Cell confluence as crucial regulator of ROS-induced toxicity:

Analysis of *t*-BuOOH-induced cell death *in vitro*

Dissertation zum Erlangen des Grades

"**Doktor der Naturwissenschaften**"

im Promotionsfach Pharmazie

am Fachbereich Chemie, Pharmazie und Geowissenschaften

der Johannes Gutenberg-Universität in Mainz

vorgelegt von

Christine Wenz

geb. am 19.08.1986 in Bad Urach

Mainz, 2019

Dekan:

1. Gutachter:

2. Gutachter:

Tag der mündlichen Prüfung: 11.09.2019

"The happiness of your life depends on the nature of your thoughts."

(translated from Marcus Aurelius)

Table of Contents

List of Abbreviations

AA	arachidonic acid
AAPH	2,2′-azobis (2-amidinopropane) dihydrochloride
ADH	alcohol dehydrogenase
ADP	adenosine 5'-diphosphate
AM	acetoxymethyl esterified
ANT	adenine nucleotide translocator
AP (site)	apurinic / apyrimidinic (site)
APAP	acetaminophen
APS	ammonium persulfate
ATF-2	cyclic AMP-dependent transcription factor 2
ATP	adenosine 5'-triphosphate
ATM	ataxia telangiectasia mutated
ATR	ataxia telangiectasia and Rad3-related protein
BAPTA (AM)	1,2-bis(o-aminophenoxy)ethane-N,N,N',N'-tetraacetic acid (acetoxymethyl esterified)
BCA	bicinchoninic acid
BER	base excision repair
BSA	bovine serum albumin
BSO	buthionine sulfoximine
Ca^{2+}	calcium (II)
CaCl	calcium chloride
Chk (1/2)	checkpoint kinase (1/2)
CHX	cycloheximide
CL	cardiolipin
CO_2	carbon dioxide
COX	cyclooxygenase
CRISPR	clustered regularly interspaced short palindromic repeats
CsA	ciclosporin A
Cu^+ / Cu^{2+}	copper (I) / copper (II)
$CuSO_4 \cdot 5H_2O$	copper sulfate pentahydrate
CypD	cyclophilin D
DDR	DNA damage response
$\Delta\psi_m$	mitochondrial membrane potential
DiOC6	3,3'-dihexyloxacarbocyanine iodide
DMSO	dimethyl sulfoxide
DNA	deoxyribonucleic acid
DSB	double-strand break
DTNB	5,5'-dithiobis-2,5-nitrobenzoic acid
DTT	dithiothreitol
EDTA	ethylenediaminetetraacetic acid
EdU	5-ethynyl-2'-deoxyuridine
EGF	epidermal growth factor
EGFR	epidermal growth factor receptor
ELISA	enzyme-linked immunosorbent-assay
EMT	epithelial-to-mesenchymal transition

ER	endoplasmatic reticulum
ERK 2	extracellular signal-regulated kinase 2
ETC	electron transport chain
EtOH	ethanol
FACS	fluorescence-activated cell scanning
FBS	fetal bovine serum
FCCP	carbonyl cyanide-4-(trifluoromethoxy)-phenylhydrazone
Fe^{2+}	iron (II)
FEN1	flap endonuclease 1
FITC	fluorescein isothiocyanate
FLAP	arachidonate 5-lipoxygenase activating protein
FS	ferrostatin-1
Gadd45A	growth arrest and DNA damage-inducible protein 45A
GPX	glutathione peroxidase
GSH	glutathione
HAT	hypoxanthine-aminopterin-thymidine
(γ-)H2AX	(phospho-) histone H2AX
H_2O_2	hydrogen peroxide
H_3PO_4	phosphoric acid
HRP	horse radish peroxidase
HSP90	heat shock protein 90
IC_{50}	half maximal inhibitory concentration
IP3	inositol 1,4,5-trisphosphate
JNK (1/2)	c-jun N-terminal kinase (1/2)
KCl	potassium chloride
K_2HPO_4	dipotassium phosphate
KOH	potassium hydroxide
LC-MS	liquid chromatography - mass spectrometry
LIG1	DNA ligase 1
LMP	low melting point
LOX	lipoxygenase
LSM	laser scanning microscopy
LX	liproxstatin-1
Mg^{2+}	magnesium (II)
MAPK	mitogen-activated protein kinase
MAPKAP	MAPK-activated protein kinase
MDA	malondialdehyde
MDC1	mediator of DNA damage checkpoint protein1
MEF	mouse embryonic fibroblast
MEK (1/2)	mitogen-activated protein kinase kinase (1/2)
MLKL	mixed lineage kinase domain-like protein
MMP	mitochondrial membrane potential
MMS	methyl methanesulfonate
MPT	mitochondrial permeability transition
mRNA	messenger ribonucleic acid
MTT	3-(4,5-dimethylthiazol-2-yl)-2,5-diphenyltetrazolium bromide

Na^+	sodium (I)
NAC	*N*-acetylcysteine
NaCl	sodium chloride
Na_2CO_3	sodium carbonate
$NAD(P)H / NAD(P)^+$	nicotinamide adenine dinucleotide (phosphate)
$NaHCO_3$	sodium hydrogen carbonate
$NaHPO_4$	sodium hydrogen phosphate
NaOH	sodium hydroxide
Nec-1	necrostatin-1
NF-κB	nuclear factor 'kappa-light-chain-enhancer' of activated B-cells
NGS	normal goat serum
Notch-1	neurogenic locus notch homolog protein-1
NOX1	NADPH oxidase 1
Nrf2	nuclear factor erythroid 2-related factor 2
$^1O_2$	singlet oxygen
$O_2^{\bullet-}$	superoxide radical anion
OGG1	8-oxoguanine DNA glycosylase
$OH^{\bullet}$	hydroxyl radical
8-oxo-dG	8-oxo-2'-deoxyguanosine
p27	cyclin-dependent kinase inhibitor 1B
p38 (MAPK)	p38 (mitogen-activated protein kinase)
p53	tumor protein p53
PAGE	polyacrylamide gel electrophoresis
PAR	poly (ADP-ribose)
PARP-1	poly (ADP-ribose) polymerase-1
PBS	phosphate buffer saline
PFA	paraformaldehyde
PES	phenazine ethosulfate
PI	propidium iodide
PVDF	polyvinylidene (di)fluoride
PS	phosphatidyl serine
(ω-3, ω-6) PUFA	(ω-3, ω-6) polyunsaturated fatty acid
Ras	rat sarcoma protein
RIPK (1,3)	receptor-interacting serine / threonine-protein kinase (1,3)
RN	regulated necrosis
$RO^{\bullet}$	alkoxyl radical
$ROO^{\bullet}$	peroxyl radical
ROS	reactive oxygen species
RSL3	RAS-Selective Lethal 3
RTK	receptor tyrosine kinase
RTP	receptor tyrosine phosphatase
SCG	single-cell gel
SDS	sodium dodecyl sulfate
siRNA	small interfering ribonucleic acid
SH-(group)	thiol- (group)
SOD	superoxide dismutase
SR	sarcoplasmatic reticulum
c-Src	(cellular sarcoma) tyrosine-protein kinase

SSB	single-strand break
TAZ	tafazzin
t-BuOOH	*tertiary*-butyl hydroperoxide
TBS (/T)	Tris-buffered saline (/ Tween 20)
TCA	tricarboxylic acid
TEMED	tetramethylethylenediamine
TGHQ	2,3,5-tris(glutathion-S-yl)hydroquinone
TNFα	tumor necrosis factor α
UV-C	ultra violet C
Wnt	wingless-type MMTV integration site family
wt	wild type
z-VAD-fmk	carbobenzoxy-valyl-alanyl-aspartyl-[O-methyl]-fluoromethylketone
($^{-/-}$)	knockout

1 Introduction

1.1 Oxidative stress: origin and consequences

Oxidative stress has been so far defined as disruption of the balance between oxidants and antioxidants in favor of an oxidative redox status of biological systems (Sies, 1985). Since the cellular redox balance is also influenced by molecular processes such as enzymatic regeneration of antioxidants or DNA repair, the current definition captures more precisely the major characteristics of oxidative stress. Thus, not only a general shift of the redox balance in favor of oxidative processes / species should be mentioned but in particular, the resulting disruption of redox signaling and related control mechanisms, and / or the accumulation of damaged macromolecules such as DNA, lipids and proteins (Valko et al., 2007; Sies, 2015; Sies et al., 2017).

1.1.1 ROS: types, sources and defense

Overproduction of as referred to reactive oxygen species (ROS) provokes oxidative stress. The harmful effect of oxidative stress is thereby conferred by free radical forms of ROS, i.e. molecules that exhibit one or more free electron in their atomic or molecular orbitals (Halliwell & Gutteridge, 1985). Thus, these electrophilic molecules or molecule fragments are highly reactive with cellular macromolecules. In biological systems, these radicals are most commonly derived from oxygen and comprise superoxide radical anion ($O_2^{\bullet-}$), hydroxyl radical ($OH\cdot$), alkoxyl ($RO^{\bullet}$) and peroxyl radicals ($ROO^{\bullet}$) as one of the most detrimental ROS (Miller et al., 1990; Pastor et al., 2000). However, also molecules with a unique electronic configuration such as singlet oxygen ($^{1}O_2$) or peroxides (H_2O_2, $ROOH$) cause oxidative stress. In this context, these molecules are sequentially reduced to free radical species via enzymatic (e.g., oxidases or superoxide dismutase (SOD)) and / or non-enzymatic (metal-catalyzed Haber-Weiss and Fenton reaction) processes (see Figure 1; Tandon et al., 2005; Valko et al., 2007; Bhattacharya et al., 2015; Sies et al., 2017).
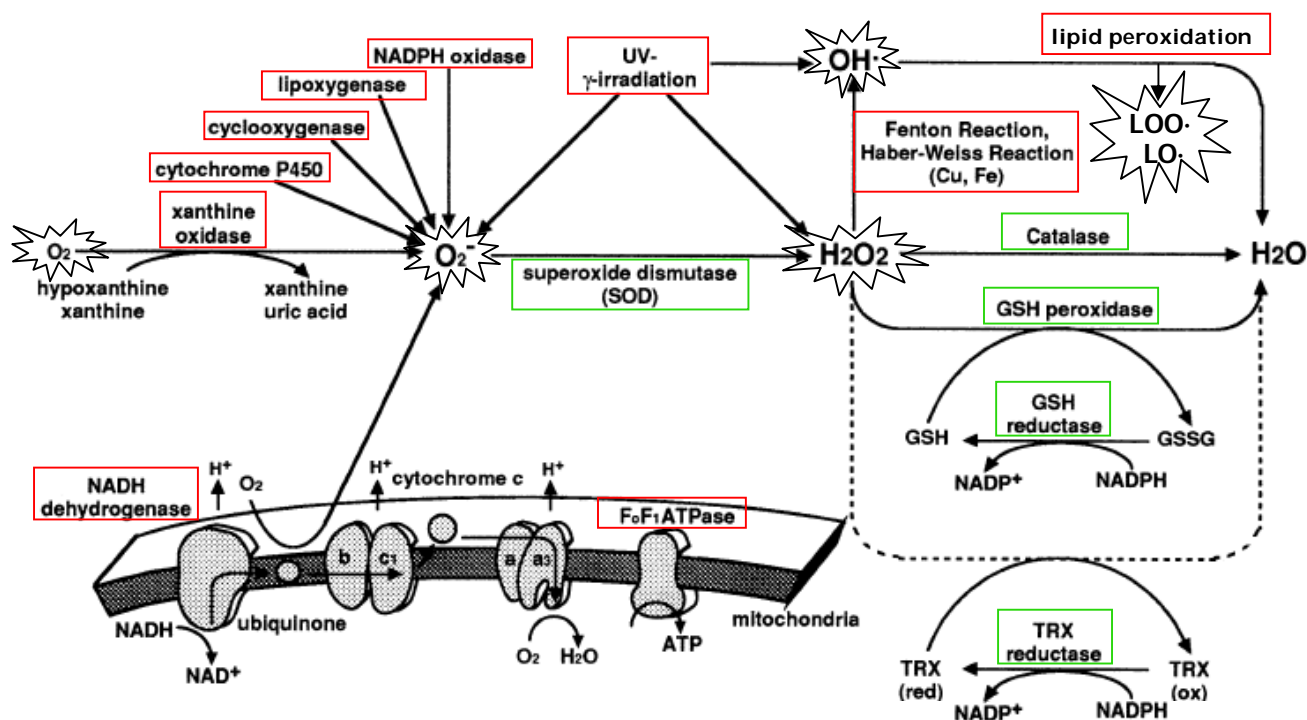
Fig. 1 Overview of ROS-generating and detoxifying systems. ROS can be derived from (i) the mitochondrial respiratory chain, (ii) enzyme-catalyzed (e.g., metabolism) or (iii) metal-catalyzed reactions (e.g,. Fenton), (iv) autooxidation (e.g., lipid peroxidation), or (v) environmental sources (e.g., γ-irradiation) (i-v: *red boxes*). Homeostasis is guaranteed by ROS detoxification (*green boxes*). Disturbance can provoke oxidative stress (related molecules*; modified after *Kamata & Hirata, 1999*).

The major endogenous sources of ROS in biological systems are (i) electron leakage of the mitochondrial respiratory chain, (ii) ROS-generating enzymes (e.g., oxidases and lipoxygenases (LOX)) involved in metabolism and the immune response, (iii) autooxidation (e.g., lipid peroxidation), as well as (iv) metal-catalyzed reactions (e.g., Fenton reaction). In addition, exposure to environmental free radicals is mainly provoked by (i) UV light, X-ray and γ-irradiation, (ii) air pollution, smoking and pesticides, (iii) food ingredients, alcohol and xenobiotics (Tandon et al., 2005; Valko et al., 2007; Sosa et al., 2013; Bhattacharya et al., 2015; Sies et al., 2017).

Experimentally, H_2O_2 and *tertiary*-butyl hydroperoxide (*t*-BuOOH) are the most frequently used chemicals to induce oxidative stress. For both, a similar mode of action is assumed regarding damage to macromolecules, as well as the mechanism of cell death. In contrast to highly reactive H_2O_2, which can freely penetrate different cellular sites, the lipophilicity of *t*-BuOOH provokes persistent oxidative stress, which is related to its predominant action on membranes and lipid peroxidation (Coleman et al., 1989; Masaki et al., 1989; Baker & He, 1991; Barr & Mason, 1995; Vroegop et al., 1995; Bergamini et al., 2004; Alia et al., 2005; Linden et al., 2008).

To counteract oxidative stress, a variety of endogenous and exogenous antioxidative defense mechanisms exists, mediating (i) prevention of ROS generation (ii) ROS interception, or (iii) repair of ROS-induced cellular lesions (Bhattacharya et al., 2015). Endogenously, the main ROS-detoxifying enzymes are SODs, catalase and glutathione peroxidases (GPXs) with the DNA damage response as secondary enzymatic defense system against oxidative stress. Non-enzymatic antioxidants that can be found in the human body are, for instance, thiols (e.g., glutathione, GSH) or bilirubin. Exogenous antioxidants are most common ingredients of natural products that contain, e.g., ascorbic acid, α-tocopherol or carotenoids (Valko et al., 2007; Pisoschi et al., 2015; Aguilar et al., 2016; Sies et al., 2017).

1.1.2 ROS-induced cellular lesions and diseases

At a high intracellular ROS concentration, a broad range of toxic effects has been described to occur via oxidation of macromolecules like the DNA, proteins and lipids (Valko et al., 2006; Wang, 2008; Avery, 2011). This process can give rise to secondary radical production of, e.g., base-, lipid- or amino acid-derived radicals followed by ROO$^\bullet$-mediated chain reactions dependent on the redox status of the cell or the site of ROS generation (Winterbourn et al., 2008).

Among oxidative DNA damage, most of mitochondrial and nuclear DNA lesions are induced by the presence of OH$\bullet$, which is able to react with all DNA components (Halliwell & Gutteridge, 1985). Besides ROS-mediated induction of, e.g., distinct oxidative DNA base modifications (e.g., 8-oxo-dG), AP sites or DNA single- and double-strand breaks (DNA SSBs and DSBs), also disturbance of the DNA repair machinery has been often described to be involved in the toxicity of ROS (Valko et al., 2006; Wang, 2008; Avery, 2011; Bhattacharya et al., 2015).

Similarly to the DNA, polyunsaturated fatty acids (PUFAs) of phospholipids, mostly located to mitochondrial and nuclear membranes, are highly sensitive to ROS-induced oxidation (Siems, Grune & Esterbauer, 1995). By the process of lipid peroxidation secondary toxic breakdown products are formed, such as malondialdehyde (MDA) and 4-hydroxynonenal (4-HNE). In addition to changes of the permeability and fluidity of cellular membranes, lipid peroxides can cross-link with the DNA or proteins, finally resulting in bulky adducts (Valko et al., 2006; Avery, 2011). Moreover, the three dimensional structure and therefore the function of

proteins can be destroyed by formation of aggregates, fragmentation or cross-linking upon ROS-induced protein oxidation (Valko et al., 2006; Avery, 2011; Bhattacharya et al., 2015). The most common secondary toxic effects of ROS-induced damage to macromolecules are, e.g., replication block, breakdown of the mitochondrial membrane potential (MMP, $\Delta\psi_m$), depletion of metabolic substrates (e.g., NAD^+ or ATP), ER stress or Ca^{2+} release (Wang, 2008; Avery, 2011; Alfadda & Sallam, 2012; Görlach et al., 2015). Besides formation of mutagenic and carcinogenic DNA lesions, cell death is one of the fatal consequences of excessive oxidative cellular damage. In addition to its key role during the onset and progression of human cancer, oxidative stress is highly involved in other acute and / or chronic pathologies, such as cardiovascular diseases, atherosclerosis, diabetes, neurological disorders and ischemia / reperfusion injury (Valko et al., 2006; Sedelnikova et al., 2010; Sosa et al., 2013; Bhattacharya et al., 2015).

1.2 A new facet of programmed cell death: regulated necrosis

To date, it is not precisely known what type of cellular damage is crucial to mediate cell death and therefore lethal toxicity upon oxidative stress. Generally, it is assumed that a low or moderate level of oxidative stress induced by, e.g., H_2O_2 is highly associated to the activation of the programmed cell death mechanism of caspase-dependent apoptosis, whereas high peroxide concentrations induce necrosis (Hampton & Orrenius, 1997; Leist et al., 1997; Nicotera & Melino, 2004; Saito et al., 2006). However, the classical image of accidently executed, chaotic necrosis has to be reconsidered due to the existence of necrotic subroutines that are tightly orchestrated upon the background of as referred to "regulated necrosis" (RN) – modes of necrotic cell death that occur upon a defined molecular setting, which can be inhibited by pharmacological or genetic interference (Galluzzi et al., 2012, 2014). Among the most intensively studied RN subroutines are cell death mechanisms, such as RIPK1 / RIPK3-mediated necroptosis, MPT-driven necrosis and PARP-1-induced parthanatos, whereas the RN subroutine of ferroptosis has been recently recognized (Galluzzi et al., 2012, 2014; Linkermann & Green, 2014; Conrad et al., 2016; Galluzzi et al., 2018).

1.2.1 Physiological and pathophysiological relevance

Inhibition of caspases via pharmacological intervention or upon certain stress conditions is one of the reasons for the evolution of RN, partially undertaking the physiological functions of apoptotic cell death (Cho et al., 2010; Dunai et al., 2011; Galluzzi et al., 2012). Physiological functions of RN pathways are related to, e.g., (post)embryonic development, tissue homeostasis, the immune response and regulation of the nervous system (Cho et al., 2010; Dunai et al., 2011). As some RN subroutines have been just recently characterized, the physiological function of, e.g., ferroptosis remains to be elucidated (Stockwell et al., 2017).

In a pathophysiological context, RN occurs in response to a broad set of exogenous and endogenous stimuli, such as (in)organic compounds, pathogens, genotoxins, oxidative stress and cell death receptors (Cho et al., 2010; Vanlangenakker et al., 2012; Vanden Berghe et al., 2014). These distinct stimuli can trigger different RN subroutines that are highly associated to ischemia / reperfusion injury in the kidney, heart, brain and liver or inflammation-related diseases, such as inflammatory bowel disease, atherosclerosis, sepsis or pancreatitis. Besides other human pathologies, also acute neurotoxicity and chronic neurodegenerative disorders can be mediated via different RN subroutines (Cho et al., 2010; Dunai et al., 2011; Galluzzi et al., 2014; Tonnus & Linkermann, 2017). On the other hand, induction of RN subroutines (e.g., necroptosis or ferroptosis) has been recognized as promising tool in cancer therapy to overcome apoptosis resistance of solid tumors (Kreuzaler & Watson, 2012; Fulda, 2014; Mohammad et al., 2015; Yu et al., 2017).

1.2.2 RN subroutines upon oxidative stress

In contrast to pyroptosis, most of RN subroutines that have been yet described in the context of oxidative stress are executed independent of caspases, such as necroptosis, MPT-driven necrosis, parthanatos and ferroptosis (Figure 2; Galluzzi et al., 2012, 2014; Linkermann & Green, 2014; Conrad et al., 2016; Galluzzi et al., 2018). In this context, including further biochemical features helps to classify these RN subroutines since classical cell death characterization might provoke misinterpretation of the underlying mechanism, regarding partially overlapping morphological characteristics (e.g., cell shrinkage upon apoptosis and ferroptosis) (Dunai et al., 2011; Dixon et al., 2012; Galluzzi et al., 2012).
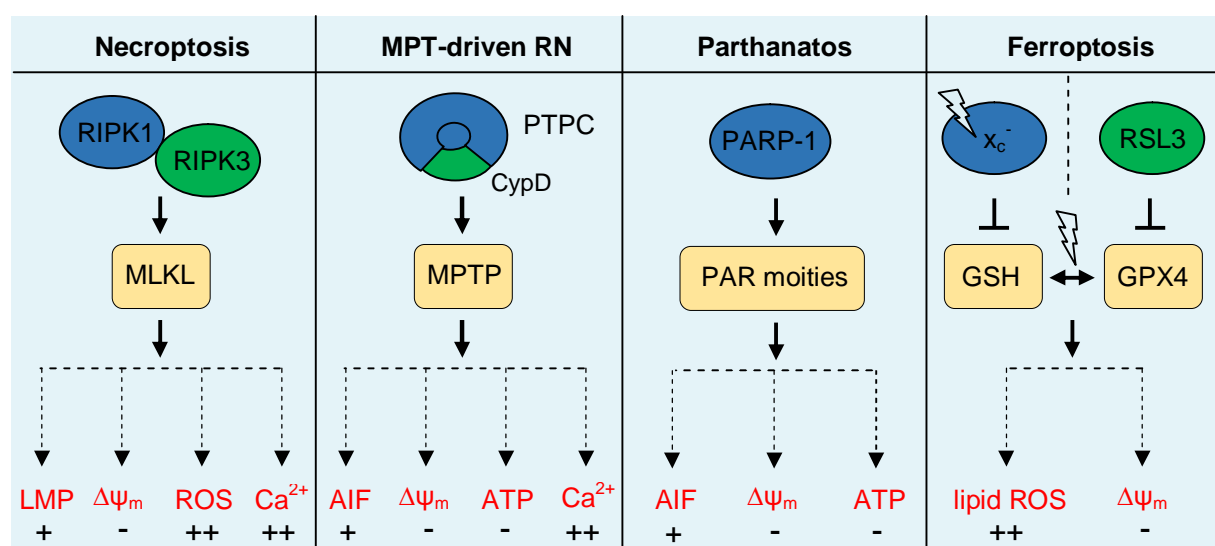
Fig. 2 Mechanisms of regulated necrosis (RN) related to oxidative stress. ROS can trigger distinct RN initiators (*blue and green colored*) and can thereby activate critical components (*orange colored*) for cell death execution, resulting in a panel of cellular stress responses (*red colored*) and finally necrosis dependent on the cellular context and RN stimulus. + = activation / release, ++ = increased generation / release, - = inhibition / inactivation. For more detailed explanations, see main text.

Necroptosis
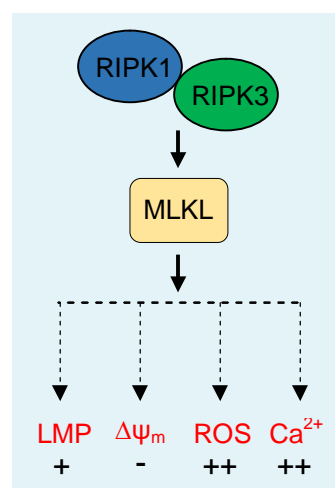
Fig. 3 Mechanism of necroptosis (see Fig.2)

As the most intensively studied RN subroutine, TNFα-induced necrosis, is the prototype of as referred to "necroptosis" – a cell death mechanism first being described in tumor cells in 1975 (Vandenabeele et al., 2010; Galluzzi et al., 2012, 2014; Linkermann & Green, 2014; Gallluzzi et al., 2018). Originally, the definition involves TNFR1 activation and the presence of RIPK1 (receptor interacting serine / threonin protein kinase 1) upon inhibition of caspase 8, whereby this type of necroptosis has been designated to be specifically blocked by the chemical necrostatin-1 (Nec-1) *in vitro* and *in vivo* (Vandenabeele et al., 2010; Galluzzi et al., 2014; Khan et al., 2014). Nowadays, the term necroptosis comprises caspase-independent necrotic subroutines that (i) can be induced by a broad range of stimuli (see chapter before), (ii) are executed in a RIPK1- and / or RIPK3- dependent manner, and (iii) can be inhibited by a set of more specific inhibitors in addition to Nec-1 (Tonnus & Linkermann, 2017; Galluzzi et al., 2018).

Interestingly, the presence of RIPK1 is not essential for the initiation and execution of necroptosis but rather the engagement of RIPK3 in a multiprotein complex (necrosome) to activate MLKL (mixed lineage kinase domain-like protein) via phosphorylation (Linkermann & Green, 2014; Vanden Berghe et al., 2014; Conrad et al., 2016; Galluzzi et al., 2018). However, downstream signaling by activated MLKL is not completely understood but so far (i) loss of the mitochondrial membrane potential (MMP / $\Delta\psi_m$), (ii) lysosomal membrane permeabilization (LMP), (iii) plasma membrane damage and Ca^{2+} influx, as well as (iv) a lethal oxidative burst via NADPH oxidases (e.g., NOX1) have been already discussed (Dunai et al., 2011; Galluzzi et al., 2014, 2018).

MPT-driven necrosis
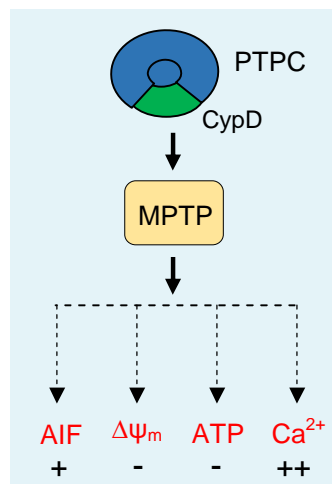
Fig. 4 Mechanism of MPT-driven necrosis (see Fig.2)

Besides a role in other types of programmed cell death, such as apoptosis, parthanatos or necroptosis, mitochondrial dysfunction is highly involved in as referred to "MPT-driven necrosis" upon oxidative stress or Ca^{2+} overload (Vandenabeele et al., 2010; Galluzzi et al., 2012, 2014; Linkermann & Green, 2014; Belizário et al., 2015; Galluzzi et al., 2018). Several studies have yet demonstrated induction of this RN subroutine due to mitochondrial permeability transition (MPT), meaning an increased entry of solutes (mainly H_2O) into the mitochondrial matrix via permanent opening of the permeability transition pore complex (PTPC) that is located between the outer and inner mitochondrial membrane (Halestrap, 2009; Galluzzi et al., 2018). In addition to proteins like adenine nucleotide translocases (ANTs) that have been yet described in the regulation of PTPC opening, cyclophilin D (CypD), which can be inhibited by the chemical cyclosporine A (CsA), remains the only, so far characterized functional component of the PT pore complex (Baines et al., 2005; Galluzzi et al., 2012, 2014, 2018). Secondary toxic events that might be triggered by MPT are, e.g., (i) mitochondrial dysfunction (loss of the MMP / $\Delta\psi_m$ and breakdown of ATP synthesis), (ii) release of cell death mediators (e.g., AIF or cytochrome C) and (iii) release of mitochondrial Ca^{2+} into the cytosol (Galluzzi et al., 2014, 2018).

Parthanatos
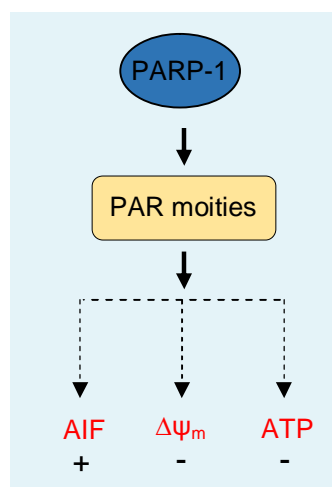
Fig. 5 Mechanism of parthanatos (see Fig.2)

As another caspase-independent RN subroutine "parthanatos", named after the Greek word *thanatos* (personification of death), has been recently discovered (Andrabi et al., 2008; David et al., 2009). Functional drivers of this necrotic pathway are nuclear enzymes of the poly (ADP-ribose) polymerase (PARP) family (Galluzzi et al., 2012, 2014, 2018). The dominant isoform PARP-1 is regulated via action of caspase 3 (Tewari et al., 1995; Amé et al., 2004). Upon covalent addition of PAR moieties to the site of DNA damage, PARP-1 facilitates the repair of SSBs, bulky DNA adducts and DSBs (Rouleau et al., 2010; Gibson & Kraus, 2012; Sfeier & Symington, 2015). In case of persistent ROS-induced DNA damage, PARP-1 becomes hyperactivated, which results in NAD^+ depletion. Due to mitochondrial accumulation of toxic PAR polymers diverse cell-death promoting lesions are induced, e.g., (i) MMP collapse ($\Delta\psi_m$), (ii) inhibition of ATP synthesis, and (iii) AIF-dependent chromatinolysis (Galluzzi et al., 2014, 2018). Notably, this RN subroutine can be inhibited via pharmacological (e.g., olaparib) or genetic interference of PARP-1 (Galluzzi et al., 2012, 2014, 2018).

Ferroptosis
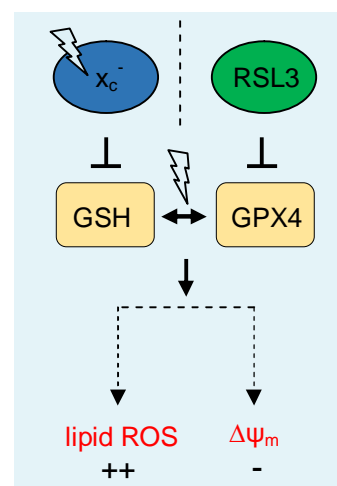
Fig. 6 Mechanism of ferroptosis (see Fig.2)

In 2012, Dixon et al. postulated a novel type of RN subroutine, characterized by excessive iron-dependent lipid peroxidation and related to a certain mitochondrial morphology (e.g., shrinkage, higher density, reduced cristae) (Xie et al., 2016; Galluzzi et al., 2018). Before notion of this RN subroutine of as referred to "ferroptosis", three distinct agents had been already discovered (erastin, RSL3 and RSL5) as inducers of this cell death in Ras-mutated tumor cells (Yu et al., 2017). Nowadays, also other ferroptosis-inducing agents have been identified and classified.

The first group of ferroptosis inducers (e.g., erastin, buthionine sulfoximine (BSO) or acetaminophen (APAP)) is characterized by GSH depletion followed by inhibition of, e.g. GPX4, and therefore blockage of lipid ROS detoxification. Besides GSH consumption through detoxification of cytosolic and lipid ROS, erastin and other drugs (e.g, sorafenib) trigger GSH depletion via inhibition of the cystine / glutamate antiporter system x_c^-, which limits the *de novo* synthesis of GSH in response to a reduced availability of cysteine. Another class of agents directly inhibits GPX4 without GSH depletion (Dixon et al. 2012, 2014; Friedmann Angeli et al., 2014; Linkermann et al., 2014; Xie et al., 2016; Yu et al., 2017; Galluzzi et al., 2018). As a unique outcome of inhibiting the GSH / GPX system, lipid peroxidation of mainly PUFAs is initiated via non-enzymatic (e.g., Fenton) and / or via enzymatic reactions (e.g., cyclooxygenase (COX) or LOX) in the presence of iron, as well as loss of the MMP (Yagoda et al., 2007; Yang et al., 2016; Yang & Stockwell, 2016). Notably, ferroptosis can be specifically inhibited by, e.g., ferrostatin-1 (FS) or liproxstatin-1 (LX), acting as ROS scavengers. Thus, also antioxidants, such as α-tocopherol, *N*-acetylcysteine (NAC) or iron chelators have been yet described to act as unspecific ferroptosis inhibitors (Yang et al., 2014; Gao et al., 2015; Lörincz et al., 2015; Xie et al., 2016; Yu et al., 2017; Galluzzi et al., 2018; Li et al., 2018; Wu et al., 2018).

1.3 The DNA damage response upon ROS-induced cell death

Upon oxidative stress, the genomic integrity of mammalian cells is secured by the DNA damage response (DDR) machinery, including proteins, such as p53, ATR, ATM, p38 and JNK. Intensive studies have demonstrated that all of these proteins are able (i) to stimulate the repair of ROS-induced DNA lesions, (ii) to induce cell cycle arrest, or (iii) to induce apoptosis when the DNA damage exceeds the repair capacity (Barzilai & Yamamoto, 2004; Roos & Kaina, 2013; Yan et al., 2014). Among the classical image of DDR pathways, activation of ATR (e.g., by UV-C-induced SSBs), ATM (e.g., by y-irradiation-induced DSBs), or their related downstream targets, Chk1 and Chk2, can result in p53 phosphorylation and induction of apoptosis upon excessive DNA damage (Yang et al., 2003). Moreover, sustained activation of p38 and JNK upon ROS-induced DNA damage has been widely demonstrated to regulate p53, as well as other mediators and inhibitors of apoptosis (Brozovic et al., 2004; Son et al., 2011; Picco & Pagés, 2013; Roos & Kaina, 2013; Shi et al., 2014).

On the other hand, first investigations of a role of these DDR components in the cell fate decision via directing to necrotic cell death mechanisms have just emerged during the last years. Interestingly, sustained activation of p38 and JNK in a necrotic cell death context has been yet found to be a result of, e.g., RIPK1 and / or RIPK3 activation during TNFα-induced necroptosis or a consequence of PARP-1 hyperactivation (Kelliher et al., 1998; Devin et al., 2003; Lee et al., 2003; Vandenabeele et al., 2010; Gautheron et al., 2014). Moreover, both MAP kinases appear also as crucial regulators of ferroptosis since pharmacological inhibition of p38 and JNK prevented erastin-induced cell death (Xie et al., 2017). In addition to a regulatory role of p53 during MPT-driven necrosis, p53 can also act in a cell-type specific manner as positive or negative regulator of ferroptosis (Vaseva et al., 2012; Xie et al., 2017). In contrast to MAP kinase and p53 signaling during RN, involvement of ATR and ATM has been so far only investigated by a few studies that suggest also a regulatory function of these DNA damage sensors in the context of parthanatos and necroptosis (Baritaud et al., 2012; Wang-Heaton, 2016).

1.4 Cell-cell contacts: regulators of the cell fate decision

In multicellular organisms, tissue homeostasis, wound healing and organ size control are orchestrated by a precise mechanism named "contact inhibition", which tightly regulates proliferation, differentiation and cell death by the presence of cell-cell contacts (Eagle & Levin, 1967; Dietrich et al., 1997; Heit et al., 2001; Nelson & Daniel, 2002; Faust et al., 2005; Weiss et al., 2008; Kango-Shing & Shing, 2009; Küppers et al., 2010; McClatchey & Yap, 2012). *In vivo* and *in vitro*, this phenomenon can be observed when non-transformed cells stop proliferation upon high density. Most of these cells thereby exit the cell cycle and reside in a quiescent state (G1 / G0 cell cycle phase), for instance by upregulation of Cdk inhibitors (e.g., p27) or activation of MAPK signaling (e.g., p38) (Lloyd et al., 1999; Wieser et al., 1999; Nelson & Daniel, 2002; Faust et al., 2005; Cheung & Rando, 2013). Although serum deprivation or stress responses have been described to mimic a G1 cell cycle arrest and to affect the same pathways, the molecular mechanism induced by the presence of cell-cell contacts is unique (Dietrich et al., 1997; Nelson & Daniel, 2002).

One of the best studied cell-cell adhesions involved in contact inhibition in fibroblast and epithelial cells are adherence junctions with two major constituents, a transmembrane protein (e.g., cadherins) and an intracellular component (e.g., catenins). Both mediate the regulation of various signaling pathways and related gene expression via cytoskeletal scaffold proteins (e.g., protein kinases) and transcription factors (Nelson & Daniel, 2002; Ebnet, 2008; Hartsock & Nelson, 2008).
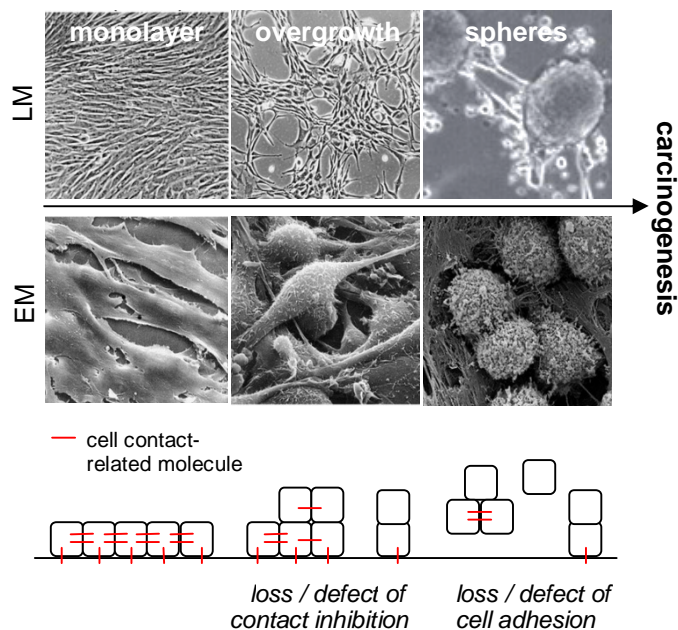
Fig. 7 Cell contact- related molecules are crucial drivers of carcinogenesis upon loss and / or defect of contact inhibition and cell adhesion. Loss and / or mutation of cell contact- related components induce overgrowth of quiescent fibroblast monolayers and finally trigger sphere formation and single cell detachment. These alterations are associated to adenoma / carcinoma formation and metastasis. Light microscopy (LM), electron microscopy (EM). Photo- graphs are taken from *Campbell & Reece, 2005*; *Liu et al., 2009*.

Importantly, loss of contact inhibition and / or mutation of cell-cell contact-related molecules are highly associated with the onset and progression of carcinogenesis (Abercrombie, 1979; Glick & Yuspa, 2005; Bhutia et al., 2010). Thus, contact inhibition provides a *bona fide* tumor suppressor mechanism, which is highlighted by cancer resistance of naked mole rats due to their hypersensitivity to contact inhibition (Seluanov et al., 2009). Remarkably, increasing evidence suggests a pivotal role of cell-cell contacts also in the regulation of the redox status and the sensitivity of mammalian cells to genotoxin- or ROS- induced cell death (Pani et al., 2000; Rancourt et al., 2002; Bakondi et al., 2003; Naderi et al., 2003; Attene-Ramos et al., 2005; Dorsey et al., 2010; Gaballah et al., 2012).

Although therapy resistance of solid tumors has been so far mainly a debate of a reduced formation of replication-dependent DNA lesions in quiescent cells, Bar et al. (2004) provided strong evidence for cell-cell contacts to provoke drug resistance independent of a G1 cell cycle arrest (Berman et al., 1978; Roos & Kaina, 2006). To date, the Wnt / β-catenin pathway, the Notch pathway and the Hippo pathway, requiring the presence of cell-cell contacts in mammalian cells, are highly discussed to be mediators of drug resistance in solid tumors (Wood, 2015; Gujral & Kirschner, 2017; Nussinov et al., 2017). Thus, a better understanding of how cell-cell contacts provide resistance against genotoxin- and ROS-induced cell death may be of great importance for novel clinical approaches.

1.5 Aims and Objectives

Since previous results of our laboratory have indicated resistance of contact-inhibited compared to proliferating fibroblasts against the toxicity of the ROS-inducing chemical *t*-BuOOH (B. Linz, MD thesis, 2013), this study aimed to analyze if cell-cell contacts may provide also resistance against ROS-induced cell death and cellular damage as independent parameter, i.e. independent of a G1 arrest. Therefore, different murine and human fibroblasts and epithelial cell lines were investigated, as well as two experimental setups were established. Moreover, characterization of the underlying cell death mechanism induced by the presence of *t*-BuOOH in proliferating cultures should provide hints towards key regulators of the cell-cell contact-driven resistance against the toxicity of *t*-BuOOH. In this context, *t*-BuOOH was chosen as a model ROS inducer since this organic peroxide is able to mimic lipid ROS patterning of oxidative stress-related pathological conditions *in vivo*, for instance, ischemia / reperfusion injury, neurological disorders and cancer (Lemasters & Nieminen, 1997; Garcia-Cohen et al., 2000; Lemasters et al., 2009; Ayala et al., 2014).

2 Materials

2.1 Laboratory Equipment

2.1.1 Large and small devices

Device	Type Designation	Manufacturer
Analytical balances	A200S	Sartorius, Göttingen, Germany
	TE64-0CE	Sartorius, Göttingen, Germany
	L2200P	Sartorius, Göttingen, Germany
Autoclave	Systec VX-150	Systec, Linden, Germany
Blotting chamber	Mini Trans-Blot cell	Bio-Rad, Munich, Germany
Centrifuges	5417R	Eppendorf, Hamburg, Germany
	5417C	Eppendorf, Hamburg, Germany
	Rotanta RPC	Hettich, Kirchlengern, Germany
Counter (for cell culture)		Becton Dickinson, Franklin Lakes, NJ, USA
Dewar vessels	1000 mL	KGW-Isotherm, Karlsruhe, Germany
Electrophoresis chambers	DNA subcell 16S/6607	Bio-Rad, Munich, Germany
	41-2025	PEQLAB, Erlangen, Germany
	Mini PROTEAN Tetra Cell	Bio-Rad, Munich, Germany
Electrophoresis equipment		Bio-Rad, Munich, Germany
Falcon tube rotator	in-house manufacturer	University Medical Center, Mainz, Germany
Flow cytometers	FACS Calibur	BD Biosciences, Heidelberg, Germany
	FACS Canto II	BD Biosciences, Heidelberg, Germany
Fluorescence microscope	Olympus BX50	Olympus, Münster, Germany
Forceps (for X-ray films)		Jobo, Gummersbach, Germany
Freezers	HERAfreeze™	Heraeus, Hanau, Germany
	GSN 3336	Liebherr, Bulle, Switzerland
Gamma irradiator	[^{137}Cs] source, Gammacell 200	Mølsgaard, Risø, Denmark
Glass devices		Schott, Mainz, Germany
Hemocytometer	Neubauer	Paul Marienfeld, Lauda-

Device	Type Designation	Manufacturer
		Königshofen, Germany
Incubator (CO$_2$)	Heracell 150	Heraeus, Hanau, Germany
Laminar flow	NuAire, Type A2	INTEGRA Biosciences, Zizers, Switzerland
Laser scanning microscope	LSM710	Carl Zeiss, Oberkochen, Germany
Light microscope	VWR$^®$ Inverted Microscope	VWR International, Radnor, PA, USA
Magnetic rods		Carl Roth, Karlsruhe, Germany
Magnetic stirrers	IKA-Combimac RCT	Janke & Kunkel, Staufen, Germany
	MR 2002	Heidolph, Schwabach, Germany
Microwave		LG, Ratingen, Germany
Microplate readers	Sunrise RC	Tecan, Männedorf, Switzerland
	Multiskan Ex	Thermofisher Scientific, Waltham, MA, USA
	TriStar² LB 942	Berthold Technologies, Bad Wildbad, Germany
pH-meter	HI 2211	Hanna Instruments, Woonsocket, RI, USA
Photometer	BioPhotometer 6131	Eppendorf, Hamburg, Germany
Pipettes	Pipet-Lite XLS, single channel	Mettler-Toledo Rainin, Oakland, CA, USA
Pipettors	Multipipette Plus	Eppendorf, Hamburg, Germany
	Pipeteboy acu	INTEGRA Biosciences, Zizers, Switzerland
Plastic tubs		Jobo, Gummersbach, Germany
Power supplies	200 / 2.0	Bio-Rad, Munich, Germany
	PowerPac™basic	Bio-Rad, Munich, Germany
Quadriperm	for 3 x 1 inch slides, 76 x 26 mm	Heraeus, Munich, Germany
Refrigerator		Siemens, Munich, Germany
		Liebherr, Bulle, Switzerland
Roller mixer	SRT9	Stuart, Staffordshire, UK
Safelight	Spot X Vario	PEHA Medizinische Geräte,

Device	Type Designation	Manufacturer
Shaker	Duomax 2030	Sulzbach, Germany Heidolph, Schwabach, Germany
Spatula	Stainless steel	VWR International, Radnor, PA, USA
Stopwatch		Junghans, Schramberg, Germany
Thermomixer	ThermoStat plus	Eppendorf, Hamburg, Germany
Tint bowl (for comet assay lysis)	Rogo Sampaic™ 143004	Thermofisher Scientific, Hampton, NH, USA
Tweezers	Stainless steel	VWR International, Radnor, PA, USA
UV-C lamp		Heraeus, Munich, Germany
Vacuum pump		Leybold, Köln, Germany
Vortex mixers	Vortex Genie 2	Bender & Hobein, Bruchsal, Germany
	REAX 2000	Heidolph, Schwabach, Germany
Water bath		GFL, Burgwedel, Germany
Water jet pump		BRAND, Wertheim, Germany
X-ray cassettes		Carl Roth, Karlsruhe, Germany

2.1.2 Expandable items

Item	Type Designation	Manufacturer
Aluminium foil	Rotilabo®	Carl Roth, Karlsruhe, Germany
Autoradiography developer and fixer	190-0943, 190-1875	Carestream Health and Kodak, Rochester, NY, USA
Cannulae	0.6 x 60 mm	B. Braun, Melsungen, Germany
	0.9 x 70 mm	B. Braun, Melsungen, Germany
Cell culture dishes	3.5 / 6 / 10 cm, Cellstar®	Greiner Bio-One, Fricken-hausen, Germany
Cell culture plates	6 / 12 / 24 / 96-well, Cellstar®	Greiner Bio-One, Fricken-hausen, Germany
Cover slips	for hemocyto-meter, 20 x 26 mm	Carl Roth, Karlsruhe, Germany
	24 x 24 mm	Carl Roth, Karlsruhe, Germany
	24 x 60 mm	Waldemar Knittel, Braun-

Item	Type Designation	Manufacturer
		schweig, Germany
Cryo vials	2 mL, Cryos™	Greiner Bio-One, Fricken-hausen, Germany
Cuvettes	1.5 mL, polystyrene	Carl Roth, Karlsruhe, Germany
Disposable gloves	powder free Level 2 (AQL< 1.5), > 480 minutes	Semperit Technische Produkte Gesellschaft, Wien, Austria
Falcon tubes	15/50 mL, Cellstar®	Greiner Bio-One, Fricken-hausen, Germany
Immersion oils	Immersol™ W 2010	Carl Zeiss, Oberkochen, Germany
	Immersol™ 518 F	Carl Zeiss, Oberkochen, Germany
Laboratory film	Parafilm M	Bemis, Neenah, WI, USA
Mounting medium	Vectashield® H-100	Vector Labs, Burlingame, CA USA
Microscopic slides	76x26 mm, 3x1 inch	DIAGONAL, Münster, Germany
Nail varnish	transparent	Sabrina Cosmetics, Lungkwitz, Germany
Pasteur capillary pipettes		Carl Roth, Karlsruhe, Germany
Pipette tips	0.5 µL - 1 mL	PEQLAB, Erlangen, Germany Greiner Bio-One, Fricken-hausen, Germany
Plastic pipettes	5-25 mL, Cellstar®	Greiner Bio-One, Fricken-hausen, Germany
Precision wipes (for LSM)		Kimberly-Clark, Irving, TX, USA
PVDF membrane	Immobilon®-P	Merck, Darmstadt, Germany
Reaction tubes	0.5 / 1.5 / 2 mL	Eppendorf, Hamburg, Germany
Rubbing alcohol	Benzinum DAB	Otto Fischar, Saarbrücken, Germany
Scalpels	No. 15	Swann-Morton Limited, Owler-ton Green, Sheffield, UK
Scraper (cell culture)	Length 290 mm, Blade wide 20 mm	SPL Life Sciences, Pocheon, Gyeonggi-do, South Korea
Syringes	Omnifix®Luer 20 mL	B. Braun, Melsungen, Germany
	Injekt®-F, 1 mL	B. Braun, Melsungen, Germany
Syringe filter	Minisart®, 0.2 µm	Sartorius, Göttingen, Germany
Weighing paper	MN 226	MACHEREY-NAGEL, Düren, Germany

Item	Type Designation	Manufacturer
Whatman filter paper	Grade 703 Blotting Paper	VWR International, Radnor, PA, USA
X-ray films	Cronex 5	Agfa Healthcare, Mortsel, Belgium
	Amersham Hyper-Film ECL	GE Healthcare, Little Chalfont, UK

2.2 Chemicals and Biochemicals

Reagent	Manufacturer
Acetic acid	Carl Roth, Karlsruhe, Germany
ADH	TCI Deutschland, Eschborn, Germany
Albumin Fraction V, BSA	Carl Roth, Karlsruhe, Germany
Aqua ad iniectabilia	B. Braun, Melsungen, Germany
Anisomycin solution (5 mg / mL)	Sigma-Aldrich, Steinheim, Germany
Annexin V-FITC	Miltenyi Biotec, Bergisch Gladbach, Germany
BAPTA AM	AAT Bioquest, Sunnyvale, CA, USA Biomol, Hamburg, Germany
Bicine (titration)	Sigma-Aldrich, Steinheim, Germany
Boric acid	Serva Electrophoresis, Heidelberg, Germany
Bradford dye concentrate	Bio-Rad, Munich, Germany
Bromphenol blue, sodium salt	Serva Electrophoresis, Heidelberg, Germany
BSO	Sigma-Aldrich, Steinheim, Germany
$CaCl_2$	Sigma-Aldrich, Steinheim, Germany
Chloroform, ROTIPURAN®	Carl Roth, Karlsruhe, Germany
CHX	Sigma-Aldrich, Steinheim, Germany
Cisplatin	Pharmacy of the University Medical Center, Mainz, Germany
CM-H2DCFDA	Invitrogen, Carlsbad, CA, USA
Coomassie Brilliant Blue G	Sigma-Aldrich, Steinheim, Germany
CsA	Santa Cruz Biotechnology, Dallas, TX, USA
$CuSO4 \cdot 5 H_2O$	PanReac AppliChem, Darmstadt, Germany
Cyclic Pifithrin α hydrobromide	Biomol, Hamburg, Germany
DCFH-DA	Sigma-Aldrich, Steinheim, Germany
DiOC6	Thermofisher Scientific, Waltham, MA, USA
DMEM (Cat.:11960044; no phenol red: 21063029; no Ca^{2+}: 21068028)	Gibco Life Technologies, Karlsruhe, Germany
DMSO	Carl Roth, Karlsruhe, Germany
DMSO (anhydrous)	Merck, Darmstadt, Germany

Reagent	Manufacturer
DTNB	Sigma-Aldrich, Steinheim, Germany
DTT	PanReac AppliChem, Darmstadt, Germany
EDTA	PanReac AppliChem, Darmstadt, Germany
EtOH, ROTIPURAN®	Carl Roth, Karlsruhe, Germany
FBS	Gibco Life Technologies, Karlsruhe, Germany
FCCP	Santa Cruz Biotechnology, Dallas, TX, USA
Ferrostatin-1	Sigma-Aldrich, Steinheim, Germany
Fluo-4 AM	Thermofisher Scientific, Waltham, MA, USA
Geniticin, G418 solution (50 mg / mL, 30000 U / mL)	Merck Millipore, Billerica, MA, USA
L-Glutamine solution (200 mM)	PAA Laboratories, Pasching, Austria
L-glutathione reduced, GSH	Sigma-Aldrich, Steinheim, Germany
Glycine	Carl Roth, Karlsruhe, Germany
GSK 2791728 A (GSK '728')	GlaxoSmithKline, Brentford, UK
GSK 2791840 B (GSK '840')	GlaxoSmithKline, Brentford, UK
GSK 3002963 A (GSK '963')	GlaxoSmithKline, Brentford, UK
GSK 2393843 A (GSK '843')	GlaxoSmithKline, Brentford, UK
GSK 2399872 A (GSK '872')	GlaxoSmithKline, Brentford, UK
HAT Supplement	Life Technologies, Carlsbad, CA, USA
HEPES	Carl Roth, Karlsruhe, Germany
HiPerFect® Transfection Reagent	Qiagen, Hilden, Germany
H_2O_2 (30 % v/v)	Sigma-Aldrich, Steinheim, Germany
H_3PO_4	Sigma-Aldrich, Steinheim, Germany
KCl	Carl Roth, Karlsruhe, Germany
K_2HPO_4	Merck, Darmstadt, Germany
KH_2PO_4	Carl Roth, Karlsruhe, Germany
KOH (pellets)	Merck, Darmstadt, Germany
Ku 60019	Apexbio Technology LLC, Houston, TX, USA
Lipofectamine® 2000 CD Reagent	Invitrogen, Carlsbad, CA, USA
Lipofectamine™ Reagent	Invitrogen, Carlsbad, CA, USA
Lipofectamine™, RNAi Max, Reagent	Invitrogen, Carlsbad, CA, USA
Low Melting Point Agarose	Bethesda Research Laboratories, Gaithersburg, USA
LumiGLO®, Reagent A (20x conc.)	Cell Signaling Technology, Danvers, MA, USA
Luperox® TBH70X, t-BuOOH solution	Sigma-Aldrich, Steinheim, Germany
MEM (Cat.: M2279)	Sigma-Aldrich, Steinheim, Germany
MEM non-essential amino acid solution (100x)	Sigma-Aldrich, Steinheim, Germany

Reagent	Manufacturer
Methanol, ROTIPURAN®	Carl Roth, Karlsruhe, Germany
MitoTracker® Red (M7512)	Life Technologies, Carlsbad, CA, USA
MMS	Sigma-Aldrich, Steinheim, Germany
MTT	Sigma-Aldrich, Steinheim, Germany
NAC, cell culture tested	Sigma-Aldrich, Steinheim, Germany
NaCl	Carl Roth, Karlsruhe, Germany
Na_2CO_3 (anhydrous)	Merck, Darmstadt, Germany
$NaHCO_3$	Merck, Darmstadt, Germany
$NaHPO_4$	Honeywell Riedel-de Haën, Seelze, Germany
NAD^+ solution (50 mM)	New England Biolabs, Ipswich, MA, USA
NaOH (pellets)	Carl Roth, Karlsruhe, Germany
Necrostatin-1	Santa Cruz Biotechnology, Dallas, TX, USA
NGS	Jackson ImmunoResearch, West Grove, PA, USA
Olaparib	Selleck Chemicals, Houston, TX, USA
Opti-MEM™ I Reduced Serum Medium	Gibco Life Technologies, Karlsruhe, Germany
PFA	Carl Roth, Karlsruhe, Germany
Passive Lysis Buffer, 5x	Promega, Madison, WI, USA
Penicillin (10.000 U / mL) / Streptomycin (10 mg / mL) solution	Sigma-Aldrich, Steinheim, Germany
Peroxide, Reagent B (20x conc.)	Cell Signaling Technology, Danvers, MA, USA
PES	Sigma-Aldrich, Steinheim, Germany
PI	Serva Electrophoresis, Heidelberg, Germany
Pierce™ BCA Solid	Thermofisher Scientific, Waltham, MA, USA
Powdered milk, blotting grade	Carl Roth, Karlsruhe, Germany
Isopropyl alcohol	AppliChem, Darmstadt, Germany
Protein ladder (biotinylated)	Cell Signaling Technology, Danvers, MA, USA
Protein ladder (Spectra ™ Multicolor Broad Range)	Thermofisher Scientific, Waltham, MA, USA
Protein Ladder (Prestained Molecular Weight Marker)	Sigma-Aldrich, Steinheim, Germany
Ribonuclease A (DNAse-free, min. 80 U / mg)	AppliChem, Darmstadt, Germany
Rotiphorese® Gel A	Carl Roth, Karlsruhe, Germany
Rotiphorese® Gel B (2 % bisacrylamide)	Carl Roth, Karlsruhe, Germany

Reagent	Manufacturer
SB203580	Jena Bioscience, Jena, Germany
SDS	Carl Roth, Karlsruhe, Germany
Sodium pyruvate solution (100 mM)	PAA Laboratories, Pasching, Austria
Sodium tartrate	Merck, Darmstadt, Germany
SP600125	Enzo Life Sciences, Lausen, Austria
StarPure Agarose (low EEO for gel electrophoresis)	STARLAB, Ahrensburg, Germany
Staurosporine	Sigma-Aldrich, Steinheim, Germany
Sucrose	Carl Roth, Karlsruhe, Germany
5-Sulfosalicyclic acid dihydrate, Reagent Plus	Sigma-Aldrich, Steinheim, Germany
SYTOX™ Blue Nucleic Acid Stain (5 mM solution)	Thermofisher Scientific, Waltham, MA, USA
TEMED	AppliChem, Darmstadt, Germany
TNFα	Preprotech, Hamburg, Germany
To-Pro™-3 iodide (1 mM solution)	Thermofisher Scientific, Waltham, MA, USA
Triton X-100	Sigma-Aldrich, Steinheim, Germany
Tris	Carl Roth, Karlsruhe, Germany
Trizma® base (titration)	Sigma-Aldrich, Steinheim, Germany
Trypan Blue	Serva Electrophoresis, Heidelberg, Germany
Trypsin solution (2.5 %)	Sigma-Aldrich, Steinheim, Germany
Tween® 20	Sigma-Aldrich, Steinheim, Germany
U0126	Cayman Chemical Company, Ann Arbor, MI, USA
VE-821	Selleck Chemicals, Houston, TX, USA
Z-VAD-fmk	Promega, Madison, WI, USA
	Enzo Life Sciences, Lausen, Austria

2.3 Synthetic Oligonucleotides

Name	Sequence (5'→ 3')
RIPK1 (mouse) siRNA	CCACUAGUCUGACUGAUG

Manufacturer	Application
Eurofins Genomics	transient knockdown of RIPK1 in NIH3T3 and MEF cells[1]

Name	Sequence (5'→ 3')
dsRed	AGUUCCAGUACGGCUCCAAtt
Manufacturer	**Application**
Ambion®, Thermo-fisher Scientific	custom siRNA[2]

[1] according to Sosna et al., 2014.

[2] according to Weiss et al., 2005 and Faust et al., 2013.

2.4 Antibodies

2.4.1 Primary antibodies

Antigen: **ATF2**	Cat-No.: sc-187	Source: rabbit, polyclonal
Manufacturer: Santa Cruz Biotech. (Dallas, TX, USA)	Application: Western Blotting (1:1000 dilution in 5 % milk powder / TBS/T)	
Antigen: **phospho-ATF2 (T71)**	Cat-No.: #9221	Source: rabbit, polyclonal
Manufacturer: Cell Signaling Techn. (Danvers, MA, USA)	Application: Western Blotting (1:1000 dilution in 5 % BSA / TBS/T)	
Antigen: **β-actin**	Cat-No.: sc-47778	Source: mouse, monoclonal
Manufacturer: Santa Cruz Biotech. (Dallas, TX, USA)	Application: Western Blotting (1:1000 dilution in 5 % milk powder / TBS/T)*	
Antigen: **phospho-c-jun (S63)**	Cat-No.: #9262	Source: rabbit, polyclonal
Manufacturer: Cell Signaling Techn. (Danvers, MA, USA)	Application: Western Blotting (1:1000 dilution in 5 % BSA / TBS/T)	
Antigen: **phospho-c-jun (S73)**	Cat-No.: #9164	Source: rabbit, polyclonal
Manufacturer: Cell Signaling Techn. (Danvers, MA, USA)	Application: Western Blotting (1:1000 dilution in 5 % BSA / TBS/T)	
Antigen: **cleaved caspase 3**	Cat-No.: sc-7148	Source: rabbit, polyclonal
Manufacturer: Santa Cruz Biotech. (Dallas, TX, USA)	Application: Western Blotting (1:1000 dilution in 5 % BSA / TBS/T)	
Antigen: **phospho-Chk1 (S345)**	Cat-No.: #2341	Source: rabbit, polyclonal
Manufacturer: Cell Signaling Techn. (Danvers, MA, USA)	Application: Western Blotting (1:1000 dilution in 5 % BSA / TBS/T)	
Antigen: **phospho-Chk2 (T68)**	Cat-No.: #2661	Source: rabbit, polyclonal
Manufacturer: Cell Signaling Techn. (Danvers, MA, USA)	Application: Western Blotting (1:1000 dilution in 5 % BSA / TBS/T)	

Antigen: **ERK2**	Cat-No.: sc-154	Source: rabbit, polyclonal
Manufacturer: Santa Cruz Biotech. (Dallas, TX, USA)	Application: Western Blotting (1:1000 dilution in 5 % milk powder / TBS/T)	
Antigen: **γ-H2AX (S139)**	Cat-No.: ab11174	Source: rabbit, polyclonal
Manufacturer: Abcam (Cambridge, UK)	Application: Western Blotting (1:1000 dilution in 5 % milk powder / TBS/T)	
Antigen: **γ-H2AX (S139)**	Cat-No.: #9718	Source: rabbit, polyclonal
Manufacturer: Cell Signaling Techn. (Danvers, MA, USA)	Application: Immunocytochemistry (1:200 - 1:1000 dilution in 0.25 % Triton-X 100 / PBS)	
Antigen: **HSP90**	Cat-No.: sc-13119	Source: mouse, monoclonal
Manufacturer: Santa Cruz Biotech. (Dallas, TX, USA)	Application: Western Blotting (1:1000 dilution in 5 % milk powder / TBS/T)*	
Antigen: **phospho-JNK (T183/Y185)**	Cat-No.: #9251	Source: rabbit, polyclonal
Manufacturer: Cell Signaling Techn. (Danvers, MA, USA)	Application: Western Blotting (1:1000 dilution in 5 % BSA / TBS/T)	
Antigen: **phospho-MAPKAP (T334)**	Cat-No.: #3007	Source: rabbit, monoclonal
Manufacturer: Cell Signaling Techn. (Danvers, MA, USA)	Application: Western Blotting (1:1000 dilution in 5 % BSA / TBS/T)	
Antigen: **MAPKAP**	Cat-No.: sc-393609	Source: mouse, monoclonal
Manufacturer: Santa Cruz Biotech. (Dallas, TX, USA)	Application: Western Blotting (1:1000 dilution in 5 % milk powder / TBS/T)	
Antigen: **MDC1**	Cat-No.: 05-1572	Source: mouse, monoclonal
Manufacturer: Merck Millipore (Billerica, MA, USA)	Application: Immunocytochemistry (1:200 dilution in 0.25 % Triton-X 100 / PBS))	
Antigen: **p27**	Cat-No.: sc-528	Source: rabbit, polyclonal
Manufacturer: Santa Cruz Biotech. (Dallas, TX, USA)	Application: Western Blotting (1:1000 dilution in 5 % milk powder / TBS/T)*	
Antigen: **p38**	Cat-No.: #9212	Source: rabbit, monoclonal
Manufacturer: Cell Signaling Techn. (Danvers, MA, USA)	Application: Western Blotting (1:1000 dilution in 5 % milk powder / TBS/T)	
Antigen: **phospho-p38** (T180/Y182)	Cat-No.: #9211	Source: rabbit, polyclonal
Manufacturer: Cell Signaling Techn. (Danvers, MA, USA)	Application: Western Blotting (1:1000 dilution in 5 % BSA / TBS/T)	
Antigen: **p53**	Cat-No.: CBL404	Source: mouse, monoclonal
Manufacturer: Merck Millipore (Billerica, MA, USA)	Application: Western Blotting (1:1000 dilution in 5 % milk powder / TBS/T)	
Antigen: **phospho-p53 (S15)**	Cat-No.: #9284	Source: rabbit, polyclonal
Manufacturer: Cell Signaling Techn. (Danvers, MA, USA)	Application: Western Blotting (1:1000 dilution in 5 % BSA / TBS/T)	

Antigen: **cleaved PARP-1**	Cat-No.: ab4830	Source: rabbit, polyclonal
Manufacturer: Abcam (Cambridge, UK)	Application: Western Blotting (1:250 dilution in TBS/T)	
Antigen: **PAR (10H antibody)**	Cat-No.: --	Source: mouse, monoclonal[1]
Manufacturer: gift of [2]	Application: Immunocytochemistry (1:300 dilution in 5 % milk powder / TBS/T)	
Antigen: **RIPK1**	Cat-No.: 610459	Source: mouse, monoclonal
Manufacturer: Becton Dickinson (Franklin Lakes, NJ, USA)	Application: Western Blotting (1:1000 dilution in 5 % milk powder / TBS/T)	
Antigen: **RIPK3**	Cat-No.: sc-135170	Source: rabbit, polyclonal
Manufacturer: Santa Cruz Biotech. (Dallas, TX, USA)	Application: Western Blotting (1:200 dilution in 5 % BSA / TBS/T)	

[1] according to Kawamitsu et al., 1984 and Fahrer et al., 2007.

[2] Prof. Dr. Alexander Bürkle, University of Konstanz, Germany.

* incubation can be performed for 1-1.5 h at RT as an alternative to overnight incubation at 4°C.

2.4.2 Secondary detection antibodies

2.4.2.1 HRP secondary antibody conjugates

Antibody: **anti-mouse IgG-HRP**	Cat-No.: sc-2005	Source: goat, polyclonal
Manufacturer: Santa Cruz Biotech. (Dallas, TX, USA)	Application: Western Blotting (1:1000 dilution in 5 % milk powder / TBS/T)	
Antibody: **anti-rabbit IgG-HRP**	Cat-No.: #7074	Source: goat, polyclonal
Manufacturer: Cell Signaling Techn. (Danvers, MA, USA)	Application: Western Blotting (1:1000 dilution in 5 % milk powder / TBS/T)	

2.4.2.2 Fluorophore-conjugated secondary antibodies

Antibody: anti-mouse IgG-Cy3 conjugate	**Cat-No.:** #115-165-003	**Source:** goat, polyclonal
Manufacturer: Jackson ImmunoResearch (West Grove, PA, USA)	**Application:** Immunocytochemistry (1:400 dilution in 0.25 % Triton-X 100 / PBS)	
Antibody: anti-mouse IgG-Alexa Fluor 488 conjugate	**Cat-No.:** #A-11001	**Source:** goat, polyclonal
Manufacturer: Thermo Fisher Scientific (Waltham, MA, USA)	**Application:** Immunocytochemistry (1:400 dilution in 5 % milk powder / TBS/T)	

Antibody: anti-rabbit IgG-Alexa Fluor 488 conjugate	**Cat-No.:** #A-11034	**Source:** goat, polyclonal
Manufacturer: Thermo Fisher Scientific (Waltham, MA, USA)	**Application:** Immunocytochemistry (1:400 dilution in 0.25 % Triton-X 100 / PBS)	

2.5 Buffers and Solutions

2.5.1 Mammalian cell culture and cell treatment

Cell cultivation medium and additives

For cultivation of NIH3T3, MEF (p53 wt; p53 $^{-/-}$), Swiss3T3, FH109, HaCaT cells:

- DMEM (Cat-No.:11960044)
- 10 % (v/v) FBS
- 2 % (v/v) L-Glutamine solution
- 1 % (v/v) Penicillin-Streptomycin solution

For cultivation of Caco-2 cells:

- MEM (Cat-No.: M2279)
- 10 % (v/v) FBS
- 2 % (v/v) L-Glutamine solution
- 1 % (v/v) Penicillin-Streptomycin solution
- 1 % (v/v) MEM non-essential amino acid solution

For cultivation of EAhy.926 cells:

- DMEM (Cat-No.:11960044)
- 10 % (v/v) FBS
- 2 % (v/v) L-Glutamine solution
- 2 % (v/v) HAT supplement
- 1 % (v/v) Penicillin-Streptomycin solution
- 1 % (v/v) MEM non-essential amino acid solution

For cultivation of NIH3T3 RIP1 $^{-/-}$ and RIP3 $^{-/-}$ cells:

- DMEM (Cat-No.:11960044)
- 10 % (v/v) FBS

- 2 % (v/v) L-Glutamine solution
- 1 % (v/v) Penicillin-Streptomycin solution
- 1 mg / mL G418 solution

Culture medium is supplemented with additives prior to use and stored at 4 °C. Aliquots of FBS, as well as of the L-Glutamine, Penicillin-Streptomycin and HAT supplement stock solutions are stored at -20 °C.

PBS (10x)

NaCl	1.368 M	80 g
Na_2HPO_4	32 mM	4.5 g
KCl	26.8 mM	2 g
KH_2PO_4	14.7 mM	2 g
H_2O_{dest}		ad 1 L

The pH is adjusted to 7.4. The PBS stock solution is diluted 1:10 with H_2O_{dest} for the final working concentration of 1x PBS. Aliquots of the PBS stock and working solution are autoclaved and stored at 4 °C.

PBS / EDTA for trypsin dilution

EDTA	0.02 % (w/v)	100 mg
1x PBS		ad 500 mL

After pH adjustment (7.4), the solution is autoclaved and stored at 4 °C.

PBS / EDTA (HaCaT pretreatment for trypsinization)

EDTA	0.05 % (w/v)	250 mg
1x PBS		ad 500 mL

After pH adjustment (7.4), the solution is autoclaved and stored at 4 °C.

EtOH solution

EtOH	70 % (v/v)	700 mL
H_2O_{dest}		ad 1 L

The solution is stored at RT.

NaCl solution

- NaCl   0.9 % (w/v)   900 mg
- H_2O_{dest} ad 100 mL

The solution is stored at 4 °C.

Trypan Blue staining solution

- Trypan Blue   0.5 % (w/v)   500 mg
- NaCl solution (0.9 %)   ad 100 mL

The solution is stored at RT.

t-BuOOH stock solution

- t-BuOOH solution (70x)   10 mM   13.84 µL
- 1x PBS (sterile)   ad 10 mL

The stock solution is stored at 4 °C up to 1 week.

H_2O_2 stock solution

- H_2O_2 (30 % v/v)   1 mM   10.2 µL
- H_2O_{dest} ad 10 mL

The stock solution is freshly prepared and immediately used for cell treatment.

TNFα stock solution

- TNFα   20 µg / mL   0.02 g
- BSA   0.1 % (w/v)   0.001 g
- 1x PBS (sterile)   ad 1 mL

The solution is sterile-filtrated and stored in aliquots at -20 °C.

NAC stock solution

- NAC   500 mM   816 mg
- H_2O_{dest} ad 10 mL

The pH is adjusted to 7.4. After sterile filtration, the stock solution is stored at 4 °C for two weeks.

BSO stock solution

- BSO   200 mM   0.44 g
- H_2O_{dest} ad 1 mL

To dissolve BSO, the solution is heated to 37 °C and mixed by vortexing. After sterile filtration, the stock solution is stored at 4 °C for several weeks.

MMS stock solution

- MMS   100 mM   9.1 µL
- H_2O_{dest} ad 1 mL

The stock solution is freshly prepared and immediately used for cell treatment. Afterwards, MMS is neutralized by adding an equal volume of NaOH (1 M).

Cisplatin stock solution

The stock solution (1 mg / mL in DMSO) was provided by the lab of Prof. Dr. Bernd Kaina (Toxicology, Mainz, Germany). The stock solution is stored at -20 °C.

Olaparib working solution

The stock solution (10 mM) of Olaparib is prepared according to the manufacturer's instructions in DMSO. Aliquots of the stock are stored at -20 °C. Shortly prior to use, the stock solution is diluted with sterile 1x PBS for the final inhibitor working concentration. The working solution can be stored at 4 °C for 1 day.

Other stock solutions for cell treatment, i.e. of chemical inhibitors are prepared and stored according to the manufacturers' instructions. In this context, suitable concentrations for the stock solutions are selected to keep the solvent concentration on a non-cytotoxic level of 0.1-0.5 % (v/v) for cell treatment.

2.5.2 Cytochemistry and flow cytometry

Binding buffer (10x)

- NaCl   1.4 M   4.09 g
- HEPES   100 mM   1.19 g
- BSA   1 % (w/v)   0.5 g
- $CaCl_2$ 25 mM   0.18 g
- H_2O_{dest} ad 50 mL

The stock solution (10x) is diluted 1:10 with H_2O_{dest} for the final working concentration of the Binding buffer (1x). Aliquots of the stock solution are stored at -20 °C. The working solution is stored at 4 °C up to 1 week.

PBS / FBS solution

- FBS   2 % (v/v)   1 mL
- PBS (sterile)   ad 50 mL

The solution is stored at 4 °C for several weeks.

Tris buffer (10 mM, pH 7.4)

- Tris   10 mM   60.57 mg
- H_2O_{dest} ad 50 mL

The pH is adjusted to 7.4 with HCl. The solution is stored at 4 °C for several weeks.

RNAse A solution

- RNAse A (min. 80 U / mg)   1562.5 U / mL   19.53 mg
- Tris · HCl (10 mM, pH 7.5)   ad 1 mL

Aliquots of the solution are stored at -20 °C.

PI stock solution

- PI   10 mg / mL   500 mg
- H_2O_{dest} ad 50 mL

The solution is stored at 4 °C in the dark.

PI staining solution (subG1)

- PI   10 mg / mL   100 µL
- RNAse A solution   11.25 U   7.2 µL
- PBS / FBS solution   ad 1 mL

The solution is freshly prepared in the dark. The staining solution volume is sufficient for max. ~ 3 x 10^5 cells.

AnnexinV-FITC / PI staining solution

- AnnexinV-FITC   5 % (v/v)   2.5 µL
- Binding buffer (1x)   ad 50 µL

Pelletized cells are resuspended in AnnexinV-FITC staining solution prior to dropwise addition of the PI staining solution.

- PI (10 mg / mL)   1 mg / mL   45 µL
- Binding buffer (1x)   ad 450 µL

The solutions are freshly prepared in the dark. The staining solution volume is sufficient for max. ~ 3 x 10^5 cells.

CM-H2DCFDA stock solution

- CM-H2DCFDA   1.25 mM   50 µg
- DMSO   ad 69.2 µL

The stock solution is freshly prepared in the dark. After freezing in liquid nitrogen, the solution can be stored once at -20 °C.

CM-H2DCFDA staining solution

- CM-H2DCFDA (1.25 mM)   5 µM   8 µL
- DMEM (no phenol red: Cat-No.: 21063029)   ad 2 mL

The staining solution is freshly prepared in the dark. The staining solution volume is sufficient for max. ~ 3 x 10^5 cells.

DCFH-DA stock solution

- DCFH-DA   40 mM   50 mg
- DMSO   ad 2.565 mL

The stock solution is prepared in the dark. Aliquots are stored at -20 °C and thawed once.

DCFH-DA staining solution

- DCFH-DA (40 mM)   100 µM   5 µL
- DMEM (no phenol red: Cat-No.: 21063029)   ad 2 mL

The staining solution is freshly prepared in the dark. The staining solution volume is sufficient for max. ~ 3×10^5 cells.

DiOC6 stock solution

- DiOC6   10 mM   100 mg
- EtOH   ad 17.47 mL

The stock solution is prepared in the dark. Aliquots are sealed with laboratory film to prevent solvent evaporation and are stored at -20 °C.

DiOC6 staining solution

- DiOC6 (10 mM)   20 nM 2×10^{-3} µL
- DMEM (no phenol red: Cat-No.: 21063029)   ad 2 mL

The staining solution is freshly prepared in the dark. If very small volumes of DiOC6 are needed, the stock solution (10 mM) is prediluted (1:10) in EtOH. The staining solution volume is sufficient for max. ~ 3×10^5 cells.

Fluo-4 AM stock solution

- Fluo-4 AM   1 mM   50 µg
- DMSO   ad 45.6 µL

The stock solution prepared in the dark. Aliquots are stored at -20 °C and thawed once.

Fluo-4 AM staining solution

- Fluo-4 AM (1 mM)   2 µM   4 µL
- DMEM (no Ca^{2+}: Cat-No.: 21068028)   ad 2 mL

The staining solution is freshly prepared in the dark. The staining solution volume is sufficient for max. ~ 3 x 10^5 cells.

2.5.3 Photometric and luciferase-based assays

MTT stock solution

- MTT   5 mg / mL   50 mg
- 1x PBS (sterile)   ad 10 mL

The stock solution is stored at 4 °C in the dark.

MTT staining solution

- MTT (5 mg / mL)   1 mg / mL   20 µL
- DMEM (Cat-No.: 11960044)   ad 120 µL

The solution is freshly prepared and sufficient to stain cells seeded on a 96-well.

HCl / Isopropyl alcohol solution

- HCl 1 M   40 mM   20 mL
- Isopropyl alcohol   ad 500 mL

The stock solution is stored at 4 °C.

KH$_2$PO4 stock solution

- KH$_2$PO$_4$ 1 M   13.61 g
- H$_2$O$_{dest}$ ad 100 mL

The stock solution is stored at 4 °C.

K$_2$HPO4 stock solution

- K$_2$HPO$_4$ 1 M   22.82 g
- H$_2$O$_{dest}$ ad 100 mL

The stock solution is stored at 4 °C.

EDTA stock solution (for GSH Assay)

- EDTA   0.5 M   14.61 g
- H$_2$O$_{dest}$ ad 100 mL

The stock solution is stored at 4 °C.

Buffer A (for GSH Assay)

- KH$_2$PO$_4$ (1 M)   125 mM   12.5 mL
- EDTA (0.5 M)   8 mM   1.6 mL
- H$_2$O$_{dest}$ ad 100 mL

The stock solution is stored at 4 °C.

Buffer B (for GSH Assay)

- K$_2$HPO$_4$ (1 M)   125 mM   12.5 mL
- EDTA (0.5 M)   8 mM   1.6 mL
- H$_2$O$_{dest}$ ad 100 mL

The stock solution is stored at 4 °C.

Buffer A / B (for GSH Assay)

- Buffer A   15 mL
- Buffer B   ad 100 mL

The stock solution is stored at 4 °C.

Sulfocalicylic acid solution (5 %)

- Sulfocalicylic acid   5 % (w/v)   5 g
- H$_2$O$_{dest}$ ad 100 mL

The stock solution is stored at 4 °C.

Sulfocalicylic acid solution (10 %)

- Sulfocalicylic acid   10 % (w/v)   10 g
- H_2O_{dest} ad 100 mL

The stock solution is stored at 4 °C.

GSH stock solution

- GSH   50 mM   15.4 mg
- H_2O_{dest} ad 1 mL

Aliquots of the stock solution are stored at -80 °C.

GSH working solution

- GSH (50 mM)   1 mM   20 µl
- Sulfocalicylic acid solution (5 %)   ad 1 mL

The solution is stored at 4 °C for one day.

DTNB solution

- DTNB   6 mM   4.8 mg
- Buffer A / B solution   ad 2 mL

The solution is freshly prepared in the dark.

Reaction mix (GSH Assay)

- DTNB solution   20 µL
- Buffer A / B solution   ad 190 µL

The staining solution is freshly prepared in the dark.

NaOH stock solution (for NAD⁺ cycling assay)

- NaOH (pellets)   1 M   20 g
- H_2O_{dest} ad 500 mL

NaOH is dissolved on ice and stored at RT.

Bicine solution

- Bicine   0.1 M   1.63 g
- H_2O_{dest} ad 100 mL

The solution is stored at 4 °C.

Phosphate Buffer

- KH_2PO_4 42.3 mM   5.75 g
- K_2HPO_4 25.8 mM   4.49 g
- H_2O_{dest} ad 100 mL

The pH is adjusted to 7.5 with KOH. The buffer is stored at 4 °C.

PES solution

- PES   40 mM   130 mg
- H_2O_{dest} ad 10 mL

The solution is stored at 4 °C in the dark.

ADH solution

- ADH   1 mg / mL   10 mg
- Bicine solution (0.1 M)   ad 1 mL

Aliquots of the solution are stored at -20 °C.

Diluent (for NAD$^+$ cycling assay)

- H_3PO_4 0.25 M   720 µL
- NaOH (1 M)   0.5 M   25 mL
- H_2O_{dest} ad 24.28 mL

The solution is stored at 4 °C.

NAD$^+$ stock solution

- NAD$^+$ solution (50 mM)   1 mM   200 µL
- Diluent (for NAD$^+$ assay)   ad 10 mL

Aliquots of the solution are stored at -80 °C and are thawed once.

MTT stock solution (for NAD⁺ cycling assay)

- MTT   4.14 mg / mL   50 mg
- H_2O_{dest} ad 12.07 mL

The solution is stored at 4 °C in the dark.

Premix (for NAD⁺ cycling assay)

- Bicine   480.5 mM   3.92 g
- EDTA   25.7 mM   375 mg
- BSA   4 mg / mL   200 mg
- EtOH   14 % (v/v)   7 mL
- MTT stock (4.14 mg / mL)   10 mL
- H_2O_{dest} ad 50 mL

Bicine is dissolved in H_2O_{dest} prior to pH adjustment (8.0) with NaOH. The solution is stored at 4 °C in the dark.

Reaction mix (for NAD⁺ cycling assay)

- Premix   35.7 µL
- PES solution (40 mM)   7.1 µL
- ADH solution (1 mg/mL)   7.1 µL

The Reaction mix is freshly prepared one ice. The volume (50 µL) is suitable for one sample (10 µL) within the NAD⁺ cycling assay.

Passive Lysis Buffer (1x)

- Passive Lysis Buffer (5x)   1x   10 mL
- H_2O_{dest} ad 50 mL

The solution is stored at 4 °C.

2.5.4 (Immuno)cytochemistry and Laser Scanning Microscopy

HCl solution (for cover slips)

- HCl   1 M   7.3 g
- H_2O_{dest} ad 200 mL

The solution is stored at RT.

PFA fixative

- PFA   4 % (w/v)   2 mL
- 1x PBS (unsterile)   ad 50 mL

PFA is dissolved at 60 °C for 30 min while stirring. Aliquots of the fixative are stored at -20 °C.

Methanol / acetone fixative

- Methanol   70 % (v/v)   140 mL
- Acetone   30 % (v/v)   60 mL

The fixative is stored at -20 °C.

Triton X-100 solution (for permeabilization)

- Triton X-100   0.5 % (v/v)   0.5 mL
- 1x PBS (unsterile)   ad 50 mL

The solution is stored at 4 °C.

Triton X-100 solution (for antibody dilution)

- Triton X-100   0.25 % (v/v)   0.25 mL
- 1x PBS (unsterile)   ad 10 mL

The solution is stored at 4 °C.

NGS blocking solution

- NGS   10 % (v/v)   5 mL
- Triton X-100   0.5 % (v/v)   125 µL
- 1x PBS (unsterile)   ad 50 mL

The solution is stored at 4 °C.

PBS "high salt"

- NaCl   0.4 M   2.3 g
- 1x PBS (unsterile)   ad 100 mL

The solution is stored at 4 °C.

PBS / BSA solution

- BSA   3 % (w/v)   3 g
- 1x PBS (unsterile)   ad 100 mL

The solution is stored at 4 °C.

To-Pro-3 stock solution (100x)

- To-Pro-3 iodide (1 mM)   100 µM   1 mL
- 1x PBS (unsterile)   ad 10 mL

Aliquots of the stock solution are stored at -20 °C in the dark.

To-Pro-3 staining solution

- To-Pro-3 stock (100x)   1 µM   0.1 µL
- 1x PBS (unsterile)   ad 10 µL

The solution is freshly prepared in the dark. The volume is sufficient to stain max. ~ 6 x 10^4 cells.

SYTOX blue stock solution (100x)

- SYTOX blue (5 mM)   100 µM   250 µL
- 1x PBS (unsterile)   ad 5 mL

Aliquots of the stock solution are stored at -20 °C in the dark.

SYTOX blue staining solution

- SYTOX blue (100x)   1 µM   0.1 µL
- 1x PBS (unsterile)   ad 10 µL

The solution is freshly prepared in the dark. The volume is sufficient to stain max. ~ 6 x 10^4 cells.

Components of other staining solutions and buffers, e.g. AnnexinV-FITC staining solution used for laser scanning microscopy, can be found in section 2.5.2 and 2.5.5.

2.5.5 Protein analysis

Tris buffer (20 mM, pH 7.4)

- Tris   20 mM   1.21 g
- H_2O_{dest} ad 500 mL

The pH is adjusted to 7.4 with HCl. The solution is stored at 4 °C.

Tris buffer (1 M, pH 6.8)

- Tris   1 M   12.1 g
- H_2O_{dest} ad 100 mL

The pH is adjusted to 6.8 with HCl. The solution is stored at 4 °C.

Tris buffer (1.5 M, pH 8.8)

- Tris   1.5 M   181.5 g
- H_2O_{dest} ad 1 L

The pH is adjusted to 8.8. The solution is stored at 4 °C.

SDS solution (10 %)

- SDS   10 % (w/v)   20 g
- H_2O_{dest} ad 100 mL

SDS is dissolved while slowly stirring. Fast SDS dissolution is achieved by heating to 65 °C. The solution is stored at RT.

SDS solution (20 %)

- SDS   20 % (w/v)   20 g
- H_2O_{dest} ad 100 mL

SDS is dissolved while slowly stirring. Fast SDS dissolution is achieved by heating to 65 °C. The solution is stored at RT.

DTT solution (1 M)

- DTT   1 M   1.54 g
- H_2O_{dest} ad 10 mL

Aliquots of the solution are stored at -20 °C. After thawing at 37 °C, DTT is again dissolved by vortexing.

Laemmli buffer (2x)

- Tris (1 M, pH 6.8)   120 mM   6 mL
- SDS solution (20 %)   10 % (v/v)   25 mL
- Sucrose   200 mg / mL   10 g
- H_2O_{dest} ad 50 mL
- qs bromphenol blue

The solution is sterile-filtrated and stored at RT.

Laemmli buffer (1x, reducing)

- Laemmli buffer (2x)   50 % (v/v)   500 µL
- DTT solution (1 M)   10 % (v/v)   100 µL
- H_2O_{dest} ad 1 mL

The solution is freshly prepared prior to use.

NaOH solution (0.1 M)

- NaOH (1 M)   0.1 M   5 mL
- H_2O_{dest} ad 50 mL

The solution is stored at RT.

BSA stock solution

- BSA   1 mg / mL   20 mg
- H_2O_{dest} ad 20 mL

BSA is dissolved by vortexing. Aliquots of the solution are stored at -20 °C.

Solution A (for BCA assay)

- BCA   29 mM   5 g
- Sodium tartrate   8.24 mM   0.8 g
- NaOH   100 mM   2 g
- Na_2CO_3 188 mM   10 g
- $NaHCO_3$ 113 mM   4.75 g
- H_2O_{dest} ad 500 mL

After pH adjustment to 11.25, the solution is stored at 4 °C.

Solution B (for BCA assay)

- $CuSO_4 \cdot 5\ H_2O$ 4 % (w/v)   4 g
- H_2O_{dest} ad 100 mL

The solution is stored at 4 °C.

BCA test solution

- Solution A   100 parts   1 mL
- Solution B   2 parts   20 µL

The solution is freshly prepared prior to use and sufficient for one protein sample within the BCA assay.

APS stock solution

- APS   10 % (w/v)   100 mg
- H_2O_{dest} ad 1 mL

Aliquots of the solution are stored at -20 °C.

SDS-PAGE gel formulations

1 gel	Separating gel				Stacking gel	
	7.5 %	**10 %**	**12.5 %**	**15 %**	**4 %**	
Rotiphorese® Gel A	1.5 mL	1.9 mL	2.5 mL	2.9 mL	Rotiphorese® Gel A	412.5 µL
Rotiphorese® Gel B	600 µL	800 µL	1 mL	1.2 mL	Rotiphorese® Gel B	170 µL
H_2O_{dest}	2.9 mL	2.3 mL	1 mL	350 µL	H_2O_{dest}	1.6 mL
Tris (1.5 M, pH 8.8)	1.5 mL				Tris (1 M, pH 6.8)	312.5 µL
SDS (20 %)	60 µL				SDS (20 %)	25 µL
APS (10 %)	30 µL				APS (10 %)	12.5 µL
TEMED	5 µL				TEMED	2.5 µL

2 gel	Separating gel				Stacking gel	
	7.5 %	**10 %**	**12.5 %**	**15 %**	**4 %**	
Rotiphorese® Gel A	3 mL	3.8 mL	4.9 mL	5.8 mL	Rotiphorese® Gel A	825 µL
Rotiphorese® Gel B	1.2 mL	1.6 mL	2 mL	2.4 mL	Rotiphorese® Gel B	340 µL
H_2O_{dest}	5.8 mL	4.6 mL	2 mL	700 µL	H_2O_{dest}	3.2 mL
Tris (1.5 M, pH 8.8)	3 mL				Tris (1 M, pH 6.8)	625 µL
SDS (20 %)	120 µL				SDS (20 %)	50 µL
APS (10 %)	60 µL				APS (10 %)	25 µL
TEMED	10 µL				TEMED	5 µL

3 gel	Separating gel				Stacking gel	
	7.5 %	**10 %**	**12.5 %**	**15 %**	**4 %**	
Rotiphorese® Gel A	4.5 mL	5.7 mL	7.4 mL	8.7 mL	Rotiphorese® Gel A	1.2375 mL
Rotiphorese® Gel B	1.8 mL	2.4 mL	3 mL	3.6 mL	Rotiphorese® Gel B	510 µL
H_2O_{dest}	8.7 mL	6.9 mL	3 mL	1.050 mL	H_2O_{dest}	4.8 mL
Tris (1.5 M, pH 8.8)	4.5 mL				Tris (1 M, pH 6.8)	937.5 µL
SDS (20 %)	180 µL				SDS (20 %)	75 µL
APS (10 %)	90 µL				APS (10 %)	37.5 µL
TEMED	15 µL				TEMED	7.5 µL

4 gel	Separating gel				Stacking gel	
	7.5 %	10 %	12.5 %	15 %	4 %	
Rotiphorese® Gel A	6 mL	7.6 mL	9.8 mL	11.6 mL	Rotiphorese ® Gel A	1.65 mL
Rotiphorese® Gel B	2.4 mL	3.2 mL	4 mL	4.8 mL	Rotiphorese ® Gel B	680 µL
H_2O_{dest}	11.6 mL	9.2 mL	4 mL	1.4 mL	H_2O_{dest}	6.4 mL
Tris (1.5 M, pH 8.8)	6 mL				Tris (1 M, pH 6.8)	1.25 mL
SDS (20 %)	240 µL				SDS (20 %)	100 µL
APS (10 %)	120 µL				APS (10 %)	50 µL
TEMED	20 µL				TEMED	10 µL

Solutions are freshly prepared. Gels are covered with H_2O_{dest}-soaked paper towels and stored in a sealed box at 4 °C.

Electrophoresis buffer (for SDS-PAGE)

- Glycine   1.44 % (w/v)   72 g
- Tris   24.76 mM   15 g
- SDS   0.125 % (w/v)   6.25 g
- H_2O_{dest} ad 5 L

The solution is stored at 4 °C and only used once for electrophoresis.

Blotting buffer (for SDS-PAGE)

- Glycine   0.3 % (w/v)   12.1 g
- Tris   118.75 mM   57.6 g
- Methanol   20 % (v/v)   800 mL
- H_2O_{dest} ad 4 L

The solution is stored at 4 °C and is reused several times for Western Blotting till voltage strength cannot be maintained anymore.

TBS (10x)

- Tris   29 mM   24 g
- NaCl   8.24 mM   80 g
- H_2O_{dest} ad 1L

After pH adjustment to 7.6, the solution is stored at 4 °C.

TBS/T

- TBS (10x) 1x 100 mL
- Tween 20 0.1 % (v/v) 1 mL
- H_2O_{dest} ad 1L

Tween 20 is slowly dissolved upon stirring. The solution is stored at 4 °C.

ECL solution

- LumiGLO®, Reagent A (20x) 1x 400 µL
- Peroxide, Reagent B (20x) 1x 400 µL
- H_2O_{dest} ad 8 mL

Components of the ECL solution are quickly mixed prior to use in the dark.

Developer solution (for autoradiography)

- Developer 50 mL
- H_2O_{dest} 200 mL

The solution is stored at 4 °C in the dark.

Fixer solution (for autoradiography)

- Fixer 50 mL
- H_2O_{dest} 200 mL

The solution is stored at 4 °C in the dark.

2.5.6 DNA damage analysis

NaOH stock solution (10 M)

- NaOH pellets 10 M 584.4 g
- H_2O_{dest} ad 1L

NaOH pellets are slowly dissolved on ice upon stirring. The solution is stored at 4 °C up to several weeks.

EDTA stock solution (100 mM)

- EDTA   100 mM   14.6 g
- H_2O_{dest} ad 500 mL

The solution is stored at RT.

Agarose solution (for slide coating)

- StarPureAgarose   1.5 % (w/v)   1.5 g
- H_2O_{dest} 100 mL

Agarose is slowly dissolved by heating of the solution in a microwave. Cooled agarose solution is stored at 4 °C.

LMP agarose solution (for sample application)

- LMP Agarose   0.5 % (w/v)   50 mg
- H_2O_{dest} 10 mL

Agarose is slowly dissolved by heating of the solution in a microwave. The solution is kept at 37 °C till usage.

Lysis buffer (for alkaline comet assay)

- NaCl   2.5 M   146.1 g
- EDTA   100 mM   37.2 g
- Tris   10 mM   1.2 g
- H_2O_{dest} ad 1L

After pH adjustment to 10 with NaOH, the buffer is stored at 4 °C. 1 % (v/v) Triton X-100 is added upon slow stirring and the buffer is pre-chilled prior to use.

Lysis buffer (for neutral comet assay)

- NaCl   2.5 M   146.1 g
- EDTA   100 mM   37.2 g
- Tris   10 mM   1.2 g
- H_2O_{dest} ad 1L

After pH adjustment to 7.5, the buffer is stored at 4 °C. 1 % (v/v) Triton X-100 is added upon slow stirring and the buffer is pre-chilled prior to use.

Electrophoresis buffer (for alkaline comet assay)

- NaOH (10 M)   300 mM   150 mL
- EDTA (100 mM)   1 mM   50 mL
- H_2O_{dest} ad 5 L

The buffer can be stored at 4 °C for several weeks. Prior to usage for electrophoresis, the pH ($\geq$ 13) of the buffer is controlled.

Electrophoresis buffer (for neutral comet assay)

- Tris   90 mM   54.5 g
- Boric acid   90 mM   27.8 g
- EDTA (100 mM)   2 mM   2.9 g
- H_2O_{dest} ad 5 L

The buffer can be stored at 4 °C for several weeks. Prior to usage for electrophoresis, a neutral pH of the buffer is controlled.

Neutralisation buffer

- Tris   0.4 M   48.5 g
- H_2O_{dest} 2 L

The solution is stored at RT.

PI staining solution (for comet assays)

- PI   20 µg / mL   1 g
- H_2O_{dest} 50 mL

The solution is stored at 4 °C in the dark.

2.6 Cell lines

2.6.1 Murine parental cell lines

NIH3T3 (origin: own laboratory)

Spontaneously, immortalized NIH (National Institutes of Health) 3T3 cells were isolated from *Mus musculus f. domestica* ("Swiss mouse") embryos and cultivated according to the "3T3" protocol (Todaro and Green, 1963). These non-transformed, adherent mouse embryonic fibroblasts represent a well-characterized model for cells underlying the mechanism of contact inhibition (Heit et al., 2001; Küppers et al. 2010) and therefore display growth in monolayers. Furthermore, these fibroblasts are supposed to undergo different cell death modalities, such as apoptosis, as well as distinct mechanisms of regulated necrosis (Wenz et al., 2018). NIH3T3 cells express p53wt (wild type) protein, which can be induced by UV-C radiation and *t*-BuOOH exposure (see 4.2.2). For cultivation and maintenance see section 2.5.1 and 3.1.2.

NIH3T3* (origin: University Hospital Kiel)

Parental NIH3T3 cells of CRISPR/Cas9 RIPK1 and RIPK3 knockout cell clones were kindly provided by Prof. Dr. Stefan Krautwald (University Hospital Schleswig-Holstein, Kiel, Germany). These immortalized, adherent murine fibroblasts are supposed to show the same characteristics as mentioned for NIH3T3 cells above. Usage of this cell line for experimental analysis is designated (*). For cultivation and maintenance see section 2.5.1 and 3.1.2.

Swiss3T3

Swiss3T3 cells were kindly provided by Dr. Albert Braeuning (Toxicology Tübingen, Germany). These immortalized, adherent mouse embryonic fibroblasts grow in monolayers with proliferation controlled via contact inhibition (Volwerk et al., 1992) and express p53wt protein, which is inducible by UV-C radiation (see 4.2.2). For cultivation and maintenance see section 2.5.1 and 3.1.2.

MEF p53wt (origin: own laboratory)

MEF (Mouse embryonic fibroblasts) cells were kindly provided by Prof. Dr. Angel Nebreda (IRB Barcelona, Spain). These immortalized, adherent murine fibroblasts grow in monolayers and underlie the mechanism of contact inhibition (Faust et al., 2005). Moreover, this fibroblast cell line potentially undergoes necroptosis (Sosna et al., 2014; Wenz et al., 2018). MEF cells express p53wt protein, which can be induced by UV-C radiation (see 4.2.2). For cultivation and maintenance see section 2.5.1 and 3.1.2.

MEF p53wt* (origin: M. Christmann, Toxicology Mainz)

MEF p53wt cells were kindly provided by Prof. Dr. Markus Christmann (Toxicology Mainz, Germany). These immortalized, adherent murine fibroblasts were isolated from p53wt littermates, simultaneously to isolation of fibroblasts from p53$^{-/-}$ mice for comparison (Lackinger et al., 2001). These fibroblasts are supposed to show the same characteristics as mentioned above for NIH3T3 and Swiss3T3 fibroblasts. Usage of this cell line for experimental analysis is designated (*). For cultivation and maintenance see section 2.5.1 and 3.1.2.

2.6.2 Murine transgenic cell lines

NIH3T3 RIPK1$^{-/-}$, NIH3T3 RIPK3 $^{-/-}$

Stable NIH3T3 RIPK1 and RIPK3 knockout cell clones, generated by the CRISPR/Cas9 method (Wenz et al., 2018), were kindly provided by Prof. Dr. Stefan Krautwald (University Hospital Schleswig-Holstein, Kiel, Germany). Immortalized, adherent NIH3T3 RIPK1$^{-/-}$ cells can undergo RIPK3-dependent necroptosis, whereby necroptosis is completely abolished in NIH3T3 RIPK3$^{-/-}$ cell clones (Galluzzi et al., 2012). For cultivation and maintenance see section 2.5.1 and 3.1.2.

MEF p53$^{-/-}$

Immortalized, adherent MEF cells isolated from p53 knockout littermates for comparison with MEF p53wt* cells (Lackinger et al., 2001). For cultivation and maintenance see section 2.5.1 and 3.1.2.

2.6.3 Human cell lines

FH109

FH109 cells are human, embryonic lung fibroblasts that are not immortalized. Despite their limited potential for cell divisions, these adherent cells underlie the mechanism of contact inhibition (Dietrich et al., 1997). FH109 cells express p53wt protein at a very low level, which can be induced by UV-C radiation (see 4.2.2). To prevent signs of cell aging, FH109 fibroblasts are cultivated only at low passages (5-11). For further information about cultivation and maintenance see section 2.5.1 and 3.1.2.

EA.hy926

Immortalized, adherent human endothelial cells from line EA.hy926 were kindly provided by Dr. Sven Horke (Pharmacology Mainz, Germany). Proliferation in EA.hy926 cells is controlled via contact inhibition and EA.hy926 cells express p53wt protein (Edgell et al., 1983; Steinkamp-Fenske, 2007; Upreti et al., 2010). For cultivation and maintenance see section 2.5.1 and 3.1.2.

HaCaT

Human, epithelial keratinocytes from line HaCaT are kindly provided by Dr. Norbert Fusenig (German Cancer Research Center Heidelberg, Germany). Proliferation in immortalized, adherent HaCaT cells is controlled via contact inhibition with the full potential of these cells for differentiation (Boukamp et al., 1988; Dietrich et al., 2001). HaCaT cells express a mutant variant of the p53 protein, displaying partial loss of function but still being inducible via p63-guided interactions (see 4.2.2; Neilsen et al., 2011). For cultivation and maintenance see section 2.5.1 and 3.1.2.

Caco-2

Human, epithelial colon carcinoma cells from line Caco-2 (sold from Cell Line Service, Heidelberg, Germany) are originally derived from a colorectal adeno-carcinoma of a Caucasian, 72 year-old man. Despite their tumorigenic characteristics, proliferation in immortalized, adherent Caco-2 cells is controlled via contact inhibition and cells have the potential for differentiation (Abraham et al., 1998; Buhrke et al., 2011). Caco-2 cells do not express p53 protein due to a p53 null

mutation (see 4.2.2; Djelloul et al., 1997; Liu and Bodmer, 2005). For cultivation and maintenance see section 2.5.1 and 3.1.2.

2.7 Kits

Click-iT® EdU Imaging Kit   Thermofisher Scientific, Waltham, MA, USA
(Alexa Fluor 555, Alexa Fluor 647)

ATP Determination Kit (A22066)   Thermofisher Scientific, Waltham, MA, USA

2.8 Software

Ascent Software 2.6	Thermofisher Scientific, Waltham, MA, USA
CellQuest Pro	BD Pharmingen, Heidelberg, Germany
EndNote	Thomson Reuters, New York City, NY, USA
FACSDiva Software 7.0	BD Pharmingen, Heidelberg, Germany
Flowing software	Turku Centre for Biotechnology, Finland
Graph Pad Prism Version 6	Graph Pad Software, La Jolla, CA, USA
ImageJ Software	Rasband, W.S., ImageJ, U.S. National Institutes of Health, Bethesda, USA
Komet 4.20.2	Kinetic Imaging, Liverpool, UK
MS Office 2007	Microsoft, Unterschleißheim, Germany
WinMDI 2.8, 2.9	Joseph Trotter; Scripps Research Institut, La Jolla, CA, USA
ZEN 2011	Carl Zeiss, Oberkochen, Germany

3 Methods

3.1 Mammalian cell culture for maintenance

3.1.1 General Remarks

Working steps with mammalian cell culture are performed under sterile conditions. The risk of contamination is reduced by conductance of cell culture under a laminar flow, careful hand disinfection with 70 % (v/v) EtOH and use of heat-stable solutions, glass wares, pipette tips and reaction tubes that are autoclaved prior to application. Heat-sensitive solutions are sterile filtrated. Solutions and culture medium are pre-warmed to 37 °C before use. Contamination of cell cultures is controlled via regularly microscopic evaluation and the pH indicator phenol red as marker for bacteria-induced acidification of the medium. Mycoplasma tests are conducted on a regular basis (every 4 - 6 weeks). All cell lines that are used in the context of this work are tested negative for mycoplasma.

3.1.2 Sub-cultivation for cell maintenance

Cells are cultivated in an appropriate culture medium (see 2.5.1) in an incubator under humidified conditions (37 °C and 5 % CO_2). Sub-cultivation of cells is performed every 3 - 4 days before > 90 % of cells reach confluence in order to avoid inhibition of cell growth via contact inhibition. For sub-cultivation, the medium is carefully aspirated with help of a Pasteur capillary pipette followed by washing with 1x PBS. Trypsin, diluted in PBS / EDTA (see 2.5.1), is added in amounts just covering the cells as a thin layer followed by incubation for 3 - 5 min at 37 °C. After microscopic evaluation of cell detachment, trypsin reaction is terminated by addition of FBS-containing medium and the cells are singularized via pipetting them several times up and down. In order to loosen tight, Ca^{2+}-dependent intercellular contacts, human keratinocytes (HaCaT) are pre-incubated for ~ 10 - 15 min with PBS / EDTA (see 2.5.1) prior to trypsin treatment. After trypsinization, parts of the cell suspension are transferred to medium-filled, new culture dishes for cell maintenance. To reach 80 - 90 % cell confluence within 3 - 4 days, two splitting ratios per cell line were applied as follows:

Splitting ratios for 3 - 4 days of cell maintenance

Cell line	Ratio (cell suspension : fresh medium)
NIH3T3	1:30 and 1:40
NIH3T3 RIPK1$^{-/-}$	1:10 and 1:20
NIH3T3 RIPK3$^{-/-}$	1:5 and 1:10
MEF p53wt	1:10 and 1:20
MEF p53$^{-/-}$	1:10 and 1:20
Swiss3T3	1:30 and 1:40
FH109	1:10 and 1:20
EA.hy926	1:10 and 1:20
HaCaT	1:5 and 1:10
Caco-2	1:5 and 1:10

3.1.3 Cell counting and Trypan Blue exclusion

To plate cells at the desired density for experimental analysis, the number of vital cells in suspension is determined with help of a Neubauer counting chamber after trypsinization (see 3.1.2). Vital cells are identified by exclusion of Trypan Blue – a dye which marks only dead cells by overcoming the damaged plasma membrane (Adan et al., 2016). 50 µL of the cell suspension are briefly mixed (1:1) with the Trypan Blue staining solution (see 2.5.1). Subsequent to staining, 10 - 20 µL of the cell suspension are applied to each chamber of the hemocytometer. Under the light microscope, vital cells are counted in at least 4 large squares per chamber. The mean cell number of two chambers is calculated as follows:

- *Chamber factor* for cell number / mL: Volume of 4 squares per chamber = 4 x (chamber area x depth) = 4 x ((edge length^2) x depth) = 4 x ((1 mm^2) x 0.1 mm) = 0.4 mm^3 = 0.4 µL $\rightarrow$ 0.4 µL x 2500 = 1 mL $\rightarrow$ Chamber factor = 2500

- *Trypan Blue dilution factor*: 2

- *Mean cell number / mL*: mean (cell number of chamber 1: cell number of chamber 2) = mean ((cell number of 4 squares chamber 1) x 2 x 2500):(cell number 4 squares chamber 2) x 2 x 2500))

3.1.4 Freezing and thawing

Cells are frozen at a confluence of 80 - 90 % to secure availability of cells from low passages by long-term storage. After trypsinization (see 3.1.2), cells are pelletized by centrifugation (5 min, 800 rpm, RT). The supernatant is carefully aspirated with a Pasteur capillary pipette and subsequently, cells are resuspended in a mixture of 90 % (v/v) FBS and 10 % (v/v) DMSO. 1 - 1.5 mL aliquots (containing 1 - 1.25 x 10^6 cells) of the cell suspension are transferred to pre-chilled cryo tubes. Cells are kept o/n at -80 °C and are finally stored in liquid nitrogen.

Cells are thawed at room temperature by repeated application of 500 µL pre-warmed, appropriate medium (see 2.5.1) followed by transfer of the cell suspension to the residual, total medium volume of 35 - 40 mL for fast DMSO dilution. Cells are pelletized by centrifugation (5 min, 800 rpm, RT) and the supernatant is carefully aspirated. Cells are resuspended in an appropriate medium volume according to the culture dish size. In order to favor cell attachment and cell proliferation during 24 h after thawing, the FBS concentration can be increased from 10 % (v/v) to 15 % (v/v). The following day, the medium is changed and if necessary the cells are washed with PBS to remove dead cells and debris.

3.2 Cell cultivation models for *t*-BuOOH exposure

3.2.1 Cell seeding and cultivation: experimental setup I

To analyze the influence of cell-cell contacts on the sensitivity of mammalian cells to *t*-BuOOH independent of a G1 cell cycle arrest, the following procedures for seeding and cultivation of confluent and semiconfluent cultures are applied according to experimental setup I. Confluent (confl.) cultures are seeded below their saturation density to avoid quiescence. Besides semiconfluent, proliferating (prol.) cultures, semiconfluent serum-depleted (sd) cells are included. Upon the following conditions, serum-depleted cultures show a comparable amount of cells in the G1 cell cycle phase as confluent cultures at the time point of *t*-BuOOH exposure, what is examined by cell cycle analysis (see Appendix I, Table 1). For each cell line, a minimal FBS concentration is determined, being sufficient to induce a cell cycle distribution with 60 - 75 % of cells in G1, but not intensively (< 25 %) causing apoptosis.

Experimental setup I

Cell population	Cell number for seeding [1]	Cultivation prior to t-BuOOH exposure [2]
confluent (confl.)	1.4×10^5 cells / cm^2	24 h cultivation medium with 10 % FBS
semiconfluent, proliferating (prol.)	5×10^3 cells / cm^2	24 h cultivation medium with 10 % FBS
semiconfluent, serum-depleted (sd)	5×10^3 cells / cm^2	1. Seeding in: cultivation medium with 10 % FBS 2. After cell attachment: 2x PBS washing + 48 h cultivation medium with low FBS concentration [3]

[1] exception for HaCaT cells: prol., sd = 8×10^3 cells / cm^2; exception for Caco-2 cells: confl. = 1.4×10^4 cells / cm^2, prol., sd = 2.5×10^3 cells / cm^2. Exceptions are made due to different cell sizes. In order to reach an equal (semi)confluence among different cell lines, the plated cell number is adapted.

[2] exception for cultivation of Caco-2 cells after seeding: confl., prol. = 48 h cultivation; sd = 72 h cultivation (24 h cell attachment + 48 h serum depletion). The exception is made due to longer duration of cell attachment.

[3] NIH3T3 / Swiss3T3 / FH109 / HaCaT = 0.1 % FBS; Caco-2 = 0.2 % FBS; MEF p53wt = 0.5 % FBS.

In order to exclude side effects of serum depletion on the sensitivity of cells to t-BuOOH, semiconfluent NIH3T3 cells (5×10^3 cells / cm^2) are alternatively arrested by the presence of the chemical MEK1/2 inhibitor U0126. After cultivation of semiconfluent cultures in the presence of U0126 (50 µM, 24 h), NIH3T3 cells demonstrate a similar amount of cells in the G1 cell cycle phase as compared to confluent or serum-depleted cultures (see 4.1.1.1, Figure 8B).

3.2.2 Cell seeding and cultivation: experimental setup II

To exclude an increased detoxification of t-BuOOH in confluent versus semiconfluent cells due to a higher cell number that is seeded for confluent cultures upon setup I, seeding and cultivation is conducted via experimental setup II, being in accordance to the experimental model used by Bar and coworkers (2004).
The cell number which is required for plating semiconfluent, proliferating (prol.) cells is calculated according to setup I (see 3.2.1). After trypsinization (see 3.1.2), pelletized cells are resuspended in an appropriate medium volume to end up with a

cell suspension that contains the aforementioned, calculated cell number in 70 µl cultivation medium. This cell suspension is carefully applied to the culture dish, either by pipetting (i) a drop to a cover slip (sterilized with 100 % EtOH, washed with PBS and dried at 37 °C) that has been placed onto the bottom of the culture dish (6-well plate or Ø 6 cm culture dish) before, or (ii) the drop is directly transferred onto the culture dish. Incubation of the cell suspension drop for 3 - 4 h at 37 °C allows cell attachment and formation of a confluent cell drop area for t-BuOOH exposure. Subsequent, cells are gently covered with the whole amount of medium according to the size of the chosen culture dish. The cell drop is cultivated in a suitable medium (see 2.5.1) in the presence of 10 % FBS for 24 h (NIH3T3, HaCaT) or 48 h (Caco-2) prior to t-BuOOH treatment. Simultaneously, semiconfluent, proliferating (prol.) cells are plated with an equal cell number as the cell drop and are cultivated according to setup I (24 h in the presence of 10 % FBS) till t-BuOOH treatment.

3.3 Cell treatment

3.3.1 Treatment with t-BuOOH and H_2O_2

To induce oxidative stress, cells are treated with t-BuOOH or H_2O_2. Stock solutions are prepared according to 2.5.1. To treat cells with a desired concentration of t-BuOOH, the stock solution is diluted by direct application of t-BuOOH to the culture medium followed by incubation at 37 °C. The same applies with respect to treating cells with H_2O_2, except for the analysis of DNA damage via the Comet assay. Due to the rapid repair of DNA lesions that are induced by short-term H_2O_2 treatment (e.g. 5 min), cells are resuspended in cold PBS. Subsequent, the H_2O_2 stock solution is diluted to the desired concentration by application of the peroxide to the cell suspension and treatment is performed on ice.

3.3.2 Treatment with chemical inhibitors and other components

Cells are pretreated with chemical inhibitors for 30 - 60 min at 37 °C. Stock solutions of chemical inhibitors and other agents (see 2.5.1) are diluted to the desired concentration for treatment by direct application to the culture medium. Thereby, an appropriate solvent concentration for cell treatment (not cytotoxic: < 0.5 %) or solvent

controls are considered. Since DMSO has been yet described to act as a ROS scavenger (Franco et al., 2007), the influence of this solvent on *t*-BuOOH-induced cell death was evaluated in the context of this work. When applied like for most of the presented experiments at a concentration of 0.1 % (v/v), DMSO did entirely not influence *t*-BOOH-induced cell death in semiconfluent NIH3T3, HaCaT and Caco-2 cells (data not shown). Genotoxic, carcinogenic or teratogenic agents like MMS, cisplatin, FCCP or cycloheximide are handled with particular caution by wearing nitrile gloves, working on surfaces that are covered with aluminium foil, special disposal of expendable items are used, and if necessary, decontamination steps are performed according to the manufacturers' instruction.

3.3.3 UV-C and γ-irradiation

Cells are irradiated with a UV-C lamp in culture dishes with opened top lid under a laminar flow. The time required for the desired irradiation dose is calculated and stopped during exposure. For ionizing radiation, cells are seeded and cultivated in Ø 6 cm culture dishes and are γ-irradiated with a Cs-137 source. After UV-C or γ-irradiation, cells are incubated at 37 °C for the desired time period.

3.4 Gene silencing via lipid-mediated siRNA transfection

Expression of a specific gene can be artificially inhibited by transfecting cells with siRNA to induce RNA interference. For stable or transient gene silencing, transfection agents like Lipofectamine 2000 and HiPerfect are used, containing cationic lipids to bind negatively charged DNA and RNA. After liposome formation, neutral co-lipids mediate binding to the plasma membrane and final delivery of siRNA to the cytoplasm of transfected cells.

Transient inhibition of *RIPK1* gene expression is induced by transfecting RIP1 siRNA in NIH3T3 cells with help of Lipofectamine 2000, as well as in MEF cells upon usage of HiPerfect. Apart from the instructions given by the manufacturer, ~ 5000 cells / cm^2 (MEF) or ~ 7000 cells / cm^2 (NIH3T3) are seeded onto 6-well culture plates. Cells are cultivated for 24 h in antibiotic-free appropriate medium (see 2.5.1; 1.5 mL / well for Lipofectamine 2000, 2.5 mL / well for HiPerfect) to reach 60 - 70 %

semiconfluence for transfection. With regard to the transfection procedure, as well as the required volume of the transfection medium, experiments are performed in compliance with the manufacturer's instructions. NIH3T3 cells are transfected with 33 nM / 50 nM and 100 nM RIPK1 siRNA (see 2.3) for 24 h and 48 h upon usage of the double amount of Lipofectamine 2000 as recommended by the instructor. MEF cells are transfected with 33 nM and 100 nM RIPK1 siRNA for 24 h, 48 h and 72 h with a HiPerfect concentration used as given by the manufacturer's instructions. Transfection agents are removed not before 22 h. After siRNA transfection, cells are plated onto new culture dishes to reach 40 - 60 % semiconfluence within 48 h and 72 h for *t*-BuOOH exposure. Simultaneously to RIPK1 siRNA transfection, cells are treated solely with transfecting agents to exclude cytotoxic effects induced by Lipofectamine 2000 or HiPerfect. On the other hand, scramble control siRNA (see 2.3) is transfected in equivalent amounts as RIPK1 siRNA to control specific inhibition of gene expression.

3.5 Cytochemistry and Flow Cytometry

3.5.1 General Remarks

To quantitatively examine morphological and biochemical characteristics of cells, cytochemistry and flow cytometry are combined. Despite the original term FACS (Fluorescence Activated Cell Sorting) has it focus on cell sorting, the used FACS devices (FACS Calibur, FACS Canto II) allow to rapidly determine various properties of a given cell population via simultaneous usage of several fluorescent dyes with distinct emission spectra (without sorting). At the beginning of each measurement, the laser voltage is adapted to a defined fluorescence intensity for stained control cells, which is applied for samples of each experiment. With regard to the analysis of cytosolic ROS, the mitochondrial membrane potential ($\Delta\psi_m$) and cytosolic Ca^{2+}, unstained control cells are included to determine autofluorescence. Furthermore, gates are chosen in a way to clearly discriminate distinct cell populations of all samples within a single experiment without changing these data evaluation parameters. Within each sample, 10 000 cells are scored and evaluated with help of CellQuest Pro and WinMDI 2.9 for FACS Calibur or BD Diva Software and flowing software for FACS Canto II.

3.5.2 SubG1 / cell cycle analysis

Flow cytometric analysis of the DNA content is achieved by staining mammalian cells with the DNA-intercalating agent propidium iodide (PI) (Hudson et al., 1968; Darzynkiewicz et al., 2010). On the one hand, this method allows determination of the cell cycle status due to the proportional increase of PI fluorescence with the DNA content, which is doubled upon progression of DNA replication – starting with a diploid genome with two homologous chromosome sets per nucleus (= 2n2c) in the G1 cell cycle phase. This is followed by the synthesis of DNA (S phase) and finally ends up with a doubled chromosome set (= 2n4c) in the G2 cell cycle phase till completion of mitosis. On the other hand, the method roughly identifies apoptotic cells as Caspase-Activated DNAses cleave internucleosomal DNA, thereby producing DNA fragments with a length of 180 bp and generating a discrete peak in the PI histogram with a low fluorescence intensity prior to G1 (subG1) (Telford et al., 1992; Kajstura et al., 2007).

To analyze the subG1 cell fraction and therefore the cell viability in addition to the cell cycle status of a given sample (max. 3×10^6 cells), the culture medium, possibly containing dead cells or debris, is collected prior to trypsinization (see 3.1.2). Trypsinized cells are combined with the supernatant and cells are pelletized by centrifugation (10 min, 800 rpm, RT). The supernatant is discarded, followed by resuspending the cell pellet in PBS and transfer of the cell suspension to a FACS tube. After repeated centrifugation and removal of the supernatant, cells are fixed via application of 200 µL cold PBS and 2 mL ice-cold 70 % EtOH (-20 °C) upon vortexing. Subsequent to fixation (at least 30 min; storage up to 1 month) at -20 °C, cells are pelletized by centrifugation (7 min, 2000 rpm, 4 °C). The supernatant is discarded and cells are permeabilized for 15 min at 37 °C via application of PBS / 20 % (v/v) Tween 20 upon vortexing. For RNA digestion, conducted to prevent false positive PI staining, cells are incubated with 1 mL of RNAse-containing PI staining solution for subG1 analysis (see 2.5.2) for 30 min in the dark at RT. Subsequent to incubation, cells are pelletized again by centrifugation (7 min, 2000 rpm, RT). The supernatant is discarded, cells are resuspended in 800 µL PBS and stored on ice in the dark till FACS analysis is conducted. For subG1 / cell cycle analysis, PI fluorescence is excited by the blue-green laser (488 nM; filter: 630/22) and detected by the FL-2 channel.

3.5.3 Cell death analysis via AnnexinV-FITC / PI staining

Apoptotic and necrotic cell death can be roughly distinguished by staining of cells with the Ca^{2+}-dependent phospholipid binding protein AnnexinV, coupled to green-fluorescent Fluorescein isothiocyanate (FITC), and with the red-fluorescent DNA intercalator PI (Vermes et al., 1995). The method is based on binding of AnnexinV to the phospholipid phosphatidylserine (PS), which is mainly located to cytoplasmic sites of the plasma membrane upon physiological conditions. During early stages of apoptosis, PS translocates to the outer layer of the plasma membrane what enables AnnexinV binding. Necrotic cells are originally characterized by cellular membrane damage, which allows for uptake of cell-impermeable PI, whereby this dye can also enter late apoptotic cells due to an increased membrane permeability (Ormerod, 1998). Hence, the combination of AnnexinV-FITC and PI staining allows differentiation of the following cell populations: vital = FITC-/PI-, early apoptotic = FITC+/PI-, late apoptotic / necrotic = FITC+/PI+, cell debris = FITC-/PI+. Thereby, late apoptotic and necrotic cells can be distinguished by performance of kinetic studies with a closer look at the onset of cell death.

Prior to trypsinization (see 3.1.2), the culture medium, possibly containing dead cells, is collected. Trypsinized cells and the culture medium are combined and cells are pelletized by centrifugation (5 min, 800 rpm, RT). The supernatant is carefully aspirated with a Pasteur capillary and cells are resuspended in PBS to remove residual phenol red of the culture medium. Subsequent to repeated centrifugation, the supernatant is one again aspirated and cells (max. 3×10^6 cells) are resuspended in 50 µL of the AnnexinV-FITC staining solution (see 2.5.2). After incubating cells for 15 - 20 min in the dark at RT, 450 µL of the PI staining solution (see 2.5.2) are dropwise applied upon vortexing in the dark. Directly after PI application, cells are stored on ice till flow cytometric analysis is performed. AnnexinV-FITC and PI are excited by the blue-green laser (488 nm) via usage of a different filter and detector channel. AnnexinV-FITC: filter = 530/30, detector = FL-1; PI: filter = 630/22, detector = FL-3.

3.5.4 Analysis of cytosolic ROS via CM-H2DCFDA and DCFH-DA

Oxidative stress is quantitatively determined by flow cytometry via staining of mammalian cells with 2,7-dichlorodihydrofluorescein diacetate (DCFH-DA) or its chloromethyl derivate (CM-H2DCFDA). Besides a longer, intracellular retention of CM-H2DCFDA, both ROS indicators passively diffuse into cells, where they are modified by intracellular esterases to accumulate as non-fluorescent, cell membrane-impermeable metabolites in the cytosol. Furthermore, these esterase-modified dyes react with radical species generated upon oxidative stress and are converted upon fluorescence emission. Instead of specifically detecting single ROS species, both dyes are suitable as general probes for cytosolic radical oxygen speies and therefore detection of the redox state of a given cell upon oxidizing conditions (Hempel et al., 1999; Armstrong, 2010).

Shortly before cell staining (max. 3 x 10^6 cells), the stock solution of DCFH-DA or CM-H2DCFDA (see 2.5.2) are thawed at RT with every following working step being performed in the dark due to the high susceptibility of these dyes for photo-oxidation. Afterwards, stock solutions are diluted in a suitable volume of phenol red-free DMEM (without FBS and antibiotics) to reach the final working concentration of DCFH-DA and CM-H2DCFDA (see 2.5.2). Cells are washed with PBS followed by application of the staining solution (2 mL for Ø 6 cm culture dish) and incubation for 30 min at 37 °C in the dark. With regard to DCFH-DA, dye loading according to the above described procedure is alternatively possible after cell treatment. Subsequent to staining, cells are washed with PBS and cells are covered with phenol red-free DMEM (with FBS and antibiotics). After cell treatment, cells are trypsinized and are pelletized by centrifugation (5 min, 800 rpm, RT). The supernatant is carefully aspirated with a Pasteur capillary and cells are resuspended in 500 µL PBS subsequent to storage of samples on ice till FACS analysis is conducted. To detect autofluorescence, unstained control cells are included. The ROS indicators are excited with the blue-green laser (488 nm, filter: 525/10) and the increase of fluorescence upon oxidative stress is detected by the FL-1 channel as mean fluorescence relative to stained control cells.

3.5.5 Simultaneous analysis of the MMP ($\Delta\psi_m$) and necrosis via DiOC6 / PI staining

The green fluorescent dye DiOC6 (3,3'-dihexyloxacarbocyanine iodide) served as marker for the mitochondrial membrane potential ($\Delta\psi_m$). This cationic molecule accumulates in mitochondria of intact cells in inverse proportion to $\Delta\psi_m$ according to the Nernst equation (Cottett-Rousselle et al., 2011). To analyze the relation between loss of $\Delta\psi_m$ and the onset of t-BuOOH-induced cell death, necrotic cells were simultaneously identified via red fluorescent PI staining. Furthermore, DiOC6 has been described to localize not only to mitochondrial structures but also to the endoplasmatic reticulum or nuclear envelope (Koning et al., 1993), as well as to indicate the plasma membrane potential ($\Delta\psi_p$) at higher dye concentrations (> 40 nM) (Rottenberg et al., 1998). Therefore, mitochondrial staining with DiOC6 was evaluated via laser scanning microscopy prior to flow cytometric analysis.

In the last few minutes of cell treatment, the stock solution of DiOC6 (see 2.5.2) is diluted in a suitable volume of phenol red-free DMEM (without FBS and antibiotics) in the dark to work with the final concentration of DiOC6 (see 2.5.2). The supernatant, possibly including dead cells, is collected and stored on ice. Adherent cells were washed with PBS and incubated with 2 mL (for max. 3 x 10^6 cells grown on a Ø 6 cm culture dish) of the DiOC6 staining solution for 20 min at 37 °C in the dark. After trypsinization (see 3.1.2), cells were pelletized together with the supernatant by centrifugation (5 min, 800 rpm, RT). The supernatant is carefully aspirated with a Pasteur capillary followed by dropwise addition of the PI staining solution upon vortexing at RT in the dark. The same concentration of PI is applied as used for AnnexinV-FITC / PI staining (see 2.5.2) and unstained control cells are examined to exclude autofluorescence. Samples are stored on ice until the analysis is performed by flow cytometry with the following parameters: DiOC6 excitation: blue-green laser (488 nm, filter: 530/30), DiOC6 detector: FL-1 channel; PI excitation: blue laser (488 nm, filter: 630/22), PI detector: FL-3 channel.

3.5.6 Analysis of cytosolic Ca^{2+} via Fluo-4 AM

Cytosolic calcium is detected by staining of cells with Fluo-4 AM followed by flow cytometric analysis. As a single-wavelength Ca^{2+} indicator Fluo-4 AM is suitable to analyze relative changes of the cytosolic Ca^{2+} level and is trapped in cells upon modification of the AM group via intracellular esterases (Paredes et al., 2008; Bootman et al., 2014).

Before cell treatment, the stock solution of Fluo-4 AM (see 2.5.2) is thawed in the dark at RT and diluted in an appropriate volume of phenol red-free DMEM (without FBS and antiobiotics) to achieve the final working concentration (see 2.5.2). Cells are washed with PBS and incubated with 2 mL of the Fluo-4 AM staining solution (for max. 3 x 10^6 cells grown on Ø 6 cm culture dish) for 30 min at 37 °C in the dark. Cells are once again washed with PBS and covered with phenol red-free DMEM (with FBS and antibiotics) before cell treatment occurred in the dark. Subsequently, cells are trypsinized (see 3.1.2), pelletized by centrifugation (5 min, 800 rpm, RT) and resuspended in 500 µL PBS. Samples are stored on ice in the dark until flow cytometric analysis is performed. Unstained control cells serve for determination of autofluorescence. Cytosolic Ca^{2+} is analyzed upon excitation of Fluo-4 AM by the blue-green laser (488 nm, filter: 530/30) and fluorescence is detected by the FL-1 channel as mean fluorescence relative to stained control cells.

3.6 Photometric functional assays

3.6.1 The MTT Assay as a measure of mitochondrial vitality

Originally developed to detect cell proliferation, as well as to identify drug-induced cytotoxicity, the MTT (3-(4,5-dimethylthiazol-2-yl)-2,5-diphenyltetrazolium bromide) assay can be further applied as a rough measure for mitochondrial vitality (Riss et al., 2016). This is due to the activity of intracellular dehydrogenases, comprising many key enzymes of the mitochondrial respiratory chain that catalyze the NADH-dependent reduction of yellow MTT to purple colored formazan crystals (Slater et al., 1963). The conversion of MTT can be photometrically assessed.

For high-throughput measurement, cells are seeded and cultivated in triplicates on 96-well culture plates according to the above described conditions for mammalian cell culture (see 3.1.2 and 3.2). To prevent proliferation-dependent

effects on formazan absorption, long-term treatment should be avoided. Moreover, cell treatment should be no longer performed as prior to drug-induced cell death for sole analysis of mitochondrial vitality. After cell treatment, the culture medium is poured away and the residual medium is removed by carefully knocking the culture plate on paper towels. Subsequently, 100 µL of the MTT staining solution (see 2.5.3) are applied to each 96-well including a triplicate of wells without seeded cells as negative controls. Cells are incubated for 3 h at 37 °C followed by removal of the staining solution from the 96-well plate as described before. Formazan crystals are dissolved by application of 120 µL HCl / Isopropyl alcohol solution (see 2.5.3) and incubation upon shaking (15 min, 500 rpm, RT). Formazan absorption is measured at 570 nm (reference wavelength: 650 nm) with a multiwell scanning spectrophotometer (ELISA reader) after 15 sec of shaking. For data evaluation, the background noise according to the mean absorption of the included negative controls is subtracted from each sample value.

3.6.2 Detection of the intracellular GSH content

Absorption measurement of the so-called Ellman's reagent (5,5'-dithiobis-2,5-nitrobenzoic acid, DTNB) allows to quantitatively analyze free thiol groups (Ellman, 1959). As glutathione (GSH) represents the most abundant non-protein thiol in most aerobic cells, the conversion of DTNB is a measure for the total amount of intracellular GSH (Meister & Tate, 1976; Riddles et al., 1979). Thereby, the reaction of DTNB and GSH generates a mixed disulfide and one equivalent of the dianion TNB^{2-} with the latter being photometrically quantified.

A similar number of confluent and semiconfluent cells is seeded for analysis in order to reduce assay-dependent deviations. Therefore, the size of the culture dishes (confluent: 24-well, semiconfluent: Ø 10cm) is accordingly selected. Subsequent to cell treatment, cells are trypsinized and pelletized by centrifugation (5 min, 2 000 rpm, 4 °C). The supernatant is discarded and cells are resuspended in 370 µL prechilled buffer A/B (see 2.5.3). 2 x 10 µL of each sample are collected for protein quantification via the Bradford assay (see 3.9.4). The residual cell suspension (350 µL) is mixed with 350 µL sulfocalicylic acid solution (10 %, see 2.5.3) upon vortexing followed by incubation for 15 min on ice. Afterwards, the suspension is centrifuged

(10 min, 14 000 rpm, 4 °C) before the thiol-containing supernatant is collected and transferred to a prechilled 1.5 mL reaction tube. By freezing samples in liquid nitrogen, the supernatant can be stored at -80 °C for several weeks before the thiol content is assessed. After storage, samples of the thiol-containing supernatant are carefully thawed on ice. 10 µL of each sample or of the GSH standards (0, 5, 25, 50, 100, 150, 200, 500 µM GSH in 5 % sulfosalicylic acid, see 2.5.3) are transferred in triplicates to a prechilled 96-well plate suitable for photometric analysis followed by application of 190 µL reaction mix (see 2.5.3) to each 96-well. After 5 min of incubation at RT, the absorption of TNB^{2-} is measured at 405 nm with an ELISA reader. With help of the GSH standards, as well as Bradford protein quantification, the intracellular GSH content (µM per mg protein) can be determined.

3.6.3 NAD$^+$ cycling assay

Determination of the intracellular NAD$^+$ level is conducted according to the NAD$^+$ cycling assay (Bernofsky and Swan, 1973). Upon oxidation of EtOH by the enzyme alcohol dehydrogenase (ADH), intracellular NAD$^+$ is reduced. In a second reaction step, NADH serves as driving force for MTT reduction mediated by phenazine ethosulfate (PES) as intermediate electron acceptor (Riss et al., 2016). The absorption of reduced MTT (formazan crystals) is photometrically assessed to quantify the intracellular availability of NAD$^+$.

To compare NAD$^+$ levels of confluent and semiconfluent cultures, additional cell cultures of each population are seeded in duplicates to determine the NAD$^+$ amount per cell via cell counting. Subsequent to treatment, cells are washed and afterwards covered with 250 µL prechilled PBS. 12 µL perchloric acid are added to the suspension followed by incubation for 15 min on ice. During incubation, additional cultures are trypsinized (see 3.1.2) and the number of vital cells is counted after Trypan Blue exclusion (see 3.1.3). After denaturation of proteins by perchloric acid, cells are scraped off from the culture dish and the suspension is centrifuged (10 min, 3800 rpm, 4 °C). 350 µL of the supernatant is transferred to a pre-chilled 1.5 mL reaction tube and 350 µL of cold phosphate buffer (see 2.5.3) are applied for $KClO_4$ precipitation. Subsequent to incubation for 15 min on ice, the solution is centrifuged (10 min, 3800 rpm, 4 °C). The NAD$^+$-containing supernatant is transferred to a pre-

chilled 1.5 mL reaction tube followed by storage at -20 °C (up to several weeks) till photometric analysis is conducted. After storage, samples are thawed on ice and again centrifuged (10 min, 3800 rpm, 4 °C) to remove residual $KClO_4$. The supernatant is transferred to a 1.5 mL reaction tube and stored on ice during preparation of the NAD^+ standards. The NAD^+ stock solution (1 mM) is diluted with the diluent for the NAD^+ cycling assay (see 2.5.3) to a concentration of 1 µM. Final NAD^+ standard concentrations are prepared on ice as follows:

Final NAD^+ standard concentration	Diluent (µL)	1 µM NAD^+ stock (µL)
0	400	0
0.01	396	4
0.02	392	8
0.04	384	16
0.08	368	32
0.12	352	48
0.24	304	96
0.48	208	192

100 µL of each NAD^+ standard concentration are transferred in triplicates to a pre-chilled 96-well plate suitable for photometric analysis. 10 µL of each sample are equally transferred in triplicates. Subsequently, 90 µL diluents (see 2.5.3) are applied to each 96-well of the NAD^+ standards and samples, respectively. The reaction mix, which contains EtOH, ADH, PES and MTT (see 2.5.3), is prepared in the dark and 50 µL are added to each 96-well. After incubation for 30 min at 37 °C in the dark, MTT absorbance is measured at 550 nm (reference wave length: 690 nm) with help of an ELISA reader.

3.7 Luciferase-mediated ATP detection

Intracellular ATP is detected upon the bioluminescent luciferase-luciferin reaction. In the presence of oxygen and ATP, the enzyme converts firefly-derived D-luciferin in a Mg^{2+}-dependent reaction to oxyluciferin. The conversion generates thereby a chemoluminescent signal, being proportional to the amount of intracellular ATP (Morciano et al., 2017).

Cells are seeded and cultivated on a 96-well culture plate according to the above described conditions for mammalian cell culture (see 3.1.2 and 3.2). Luciferase reaction is provided by an ATP determination kit (see 2.7) including ATP for preparation of standard solutions. The reaction solution and the ATP standard solutions are prepared according to the manufacturer's instructions. Subsequent to cell treatment, the culture medium is poured away and cells are washed with cold PBS upon usage of a beaker. After removal of PBS and carefully knocking the plate on paper towels, cells are lysed by application of 100 µL Passive Lysis Buffer (1x, see 2.5.3) to each 96-well. For release of intracellular ATP, cells are incubated for 10 - 20 min at 37 °C upon shaking. 10 µL of each sample or each ATP standard solution is transferred in triplicates to a 96-well plate, which is suitable for luminescence measurement. Subsequent to application of 90 µL reaction mix in the dark, the conversion of D-luciferin is detected by a luminometer.

3.8 (Immuno)cytochemistry and Laser Scanning Microscopy
3.8.1 General Remarks

The combination of (immuno)cytochemistry and confocal laser scanning microscopy enables detection of cellular characteristics, such as cell vitality, localization of nuclei, the MMP ($\Delta\psi_m$), and others. Besides usage of fluorophores, such as the DNA intercalator PI, distinct primary antibodies are used that specifically bind to a certain antigen via complementary-determining regions (Janeway et al., 2001). These primary antibodies are in turn recognized by specific secondary antibodies with each of them coupled to a distinct fluorophore. This technique provides the ability to simultaneously detect different marker proteins, e.g. γ-H2AX and MDC1 to identify DSBs (Stewart et al., 2003), through excitation of fluorophores at different wavelength. Fluorescence images are taken by the laser scanning microscope LSM710 according to the manufacturer's instructions. For detection of green fluorescence (e.g., FITC) the Argon laser (3 laser lines: 458 nm, 488 nm, 514 nm) is used. Orange fluorescence (e.g., Cy3) is detected by the DPSS laser with a laser line of 561 nm and far-red fluorescence (e.g., Alexa Fluor 647) by the HeNe laser with 633 nm. Due to so-called dual fluorescent dyes (e.g., PI) that can be excited at two wavelengths, respectively, the laser setting was chosen in a way to

avoid strong overlapping of fluorescence emission. In addition to qualitative microscopic analysis with the ZEN2009 software, the percentage of fluorescence-labelled cells (of 5-6 images, at least 15-20 per image) is quantitatively assessed by ImageJ software (e.g., for EdU). Alternatively, the mean fluorescence intensity (e.g., for γ-H2AX foci) is determined by usage of the "BIC Macro Toolkit" (https://www.bioimaging-center.uni-konstanz.de/image-analysis/bic-macro-toolkit/).

3.8.2 Preparation of sample slides

Before cell seeding, cover slips are sterilized by incubation for 20 min in diethyl ether. Subsequent, cover slips are washed in the following order with 100 % (v/v) EtOH, 70 % (v/v) EtOH and H_2O_{dest}. Afterwards, cover slips are washed with 1 M HCl for 20 min upon shaking followed by washing with H_2O_{dest} and storage in 70 % (v/v) EtOH at 4 °C. Subsequent to cell staining, cover slips are sealed with clean slides by application of a drop of mounting medium (~ 10 - 20 µL; with or without nucleic acid dye, see 3.8.3) onto clean slides and cover slips are transferred onto the slides and fixed with nail polish. For confocal microscopy, a drop of either Immersol™ 518 F (for 63x oil immersions objective) or Immersol™ W 2010 (for 40x water immersions objective upon usage of transmitted light) is placed in the centre of the sample slide for microscopic analysis. Afterwards, sample slides are carefully cleaned with rubbing alcohol and stored in the dark at 4 °C. Samples can be analyzed up to several weeks without the risk of fluorescence bleaching.

3.8.3 Nuclei counterstaining by To-Pro-3 and SYTOX Blue

To assign fluorescence signals of dyes and antibodies to individual cells, cell nuclei are counterstained with DNA-binding dyes such as To-Pro-3 or Sytox Blue. After staining cells directly with fluorophores or fluorophor-coupled antibodies, sample cover slips are either incubated with 1 mL To-Pro-3 staining solution or SYTOX Blue staining solution (see 2.5.4) for 15 min in the dark at RT prior to application of antifade medium and sealing of cover slips with clean slides. Alternatively, antifade medium can be supplemented with 1 µM of To-Pro-3 or SYTOX Blue (see 2.5.4). Subsequent, the solution is dropped onto clean slides and

cover slips are sealed as described before (see. 3.8.2). For presentation purposes, the red fluorescence of To-Pro-3 is illustrated blue colored.

3.8.4 Cell death analysis via AnnexinV-FITC / PI staining

In addition to quantitative cell death analysis by flow cytometry, apoptosis and necrosis can be qualitatively discriminated via AnnexinV-FITC / PI staining followed by confocal microscopic analysis.

Cells are seeded and cultivated on sterile cover slips in 6-well culture plates according to the above described conditions for mammalian cell culture (see 3.1.2 and 3.2). After treatment, cover slips are removed from the culture medium and covered with AnnexinV-FITC staining solution as described for flow cytometry (see 2.5.2). Subsequent, cells are washed with 1x Binding buffer (see 2.5.2) and incubated with the same concentration of PI as used for flow cytometry (see 2.5.2) for 5 min in the dark at RT. After incubation and repeated washing, cells are covered with the PFA fixative (see 2.5.4) for 15 min in the dark at RT. To remove PFA, cells are again carefully washed and covered by clean slides as already reported (see 3.8.2). For microscopic analysis a suitable laser and detector setup is chosen for the following parameters: AnnexinV-FITC excitation: 495 nm, emission: 519 nm; PI excitation: 356 nm or 535 nm, emission: 617 nm. To distinguish confluent and semiconfluent cells, confocal images are additionally taken upon transmitted light.

3.8.5 Determination of the proliferation rate via EdU incorporation

The amount of S phase cells in a given sample is determined by incorporation of the thymidine analog EdU (5-ethynyl-2'-deoxyuridine) and laser scanning microscopy. In this context, EdU is labeled with a fluorescent dye by a so-called click reaction, which covalently binds an alkyne (contained in EdU) to an azide (contained in dye) in the presence of copper ions (Breinbauer & Köhn, 2003).

Cells are seeded and cultivated on sterile cover slips in 6-well culture plates according to the above described conditions for mammalian cell culture (see 3.1.2 and 3.2). Afterwards, EdU incorporation is conducted according to the manufacturer's

instructions of the Click-iT$^®$ EdU Imaging Kit (Alexa Fluor 555, see 2.7). To-Pro-3 is used for counterstaining cell nuclei (see 3.8.3). To combine DSB marker staining (see 3.8.8), EdU incorporation is conducted up to working step 4.6 according to the manufacturer's protocol with the exception that samples are permeabilized and fixed with methanol / acetone solution (see 2.5.4) for 8 - 9 min at -20 °C. Afterwards, cover slips are washed three times with PBS for 5 min at RT prior to application of the Click-iT$^®$ reaction cocktail. Subsequent to working step 4.6, primary antibody incubation follows according to the staining procedure for DSB markers (see 3.8.8). Microscopic analysis of EdU fluorescence is performed according to the following parameters: EdU excitation: 555 nm, emission: 565 nm; To-Pro-3 excitation: 642 nm, emission: 661 nm. To calculate the proliferation rate of cells, EdU incorporation is quantitatively evaluated, whereby not only S phase cells are marked by this nucleoside analog but also cells with active DNA synthesis, e.g. related to DNA repair (Jia et al., 2015). Hence, additional proliferation markers have to be considered.

3.8.6 Analysis of the MMP ($\Delta\psi_m$) via MitoTracker Red CMXROS staining

Besides analysis of the mitochondrial membrane potential ($\Delta\psi_m$) in living cells by carbocyanine dyes such as DiOC6, aldehyde-fixed samples can be stained with the mitochondria-selective probe MitoTracker Red CMXROS – a dye accumulating in active mitochondria dependent on $\Delta\psi_m$ and being retained upon fixation. In this context, the loss of $\Delta\psi_m$ is proportional to the loss of MitoTracker Red fluorescence what can be detected by confocal laser scanning microscopy.

Cells are seeded and cultivated on sterile cover slips in 6-well culture plates according to the above described conditions for mammalian cell culture (see 3.1.2 and 3.2). Afterwards, MitoTracker staining is conducted according to the manufacturer's instructions for MitoTracker Mitochondrion-Selective Probes (MitoTracker Red CMXROS, see 2.2) with the following exceptions. Cells are stained with 250 nM MitoTracker Red CMXROS for 15 min in the dark at 37 °C. To fix cells, cover slips are incubated with 4 % (v/v) PFA diluted in culture medium (without FBS and antibiotics) for 15 min at 37 °C. After washing cells in PBS (3x, 5 min, RT), cells are permeabilized with ice-cold acetone (5 min, -20 °C) and rehydrated by washing with PBS once again. Subsequent to staining, cover slips are sealed as described

before (see 3.8.2). The following parameters are applied for confocal microscopic analysis: MitoTracker Red CMXROS excitation: 579 nm, emission: 599 nm. To assign mitotracker fluorescence to single cells, confocal images are additionally taken upon transmitted light.

3.8.7 Detection of PARP-1 activation

Induction of the DDR-related enzyme PARP-1 can be verified by detection of NAD^+ polymers that are attached by PARP-1 to single-stranded DNA. Polymers with a size of over 20 poly(ADP-ribose) (PAR) residues, so-called PAR foci, are detected by the antibody 10H, which has been generated in hybridoma cells (Kawamitsu et al., 1984; Fahrer et al., 2007). To visualize PARP-1 activation, anti-10H antibody is recognized by a secondary antibody, which is coupled to green fluorescent Alexa Fluor 488 for analysis via laser scanning microscopy.

Cells are seeded on sterile cover slips in 6-well culture plates according to the above described conditions for mammalian cell culture (see 3.1.2 and 3.2). Subsequent to treatment, cells are fixed in methanol (7 min, -20 °C). After washing with PBS (3x, 5 min, RT), cover slips are incubated with 5 % (w/v) milk powder, diluted in PBS / 0.1 % (v/v) Tween 20. Subsequent to incubation (30 min, RT), the primary antibody for PAR foci detection (anti-10H antibody, 1:300; see 2.4.1) is applied for 1 h at RT. Afterwards, cells are washed in PBS once again and are incubated with Alexa Fluor 488-labeled secondary antibody (1:400, see 2.4.2). Subsequent to incubation (1 h, RT, in the dark), cover slips are washed with PBS (3x, 5 min, RT). Prior to sealing of cover slips (see 3.8.2), nuclei are counterstained with To-Pro-3 (see 3.8.3). Confocal microscopic analysis is conducted upon the following parameters: Alexa Fluor 488 excitation: 491 nm, emission: 515 nm; To-Pro-3 excitation: 642 nm, emission: 661 nm.

3.8.8 Examination of DNA DSBs via γ-H2AX (/ MDC1) staining

First hints towards the induction of DNA DSBs are provided by the phosphorylation of the histone H2A (γ-H2AX). In this context, the co-localization of γ-H2AX and MDC1 – both coordinating the formation of DSB foci in order to stimulate their repair (Dickey et al., 2011) – can be applied as DSB marker. Upon binding of γ-H2AX and MDC1 by specific primary antibodies and detection of these antibodies by fluorescence-labeled (Alexa Fluor 488 and Cy3) secondary antibodies, the local phosphorylation of H2AX (γ-H2AX foci), as well as the co-localization of γ-H2AX and MDC1 foci are determined by laser scanning microscopy.

Cells are seeded and cultivated on sterile cover slips in 6-well culture plates according to the above described conditions for mammalian cell culture (see 3.1.2 and 3.2). Subsequent to treatment, cover slips are removed from the culture medium and are shortly rinsed with PBS. Cells are fixed with the methanol / acetone fixative (see 2.5.4). After fixation (8 - 9 min at -20 °C), cells are washed with PBS (3x, 5 min, RT) followed by blocking of cells with 10 % NGS in Triton X-100 solution (0.25 %, see 2.5.4) for 1 h at RT. The blocking agent is removed prior to incubation (o/n, 4 °C) with anti-γ-H2AX (S139) antibody (1:1000; 1:200 in combination with MDC1; see 2.4.1) and anti-MDC1 antibody (1:200; see 2.4.1), both diluted in Triton X-100 solution (0.25 %, see 2.5.4). After washing with PBS (3x, 5 min, RT), cells are incubated with Alexa Fluor 488- conjugated secondary antibody (1:400; see 2.4.2) and Cy3-conjugated secondary antibody (1:400; see 2.4.2), both diluted in Triton-X 100 solution (0.25 %; see 2.5.4). After incubation (1 h, RT), cells are again washed with PBS (3x, 5 min, RT). Prior to sealing of cover slips (3.8.2), cell nuclei are counterstained with To-Pro-3 or SYTOX Blue (see 3.8.3). Microscopic analysis is performed according to the following parameters: Alexa Fluor 488 excitation: 491 nm, emission: 515; Cy3 excitation: 512 or 532, emission: 565, 615; SYTOX Blue excitation: 431 nm, emission: 480 nm; To-Pro-3 excitation: 642 nm, emission: 661 nm.

3.9 Protein analysis

3.9.1 Generation of total cell extracts

Total cell extracts for Western Blot analysis are gained by application of hot Laemmli buffer (Laemmli, 1970). Besides inactivation of proteases due to heat-induced denaturation, the buffer contains reducing agents, such as DTT or β-mercapto-ethanol, to block formation of disulphide bonds that provide the basis for secondary and tertiary protein structures or dimer formation.

Shortly before use, a suitable volume (~ 1 mL per Ø 10 cm culture dish) of Laemmli buffer (1x, see 2.5.5) is mixed with DTT and heated to 95 °C. After cell treatment, the culture medium is aspirated and cells are washed with Tris buffer (20 mM; see 2.5.5) followed by application of hot Laemmli buffer (500 µL for Ø 6 cm culture dish; 1 mL for Ø 10 cm culture dish). After distributing the buffer over the whole culture dish with help of a cell scraper, the cell extract is transferred to a 1.5 mL reaction tube and again heated at 95 °C for 10 min. To collect evolved condensation water, samples are centrifuged (1 min, 14 000 rpm, RT) prior to protein concentration analysis (see 3.9.3) or stored at 4 °C up to several weeks. If samples are stored, cell extracts are shortly heated at 95 °C followed by quick centrifugation prior to further usage.

3.9.2 Chloroform-methanol precipitation

Chloroform-methanol precipitation of proteins is applied to concentrate protein dilutions and to clean up cell extracts for protein concentration analysis and Western Blotting. By a defined ratio of protein, water, chloroform and methanol, proteins accumulate at the interphase of both solvent groups with a top aqueous methanol layer, which contains, e.g. nucleic acids and carbohydrates, and a chloroform lipid-containing layer at the bottom of the reaction tube (Wessel & Flügge, 1983).

The desired amount of cell extract is diluted with H_2O_{dest} to a final volume of 100 µL (dilution to 200 µL if cell extract volume > 100 µL) within a 1.5 mL reaction tube. Afterwards, 100 µL chloroform, 400 µL methanol and 300 µL H_2O_{dest} (or rather 200 µL if cell extract volume > 100 µL) are applied and the solution is carefully mixed upon vortexing. Subsequent to centrifugation (3 min, 14 000 rpm, RT), the top

aqueous methanol layer is removed by a syringe without affecting the intermediate phase of the protein solution. 300 µL of methanol are applied to wash the protein pellet by gently tapping till precipitated proteins are dropped down to the bottom of the reaction tube. Methanol is carefully removed by a syringe after repeated centrifugation (5 min, 14 000 rpm, RT) and the protein pellet is air-dried. The protein pellet is dissolved, either in 50 µL 0.1 M NaOH for the BCA assay (see 2.5.5) or in a suitable amount (10-20 µL) of hot, reducing Laemmli buffer for SDS-PAGE (see 3.9.5) upon vortexing. Dissolved Protein pellets for SDS-PAGE can be stored at 4 °C up to several weeks.

3.9.3 BCA assay

In the same way as protein quantification via the Lowery method, but being more robust against interfering compounds (e.g., detergents), the BCA (bicinchoninic acid) assay is based on the conversion of Cu^{2+} to Cu^+ upon aqueous alkaline conditions (Buiret reaction). Binding of peptide bonds catalyzes the copper-driven color change of beige BCA to a purple-colored complex compound. The absorbance of this resulting compound can be photometrically assessed and the absolute protein concentration is determined with help of a protein standard (Smith et al., 1985).

Due to interference with the BCA assay, carbohydrates are initially removed from cell extracts (20 µL in duplicates per sample) via chloroform-methanol precipitation and protein samples are dissolved in NaOH (see 3.9.2). BSA protein standards are prepared in duplicates via dilution of the BSA stock solution (1 mg / mL, see 2.5.5) according to the following scheme:

	Protein concentration (mg / mL)	BSA stock (µL)	H_2O_{dest} (µL)
Blank sample	0	0	50 µL
Standard 1	0.005	5 µL	45 µL
Standard 2	0.01	10 µL	40 µL
Standard 3	0.025	25 µL	25 µL
Standard 4	0.5	50 µL	0

Till quantification, protein and standard samples are kept on ice and the BCA test solution (see 2.5.5) is freshly prepared. Afterwards, 1 mL of the BCA test solution is applied to each sample followed by incubation for 30 min at 37 °C. The Buiret reaction is terminated by cooling the samples on ice. Subsequent to calibration of the photometer with the blank sample, BCA conversion is photometrically quantified with an absorbance maximum at 562 nm. The sample protein concentration is calculated via linear regression according to the BSA standard curve.

3.9.4 Bradford assay

In the course of intracellular GSH detection (see 3.6.2), the protein concentration was assessed by the method according to Bradford (Bradford, 1976). The method is based on the fact that aromatic and non-polar residues of amino acids form a non-covalent bond between the red colored dye Coomassie Brilliant Blue G250 and proteins within a given sample. Upon dye binding, an absorbance shift is induced which finally results in a color change of the dye to a blue colored compound. The absorbance of this compound at 595 nm can be photometrically assessed and the absolute protein concentration is calculated via a protein standard. During preparation of BSA standards, cell extracts (10 µL in duplicates per sample) from the GSH assay are kept on ice. A suitable amount of a BSA stock solution (5 mg/mL in H_2O_{dest}) is freshly prepared and kept on ice. The BSA standards are prepared in duplicates via dilution of the stock solution (5 mg / mL) as follows:

	Protein concentration (mg / mL)	BSA stock (µL)	H_2O_{dest} (µL)
Blank sample	0	0	50 µL
Standard 1	1	10 µL	40 µL
Standard 2	2	20 µL	30 µL
Standard 3	3	30 µL	20 µL
Standard 4	4	40 µL	10 µL
Standard 5	5	50 µL	0

The protein standards are kept on ice during dilution of the Bradford dye concentrate (1:5 with H_2O_{dest}) shortly before use. 10 µL of each standard sample and protein sample from the GSH assay are transferred to a 96-well plate, being appropriate for photometric analysis. 90 µL of the Bradford reagent solution are applied to each sample and 100 µL to two further 96-wells to compensate for background noise. After incubation for 5 min in the dark at RT, the absorbance is measured at 595 nm with help of an ELISA reader. The sample protein concentration is calculated via linear regression according to the BSA standard curve.

3.9.5 Discontinuous SDS-PAGE

To separate proteins according to their molecular weight, polyacrylamide gel electrophoresis (PAGE) is conducted. PAGE technique discriminate proteins according to their molecular weight and not only according to their electrophoretic mobility due to different gel pore sizes (Davis et al., 1959; Smithies, 1959). By combined usage of sodium dodecyl sulfate (SDS), secondary and tertiary protein structures are denatured and a constant negative charge is conferred to proteins relative to their mass (Shapiro et al., 1967). To increase resolution of electrophoretic separation, discontinuous SDS-PAGE is performed with help of a multiphase (discontinuous) buffer system. Therefore, samples are concentrated within a stacking gel with a relatively low acrylamide concentration and large gel pores. Afterwards, proteins are separated in the running gel with relative small pore sizes due to higher polymer concentration. The molecular weight of separated proteins can be determined by a protein standard marker and their identity by subsequent performance of Western Blot analysis (see 3.9.6).

For preparation of acrylamide gels, glass plates (for SDS-PAGE) are cleaned with 70 % EtOH. Afterwards, glass plates are placed into the casting frames followed by transfer to the casting stands of the Mini PROTEAN tetra cell system. To control safe sealing at the bottom of the plates, a small volume of H_2O_{dest} is poured between the plates. Subsequent to removal of H_2O_{dest} with Whatman filter paper, the running gel for SDS-PAGE is prepared with TEMED and APS, being applied at last to start acrylamide polymerization (see 2.5.5). For good separation of proteins with a low molecular weight, a gel with a high acrylamide concentration is selected (e.g. 15 %

SDS-PAGE gel for γ-H2AX) and *vice versa*. After pouring the running gel between the plates followed by gel polymerization, the stacking gel is prepared accordingly (see 2.5.5) and the comb is finally placed between the two plates. Polymerized acrylamide gels should be stored at least o/n at 4 °C (see 2.5.5) for complete polymerization and more defined gel pockets. Prior to use for gel electrophoresis, the comb is carefully removed and the gel is placed into the Mini PROTEAN tetra cell electrode assembly (for 2 gels, otherwise add buffer dam; use companion running module for 4 gels) followed by transfer to the buffer tank. Subsequently, the inner chamber (anode compartment) of the electrophoresis system is filled up with electrophoresis buffer for SDS-PAGE (see 2.5.5) till the appropriate calibration mark at the outer chamber (cathode compartment) of the system is reached. Residual acrylamide is carefully removed from the gel pockets by washing with electrophoresis buffer with help of a syringe. After storage at 4 °C, cell extracts or protein samples, being cleaned up by chloroform-methanol precipitation (see 3.9.2), are heated to 95 °C followed by quick centrifugation prior to usage for SDS-PAGE. The volume needed for a defined amount (20-80 µg) of protein is calculated for each sample according to results of the BCA assay (see 3.9.3) and applied by pipetting to the gel pockets. In addition, 5 µL of a molecular weight protein marker (either Spectra ™ Multicolor broad range or Prestained Molecular Weight Marker, see 2.2) are applied to one pocket of each gel. For subsequent detection of proteins upon antibody binding and chemoluminescence, 5 µL of a biotinylated protein ladder are mixed with the molecular weight protein marker before application to the gel. For better concentration of proteins within the stacking gel, a low voltage of 80-90 mV is used to start gel electrophoresis. Once the protein samples reach the running gel, the voltage is increased to 140 mV. SDS-PAGE is completed when the front line of the blue-colored Laemmli sample buffer reaches the lower end of the gel. The gels are removed from the buffer tank for Western Blot analysis (see 3.9.6).

3.9.6 Western Blotting

Western Blotting represents an analytical technique to immunochemically detect proteins in cell extracts or other protein samples. The term "blotting" is originally defined by Erwin Southern in 1971 as the transfer of electrophoretically separated macromolecules like DNA, RNA or proteins to filter membranes. Later on, modifications of this technique have resulted in the development of Western Blotting by two independent working groups in 1979 (Towbin et al., 1979; Renart et al., 1979). Proteins that are separated by SDS-PAGE are transferred from the gel to a nitrocellulose or PVDF membrane by performance of so-called tank-blotting (Bittner et al., 1980). Thereby, acrylamide gels are embedded between an appropriate membrane and Whatman filter papers (sandwich technique). SDS-loaded, negatively charged proteins migrate towards the anode and are thereby transferred to the membrane. In general, PVDF membranes are more suitable for Western Blotting due to higher protein binding capacity, better resistance to organic solvents and signal-to-noise ratio in comparison to cheaper nitrocellulose membranes.

Before SDS-PAGE (see 3.9.5) is finished, the PVDF membrane is activated via short application of methanol. After removal of the solvent, the membrane is moistened with H_2O_{dest} for 5 min at RT upon shaking. Acrylamide gels are removed from the buffer tank and glass plates are disentangled with help of a scalpel. Within a plastic box, which is filled with blotting buffer (see 2.5.5), the gel holder cassette is placed with the transparent cathode side directing to the bottom of the box. According to the sandwich technique, the foam pad and three layers of Whatman filter paper (comparably sized as acrylamide running gels) are applied. Air bubbles between the different layers are removed by gently bending over with help of a glass rod prior to removal of acrylamide gels from the SDS-PAGE buffer tank. After disentangling glass plates with help of a scalpel and removal of the stacking gel, the running gel is transferred upon usage of moistened gloves to the layers of Whatmann filter paper with opposing orientation. The gel is gently smoothened with help of the glass rod followed by application of the activated PVDF membrane (touch only with tweezer at the corners). During removal of air bubbles after application of each sandwich layer, three further layers of Whatman filter paper and a second foam pad are placed onto the membrane. The gel holder cassette is closed and transferred to the buffer tank of the blotting module, which is filled up with pre-chilled blotting buffer.

After placing an agitator and a cooling unit to the bottom of the buffer tank, the module is closed and upon gently stirring of the blotting buffer, the protein transfer is conducted upon constant voltage (100 V) for 90 min. Subsequent to Western Blotting, the PVDF membrane is removed from the gel. The membrane is incubated with a suitable blocking buffer for immunochemical protein detection (see 2.9.6) and can be stored at -20 °C (protected with plastic foil) till further working steps are conducted.

3.9.7 Detection of HRP-conjugated antibody signals

To detect proteins on PVDF membranes after Western Blotting, antigen-specific primary antibodies are used that are in turn recognized by HRP (horseradish peroxidase)-conjugated secondary antibodies. Upon usage of HRP as reporter enzyme, small amounts of a specific protein can be detected via oxidation of the HRP substrate luminol to 3-aminophthalate. The generated, intermediate dianion emits low-intensity light at 428 nm, which is strongly (10-100x) increased by addition of, e.g. H_2O_2. Due to enhanced chemoluminescence (ECL), the signal of the HRP-conjugated antigen-antibody complex can be detected due to local blackening of X-ray films.

Subsequent to Western Blotting (see 3.9.6), PVDF membranes are cut to size on a glass plate with help of scalpel. Cutting is performed in a way to detect the protein of interest and a ubiquitously expressed protein as loading control on two separated membrane pieces. Furthermore, the size of the membranes is generally reduced to a maximum extent in order to detect proteins with the smallest possible amount of antibody. Afterwards, PVDF membranes are incubated in TBS/T (see 2.5.5) supplemented, either with 5 % (w/v) BSA or milk powder, for 1 h at RT upon shaking according to the primary antibody used (see 2.4.1). If membranes are subsequently stored at -20 °C till further working steps are performed, membranes are thawed at RT prior to application of primary antibodies. After blockage of unspecific binding sites on the membranes, a specific primary antibody (5 mL total volume of antibody solution; see 2.4.1) for detection of each single protein is applied and blots are preferentially incubated o/n at 4 °C within a Falcon tube upon shaking. Subsequently, blots are shortly washed with TBS/T followed by two further washing

steps for 5 min at RT upon shaking. After removal of the primary antibody, membranes are incubated with a suitable HRP-conjugated secondary antibody (5 mL total amount of antibody solution, see 2.4.2) for 1 h at RT within a Falcon tube upon shaking. Again, membranes are washed with TBS/T as described above to remove unbound secondary antibody. Washed membranes can be stored at 4 °C till HRP-mediated detection of proteins. Upon red-coloured safelight, the ECL solution is freshly prepared (see 2.5.5) and applied to PVDF membranes for at least 90 sec (better: 5 min) to start HRP-catalyzed luminol conversion. During incubation, the X-ray film is cut to size in order to use the smallest possible pieces for detection. Afterwards, membranes are positioned between plastic foils within the X-ray cassette, whereby air bubbles upon membranes should be avoided. The X-ray film is placed on top and the cassette is closed for a certain time span (10 sec up to 20 min; first try: 1-2 min) which is dependent on the signal strength of the applied antibodies and has to be figured out for each analysis. Subsequently, the X-ray film is removed from the cassette with help of a tweezer (only touch at corners) and is shortly incubated in the fixer solution (see 2.5.5). The following application of the film to the developer solution (see 2.5.5) makes the antibody signal visible after a few seconds. Finally, the X-ray film is washed in H_2O_{dest} prior to air drying.

3.10 DNA damage analysis via the Comet assay
3.10.1 Sample preparation and cell lysis

Microscopic slides are coated with agarose solution (see 2.5.6) and are air-dried o/n at RT. Cells are seeded and cultivated on Ø 6 cm culture dishes according to the above described conditions for mammalian cell culture (see 3.1.2 and 3.2). To secure technical functionality of the Comet assay, cell treatment should include a positive control for DNA damage, e.g. induction of SSBs and DSBs upon H_2O_2 exposure (see 3.3.1). Shortly before cell treatment is completed, a suitable volume of LMP agarose is heated and kept within 1.5 mL reaction tubes (120 µL per sample) at 37 °C. After treatment, cells are trypsinized (see 3.1.2) and pelletized by centrifugation (800 rpm, 5 min, 4 °C). The culture medium is carefully removed with help of a syringe and the cell pellet is resuspended in cold PBS (50-70 µL, 1.7-3.3 x 10^5 cells per mL PBS). Subsequently, 5-10 µL of the cell suspension are mixed with

120 µL of LMP agarose followed by dropwise application of the cell agarose mix (120 µL) in one line over the agarose-coated, microscopic slides. By gently putting on a cover slip (24 x 60 mm) on the agarose mix, cells are equally distributed over the whole microscopic slide, whereby the formation of air bubbles should be avoided. Following incubation of microscopic slides for a few minutes at 4° C in order to gel the cell agarose mix, cover slips are removed and microscopic slides are transferred to a tint bowl, which is filled up with pre-chilled suitable lysis buffer (either alkaline or neutral conditions, see 2.5.6). The time span for cell lysis is dependent on the cell type / cell line that is used: NIH3T3 cells are lysed for 50 min at 4 °C and Caco-2 cells are lysed for 20 min at 4 °C. Afterwards, further working steps for single gel electrophoresis are conducted either to detect DNA single-strand breaks (SSBs via alkaline comet assay, see 3.10.2) or to analyze double-strand breaks (DSBs via neutral comet assay, see 3.10.3).

3.10.2 Alkaline single gel electrophoresis for DNA SSB detection

The single-cell gel (SCG) electrophoresis or Comet Assay is suitable for genotoxicity testing *in vitro* and *in vivo* (Tice et al., 2000). After being developed in 1984, the technique has been modified to primarily detect DNA SSBs upon alkaline assay conditions (Fairbairn et al., 1995). At a pH of < 13, DNA unwinding is induced and alkali labile sites are expressed as SSBs. Upon electrophoresis, DNA fragments migrate into the direction of the anode. The DNA migration pattern of each cell is referred to as "Comet". Subsequent to electrophoresis, SSBs are detected by PI staining and fluorescence microscopy.

After cell lysis (see 3.10.1), sample slides are placed into an electrophoresis chamber, which is suitable for Comet assay, and are carefully covered (2-3 mm) with pre-chilled electrophoresis buffer for alkaline comet assay (see 2.5.6). Subsequent to DNA unwinding upon incubation of sample slides in electrophoresis buffer for 20 min in the dark at 4 °C, electrophoresis is conducted with the following parameters adapted to NIH3T3 and Caco-2 cells: 15 min (Caco-2) or 20 min (NIH3T3), 23 V (small chamber) or 28 V (big chamber), 300 mA. Upon constant voltage, the current is adjusted for electrophoresis via adapting the volume of the electrophoresis buffer. After electrophoresis, sample slides are transferred to neutralization buffer (see

2.5.6) for 5 min at RT. The buffer is removed and sample slides are washed twice in neutralization buffer (5 min, RT) followed by short washing of slides in H_2O_{dest}. Subsequent to sample fixation in 100 % EtOH (5 min, RT), slides are air-dried and stored at 4 °C till microscopic analysis (see 3.10.4) is conducted.

3.10.3 Neutral single gel electrophoresis for DNA DSB detection

Upon neutral conditions of the above described SCG electrophoresis (see 3.10.2), the induction and the repair of DNA DSBs can be analyzed. The neutral variant of SCG electrophoresis is conducted for NIH3T3 and Caco-2 cells according to the protocol for alkaline SCG (see 3.10.1, 3.10.2) with the following exceptions. Directly after cell lysis in lysis buffer that is suitable for neutral Comet assay, electrophoresis is conducted without performance of DNA unwinding upon usage of neutral electrophoresis buffer (see 2.5.6). Due to neutral conditions, there is no need to neutralize sample slides in neutralization buffer after electrophoresis and the current is not adapted due to usage of constant voltage strength.

3.10.4 Sample analysis via fluorescence microscopy

After SCG electrophoresis, the DNA is stained with PI as a fluorescent, DNA-intercalating dye. As a measure for the migration of DNA SSBs and DSBs, the tail intensity or the tail moment of the Comet of each single cell is calculated according to the microscopically detected fluorescence signals.

To detect SSBs or DSBs after performance of alkaline or neutral SCG electrophoresis (see 3.10.2, 3.10.3), sample slides are stained with 60-80 µL of the PI staining solution for Comet assay (see 2.5.6) in the dark by dropwise application of the solution in one line over the sample slide. By gently putting on a cover slip (24 x 60 mm), the PI staining solution is equally distributed over the whole slide, whereby the formation of air bubbles should be avoided. The tail intensity or tail moment of 50 cells per sample slide are calculated via usage of the software Komet 4.20.2 and fluorescence microscopy (PI excitation wavelength: 356 nm). To avoid scoring the same cell within on sample, microscopic slides are analyzed by moving over in a

defined pattern: from the upper left corner of the slide to the upper right corner followed by a shift downwards and analysis from the right to the left corner and so on.

3.11 Statistical data evaluation

Although the results are obvious, comparisons between treatments were made by one- or two-way analysis of variance (ANOVA) followed by Tuckey's multiple comparisons test. Significance is determined upon p value calculation and defined as follows: * $p \leq 0.05$, ** $p \leq 0.01$, *** $p \leq 0.001$.

4 Results

4.1 Cell confluence protects against *t*-BuOOH-induced toxicity

4.1.1 Resistance against *t*-BuOOH-induced cell death is mediated by the presence of cell-cell contacts independent of cell cycle arrest

Starting point for my work was the observation that confluent, G1-arrested (contact-inhibited) NIH3T3 cells are protected against *t*-BuOOH-induced cell death when compared to semiconfluent, proliferating cells (B. Linz, MD thesis, 2013). I first addressed the question whether cell-cell contacts provide resistance as independent parameter against *t*-BuOOH-induced toxicity or whether resistance against ROS is mediated by cell cycle arrest. To this end, two experimental setups were included.

4.1.1.1 Experimental setup I:
The sensitivity of confluent versus semiconfluent cells to *t*-BuOOH

Murine fibroblasts (NIH3T3) and human epithelial cells (HaCaT, Caco-2) were seeded to confluence, but below their saturation density and cultured in the presence of 10 % FBS for 24 h ("confluent"). Setup I should thereby allow the establishment of cell-cell contacts without inducing quiescence at the time point of *t*-BuOOH exposure. Confluent cells were compared to semiconfluent cultures, either cultivated (i) in the presence of 10 % FBS for 24 h ("proliferating"), or (ii) under serum-depletion for 48 h ("serum-depleted"). In this context, the latter cell population served to control for possible cell cycle-driven effects (Figure 8A).

The analysis of the cell cycle distribution via PI staining and flow cytometry allowed the selection of appropriate conditions for serum depletion (0.1-0.5 % FBS, see 3.2.1) in order to achieve a comparable amount of cells in the G1 phase (NIH3T3, HaCaT: ~ 75 %, Caco-2: ~ 50 %) as observed in confluent cultures (Figure 8B). Comparatively, a lower amount of cells (NIH3T3, HaCaT: ~ 50; Caco-2: ~ 40 %) was found in G1 in proliferating cultures. Similar results were obtained in other fibroblast cell lines (MEF, Swiss3T3, FH109; Appendix I, Table 1). Importantly, the data confirm that confluent cells were not quiescent at the time point of *t*-BuOOH exposure when seeded and cultivated upon setup I.
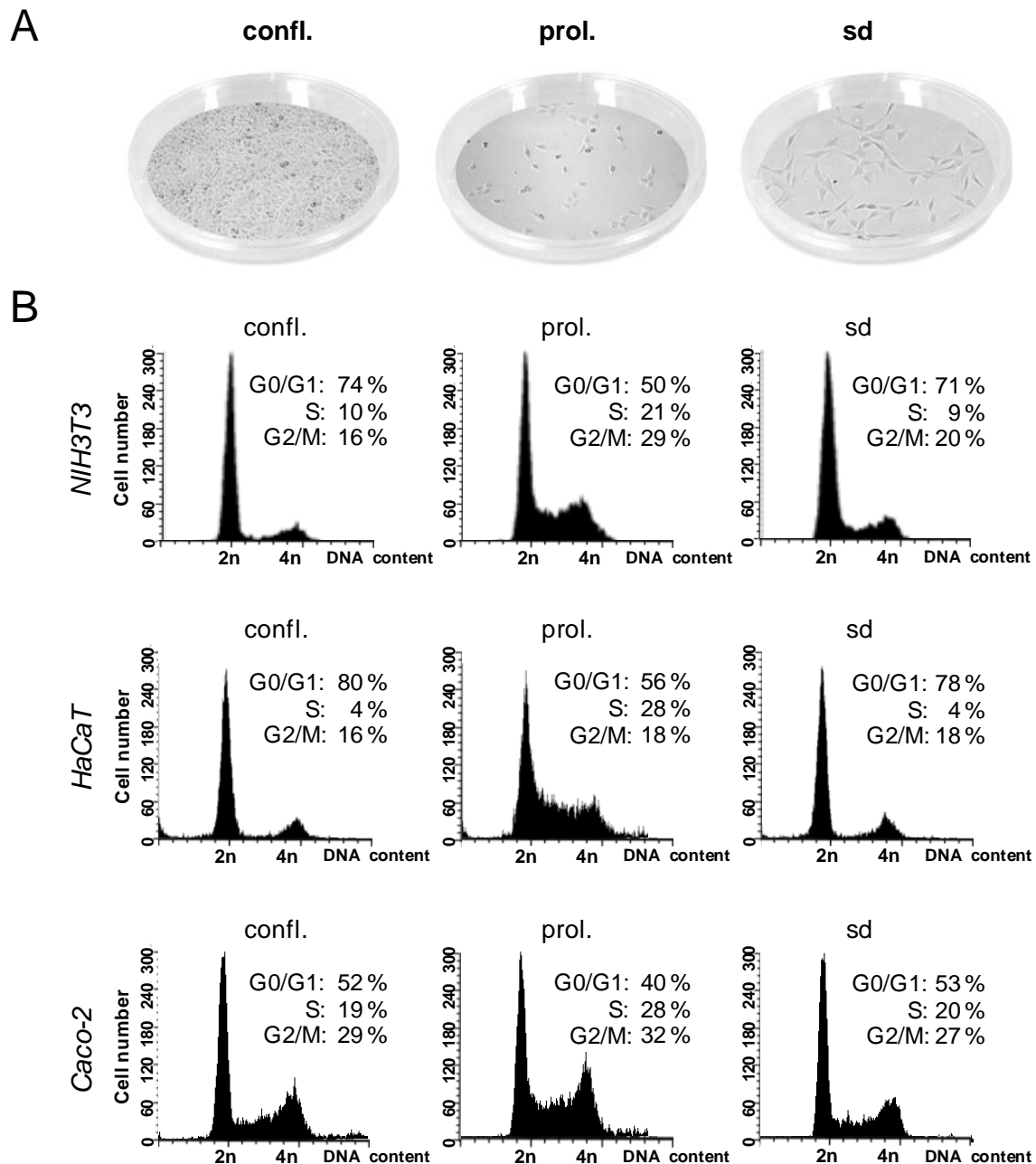
Fig. 8 Setup I: Confluent and serum-depleted murine fibroblasts (NIH3T3) and human epithelial cells (HaCaT, Caco-2) show a similar cell cycle distribution and confluent cells are not arrested in G1 at the time point of *t*-BuOOH exposure. **a, b** Confluent (confl.) and semiconfluent, proliferating (prol.) cells were cultivated for 24 h in the presence of 10 % FBS. Semiconfluent, serum-depleted cells (sd) were cultivated for 48 h in the presence of 0.1 % (NIH3T3, HaCaT) or 0.2 % (Caco-2) FBS. **a** Representative phase contrast images of NIH3T3 cells according to setup I. **b** Cell cycle analysis at the time point of *t*-BuOOH exposure via PI staining and flow cytometry (representative out of *n* = 2-3).

Further evidence that confluent cells are not contact-inhibited at the time point of *t*-BuOOH exposure was provided by Western Blot analysis of p27 – a central mediator of the G1 arrest upon high cell density (Polyak et al., 1994; Hengst & Reed, 1996; Dietrich et al., 1997). According to Figure 9A, the maximum expression of p27

and therefore quiescence was not yet reached in confluent NIH3T3 cells at the time point of *t*-BuOOH exposure (24 h after seeding), but after 48 h. Regardless from a high amount of cells in the G1 phase as demonstrated before, confluent NIH3T3 cells were still able to nearly double their number between 24 h and 48 h after seeding, i.e. during the time span intended for *t*-BuOOH treatment (Figure 9B). Despite cells had established cell-cell contacts, these findings prove that confluent cells proliferated and were not quiescent at the time point of *t*-BuOOH exposure.
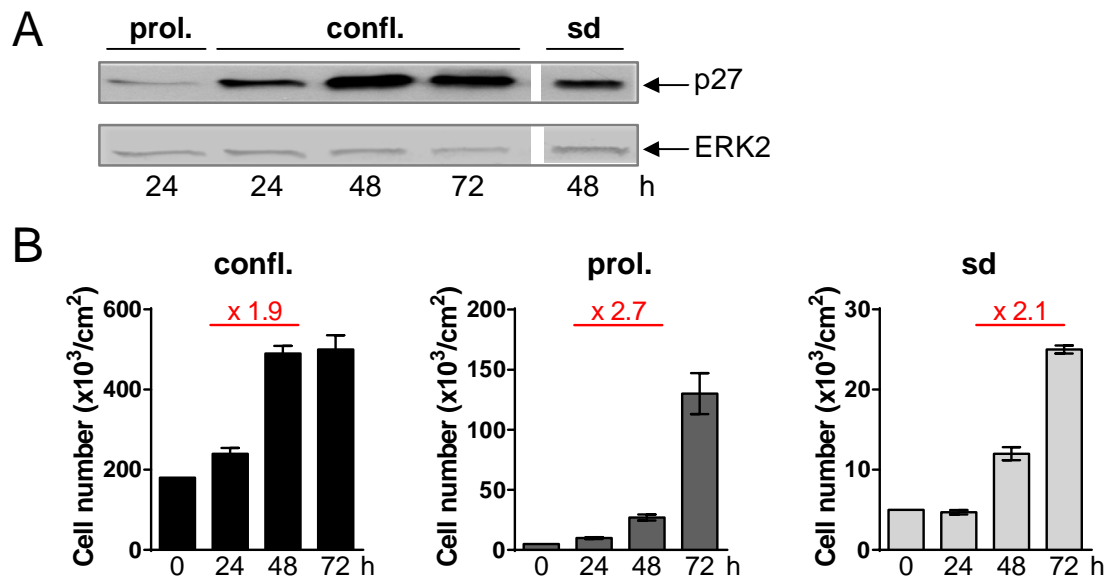
Fig. 9 Confluent NIH3T3 cells are not quiescent and proliferate at the time point of *t*-BuOOH exposure. **a, b** Confluent (confl.) and semiconfluent (proliferating, prol., serum-depleted, sd) cells were seeded according to setup I. After cultivation for the indicated time points, cells were either (**a**) harvested to analyze p27 expression via Western Blot analysis with ERK2 as loading control, or (**b**) the proliferation rate (marked red) was calculated after Trypan Blue staining and counting of vital cells (mean ± SD of a representative experiment out of *n* = 2 in duplicates; conducted by D. Faust).

After setup I was evaluated as suitable model to analyze the effects of cell-cell contacts, I first investigated the sensitivity of confluent versus semiconfluent (prol., sd) NIH3T3 cells to *t*-BuOOH (Figure 10). Trypan Blue exclusion and cell counting clearly showed survival of at least 50 % of confluent cells after 24 h of *t*-BuOOH treatment, even when cells were exposed to the highest applied concentration of 100 µM. In contrast to that, entire cell death in semiconfluent NIH3T3 cultures (prol., sd) was already induced at a concentration of ≥ 30 µM t-BuOOH. According to the concentration-response relationship, a toxic threshold concentration of around 20 µM *t*-BuOOH was determined for proliferating cells and around 10 µM *t*-BuOOH for serum-depleted cells (Wenz et al. 2018). Importantly, proliferating and serum-

depleted cultures showed a similar sensitivity to *t*-BuOOH independent of the amount of cells in G1. On the other hand, confluent NIH3T3 cells tolerated an approximately threefold higher concentration of *t*-BuOOH as compared to proliferating or serum-depleted cultures.
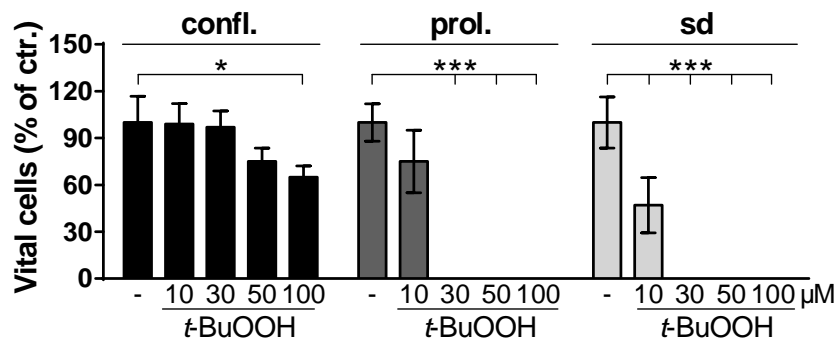
Fig. 10 Confluent (confl.) compared to semiconfluent (proliferating, prol.; serum-depleted, sd) NIH3T3 cells are more resistant to *t*-BuOOH-induced toxicity. Cells were seeded and cultivated according to setup I. After treatment with *t*-BuOOH for 24 h, the number of vital cells (relative to control) was assessed via Trypan Blue exclusion and cell counting (mean ± SD of $n = 3$ in duplicates). Significance between control and vehicle-treated cells was calculated with * $p \leq 0.05$, *** $p \leq 0.001$. ctr. = control

To exclude side effects that might arise from serum depletion, semiconfluent NIH3T3 cells were alternatively treated with the MEK1,2 inhibitor U0126 in the presence of 10 % FBS (English et al., 2002). As shown by flow cytometric analysis after PI staining, treatment with U0126 arrests ~ 70 % of semiconfluent NIH3T3 cells in G1 which is comparable to serum-depleted cultures (Figure 11A). Furthermore, Trypan Blue exclusion and cell counting proved an equal sensitivity of U0126-treated and proliferating NIH3T3 cells (Figure 11B). Hence, these data additionally confirm that the amount of cells in G1 did not influence the sensitivity of cells to *t*-BuOOH but rather the presence of cell-cell contacts.
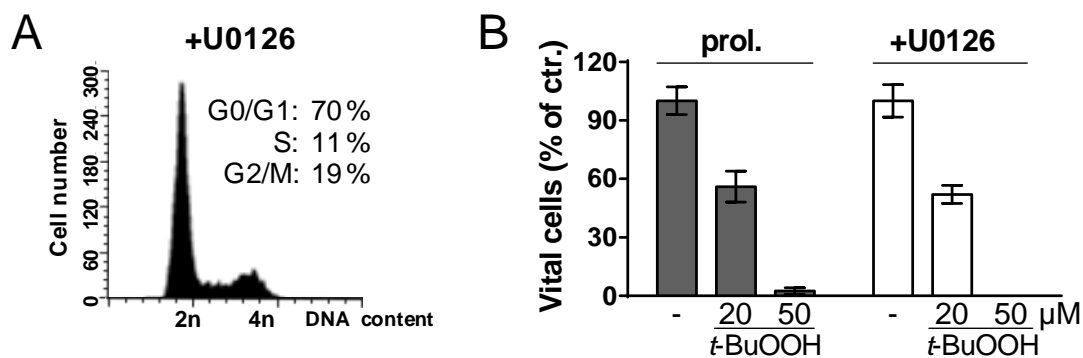
Fig. 11 U0126-treated NIH3T3 cells show a comparable amount of cells in G1 as confluent cells but are as sensitive to *t*-BuOOH as proliferating cultures. **a, b** Semiconfluent cells were seeded according to setup I. Cells were cultivated in the presence of 10 % FBS and were either untreated (proliferating,

prol.) or simultaneously treated with U0126 (50 µM; + U0126) for 24 h. **a** Cell cycle analysis via PI staining followed by flow cytometry (representative out of $n = 2$). **b** After 24 h t-BuOOH treatment, the number of vital cells (relative to control, ctr.) was determined via Trypan Blue exclusion followed by cell counting (mean ± SD of $n = 3$ in duplicates).

Besides t-BuOOH, H_2O_2 is one of the most frequently used compounds to experimentally induce oxidative stress due to its pivotal role as endogenous signaling molecule (Gough & Cotter, 2011). Thus, also a possible resistance of confluent NIH3T3 cells against H_2O_2 was investigated. Since H_2O_2 is a lesser stable ROS donor as t-BuOOH (Alia et al., 2005; Baker et al., 1991), higher H_2O_2 concentrations were applied to induce similar cytotoxic effects in semiconfluent cultures. According to Figure 12A, indeed a higher number of confluent compared to semiconfluent (prol., sd) NIH3T3 cells survived treatment with H_2O_2 at all indicated concentrations. In this context, 300 µM H_2O_2 were determined to induce an equitoxic effect as compared to 50 µM t-BuOOH in proliferating NIH3T3 cells (Wenz et al., 2018).
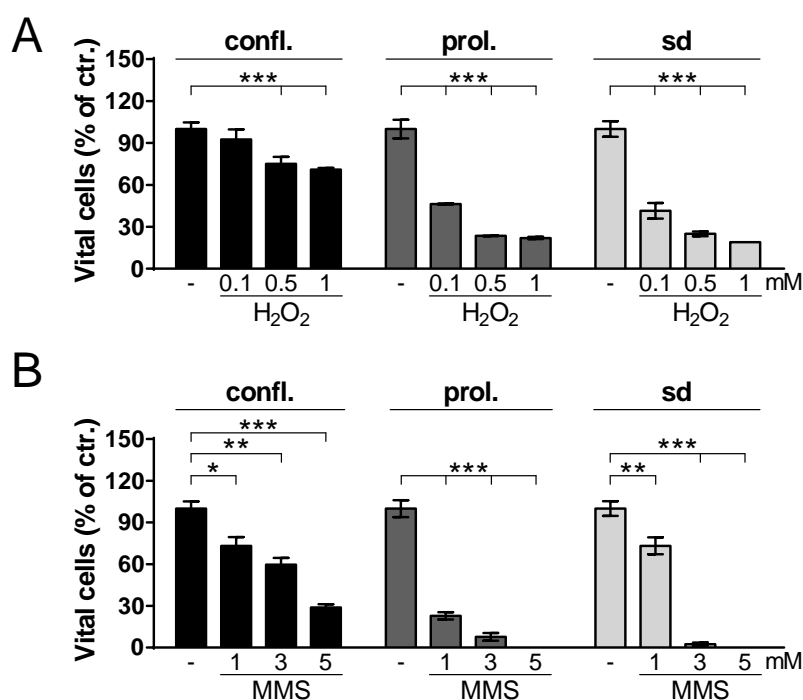
Fig. 12 Confluent (confl.) NIH3T3 cells are more resistant against H_2O_2 and MMS as semiconfluent (proliferating, prol.; serum-depleted, sd) cultures. **a,b** Cells were seeded and cultivated according to setup I. Then, cells were either treated with (**a**) H_2O_2 for 24 h (mean ± SD of $n = 3$ in duplicates, conducted by D. Faust) or (**b**) MMS for 24 h (mean ± SD of a representative experiment out of $n = 2$-3 in duplicates) followed by Trypan Blue exclusion assay. Significance between control and vehicle-treated cells was calculated with * $p \le 0.05$, ** $p \le 0.01$, *** $p \le 0.001$. ctr. = control

Apart from these peroxides, I additionally investigated resistance of confluent NIH3T3 cells against the genotoxin MMS. Although resistance of confluent compared to semiconfluent (prol., sd) cultures was not that prominent as seen against peroxides, still a higher number of confluent compared to semiconfluent cells

survived treatment with a MMS concentration of ≥ 3 mM for 24 h (Figure 12B). First results also hint towards resistance of confluent NIH3T3 cells against ROS-inducing UV-C radiation (data not shown). These data provide evidence that resistance of confluent NIH3T3 cells was not limited to a specific type of agent or noxa. Furthermore, a general mechanism for the resistance of confluent fibroblasts against t-BuOOH-induced toxicity was assumed since confluent cultures of other murine and human fibroblast cell lines (MEF p53wt, Swiss3T3, FH109) displayed a similar resistance to t-BuOOH as observed in confluent NIH3T3 cells (Figure 13A-C).
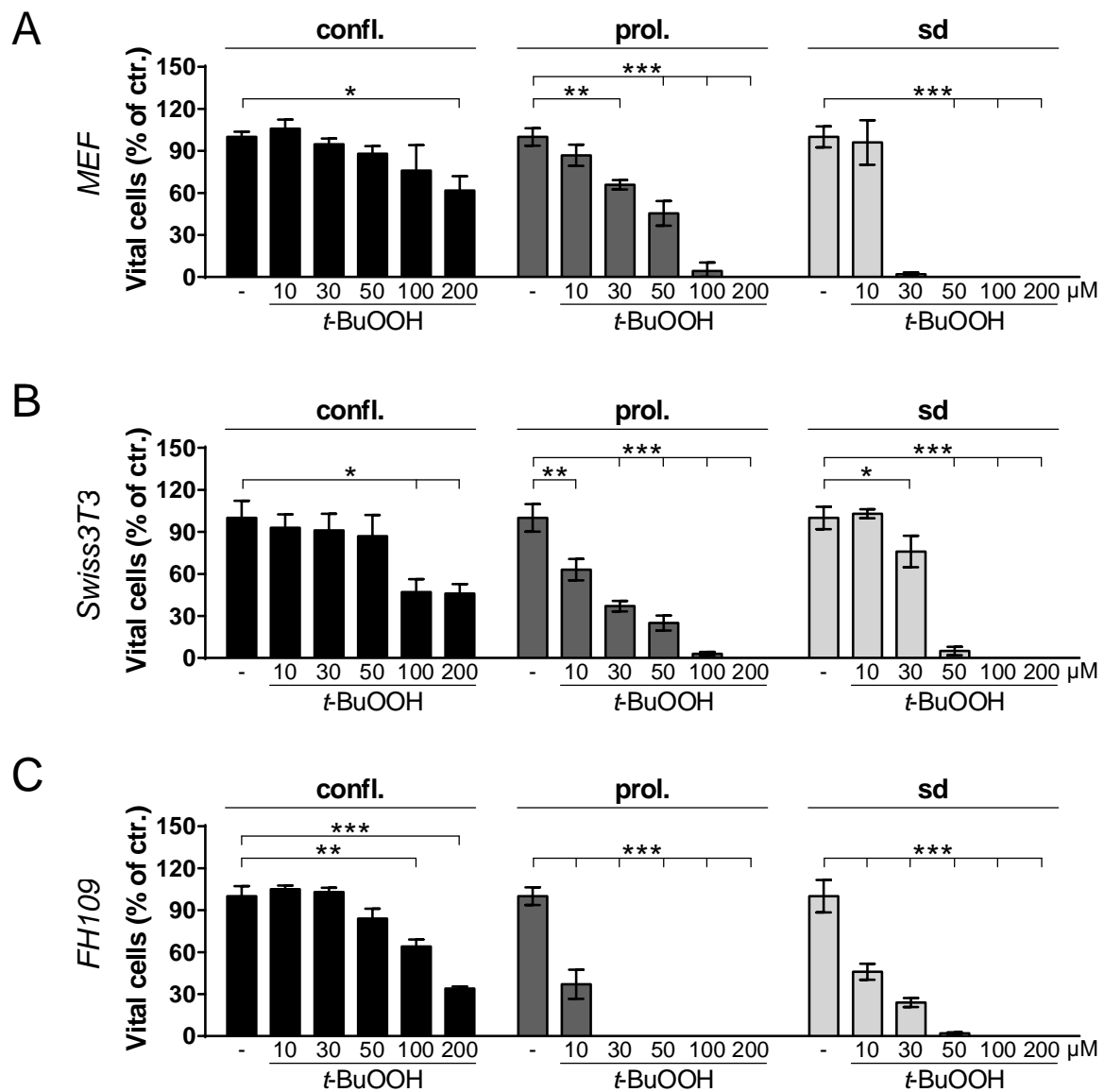
Fig. 13 Distinct fibroblast cell lines are more resistant to t-BuOOH upon confluence (confl.) as compared to corresponding semiconfluent (proliferating, prol.; serum-depleted, sd) cultures. Murine MEF p53wt (**a**) and Swiss3T3 (**b**) cells, as well as human FH109 (**c**) cells were seeded and cultivated according to setup I. After treatment with t-BuOOH for 24 h, the cell vitality (relative to control) was assessed by Trypan Blue exclusion and cell counting (mean ± SD of n = 2-3 (**a**) or of a representative

experiment out of $n = 2$ (**b**,**c**) in duplicates). Significance between control and vehicle-treated cells was calculated with * $p \leq 0.05$, ** $p \leq 0.01$, *** $p \leq 0.001$. ctr. = control

To further examine if confluence-mediated protection against t-BuOOH might be restricted to a specific cell type, confluent and semiconfluent cultures of human epithelial cell lines (HaCaT, Caco-2) were additionally exposed to t-BuOOH. According to results of the Trypan Blue exclusion assay (Figure 14A-B), at least 50 % of confluent HaCaT and Caco-2 cells survived 24 h exposure to 300 µM (HaCaT) or 100 µM (Caco-2) of t-BuOOH, respectively. In contrast to that, these concentrations induced entire cell death in the corresponding semiconfluent cultures (prol., sd), whereby t-BuOOH significantly attenuated the vitality of these cells already at a concentration of ≥ 30 µM. As similar results were obtained in distinct fibroblast cell lines as shown before, resistance of confluent cultures against t-BuOOH-induced toxicity was not limited to a specific cell type.
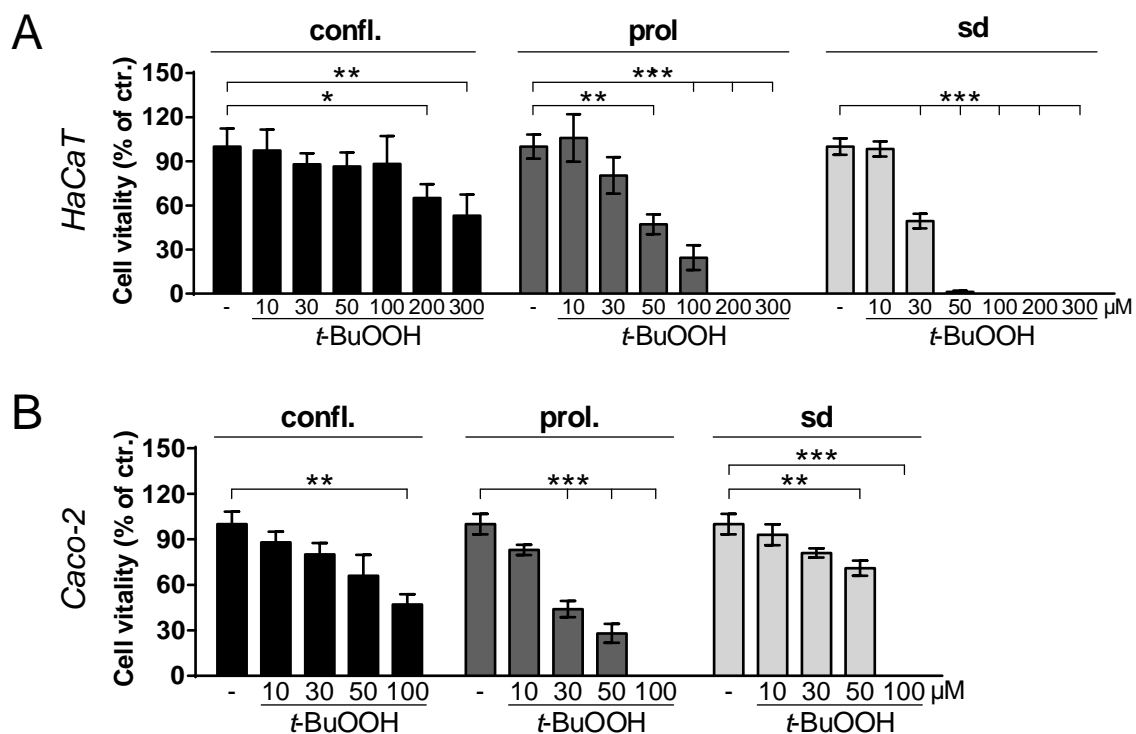
Fig. 14 Confluent (confl.) compared to semiconfluent (proliferating, prol.; serum-depleted, sd) cultures of epithelial cell lines (HaCaT, Caco-2) are more resistant against t-BuOOH-induced toxicity. Human keratinocytes (HaCaT, **a**) and colon carcinoma cells (Caco-2, **b**) were seeded and cultivated according to setup I. After treatment with t-BuOOH for 24 h, the cell vitality (relative to control) was assessed by Trypan Blue exclusion and cell counting (mean ± SD. of $n = 2$-3 in duplicates). Significance between control and vehicle-treated cells was calculated with * $p \leq 0.05$, ** $p \leq 0.01$, *** $p \leq 0.001$. ctr. = control

For further analysis, the following concentrations were selected, just sufficient to induce entire cell death in semiconfluent but not in confluent cells during 24 h treatment: NIH3T3 = 30 µM, 50 µM; HaCaT = 200 µM; Caco-2 = 100 µM. For NIH3T3 cells, two different concentrations of *t*-BuOOH were chosen in order to study cell death more detailed. In this context, AnnexinV-FITC / PI staining and flow cytometry confirmed resistance of confluent compared to semiconfluent (prol., sd) NIH3T3 cells against *t*-BuOOH-induced cell death (Figure 15A-B). *t*-BuOOH induced the onset of cell death in semiconfluent cultures already after 3-4 h treatment, ending up with entire cell death after ≥ 24 h of exposure. Although serum-depleted NIH3T3 cells showed ~ 20 % of basal cytotoxicity, these cells similarly died from *t*-BuOOH exposure as proliferating cells when treated with 30 µM and 50 µM *t*-BuOOH, respectively. In contrast to semiconfluent cultures, confluent NIH3T3 cells were resistant against *t*-BuOOH-induced cell death.
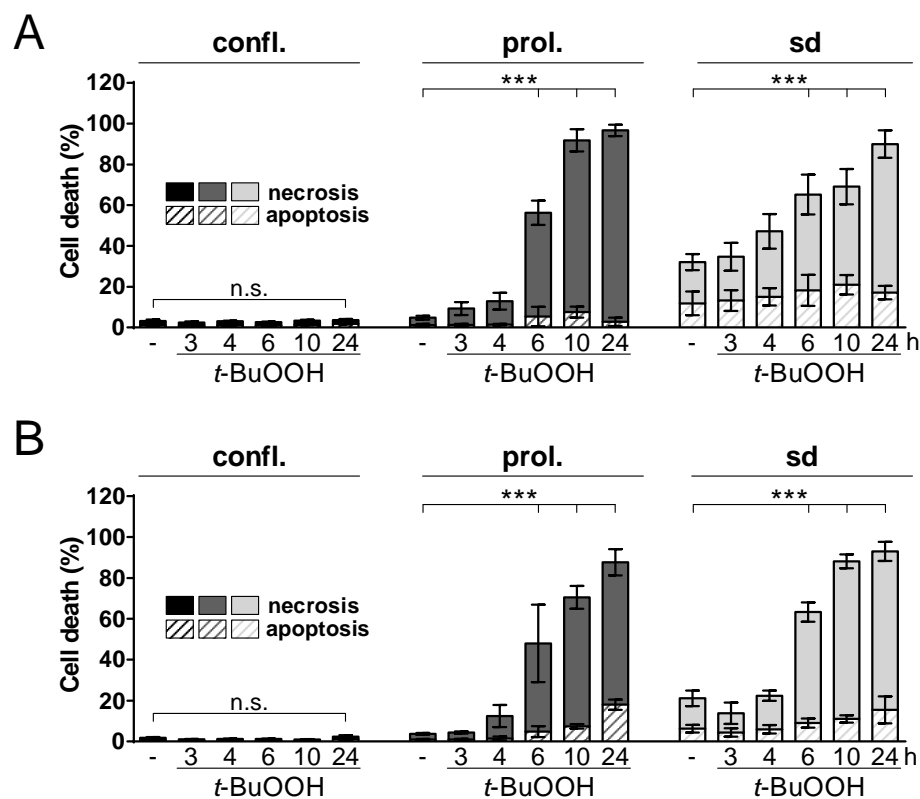
Fig. 15 Confluent compared to semiconfluent NIH3T3 cells are resistant against *t*-BuOOH-induced necrosis. **a,b** Confluent (confl.) and semiconfluent (proliferating, prol.; serum-depleted, sd) cells were seeded and cultivated upon setup I. After treatment with *t*-BuOOH (**a**: 30 µM, **b**: 50 µM), cells were stained with AnnexinV-FITC (early apoptosis) and PI (late apoptosis / necrosis) followed by flow cytometric analysis (mean ± SD of n = 2-3 in duplicates). Significance of *t*-BuOOH-induced necrosis was calculated with *** $p \leq 0.001$, n.s. = not significant.

The fast onset and progression of *t*-BuOOH-induced cell death in semiconfluent cells, as well as resistance of confluent cultures was also observed in HaCaT and Caco-2 cultures (Figure 16A-B). In this context and in the most cases of the following analyses, confluent Caco-2 cultures were only compared to proliferating cultures. Although AnnexinV-FITC / PI staining (Vermes et al., 1995) cannot discriminate between late apoptotic and necrotic cells (both: AnnexinV-FITC+ / PI+), necrosis was assumed as the main cell death mechanism induced by *t*-BuOOH since (i) only the fraction of double-stained cells (AnnexinV-FITC+ / PI+) increased at early treatment time points, whereas (ii) the amount of early apoptotic cells (AnnexinV-FITC+ / PI-) did not remarkably change during 24 h exposure. Moreover, a time-dependent, significant increase in double-stained (AnnexinV-FITC+ / PI+) cells was observed in semiconfluent cultures. Thus, cell death analysis supports resistance of confluent fibroblasts and epithelial cells against *t*-BuOOH-induced necrosis.
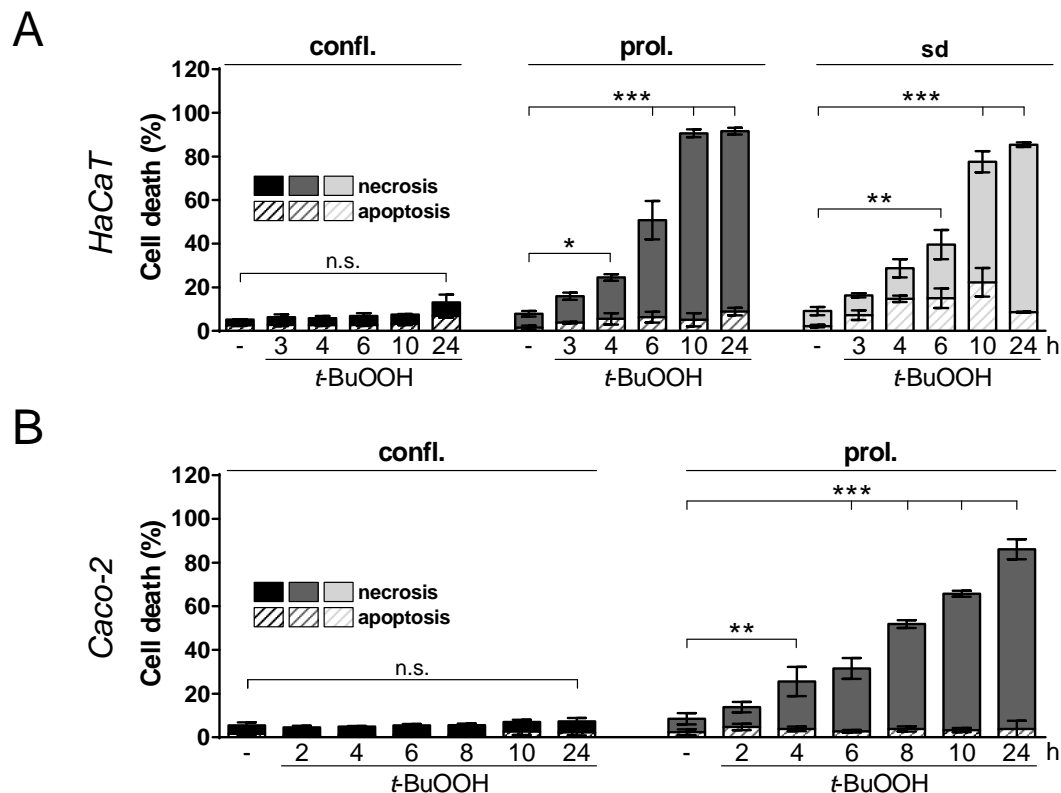
Fig. 16 Confluent compared to semiconfluent HaCaT and Caco-2 cells are resistant against *t*-BuOOH-induced necrosis. **a**,**b** Confluent (confl.) and semiconfluent (proliferating, prol.; serum-depleted, sd) cells were seeded and cultivated upon setup I. After treatment with *t*-BuOOH (**a**: 200 µM, **b**: 100 µM), cells were stained with AnnexinV-FITC (early apoptosis) and PI (late apoptosis / necrosis) followed by flow cytometric analysis (mean ± SD of *n* = 2-3 in duplicates). Significance of *t*-BuOOH-induced necrosis was calculated with * $p ≤ 0.05$, ** $p ≤ 0.01$, *** $p ≤ 0.001$, n.s. = not significant.

Interestingly, long-term treatment (48 h, 72 h) of proliferating NIH3T3 cells with low amounts of t-BuOOH (10 µM, 20 µM) near the toxic threshold concentration was not sufficient to remarkably induce cytotoxicity, whereas t-BuOOH treatment of serum-depleted cultures (20 µM for 48 h; 10 µM, 20 µM for 72 h) shifted cell death towards apoptosis (Figure 17). Nevertheless, flow cytometric analysis provided first evidence for t-BuOOH to primarily induce a necrotic-like cell death mechanism above the toxic threshold concentration as described before.
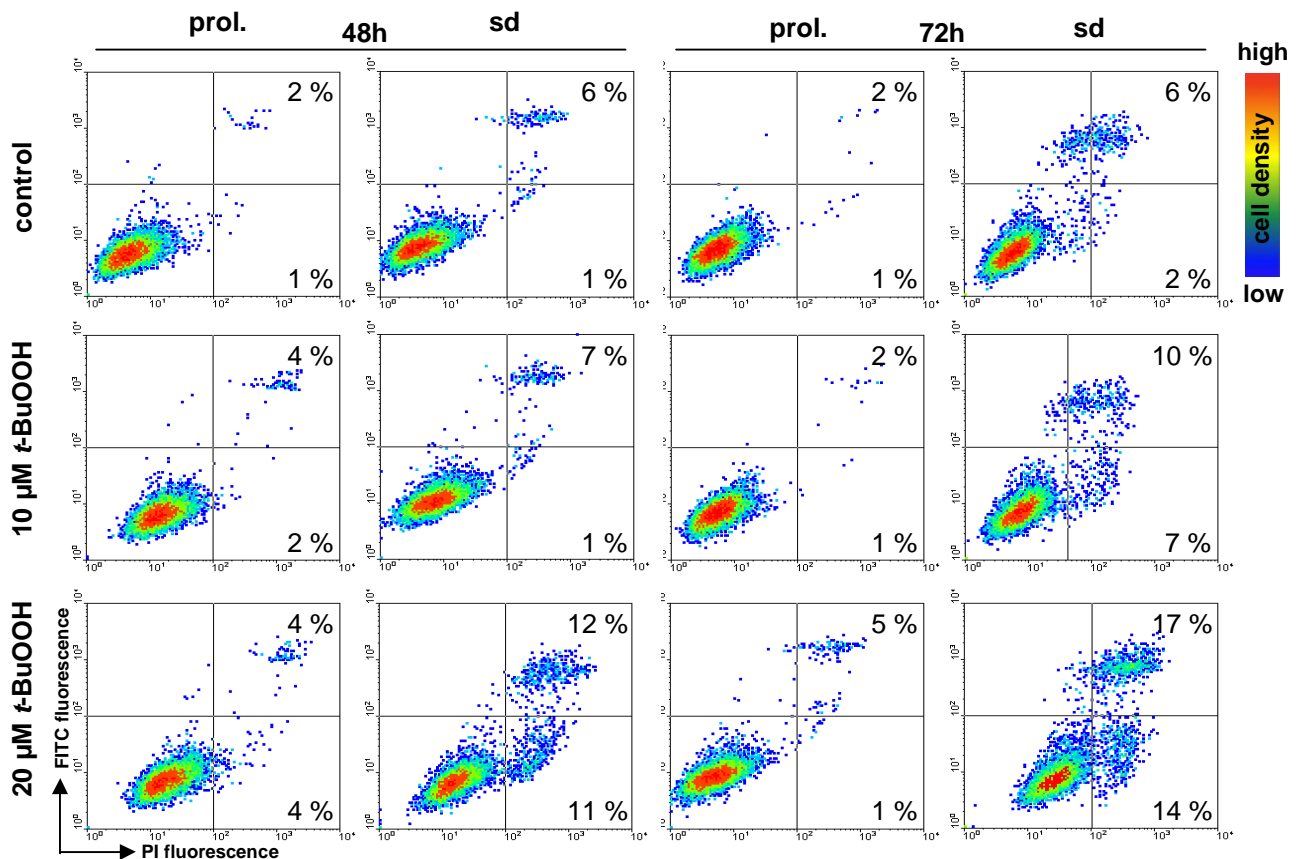
Fig. 17 Long-term exposure of semiconfluent (proliferating, prol.; serum-depleted, sd) NIH3T3 cells to low amounts of t-BuOOH is not sufficient to induce necrosis but shifts cell death towards apoptosis in serum-depleted cells. Cells were seeded and cultivated according to setup I. Afterwards, cells were either untreated (= control) or treated with t-BuOOH for the indicated time points. The amount of early apoptotic cells (AnnexinV-FITC+, lower right quadrant) and late apoptotic / necrotic cells (AnnexinV-FITC+/PI+, upper right quadrant) was analyzed by flow cytometry and is expressed in % of the total cell number. Representative density blots of a single experiment performed in duplicates.

In order to get hints towards the toxic event that might be the driving force for t-BuOOH-induced necrosis, semiconfluent NIH3T3 and Caco-2 cells were additionally exposed to different short pulses of t-BuOOH, and afterwards cultivated for another 20 h. According to Figure 18, already 1 h exposure to t-BuOOH was sufficient to significantly reduce the viability of proliferating NIH3T3 cells.

2-3 h treatment with t-BuOOH induced almost entire cell death in proliferating NIH3T3 and Caco-2 cultures. Hence, the finally toxic event upon t-BuOOH exposure occurred within the initial treatment phase of 1-3 h, leading to the onset and rapid execution of a necrotic cell death mechanism in semiconfluent cultures.
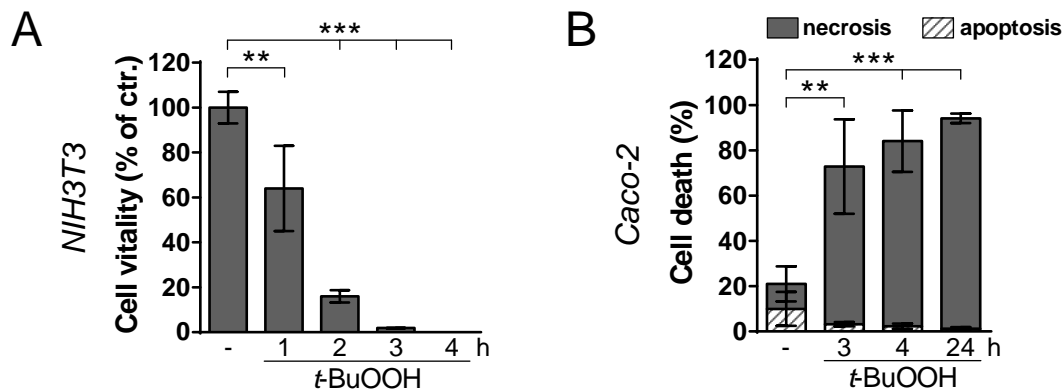
Fig. 18 A short pulse (1-3 h) of t-BuOOH above the toxic threshold concentration is sufficient to induce necrosis in semiconfluent cultures. **a,b** Cells were seeded and cultivated upon setup I. After t-BuOOH treatment (NIH3T3: 50 µM, Caco-2: 100 µM) for the indicated time points, cells were cultivated for another 20 h followed by either (**a**) Trypan Blue staining and cell counting, or (**b**) AnnexinV-FITC (apoptosis) / PI (necrosis) staining and flow cytometry (mean ± SD of n = 3 in duplicates). Significance of toxicity or necrosis was calculated with ** $p ≤ 0.01$, *** $p ≤ 0.001$. ctr. = control

4.1.1.2 Experimental setup II:
The sensitivity of confluent versus semiconfluent cells to t-BuOOH

Since I could not exclude a more efficient detoxification of t-BuOOH in confluent cells due to a higher cell number compared to semiconfluent cultures, the resistance of confluent cells against t-BuOOH was additionally evaluated in a second experimental setup (Bar et al., 2004). To this end, an equal cell number was seeded either (i) to confluence via plating cells as a drop, or (ii) to semiconfluence ("proliferating") and cultivated for 24 h in the presence of 10 % FBS. Setup II allowed thereby treatment of confluent and semiconfluent cells with a comparable amount of t-BuOOH molecules per cell. In line with setup I, incorporation of the S phase marker EdU (5-ethynyl-2'-deoxyuridine) and laser scanning microscopy proved that confluent cells were not quiescent and proliferated at the time point of t-BuOOH exposure – even at a high cell density in the center of the drop area. Moreover, cells at the drop edge and proliferating control cultures exhibited an almost equal incorporation of EdU (Figure 19A-C).
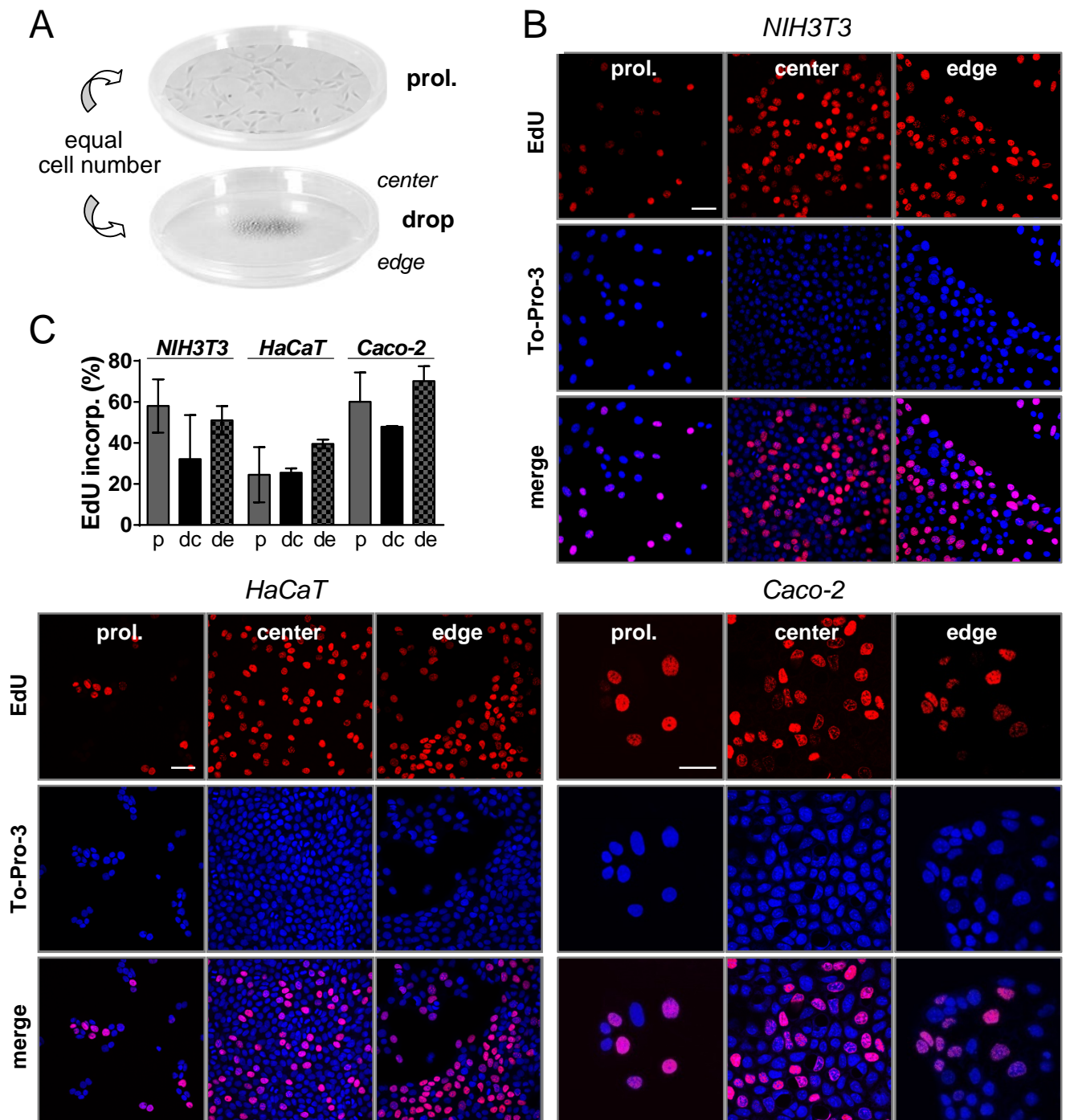
Fig. 19 Confluent and semiconfluent fibroblasts (NIH3T3) and epithelial cells (HaCaT, Caco-2) exhibit a similar proliferative capacity at the time point of *t*-BuOOH exposure upon setup II. **a** Setup II: An equal cell number was seeded either (i) to confluence via formation of a drop with a center (dc) and edge (de) area or (ii) to semiconfluence (proliferating; prol./ p). **b-c** After cultivation, cells were stained with the S phase marker EdU followed by (**b**) qualitative and (**c**) quantitative analysis of EdU incorporation (incorp.) via laser scanning microscopy (bar = 10 µm). Nuclei were counterstained with To-Pro-3 (analysis of NIH3T3 was conducted by D. Faust and C. Wenz). In (**c**), the mean ± SD of *n* = 2-3 is represented with 3-6 images counted per experiment.

Light microscopy further confirmed resistance of confluent versus semiconfluent cells (NIH3T3, HaCaT Caco-2) against t-BuOOH-induced cell death upon setup II (Figure 20).
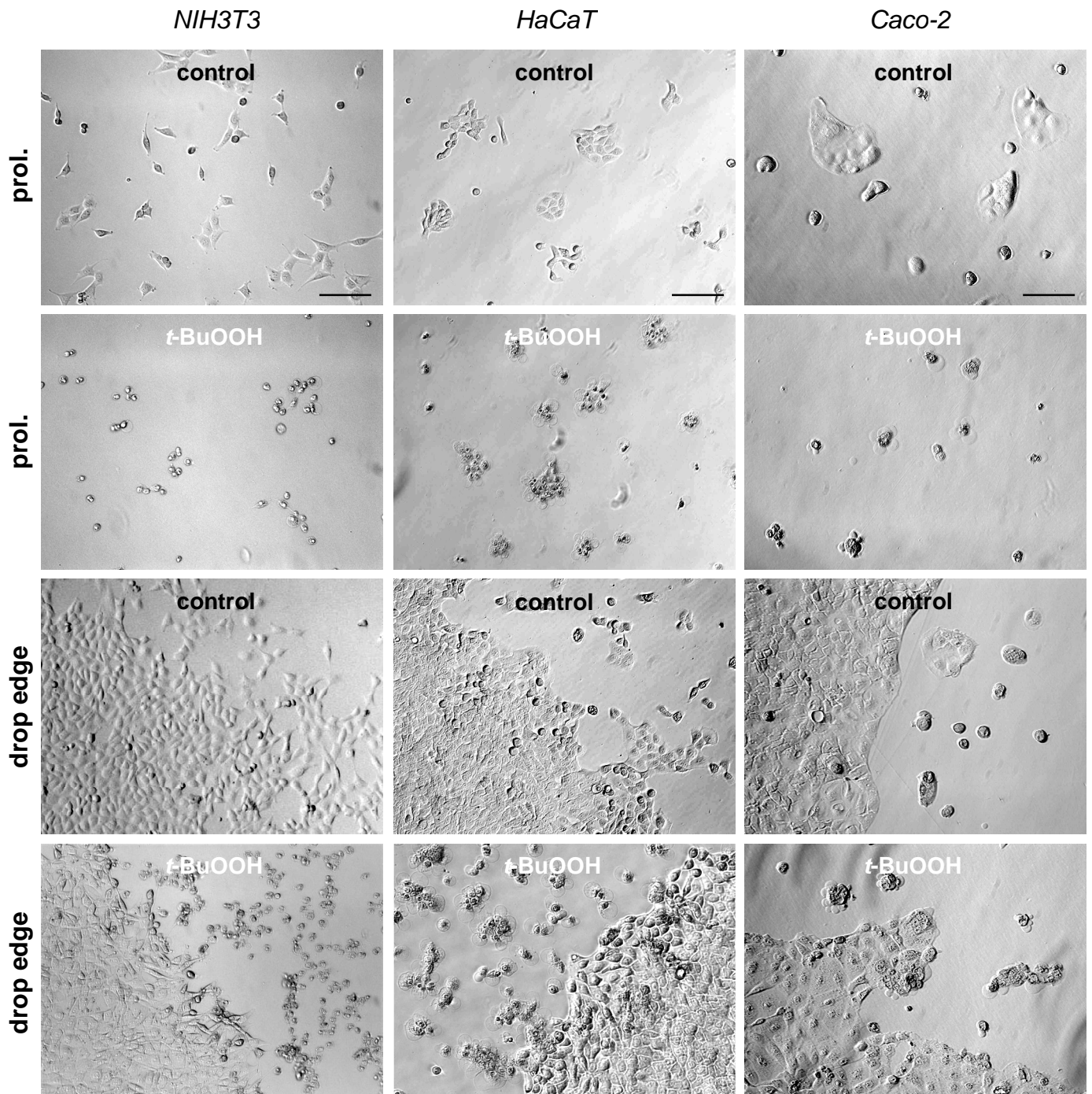
Fig. 20 Setup II confirms the resistance of confluent cells against t-BuOOH-induced cell death. Cells were seeded and cultivated upon setup II. Afterwards, cells were untreated (= control) or treated with t-BuOOH (NIH3T3: 50 µM, HaCaT: 200 µM, Caco-2: 100 µM) for 6 h. In contrast to survival of cells within the confluent drop area, semiconfluent cells at the drop edge and proliferating (prol.) control cells died from t-BuOOH-induced cell death, which was determined by light microscopic analysis of a necrosis-related morphology (cytosolic swelling, nuclei intact: see Figure 21 in detail; bar = 20 µm).

In contrast to survival of cells located within the confluent drop area, *t*-BuOOH induced a necrotic-like cell death in semiconfluent cells at the outer edge of the cell drop and – as expected – in proliferating control cultures according to necrosis-related morphological changes, as well as qualitative and quantitative analysis of AnnexinV-FITC / PI staining (Figure 21). Hence, these data exclude that resistance of confluent cells can be explained by distinct amounts of *t*-BuOOH molecules entering the cells but rather by the presence of cell-cell contacts.
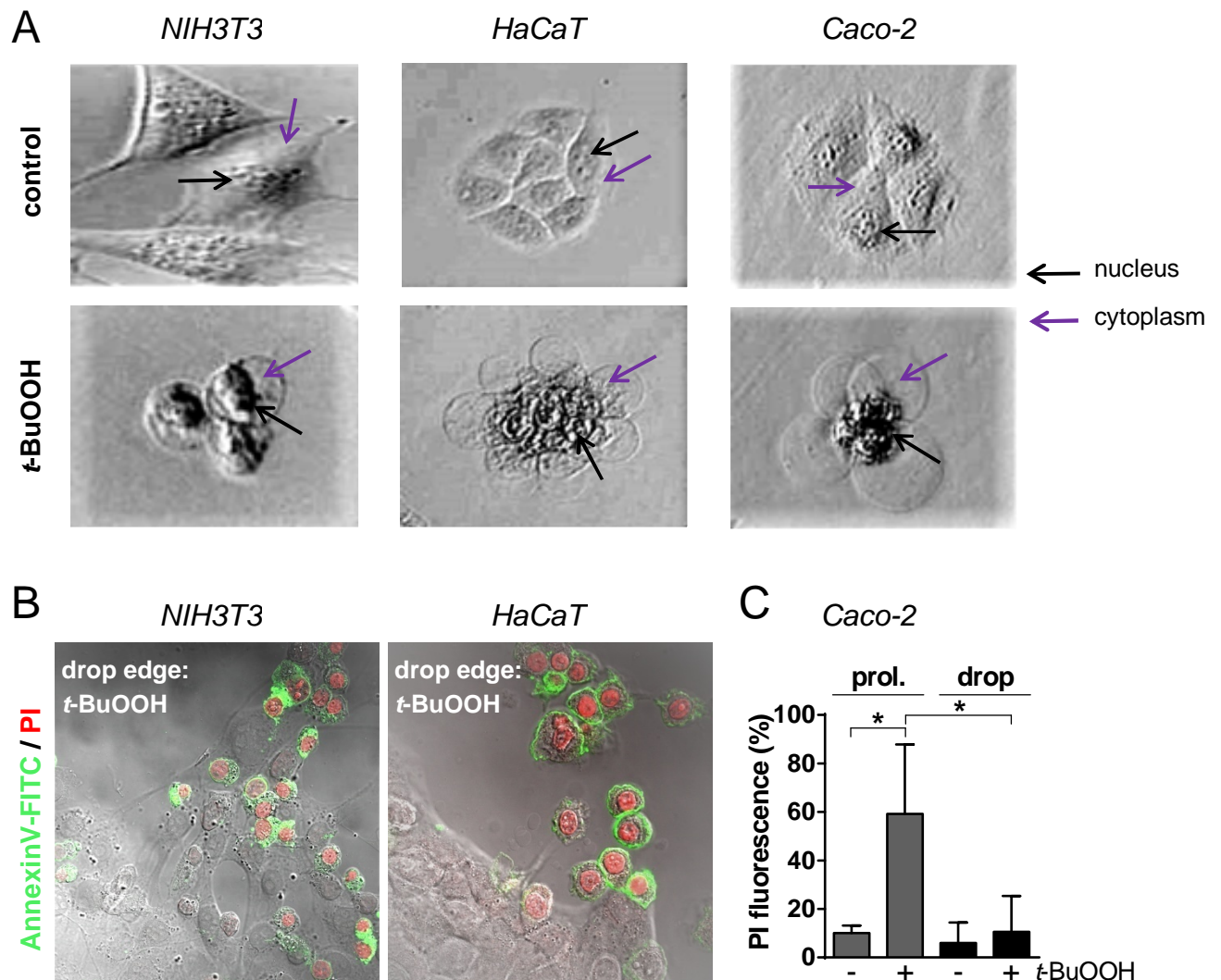
Fig. 21 Semiconfluent cells die from *t*-BuOOH-induced necrosis in contrast to resistant confluent cells upon setup II. **a-c** Cells were seeded and cultivated according to setup II followed by *t*-BuOOH treatment (NIH3T3: 50 µM; HaCaT: 200 µM; Caco-2: 100 µM; control = untreated) for 6-8 h. Necrosis in semiconfluent cells at the drop edge was supported by (**a**) light microscopy of necrosis-related morphological changes, e.g. cytosolic swelling but nuclei intact (2000-fold magnification) or by AnnexinV-FITC / PI staining, which was either (**b**) qualitatively assessed by laser scanning microscopy (bar = 20 µm) or (**c**) quantitatively by flow cytometric analysis (mean ± SD out of *n* = 2). Significance of necrosis was calculated with * *p* ≤ 0.1.

4.1.2 The redox state of confluent versus semiconfluent cells

t-BuOOH has been already described to induce a variety of different ROS species *in vitro* (Cadenas & Sies, 1982; Hix et al., 2000). On the other hand, a reduced generation of ROS (e.g., by H_2O_2) has been demonstrated upon an increased cell density of fibroblast and epithelial cultures (Day & Suzuki, 2006). Therefore, I have investigated the redox state of confluent versus semiconfluent cells.

To this end, a general ROS indicator, the chloromethyl derivative of 2-7-dichlorodihydrofluorescein diacetate (CM-H2DCFDA), was used to directly measure intracellular free radical production via flow cytometric analysis (Armstrong, 2010). Murine NIH3T3 cells and human Caco-2 cells were analyzed as model cell lines. According to Figure 22A, confluent and semiconfluent (prol., sd) NIH3T3 cells exhibit a similar ROS level prior to t-BuOOH exposure. Moreover, t-BuOOH induced an almost equal ROS increase (~ 2.5-fold) in confluent and proliferating cells over time. Despite serum-depleted cells demonstrated a slightly earlier and stronger increase (3-fold) in t-BuOOH-induced ROS – possibly due to a lower amount of FBS in the culture medium and therefore a lower level of exogenous ROS scavengers (Francis, 2010; Oberley et al., 1995) – free radical production was comparable to confluent cultures after 2 h of t-BuOOH exposure prior to necrosis induction (Figure 22B).
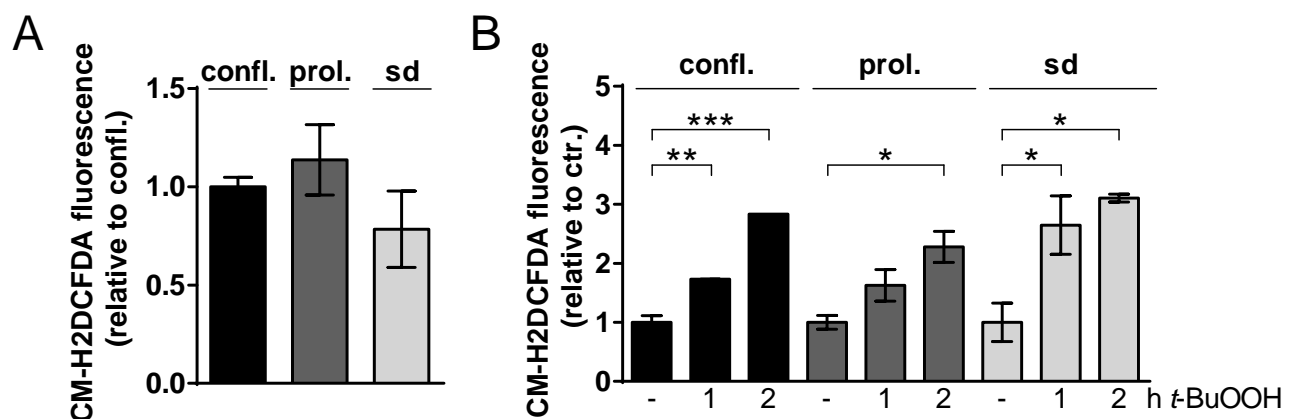
Fig. 22 Confluent (confl.) and semiconfluent (proliferating, prol.; serum-depleted, sd) NIH3T3 cells show a similar redox state in the absence and presence of t-BuOOH. **a,b** Cells were seeded and cultivated according to setup I. (**a**) Prior and (**b**) after exposure to 50 µM t-BuOOH for the indicated time points, cells were stained with CM-H2DCFDA followed by flow cytometric analysis. Fluorescence is presented relative to confluent cells or to untreated control cells (= 1; ctr.) as mean ± SD of n = 2-3 in duplicates. Significance between control and respective vehicle-treated cells was calculated with * p ≤ 0.05, ** p ≤ 0.01, *** p ≤ 0.001.

Similar results with regard to the redox state of confluent and semiconfluent cultures (prol., sd) were obtained in Caco-2 cells. In the absence of *t*-BuOOH, free radical production was almost the same, and also prior to induction of necrosis after 3 h of *t*-BuOOH exposure, ROS production (2-2.5-fold) was similar in confluent and semiconfluent Caco-2 cells (Figure 23A-B). This data support the assumption that – even upon experimental setup I – a similar amount of *t*-BuOOH molecules reaches confluent and semiconfluent cultures. In addition, it could be so far excluded that confluent cells are protected against *t*-BuOOH due to an increased detoxification.
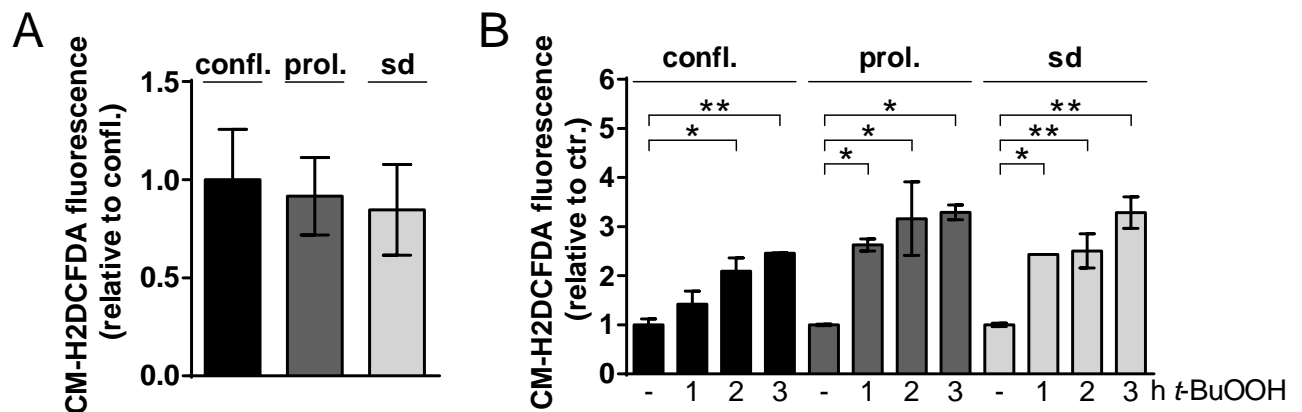
Fig. 23 Confluent (confl.) and semiconfluent (proliferating, prol.; serum-depleted, sd) Caco-2 cells show a similar redox state in the absence and presence of *t*-BuOOH. **a,b** Cells were seeded and cultivated upon setup I. (**a**) Prior and (**b**) after exposure to 100 µM *t*-BuOOH for the indicated time points, cells were stained with CM-H2DCFDA followed by flow cytometry. Fluorescence is presented relative to confluent cells or to untreated cells (= 1) as mean ± SD of *n* = 4 (**a**) or of a representative experiment out of *n* = 4-5 (**b**) in duplicates. Significance between control (ctr.) cells and respective vehicle-treated cells was calculated with * $p \leq 0.05$, ** $p \leq 0.01$, *** $p \leq 0.001$.

To further confirm results for an equal detoxification of *t*-BuOOH in confluent and semiconfluent (prol., sd) NIH3T3 and Caco-2 cells, the availability of GSH as the most abundant intracellular ROS scavenger was analyzed (Forman et al., 2009). Absorption measurement of the so-called Ellman's reagent (DTNB) demonstrated a similar GSH level in confluent and semiconfluent cells at the time point of *t*-BuOOH exposure (Figure 24A). Comparable results were obtained in HaCaT and MEF cells (data not shown). Unexpectedly, the basal GSH content was even diminished in confluent compared to proliferating Caco-2 cells (Figure 24B). Upon further analysis of the GSH regeneration capacity in the presence of *t*-BuOOH, the low assay sensitivity did not allow secure data reproduction but hinted towards a similar, time-dependent GSH consumption in confluent and semiconfluent NIH3T3 cells, whereas

confluent and semiconfluent Caco-2 cells rather exhibited an upregulation of this ROS scavenger upon t-BuOOH challenge (data not shown). Nevertheless, analysis of the basal GSH availability further supports the assumption that confluent cells are not protected against t-BuOOH-induced toxicity due to an increased ROS detoxification capacity.
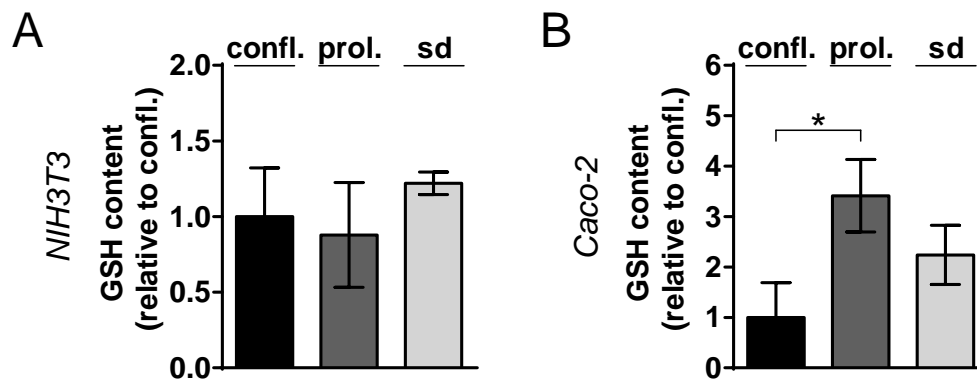
Fig. 24 Confluent (confl.) compared to semiconfluent (proliferating, prol.; serum-depleted, sd) cells display no upregulation of GSH at the time point of t-BuOOH exposure. **a-b** Cells were seeded and cultivated via setup I. Afterwards, the intracellular GSH content (relative to confluent, confl. = 1) was determined by the GSH assay and the protein concentration was assessed via the Bradford assay. Mean ± SD of n = 3 in triplicates. Significance was calculated with * $p \leq 0.05$.

4.1.3 Cell confluence inhibits t-BuOOH-induced mitochondrial damage

With the synthesis of vital ATP located to the mitochondria, the functionality of these organelles has been demonstrated to decide on cell survival and cell death (Neustadt & Pieczenik, 2008). Upon oxidative stress, the deregulation of the MMP ($\Delta\psi_m$) - an electrical gradient enabling ATP synthesis – has already resulted in the execution of necrotic cell death (Pastorino et al., 1999; Zong & Thompson, 2006). Thus, the functionality of these organelles was investigated in confluent versus semiconfluent cells upon t-BuOOH exposure.

As a rough measure for mitochondrial vitality, the activity of intracellular dehydrogenases was photometrically assessed via the MTT assay. According to Figure 25A-C, t-BuOOH induced a time-dependent reduction of the intracellular dehydrogenase activity in semiconfluent cultures (NIH3T3, HaCaT, Caco-2), whereas confluent cells were completely resistant. In addition, U0126-treated NIH3T3 cells demonstrated a similar decrease in dehydrogenase activity as proliferating cultures during t-BuOOH treatment (Appendix I, Figure A1).

Fig. 25 Confluent (confl.) compared to semiconfluent (proliferating, prol.; serum-depleted, sd) cells are protected against the time-dependent reduction of the intracellular dehydrogenase acitivity in the presence of t-BuOOH. **a-c** Cells were seeded and cultivated upon setup I followed by t-BuOOH treatment (NIH3T3: 30 μM, HaCaT: 200 μM; Caco-2: 100 μM). After incubation with MTT, formazan absorbance was assessed as a rough measure for intracellular dehyrogenase activity. Results are presented as mean ± SD of (**a-b**) n = 2-3 or of (**c**) a representative experiment out of n = 2, each 3-6 replicates. Significance of untreated control cells (= 1; ctr.) and respective vehicle-treated cells was calculated with * $p \leq 0.05$, ** $p \leq 0.01$, *** $p \leq 0.001$.

The decrease in intracellular dehydrogenase activity in t-BuOOH-treated semiconfluent cultures varied among the analyzed cell lines with regard to the final extent, onset and time-dependent progression. Interestingly, t-BuOOH started to affect the dehydrogenase activity in semiconfluent NIH3T3 and HaCaT cells within

the first 2-3 h of treatment, and therefore clearly prior to AnnexinV-FITC / PI-assessed induction of necrosis (see section 4.1.1.1). In contrast to that, the reduction of the dehydrogenase activity rather accompanied necrosis in semiconfluent Caco-2 cells at later treatment time points of 5-6 h.

Since results of the MTT assays hinted towards induction of mitochondrial damage upon t-BuOOH exposure in semiconfluent but not in confluent cultures, the mitochondrial vitality was more intensively investigated with help of the fluorescent dye DiOC6 (3,3′-dihexyloxacarbocyanine iodide) and flow cytometry. In the course of this, DiOC6 served as marker for the MMP ($\Delta\psi_m$) and therefore as an indicator for mitochondrial vitality in living cells. Necrotic cells were identified by simultaneous PI staining. Analysis of $\Delta\psi_m$ was only conducted in NIH3T3 and Caco-2 cells since results of the MTT assay were comparable in NIH3T3 and HaCaT cells. According to Figure 26A-B, confluent and semiconfluent cultures displayed a similar, not significantly different $\Delta\psi_m$ value at the time point of t-BuOOH exposure.

Fig. 26 Confluent (confl.) compared to semiconfluent (proliferating, prol.; serum-depleted, sd) cells exhibit a similar MMP ($\Delta\psi_m$) at the time point of t-BuOOH exposure. **a-b** Cells were seeded and cultivated upon setup I. Afterwards, cells were stained with DiOC6 and $\Delta\psi_m$ was assessed by flow cytometric analysis. Fluorescence is presented relative to confluent cells (= 1) as mean ± SD of (**a**) n = 3 or (**b**) of a representative experiment out of n = 3-4 in duplicates.

Moreover, the presence of t-BuOOH provoked a time-dependent reduction of $\Delta\psi_m$ in semiconfluent NIH3T3 and Caco-2 cells, whereas the MMP of confluent cells was hardly affected (Figure 27A-B). Interestingly, $\Delta\psi_m$ of semiconfluent NIH3T3 cells was already diminished prior to t-BuOOH-induced necrosis. On the other hand, a remarkable decrease in DiOC6 fluorescence was at first detected when t-BuOOH-mediated necrosis was already induced in semiconfluent Caco-2 cultures. In addition to that, an impact of cell cycle-driven effects on the resistance of confluent cells

against the loss of the MMP were excluded since serum-depleted and U0126-treated NIH3T3 cells demonstrated a similar, time-dependent decline in $\Delta\psi_m$ as proliferating cells upon t-BuOOH exposure (Figure 27A; Appendix I, Figure A2).
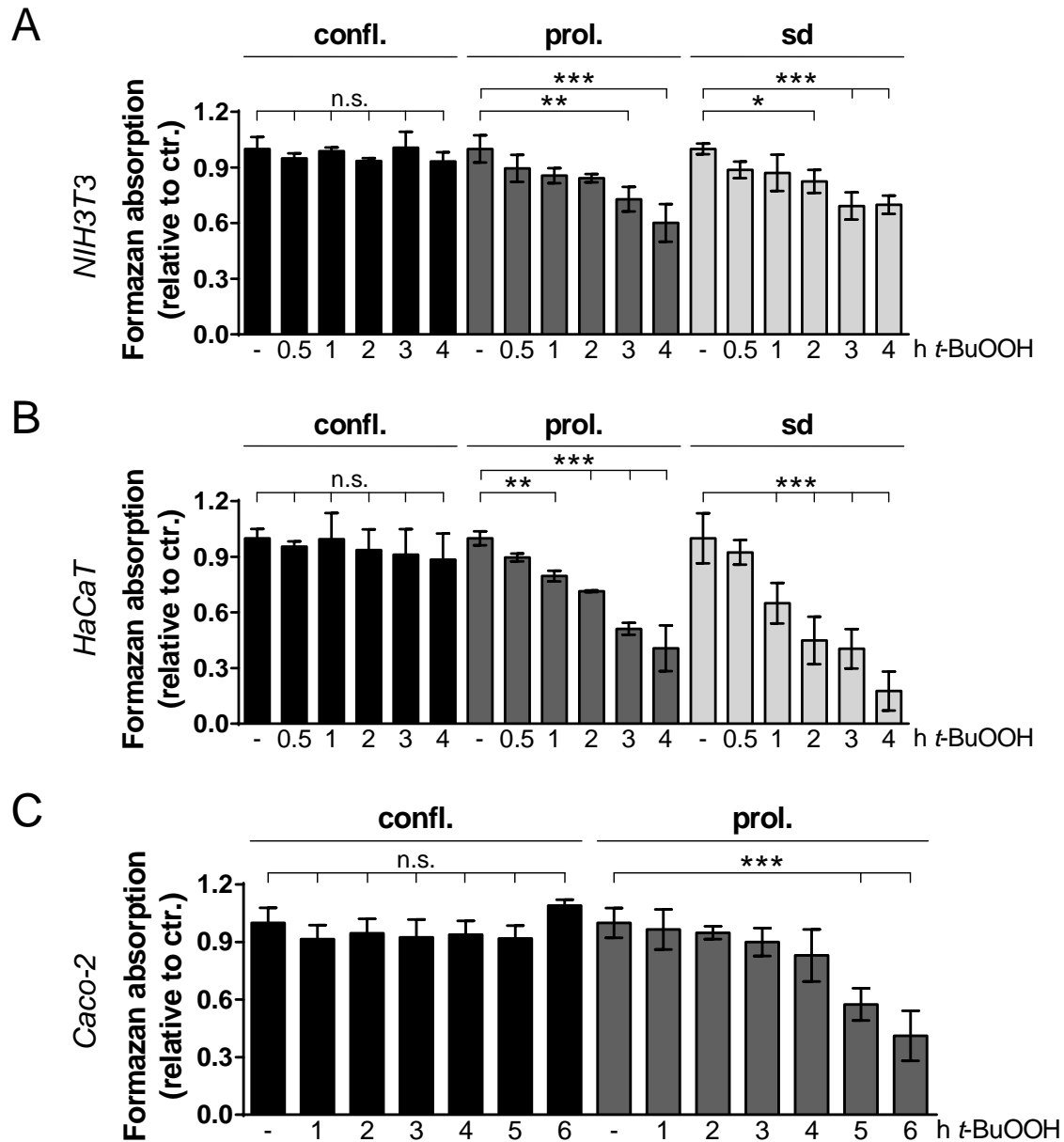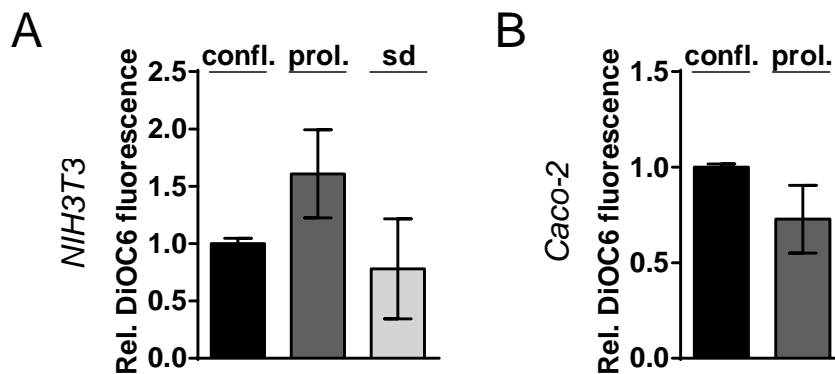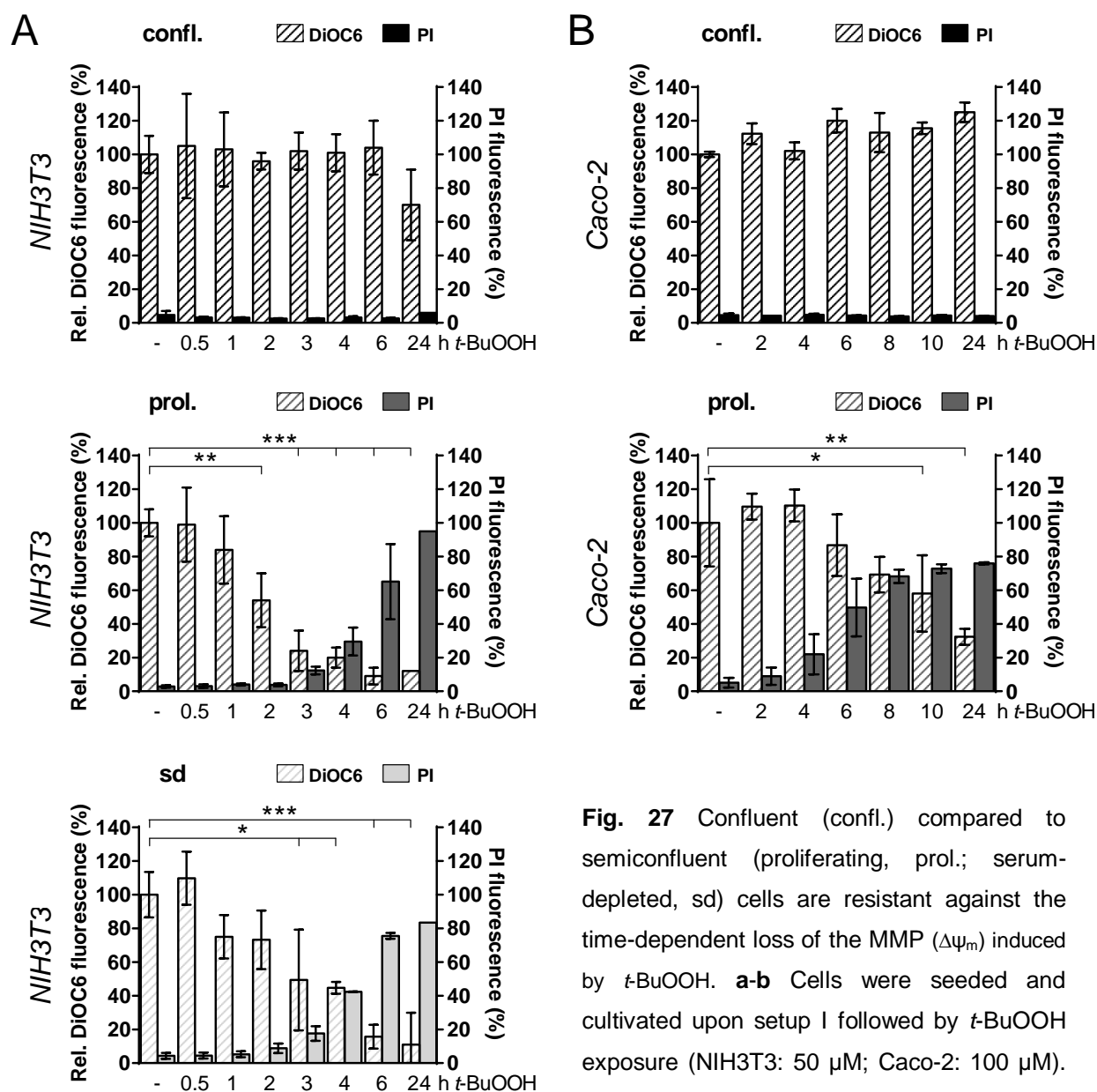

Fig. 27 Confluent (confl.) compared to semiconfluent (proliferating, prol.; serum-depleted, sd) cells are resistant against the time-dependent loss of the MMP ($\Delta\psi_m$) induced by t-BuOOH. **a-b** Cells were seeded and cultivated upon setup I followed by t-BuOOH exposure (NIH3T3: 50 µM; Caco-2: 100 µM). Afterwards, cells were stained with DiOC6 to assess $\Delta\psi_m$ and with PI to detect necrosis by flow cytometric analysis. DiOC6 fluorescence is presented relative to untreated control cells (= 100 %) as mean ± SD of (**a**) n = 3 or (**b**) of a representative experiment out of n = 2-3 in duplicates.

To further confirm the resistance of confluent cells against the loss of the MMP by t-BuOOH, $\Delta\psi_m$ was additionally analyzed with help of the dye MitoTracker Red CMXROS in confluent versus semiconfluent NIH3T3 cells. This dye accumulates in vital mitochondria due to a highly negative $\Delta\psi_m$ value, which occurs upon physiological conditions (Poot et al., 1996). According to Figure 28, laser scanning

microscopy further proved resistance of confluent cells against the loss of $\Delta\psi_m$ in the presence of *t*-BuOOH since MitoTracker Red CMXROS fluorescence was almost stable throughout 24 h treatment. In contrast, already 4 h *t*-BuOOH exposure drastically reduced mitochondrial MitoTracker Red CMXROS accumulation and therefore fluorescence in proliferating NIH3T3 cells. Hence, these data finally indicate that confluence protects against the loss of the MMP ($\Delta\psi_m$) induced by *t*-BuOOH.
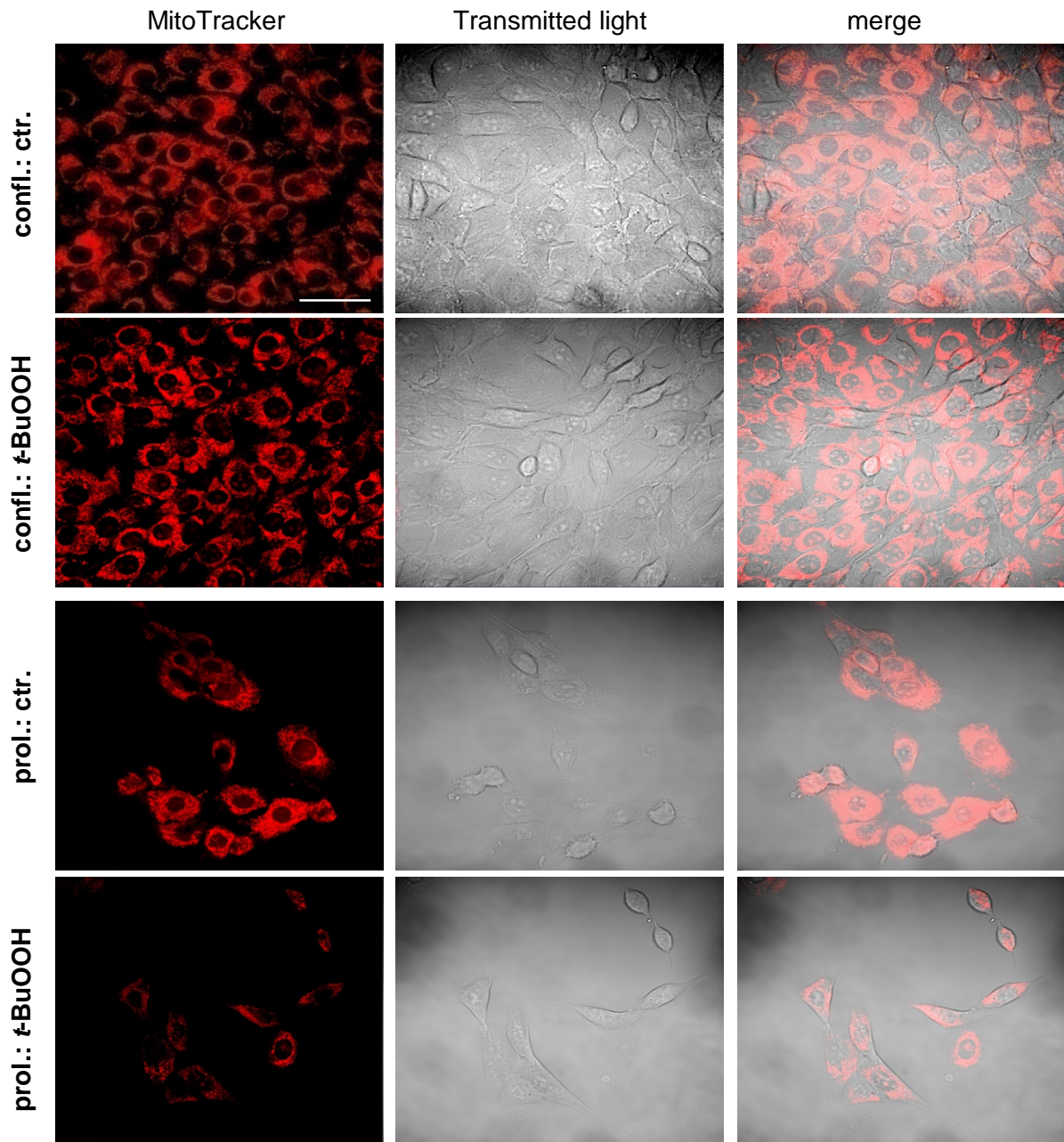
Fig. 28 Confluent (confl.) versus semiconfluent (proliferating, prol.) NIH3T3 cells are protected against *t*-BuOOH-induced mitochondrial damage. Cells were seeded and cultivated upon setup I. Afterwards, cells were treated with *t*-BuOOH (confl.: 24 h, 50 µM; prol.: 4 h, 50 µM) and stained with MitoTracker Red CMXROS as marker for $\Delta\psi_m$ followed by laser scanning microscopy (bar = 50 µm). ctr.= control

As loss of the MMP ($\Delta\psi_m$), as well as the lack of intracellular NAD^+ are tightly associated to failing of mitochondrial ATP synthesis followed by necrosis, the impact of t-BuOOH on the intracellular ATP and NAD^+ content was also examined in confluent versus semiconfluent NIH3T3 and HaCaT cultures (Galluzzi et al., 2014). Measurement of firefly luciferase activity, catalyzing the ATP-driven chemical conversion of luciferin and thereby luminescence, hinted towards an increased but, in the end, not significantly different amount of ATP in confluent versus semiconfluent (prol., sd) cells at the time point of t-BuOOH exposure (Figure 29A).
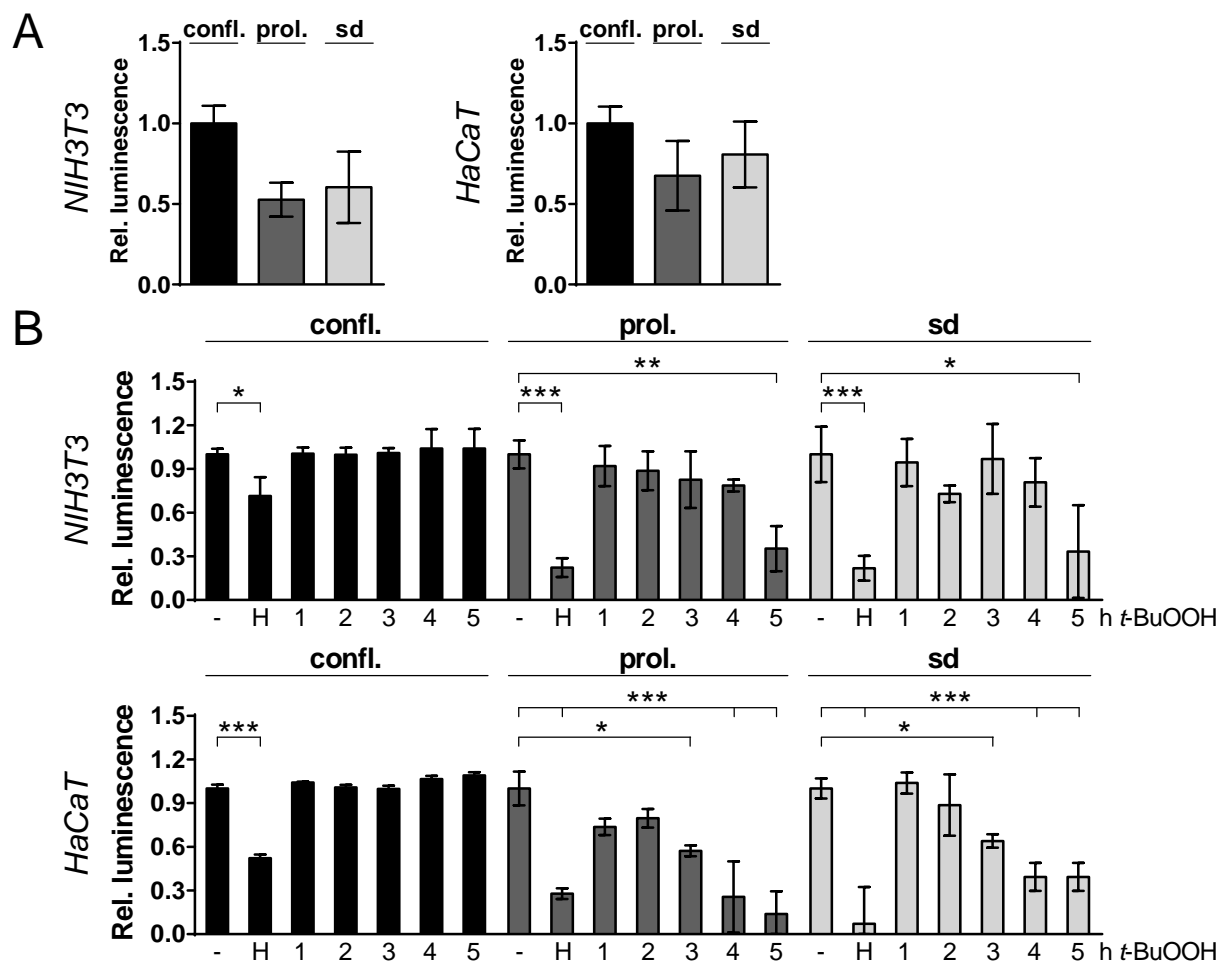
**Fig. 29** Upon a similar basal ATP level, confluent (confl.) compared to semiconfluent (proliferating, prol.; serum-depleted, sd) cells are resistant against the time-dependent loss of ATP in the presence of t-BuOOH. **a-b** Cells were seeded and cultivated upon setup I. Afterwards, (**a**) cells were either untreated or (**b**) cells were either treated with H_2O_2 (H: 10 mM, 10 min) or with t-BuOOH (NIH3T3: 50 µM; HaCaT: 200 µM). Intracellular ATP stores were calculated via measurement of firefly luciferase luminescence after cell lysis. Results are presented relative to confluent cells (**a**) or to untreated control cells (**b**) as mean ± SD of n = 2-3 (NIH3T3) or of a representative experiment out of n = 3 (HaCaT) in triplicates. Significance of untreated control cells (= 1) and respective vehicle-treated cells was calculated with * $p \leq 0.05$, ** $p \leq 0.01$, *** $p \leq 0.001$.

Caco-2 cells were not investigated since these cells exhibited a late decrease in $\Delta\psi_m$, rather accompanying necrosis. Furthermore, short-term treatment with H_2O_2 (10 mM) served as a positive control for ATP depletion. According to Figure 29B, t-BuOOH did not provoke initial depletion but rather a time-dependent reduction of the ATP level in semiconfluent cultures (prol., sd) prior to necrosis, whereby ATP stores of confluent cells were entirely not affected by the presence of t-BuOOH. The time-dependent reduction in ATP seen in semiconfluent cultures upon t-BuOOH exposure was accompanied by a time-dependent decline in cellular NAD^+ as detected by the photometric NAD^+ cycling assay (NIH3T3, HaCaT, Caco-2) (Figure 30).
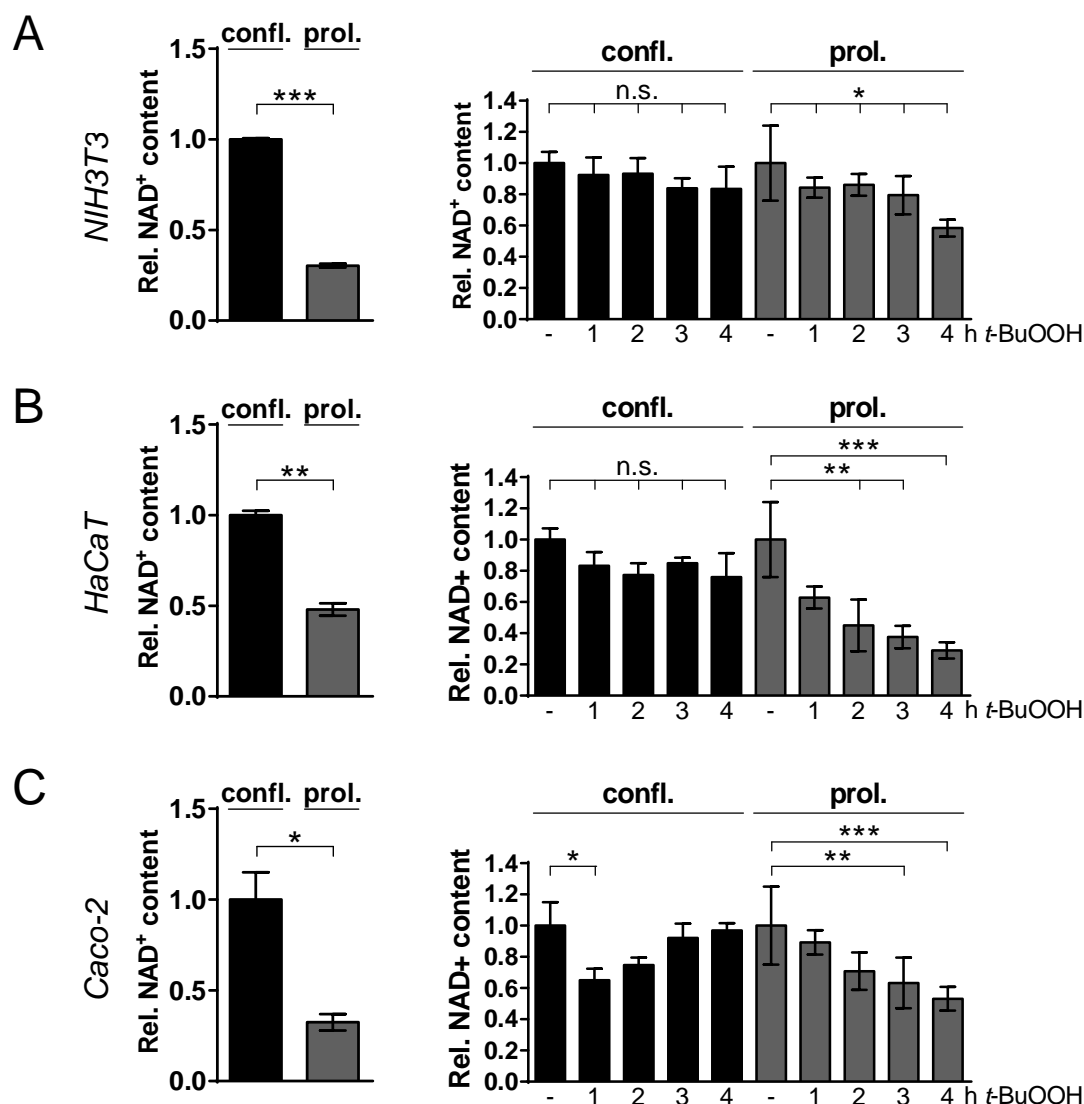
Fig. 30 Confluent (confl.) compared to semiconfluent (proliferating, prol.) cells exhibit a higher basal NAD^+ level and are protected against the time-dependent reduction of the NAD^+ level in the presence of t-BuOOH. **a-c** Cells were seeded and cultivated upon setup I. Afterwards, (*left*) cells were either untreated or (*right*) cells were treated with t-BuOOH (NIH3T3: 50 µM; HaCaT: 200 µM; Caco-2: 100 µM). The intracellular NAD^+ content was calculated via the NAD^+ cycling assay. Results are presented

relative to confluent cells (*left*) or to untreated control cells (*right*) as mean ± SD of $n = 3$ in triplicates. Significance was calculated with * $p \leq 0.05$, ** $p \leq 0.01$, *** $p \leq 0.001$.

Besides a significantly increased level of NAD$^+$ in confluent compared to semiconfluent cultures at the time point of *t*-BuOOH exposure, the intracellular NAD$^+$ content of confluent NIH3T3 and HaCaT cells was even stable in the presence of *t*-BuOOH. Unexpectedly, confluent Caco-2 cells exhibited an early, transient decrease in NAD$^+$, with control levels being restored within 4 h of *t*-BuOOH exposure.

4.1.4 Cell confluence inhibits *t*-BuOOH-induced DNA damage

So far, the resistance of confluent cells against replication-dependent, toxic DNA damage (e.g., DSBs) upon oxidative stress has been explained by cell cycle arrest (Jyonouchi et al., 1998; Persinger et al., 2001; Rancourt et al., 2002; Bakondi et al., 2003). In this context, mutagenic but not toxic DNA lesions (e.g., 8-oxo-dG or SSBs) that have been yet reported upon *t*-BuOOH exposure can be efficiently repaired via base excision repair (BER) in contrast to error-prone DSB repair mechanisms (Latour et al., 1995; Christmann et al., 2003; Tormos et al., 2004). In order to evaluate *t*-BuOOH-induced genotoxicity and to elucidate a possible role of cell-cell contacts in the regulation of DNA repair, *t*-BuOOH-induced DNA damage was investigated in confluent versus semiconfluent cultures.

First, the induction and repair capacity of DNA SSBs induced by *t*-BuOOH were analyzed in NIH3T3 cells as murine fibroblast cell line, as well as in Caco-2 cells as human epithelial model system (Figure 31-32). Microscopic analysis after performance of the alkaline Comet assay and PI staining revealed a similar SSB induction in confluent and semiconfluent (prol., sd) NIH3T3 cells after 20 min exposure to 30 µM or 50 µM *t*-BuOOH, respectively (Figure 31A). By comparison, confluent Caco-2 cells showed a significantly lower level of *t*-BuOOH-induced DNA SSBs when compared to proliferating cells (Figure 31B).
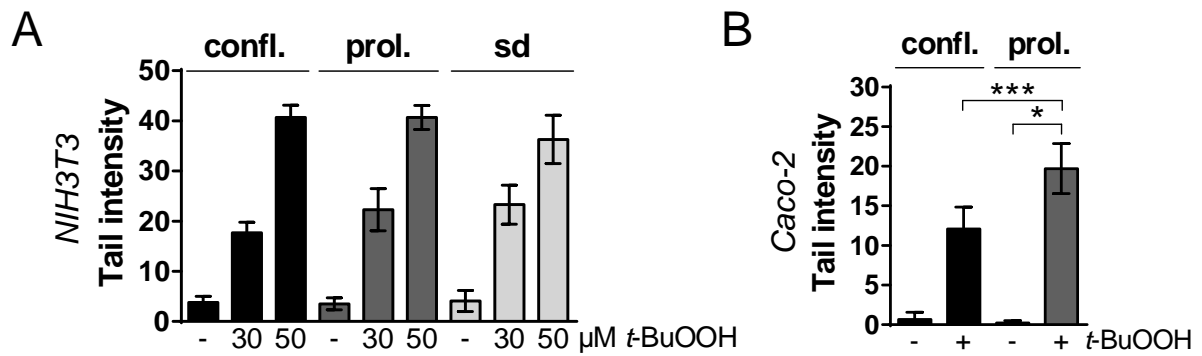
Fig. 31 Analysis of DNA SSBs induced by *t*-BuOOH in confluent (confl.) compared to semiconfluent (proliferating, prol.; serum-depleted, sd) cells. **a-b** Cells were seeded and cultivated upon setup I. After 20 min treatment with *t*-BuOOH (Caco-2: 100 µM), the alkaline Comet assay was conducted for detection of SSBs. Results are expressed as tail intensity and presented as mean ± SD of n = 2-3 with 50 cells analyzed per sample. Significance was calculated with * $p ≤ 0.05$, *** $p ≤ 0.001$.

Moreover, pulse treatment of NIH3T3 and Caco-2 cells followed by a recovery phase in the absence of *t*-BuOOH demonstrated an almost identical SSB repair velocity, with half of the lesions being repaired in confluent and proliferating cultures within ~ 30 - 40 min (Figure 32A-B). Even though serum-depleted NIH3T3 cells demonstrated a slightly higher level of initially induced SSBs (0 min after *t*-BuOOH pulse), these cells finally displayed a comparably efficient SSB repair capacity as seen in confluent and proliferating cells (240 min after *t*-BuOOH pulse).
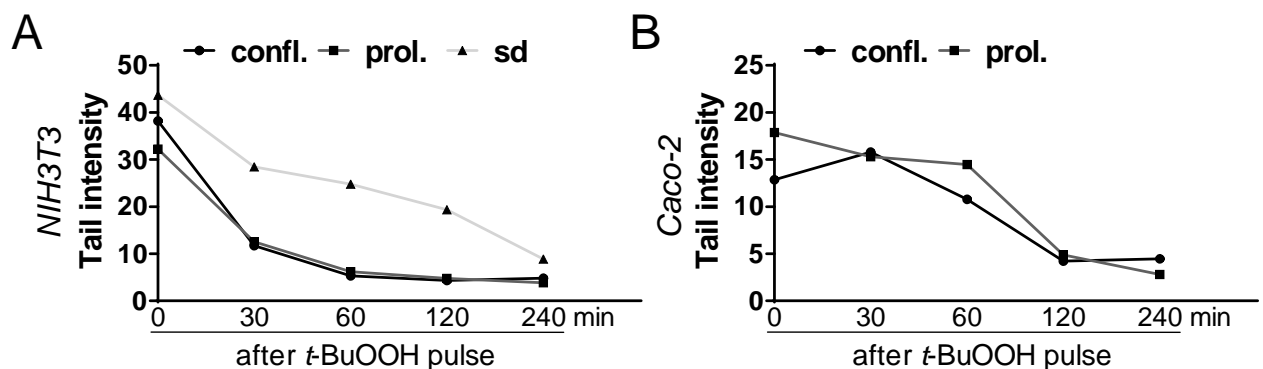
Fig. 32 Confluent (confl.) compared to semiconfluent (proliferating, prol.; serum-depleted, sd) cells demonstrate a similar repair velocity of *t*-BuOOH-induced DNA SSBs. **a-b** Cells were seeded and cultivated upon setup I. Afterwards, cells were treated for 20 min with *t*-BuOOH (NIH3T3: 50 µM; Caco-2: 100 µM) followed by performance of the alkaline Comet assay after the indicated recovery time points. Results are expressed as tail intensity and presented as mean ± SD of a representative experiment out of n = 2-3 with 50 cells analyzed per sample.

Upon a similar induction and repair of *t*-BuOOH-induced DNA SSBs, confluent NIH3T3 and Caco-2 cells were resistant against the time-dependent increase in DNA DSBs compared to *t*-BuOOH-treated semiconfluent (prol., sd) cultures as shown by the neutral Comet assay (Figure 33A-B). Interestingly, confluent Caco-2 cells were able to recover DSBs to the level of untreated controls within 4 h of *t*-BuOOH exposure, whereby confluent NIH3T3 cells displayed a kind of DSB steady state in the presence of *t*-BuOOH. In addition, U0126-treated NIH3T3 cells exhibited a similar amount of *t*-BuOOH-induced DSBs as proliferating cultures, indicating thereby again that not cell-cycle driven effects but rather the presence of cell-cell contacts provides resistance against *t*-BuOOH-induced DSBs (Appendix I, Figure A3).
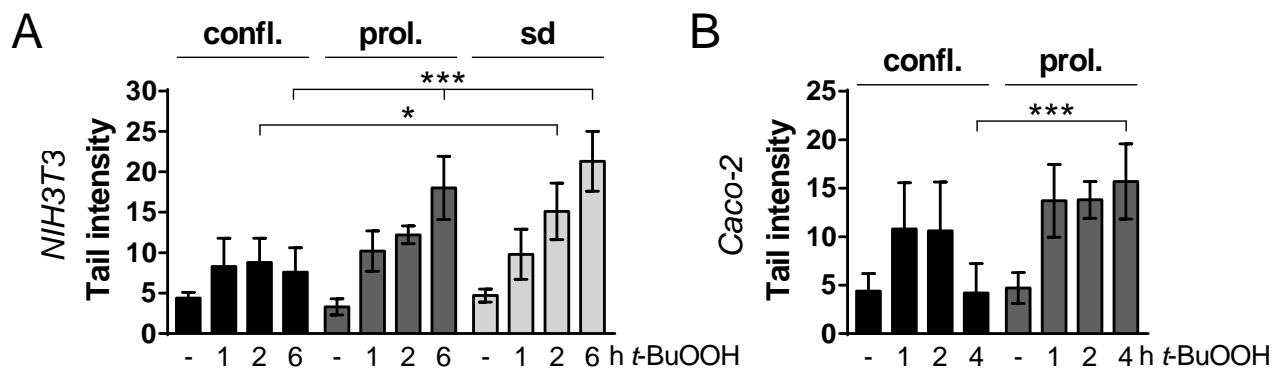
Fig. 33 Confluent (confl.) compared to semiconfluent (proliferating, prol.; serum-depleted, sd) cells are resistant against the time-dependent increase in DNA DSBs in the presence of *t*-BuOOH. **a-b** Cells were seeded and cultivated upon setup I. Afterwards, cells were treated with *t*-BuOOH (NIH3T3: 50 µM; Caco-2: 100 µM) for the indicated time points followed by performance of the neutral Comet assay. Results are expressed as tail intensity and presented as mean ± SD of n = 2-4 with 50 cells analyzed per sample. Significance was calculated with * $p ≤ 0.05$, *** $p ≤ 0.001$.

In the end, resistance of confluent cells against the time-dependent increase in *t*-BuOOH-induced DNA DSBs was confirmed by immunochemical analysis of phosphorylated histone 2A (γ-H2AX), recruiting proteins of the DNA damage response machinery for DSB repair (Chapman et al., 2012). Besides detection of γ-H2AX, also a possible DNA replication block was examined via EdU incorporation in NIH3T3 and Caco-2 cells. Laser scanning microscopy provided evidence for strongly elevated levels of γ-H2AX foci in semiconfluent control cells (prol.) and semiconfluent cells at the drop edge upon *t*-BuOOH exposure (Figure 34A, 35). In contrast to that, hardly any increase in this DSB marker was found in confluent cells / drop center upon setup I + II. Moreover, qualitative microscopic analysis of EdU incorporation indicates a similar block of replication in confluent and semiconfluent NIH3T3 and

Caco-2 cells (Figure 34B, 35). Hence, these data indicate that (i) *t*-BuOOH induces block of DNA replication independent of the confluence status, but at the same time that (ii) resistance against *t*-BuOOH-induced DSBs is mediated by cell-cell contacts.
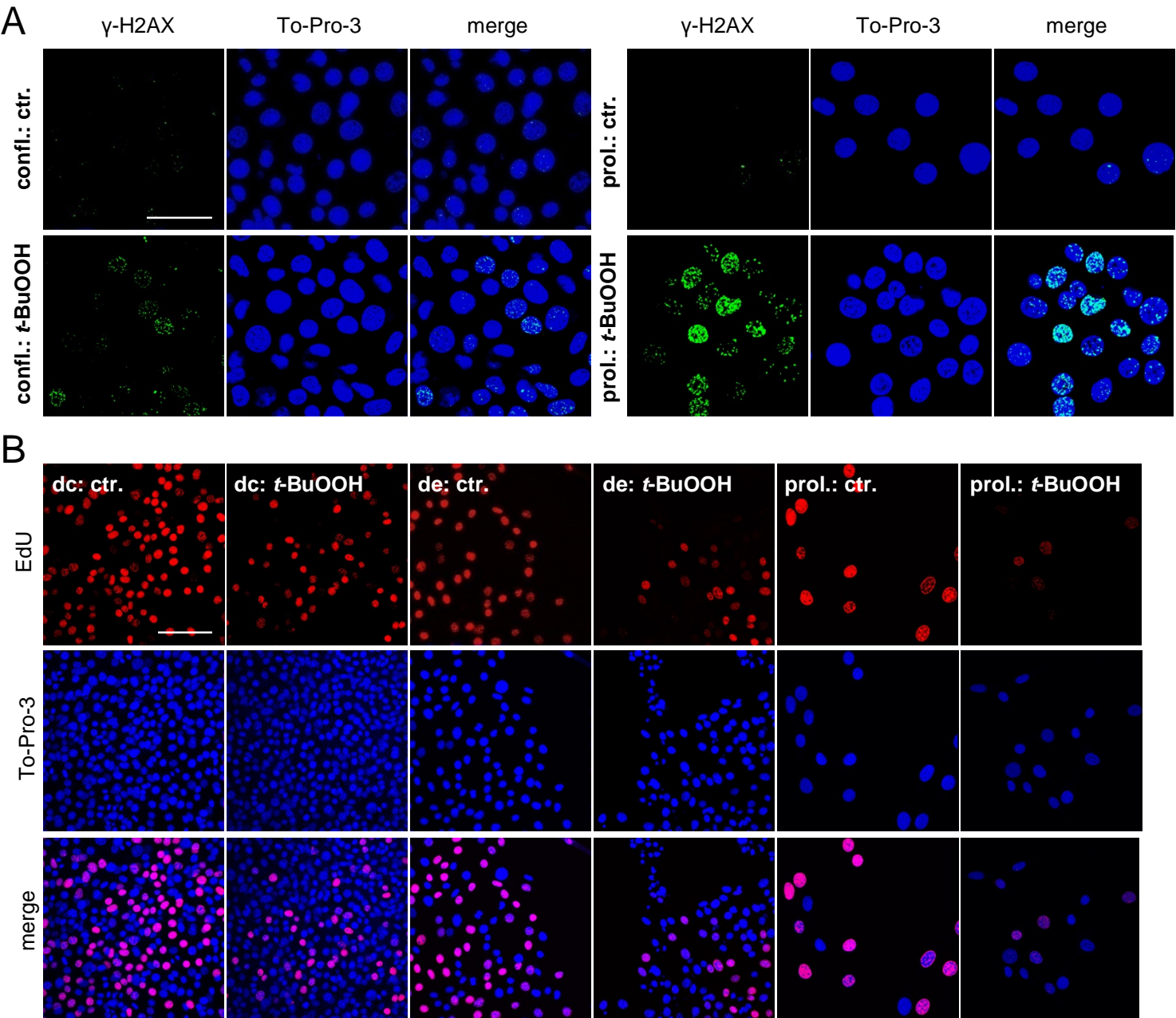
Fig. 34 Upon a similar block of replication, confluent compared to semiconfluent NIH3T3 cells are more resistant against the increase in γ-H2AX foci in the presence of *t*-BuOOH. **a-b** Cells were seeded and cultivated either (**a**) upon setup I (confluent, confl.; proliferating; prol.) or (**b**) upon set up II (dc = drop center; de = drop edge). Cells were either (**a**) treated with *t*-BuOOH (50 µM, 4 h) and stained with primary and secondary antibody for detection of γ-H2AX foci, or (**b**) cells were incubated with the S phase marker EdU followed by *t*-BuOOH treatment (50 µM, 4 h). To determine cell confluence, nucleic DNA was stained with To-Pro-3 prior to qualitative evaluation via laser scanning microscopy (bar = 50 µm). Analysis of NIH3T3 was conducted by D. Faust and C. Wenz. ctr. = control
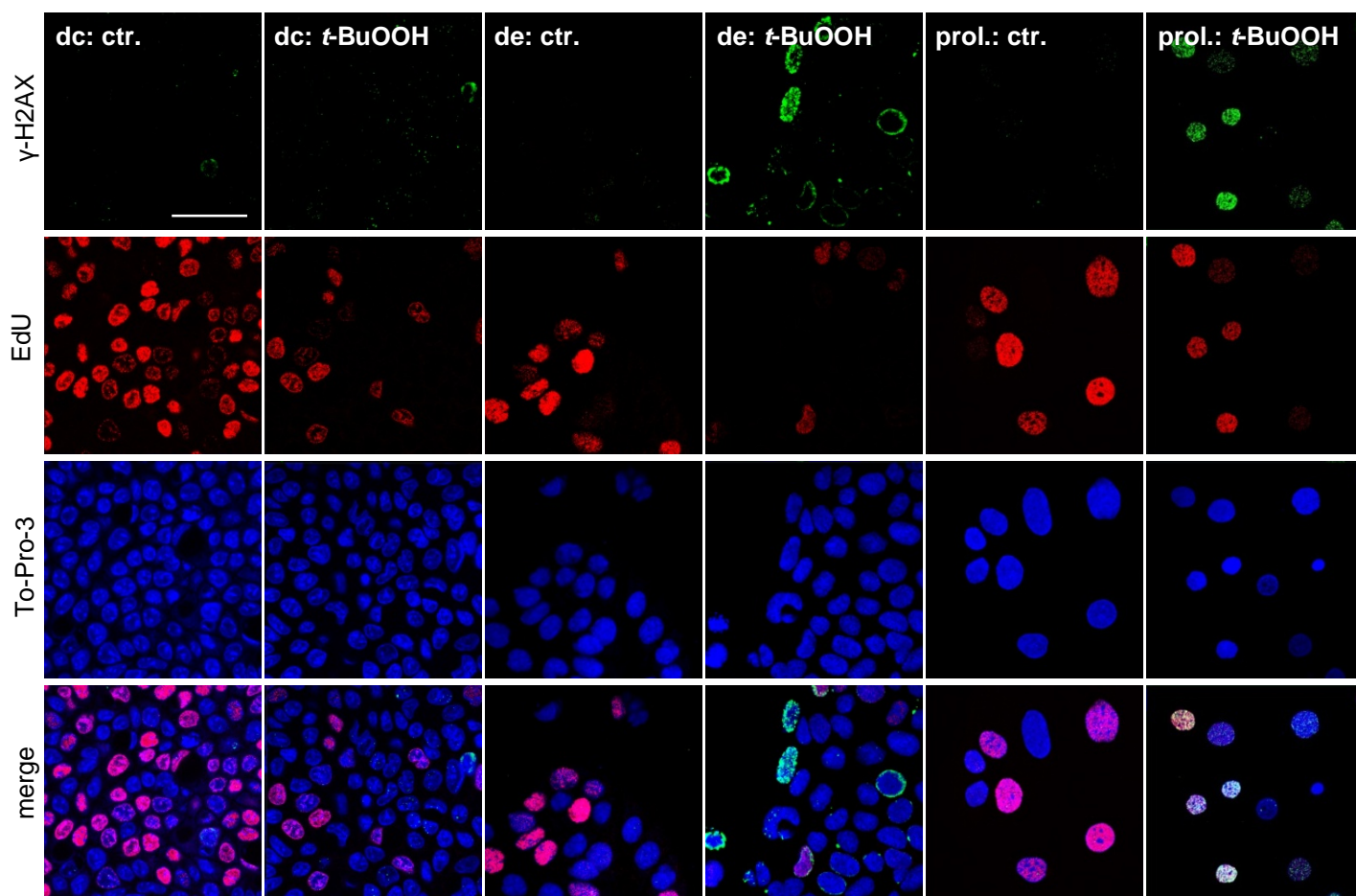
Fig. 35 Upon a similar block of DNA replication, confluent (drop center: dc) Caco-2 cells compared to semiconfluent control cells (proliferating, prol) and semiconfluent cells at the drop edge (de) are more resistant against the increase in γ-H2AX foci in the presence of t-BuOOH. Cells were seeded and cultivated upon set up II. Cells were incubated with the S phase marker EdU followed by treatment with 100 µM t-BuOOH for 4 h. Afterwards, cells were stained with primary and secondary antibody for detection of γ-H2AX foci. To determine cell confluence, nucleic DNA was stained with To-Pro-3 prior to qualitative evaluation via laser scanning microscopy (bar = 50 µm). ctr. = control

4.2 Characterization of *t*-BuOOH-induced cell death

With first results demonstrating a necrotic-like cell death induced by *t*-BuOOH, the secondary part of my work focused on the molecular mechanisms that mediate cellular damage and finally necrosis by this ROS inducer. Almost nothing is so far known about the exact cell death mechanism underlying *t*-BuOOH-induced necrosis. In this context, the classical image of chaotic necrosis has to be reconsidered due to the existence of necrosis subroutines that are tightly orchestrated upon the background of as referred to regulated necrosis (RN) (Galluzzi et al., 2014; Conrad et al., 2016; Galluzzi et al., 2018). Thus, distinct RN pathways, as well as the DNA damage response (DDR) machinery were investigated in proliferating fibroblasts (NIH3T3, MEF) and epithelial cells (HaCaT, Caco-2) to unravel the molecular mechanism of *t*-BuOOH-induced necrosis and thereby to elucidate the resistance of confluent cultures.

4.2.1 *t*-BuOOH-induced necrosis is executed independent of caspases

The execution of different RN subroutines has yet occurred either upon activation (e.g., pyroptosis) or inhibition (e.g., necroptosis) of certain caspases (Galluzzi et al., 2012, 2014, 2018). Therefore, a possible involvement of caspases in *t*-BuOOH-induced necrosis was analyzed in NIH3T3 and Caco-2 cells (Figure 36).

Since caspase 3 is one of the most frequently involved caspase in the execution of apoptosis but also of necrotic cell death modalities (Higuchi et al., 1998; Yuan et al., 2016), the activation and therefore cleavage of caspase 3 by *t*-BuOOH was investigated by Western Blot analysis. According to Figure 36A, the larger fragment (17 kDa) of cleaved caspase 3 became clearly visible when treating NIH3T3 cells with cisplatin or staurosporine – both described to induce apoptosis (Harr & Distelhorst, 2010). Contrarily to that, caspase 3 was entirely not activated by the presence of *t*-BuOOH. Similar results were obtained in confluent and serum-depleted NIH3T3 cultures (Appendix I, Figure A4), as well as in proliferating HaCaT cells (Wenz et al., 2018).
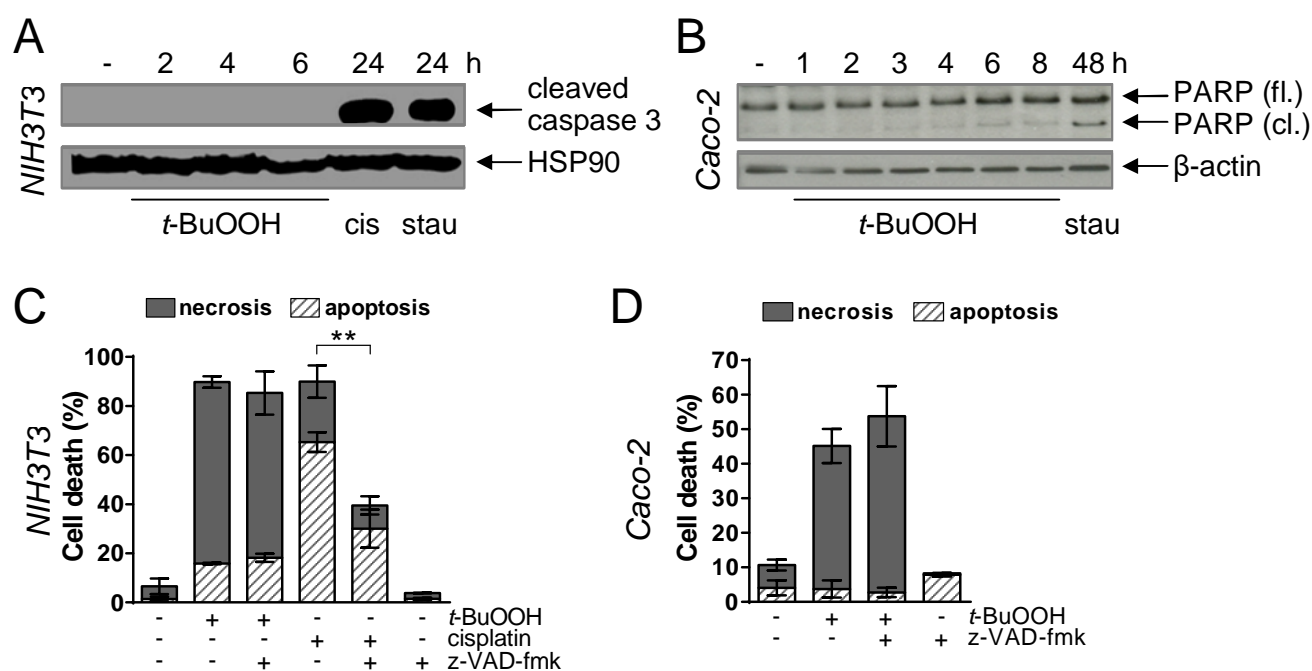
Fig. 36 *t*-BuOOH-induced necrosis is executed independent from caspases. **a-b** Cells were treated with *t*-BuOOH (a: 50 µM; b: 100 µM) or with positive controls for caspase activation: cisplatin (cis, 40 µM) and / or staurosporine (stau, 1 µM) for the indicated time points. Afterwards, cells were harvested for Western Blot analysis to detect either (**a**) activation of caspase 3 with HSP90 as loading control (conducted by D. Faust) or (**b**) caspase-dependent cleavage of PARP-1 with β-actin as loading control. **c-d** Cells were treated with *t*-BuOOH (c: 50 µM, 6 h; d: 100 µM, 8 h) or with cisplatin (c: 40 µM, 48 h) in the absence or presence of the pancaspase inhibitor z-VAD-fmk (20 µM). Cell death was analyzed via AnnexinV-FITC (apoptosis) / PI (necrosis) staining and flow cytometry (mean ± SD of *n* = 2 in duplicates). Significance was calculated with ** *p* ≤ 0.01. fl. = full-length; cl. = cleaved

Cleavage of PARP-1, which is known to occur upon caspase-mediated cell death (Chaitanya et al., 2010), was evaluated as alternative marker for caspase activity since no signal of the caspase 3 antibody was detectable in Caco-2 cells. In contrast to a visible activation and therefore cleavage of PARP-1 by staurosporine, cleaved PARP-1 was hardly detectable at early time points of *t*-BuOOH exposure (< 4 h) (Figure 36B). Despite PARP-1 cleavage slightly increased at later time points of *t*-BuOOH exposure, a crucial role of caspases in the regulation of *t*-BuOOH-induced necrosis was so far excluded since PARP-1 was not cleaved prior to the induction of necrosis (< 4 h) in Caco-2 cells.

Besides subG1 analysis did not demonstrate a sign for caspase-related DNA fragmentation (Appendix I, Table 2), independence of *t*-BuOOH-induced necrosis from caspase activity was finally confirmed by the chemical inhibitor z-VAD-fmk, which is able to inhibit cellular caspase activity (Van Noorden et al., 2001). In contrast to significant inhibition of cisplatin-induced apoptosis in NIH3T3 cells, z-VAD-fmk had

no remarkable effect on *t*-BuOOH-induced necrosis in NIH3T3 and Caco-2 cells (Figure 36C-D). Hence, *t*-BuOOH induces a necrotic cell death mechanism, which is executed independent of caspases.

4.2.2 p53 is not crucial for *t*-BuOOH-induced necrosis

Since the DNA damage sensor p53 has been yet described to induce caspase-independent RN pathways, such as MPT-driven necrosis or PARP-1-mediated necrosis upon H_2O_2 exposure (Vaseva et al., 2012; Montero et al., 2013), a possible regulatory function of p53 in *t*-BuOOH-induced necrosis was investigated.

Western Blot analysis revealed accumulation of p53 upon UV-C radiation of NIH3T3 cells in accordance to their genetic p53 wild type (wt) status. In contrast, no upregulation of p53 total protein was detected in the presence of *t*-BuOOH (Figure 37A). However, a transient phosphorylation (Ser15) of p53 was induced by *t*-BuOOH prior to necrosis induction, most likely in response to the rapid formation of t-BuOOH-induced DNA damage (Figure 37B).
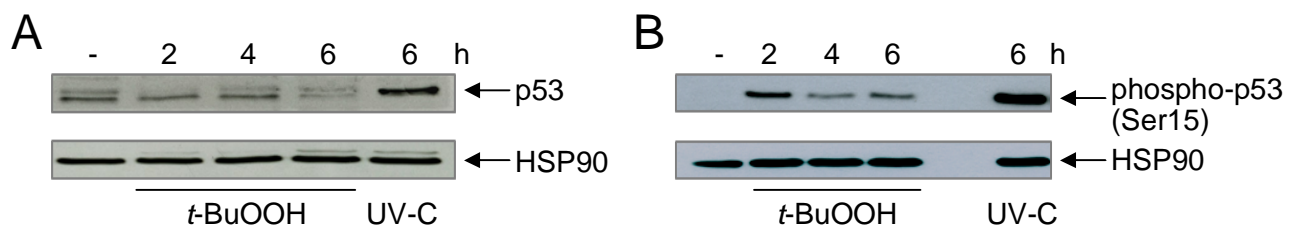
Fig. 37 *t*-BuOOH induces no accumulation but transient phosphorlyation of p53. **a-b** NIH3T3 cells were either exposed to UV-C radiation (20 J / m^2) as positive control or treated with *t*-BuOOH (50 µM). After the indicated time points, cells were harvested for Western Blot analysis of either (**a**) p53 total protein or (**b**) phosphorylation (Ser15) of p53 with HSP90 as loading control (conducted by D. Faust).

The hypothesis of *t*-BuOOH-induced necrosis to be executed independent of p53 was supported by cell death analysis of p53wt and p53 knockout ($^{-/-}$) MEFs. Western Blot analysis confirmed the p53 genotype status of these cells and flow cytometric analysis after AnnexinV-FITC / PI staining indicated a similar amount of necrosis in *t*-BuOOH-treated p53wt and p53$^{-/-}$ MEF cells (Figure 38A-B).
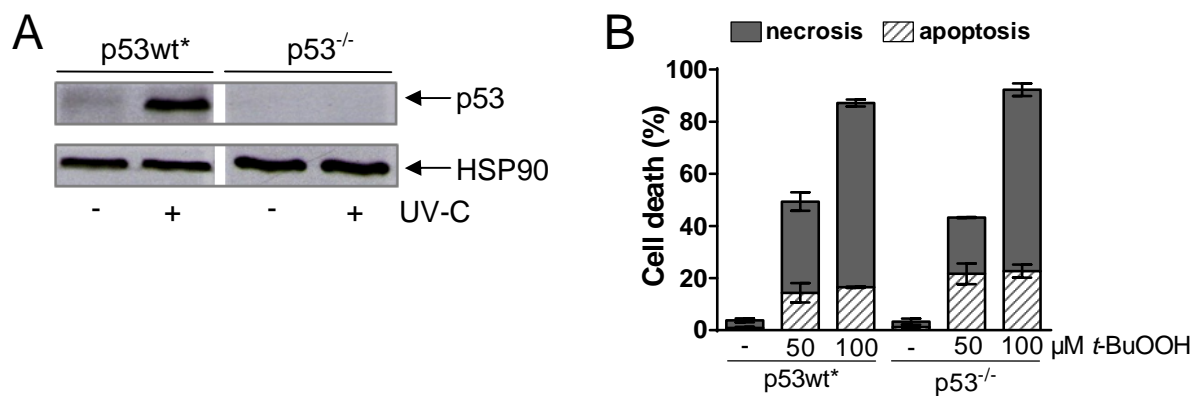
Fig. 38 *t*-BuOOH-induced necrosis is executed independent of p53. **a-b** MEF p53wt* and MEF p53$^{-/-}$ cells (see 2.6) were either (**a**) exposed to UV-C radiation (20 J / m^2) as positive control followed by Western Blot analysis of p53 expression with HSP90 as loading control after 6 h (conducted by D. Faust) or (**b**) cells were treated with *t*-BuOOH for 6 h. Cell death was analyzed via AnnexinV-FITC (apoptosis) / PI (necrosis) staining and flow cytometry (mean ± SD of *n* = 2 in duplicates).

A crucial regulatory function of p53 in *t*-BuOOH-induced necrosis was further excluded due to similar cell death execution in all of the tested murine and human cell lines upon a distinct genetic background with regard to p53. Compared to the afore mentioned p53wt status of NIH3T3 cells and other analyzed fibroblast cell lines (MEF, Swiss3T3, FH109), Western Blot analysis provided evidence for (i) expression of mutated p53 in HaCaT cells (Boukamp et al., 1988; Dietrich et al., 2001) and for (ii) a p53 null mutation in Caco-2 cells (Abraham et al., 1998; Djelloul et al., 1997; Liu & Bodmer, 2005), which results in lacking p53 expression (Figure 39). Despite a transient phosphorylation of p53 in NIH3T3 cells, these data indicate that p53 is not crucially involved in *t*-BuOOH-induced necrosis.
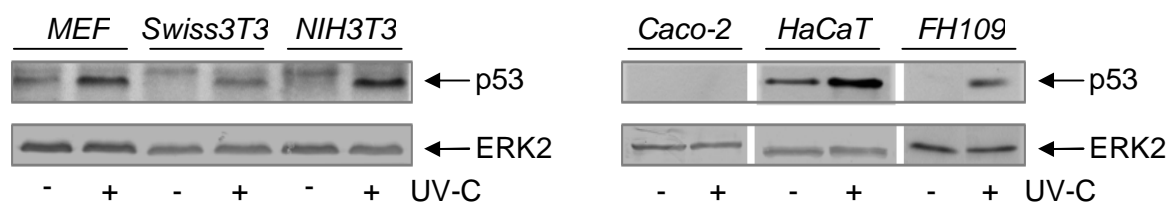
Fig. 39 p53 expression in murine and human cell lines that similarly die from t-BuOOH-induced necrosis upon a distinct p53 genotype status. Murine (*left*; MEF, Swiss3T3, NIH3T3: p53wt) and human (*right*; HaCaT: p53 mutated; Caco-2: p53 null mutation; FH109: p53wt) cells were either untreated or radiated with UV-C (20 J / m^2) as positive control. After 6 h, cells were harvested and Western Blot analysis was performed to detect p53 expression with ERK2 as loading control (conducted by D. Faust and C. Wenz).

4.2.3 A role of p38 and JNK1/2 in *t*-BuOOH-induced necrosis?

The stress kinases p38 and JNK1/2 have been widely characterized as crucial mediators of apoptotic, as well as necrotic cell death upon H_2O_2-induced DNA damage (Shen et al. 2004; Zhang et al. 2007; Kim et al. 2009; Xia et al. 2009; Gaballah et al. 2012; Watanabe et al. 2015). On the other hand, p38 and JNK1/2 can exhibit prosurvival functions (Sabapathy et al. 1999; Deng et al. 2001; Pereira et al. 2013). Therefore, a possible role of p38 and JNK1/2 in the regulation of *t*-BuOOH-induced necrosis was analyzed in NIH3T3 and Caco-2 cells.

The activation and therefore phosphorylation of p38 (Thr180 / Tyr182) and JNK1/2 (Thr183 / Tyr185) was investigated with help of the positive control anisomycin – a prominent inducer of p38 and JNK1/2 (Rennefahrt et al., 2002; Faust et al., 2012). According to Figure 40A-B, a strong phosphorylation of p38 and JNK1/2 upon anisomycin treatment proved the ability of NIH3T3 and Caco-2 cultures to activate both stress kinases. A time-dependent, persistent activation of p38 was also detected in both cell lines upon *t*-BuOOH exposure, whereby the maximum antibody signal occurred when necrosis was already executed (> 4 h). In contrast to that, NIH3T3 cells demonstrated only a transient activation of JNK1/2 prior (< 4 h) to *t*-BuOOH-induced necrosis. Unexpectedly, *t*-BuOOH treatment rather likely diminished the basal level of JNK phosphorylation in Caco-2 cells.
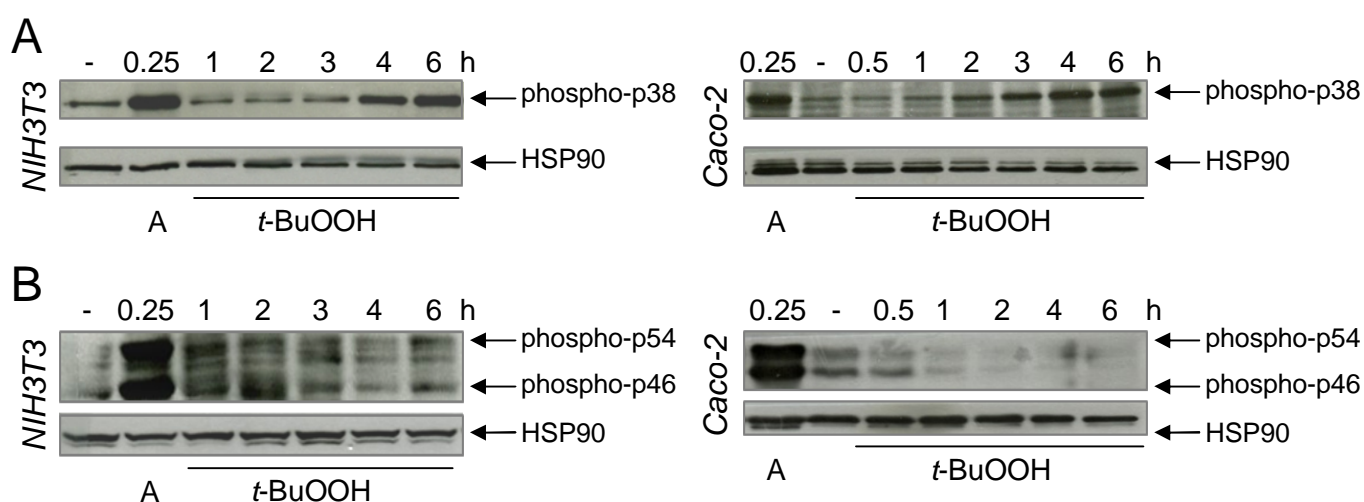
Fig. 40 Activation of p38 and JNK1/2 upon *t*-BuOOH exposure. **a-b** Cells were either exposed to anisomycin (A: 5 µg / µL; 15 min) as positive control or treated with *t*-BuOOH (NIH3T3: 50 µM; Caco-2: 100 µM) for the indicated time points. Afterwards, cells were harvested for Western Blot analysis to detect either (**a**) phosphorylation of p38 (Thr180 / Tyr182) with HSP90 as loading control, or (**b**) phosphorylation of JNK1/2 (p54, p46: Thr183 / Tyr185) with HSP90 as loading control.

To further elucidate the role of both stress kinases in *t*-BuOOH-mediated necrosis, p38 was pharmacologically inhibited by SB203580 (Cuenda et al., 1995) and JNK1/2 by SP600125 (Bennett et al., 2001). The specificity of these inhibitors was supported by Western Blot analysis (Figure 41A-B). In NIH3T3 cells, SB203580 and SP600125 clearly diminished anisomoycin-induced phosphorylation of the p38 downstream target MAPKAP kinase 2 (Thr334) or JNK1/2-activated ATF-2 (Thr71), respectively. Since the JNK inhibitor SP600125 had no effect on ATF-2 phosphorylation in Caco-2 cells (data not shown), phosphorylated c-jun (Ser63) was investigated as an alternative prototype of a JNK1/2-activated downstream target (Bogoyevitch & Kobe, 2006). Moreover, specificity of SB203580 was directly evaluated in Caco-2 cells by means of p38 phosphorylation. Western Blot analysis finally proved specificity of both inhibitors also in Caco-2 cells.
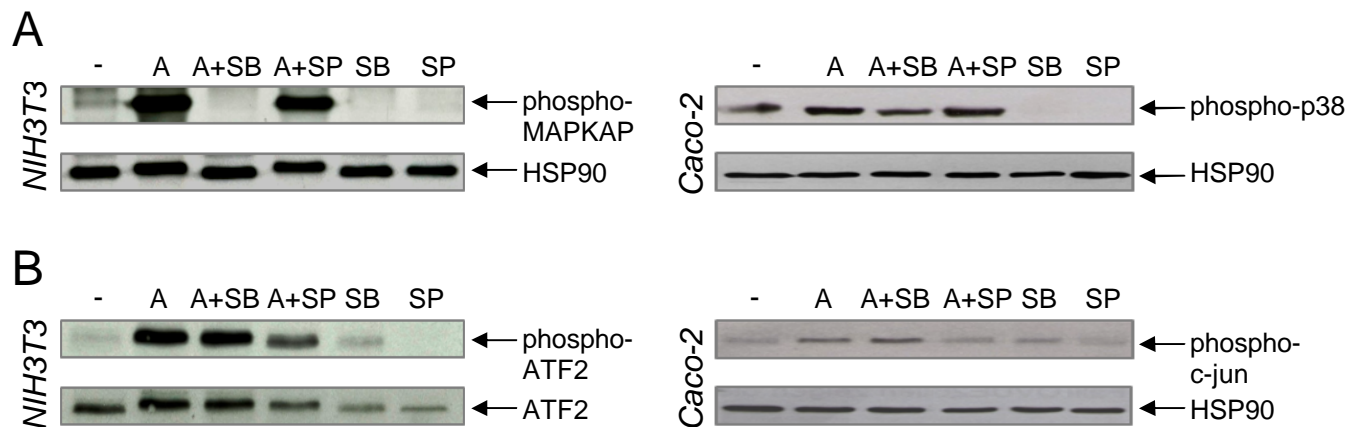
Fig. 41 Specific inhibition of p38 by SB203580 and JNK1/2 by SP600125. **a-b** Cells were exposed to anisomycin (A: 5 μg / μL; 15 min) as positive control in the absence or presence of the p38 inhibitor SB203580 (SB: 10 μM) or the JNK inhibitor SP600125 (SP: 25 μM). Afterwards, cells were harvested for Western Blot analysis to detect either (**a**) phosphorylation of the p38 downstream target MAPKAP (Thr334) or p38 phosphorylation (Thr180 / Tyr182) with MAPKAP or HSP90 as loading control, or (**b**) phosphorylation of the JNK1/2 downstream targets ATF2 (Thr71) or c-jun (Ser63) with ATF2 or HSP90 as loading control. Analysis of NIH3T3 cells was conducted by D. Faust.

Interestingly, AnnexinV-FITC / PI staining and flow cytometry revealed a prosurvival role of JNK1/2 in NIH3T3 and Caco-2 cells since *t*-BuOOH-induced necrosis was significantly enhanced by SP600125. On the other hand, inhibition of p38 by SB203580 strongly promoted *t*-BuOOH-induced necrosis in NIH3T3 cells but only slightly in Caco-2 cells (see Figure 42A-B). Nevertheless, p38 and JNK1/2 appear not essential for the execution of *t*-BuOOH-induced necrosis but seem to have a prosurvival, anti-necrotic function in this context.
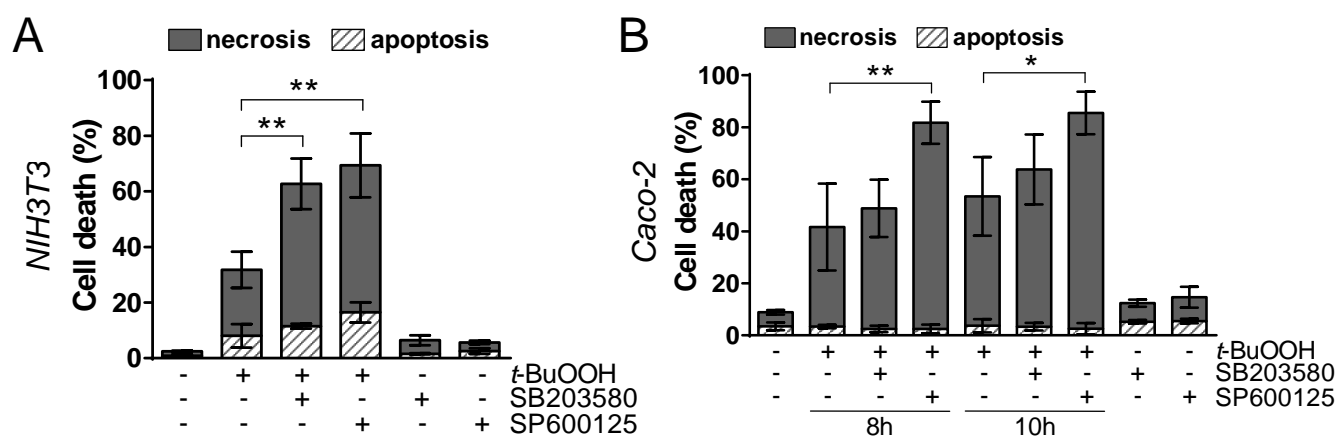
Fig. 42 Inhibition of p38 and JNK accelerates *t*-BuOOH-induced necrosis. **a-b** Cells were either untreated or treated with *t*-BuOOH (**a**: 30 µM, 6 h; **b**: 100 µM) in the absence or presence of the p38 inhibitor SB203580 (10 µM) or the JNK inhibitor SP600125 (25 µM). Subsequently, cells were stained with AnnexinV-FITC (apoptosis) / PI (necrosis) and cell death was analyzed via flow cytometry (mean ± SD of n = 2-5 in duplicates). Significance was calculated with * $p \leq 0.05$, ** $p \leq 0.01$.

4.2.4 ATR but not ATM inhibition reinforces *t*-BuOOH-induced necrosis

Besides p38 and JNK, also ATR and ATM kinase, as well as their related downstream targets, Chk1 and Chk2, have been widely implicated in the regulation of DNA damage-induced necrosis upon oxidative stress (Baritaud et al., 2012; Yan, 2014). Furthermore, pharmacological inhibition of ATR and ATM kinase is a promising tool in cancer therapy with regard to the radiosensitizing effect of both inhibitors (Weber et al., 2015). Thus, modulation of *t*-BuOOH-induced necrosis via ATR and ATM kinase was explored with a focus on tumorigenic Caco-2 cells.

According to Figure 43A-B, Western Blot analysis of Caco-2 cells provides evidence for (i) UV-C to induce activation and therefore phosphorylation (Ser345) of the ATR target Chk1 upon SSB formation, and (ii) phosphorylation (Thr68) of the ATM target Chk2 upon DSB induction by y-irradiation (Matsuoka et al., 2000; Mimmler et al., 2016). In this context, UV-C-induced Chk1 phosphorylation occurred slightly earlier than y-radiation-mediated Chk2 phosphorylation. A similar temporal sequence in Chk1 and Chk2 activation was observed in the presence of *t*-BuOOH but at later time points (3-5 h) when compared to both positive controls (0.5-2 h). However, while Chk1 phosphorylation was only transiently induced by *t*-BuOOH, Chk2 phosphorylation rather persisted throughout the whole treatment.

A

B
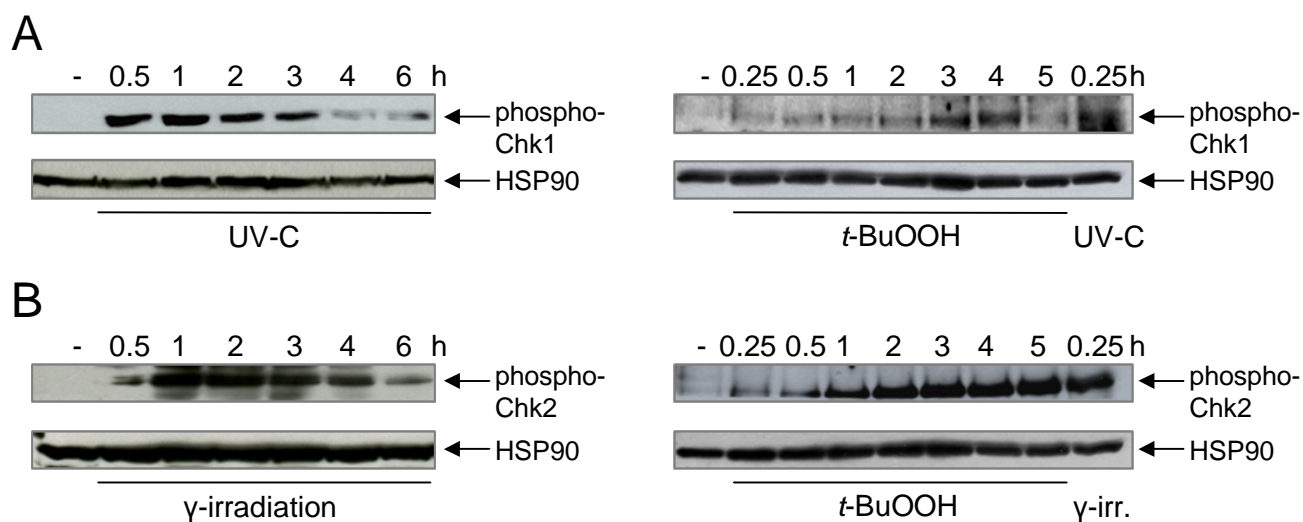
Fig. 43 *t*-BuOOH activates Chk1 and Chk2 in Caco-2 cells. **a-b** Cells were either exposed to UV-C (20 J / m^2) or γ-irradiation (γ-irr., 8 Gy) as positive control, or were treated with *t*-BuOOH (100 µM). After the indicated time, cells were harvested for Western Blot analysis to detect either (**a**) Chk1 (Ser345) phosphorylation or (**b**) Chk2 (Thr68) phosphorylation with HSP90 or β-actin as loading control.

Since *t*-BuOOH activated Chk1 and Chk2 as downstream targets of ATR and ATM in Caco-2 cells, cell death was analyzed in the presence of an ATR (VE-821) or ATM (Ku60019) inhibitor (Figure 44). Unexpectedly, solely pharmacological inhibition of ATR and not of ATM kinase resulted in significant sensitization of Caco-2 cells towards *t*-BuOOH-induced necrosis as assessed by AnnexinV-FITC / PI staining and flow cytometry. With a high specificity of these inhibitors determined by control experiments in murine and human epithelial cells in our laboratory (C. Turmann, MD thesis, in preparation), the above described results support ATR but not ATM inhibition to promote *t*-BuOOH-induced necrosis in Caco-2 cells.
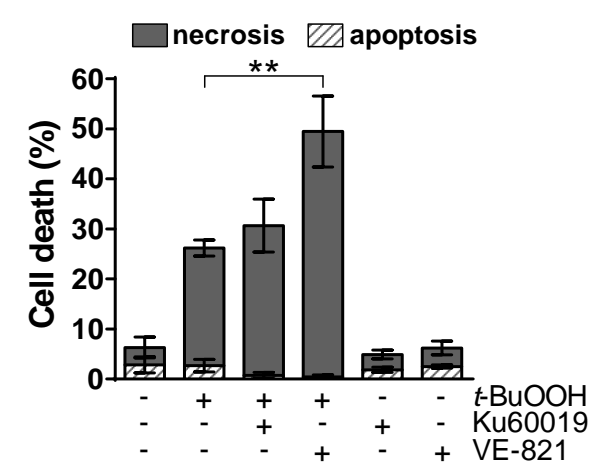
Fig. 44 Inhibition of ATR but not of ATM promotes *t*-BuOOH-induced necrosis in Caco-2 cells. Cells were either untreated or treated with *t*-BuOOH (100 µM, 6 h) in the absence or presence of the ATM inhibitor Ku60019 (3 µM) or the ATR inhibitor VE-821 (10 µM). Subsequently, cells were stained with AnnexinV-FITC (apoptosis) / PI (necrosis) and cell death was analyzed via flow cytometry (mean ± SD of *n* = 3 in duplicates). Significance was calculated with ** $p \leq 0.01$.

4.2.5 PARP-1 activation is not responsible for *t*-BuOOH-induced necrosis

Among distinct RN pathways, the mechanism of parthanatos has been already described to directly link ROS-induced DNA damage with the induction of cell necrosis (Galluzzi et al., 2012, 2014; Conrad et al., 2016; Galluzzi et al., 2018). In this context, hyperactivation of the key enzyme PARP-1, which catalyzes the attachment of NAD^+ polymers to single-stranded DNA, can lead to the depletion of NAD^+ and therefore inhibition of mitochondrial ATP synthesis. Since *t*-BuOOH provoked DNA damage, as well as a time-dependent loss of NAD^+ and ATP (see 4.1.3; 4.1.4), a possible role of PARP-1 in *t*-BuOOH-induced necrosis was evaluated.

Activation of PARP-1 was analyzed via immunochemical detection of ADP-ribose polymers (PAR foci) via laser scanning microscopy. HaCaT cells served as model system since several studies have demonstrated activation of PARP-1 when this specific cell type was treated with high concentrations of H_2O_2 (Bakondi et al., 2004; Dahl et al., 2014). According to Figure 45A, treatment of HaCaT cells with H_2O_2 (10 mM, 7 min, diluted in PBS) indeed caused a strong activation of PARP-1. Similarly, *t*-BuOOH (5 mM, 7 min, diluted in PBS) was able to induce PARP-1-dependent foci formation. Although high peroxide concentrations were used, the presence of the chemical PARP-1 inhibitor olaparib effectively abolished H_2O_2- and *t*-BuOOH-induced PAR foci formation in HaCaT cells.

Protein PARylation was additionally analyzed upon experimental conditions that were so far used in the context of cell death analysis. According to Figure 45B, laser scanning microscopy provided evidence for rapid activation of PARP-1, even when HaCaT cells were exposed to a lower amount of *t*-BuOOH (200 µM) with the latter being diluted in FBS-containing culture medium instead of PBS. Interestingly, t-BuOOH-mediated activation of PARP-1 was only transiently observable in the whole HaCaT cell population up to 20 min of exposure, whereby only single cells displayed PARP-1-induced foci formation till the onset of necrosis (4 h).
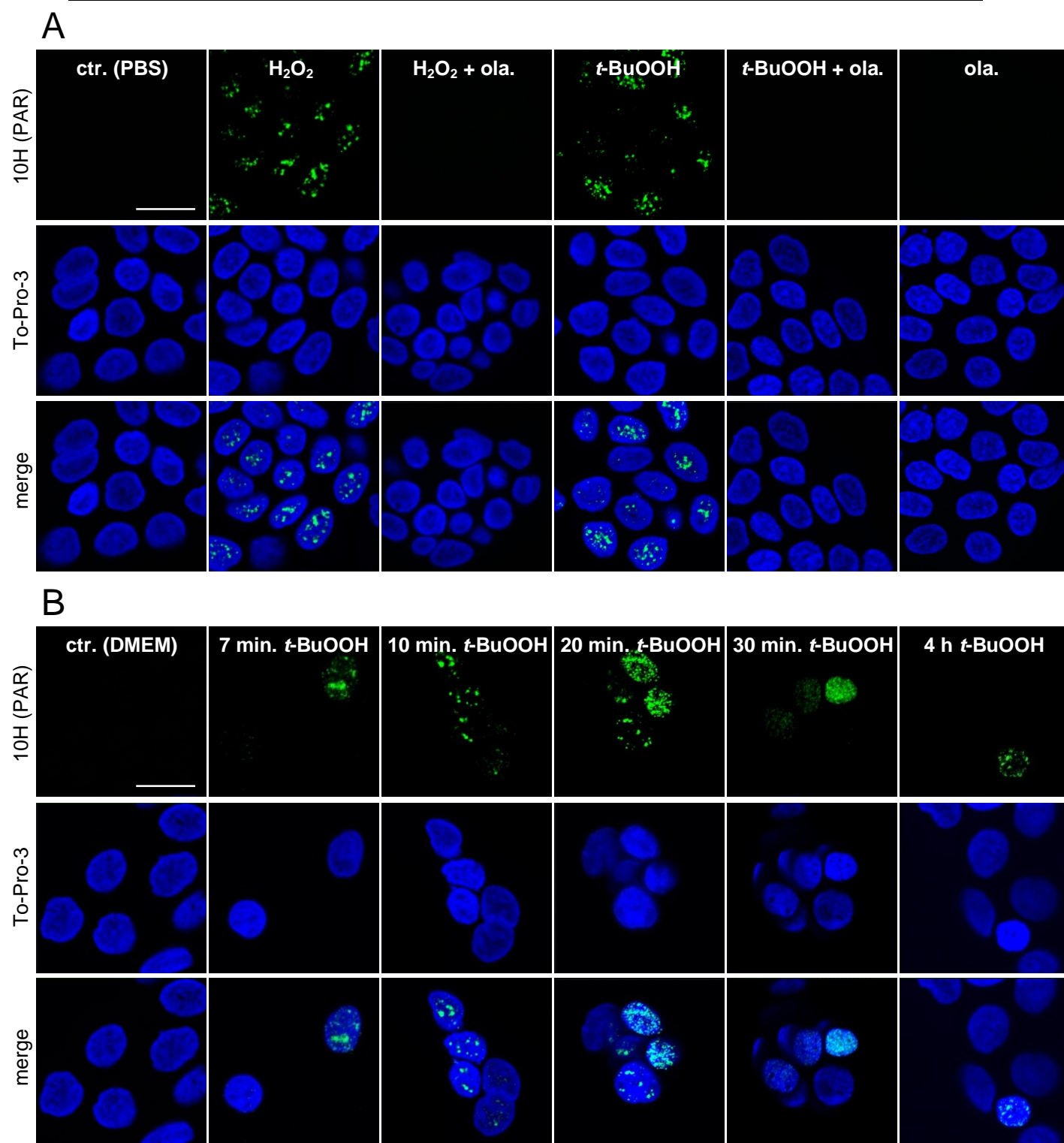
Fig. 45 PARP-1 is activated in HaCaT cells upon H_2O_2 and t-BuOOH exposure and can be inhibited by the presence of olaparib. **a-b** HaCaT cells were either (**a**) exposed for 7 minutes to a high concentration of H_2O_2 (10 mM) or t-BuOOH (5 mM), each diluted in PBS, in the absence or presence of the PARP-1 inhibitor olaparib (0.5 µM), or cells were (**b**) exposed to a low amount of t-BuOOH (200 µM), diluted in FBS-containing DMEM. After treatment, cells were stained with primary and secondary antibody for detection of PAR foci. Nucleic DNA was stained with To-Pro-3 prior to qualitative evaluation via laser scanning microscopy (bar = 20 µm). ctr. = control, ola. = olaparib, min. = minutes.

To finally elucidate a role of PARP-1 in *t*-BuOOH-induced necrosis, a possible restoration of the intracellular NAD$^+$ level, as well as inhibition of cell death by the presence of the PARP-1 inhibitor olaparib was investigated in NIH3T3, HaCaT and Caco-2 cells (Figure 46A-C). Olaparib indeed partially restored NAD$^+$ levels, even though the inhibitor alone exhibited a strong effect on the intracellular NAD$^+$ level in NIH3T3 cells. However, flow cytometric analysis after AnnexinV-FITC / PI staining did not reveal any significant modulation of *t*-BuOOH-mediated necrosis by olaparib. Similar results were obtained for serum-depleted cells (Appendix I, Figure A5). Although various higher olaparib concentrations were investigated (data not shown), olaparib was not able to block *t*-BuOOH-induced necrosis. Hence, PARP-1 activation is not crucially involved, but rather accompanied *t*-BuOOH-induced cell death.
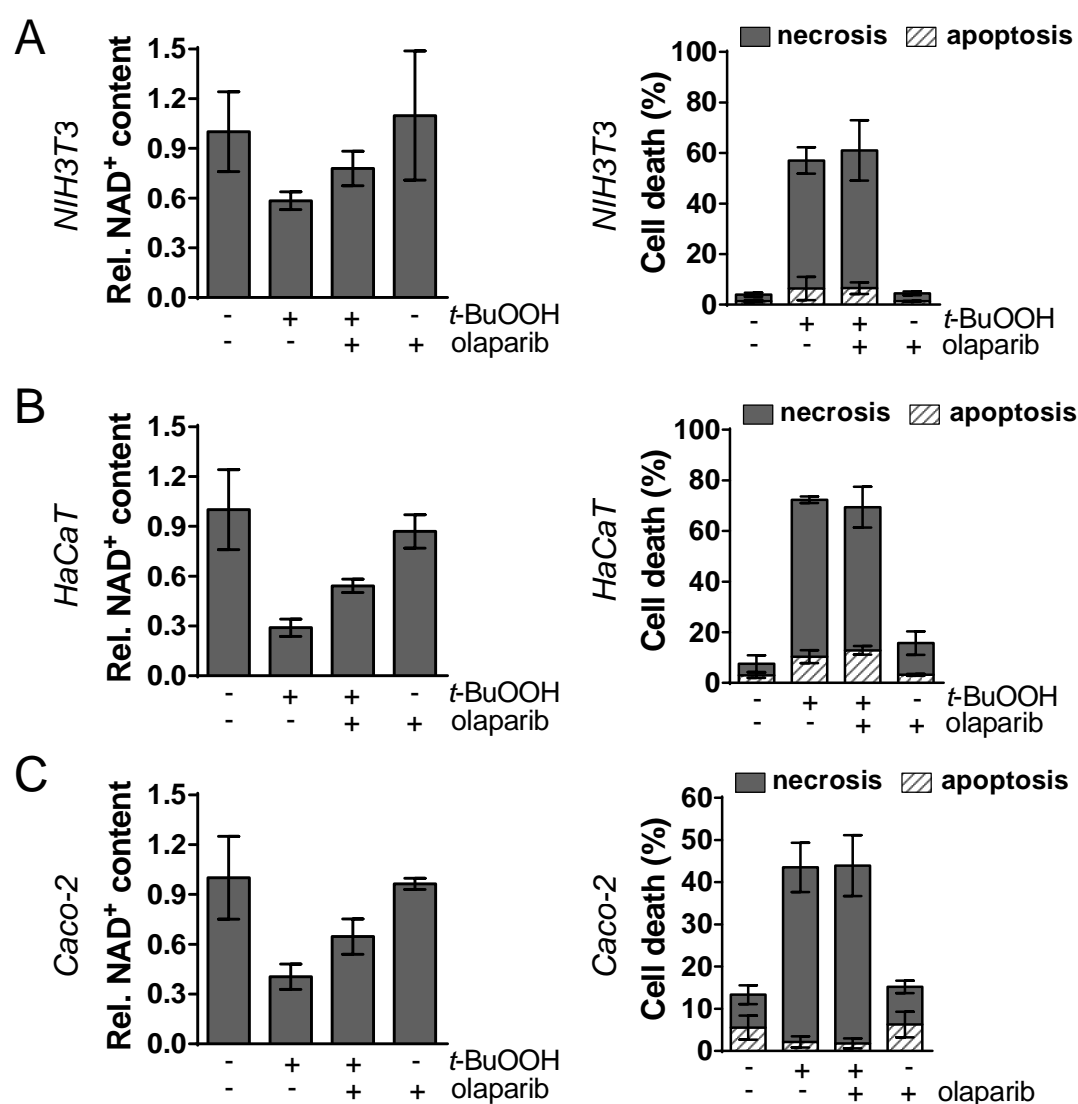
Fig. 46 PARP-1 inhibition partially restores the intracellular NAD$^+$ level but fails to block necrosis in the presence of *t*-BuOOH. **a-c** Cells were either untreated or treated with *t*-BuOOH (a: 50 μM; b: 200 μM; c: 100 μM; a-c, *left*: 4 h; a-c, *right*: 6 h) in the absence or presence of the PARP-1 inhibitor olaparib

(0.5 μM). Subsequently, (**a-c**, *left*) the intracellular NAD$^+$ level was determined via the NAD$^+$ cycling assay, or (**a-c**, *right*) cells were stained with AnnexinV-FITC (apoptosis) / PI (necrosis) and cell death was analyzed via flow cytometry (mean ± SD of n = 2-3 in duplicates or triplicates).

4.2.6 *t*-BuOOH-induced loss of the MMP ($\Delta\psi_m$) is not crucial for necrosis

Besides parthanatos, other RN pathways are a direct consequence of mitochondrial damage, such as loss of the MMP ($\Delta\psi_m$) by H_2O_2 or inhibition of ATP synthesis in the presence of TNFα (Hanstein, 1976; Jarvis et al., 2007; Degasperi et al., 2008). In this context, loss of the MMP ($\Delta\psi_m$) was provoked by MPT in a CypD-dependent manner (Baines et al. 2005; Halestrap et al., 2009; Linkermann et al. 2013). Since loss of $\Delta\psi_m$ occurred prior to *t*-BuOOH-induced necrosis in semiconfluent NIH3T3 cells, a possible effect of the chemical CypD inhibitor ciclosporin A (CsA) on *t*-BuOOH-mediated necrosis was investigated (Nakagawa et al., 2005).

According to Figure 47, flow cytometric analysis after DiOC6 / PI staining revealed a slight but no significant restoration of $\Delta\psi_m$ in the presence of CsA. Moreover, CsA failed to prevent *t*-BuOOH-induced necrosis.
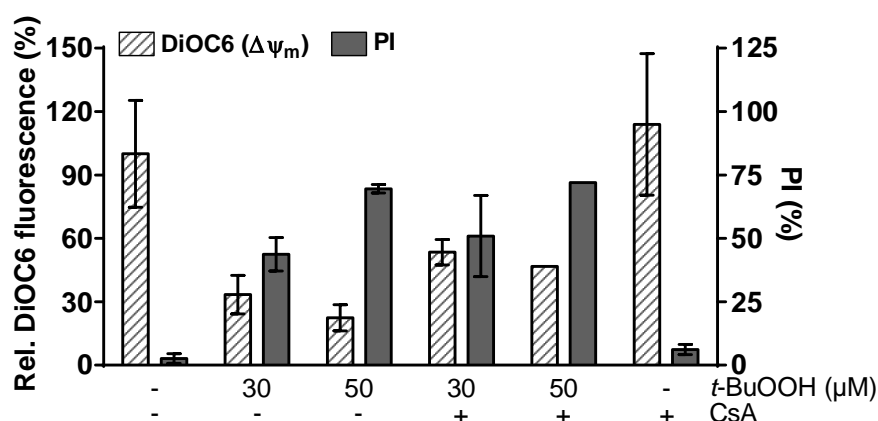
Fig. 47 CsA fails to prevent *t*-BuOOH-induced loss of the MMP ($\Delta\psi_m$) and necrosis. NIH3T3 cells were treated with the indicated concentrations of *t*-BuOOH in the absence or the presence of the CypD inhibitor CsA (100 nM) for 6 h. Afterwards, cells were stained with DiOC6 to assess the mitochondrial membrane potential ($\Delta\psi_m$) and with PI to detect necrosis by flow cytometric analysis. DiOC6 fluorescence is presented relative to untreated control cells (= 100 %) as mean ± SD of n = 2-3 in duplicates.

In addition, t-BuOOH-induced necrosis was also not inhibited but rather increased by the presence of the protonophore FCCP (carbonyl cyanide-4-(trifluoromethoxy)phenylhydrazone) (Figure 48) – a substance which uncouples ATP synthesis from mitochondrial oxidative phosphorylation and yet described to inhibit TNFα-induced necrosis (Hanstein, 1976; Jarvis et al., 2007). Since partial restoration of $\Delta\psi_m$ and uncoupling of ATP synthesis did not prevent t-BuOOH-induced cell death, as well as $\Delta\psi_m$ started to decline not before cell death was induced in Caco-2 cells (see 4.1.3), loss of the MMP appears not crucially involved in t-BuOOH-mediated necrosis.
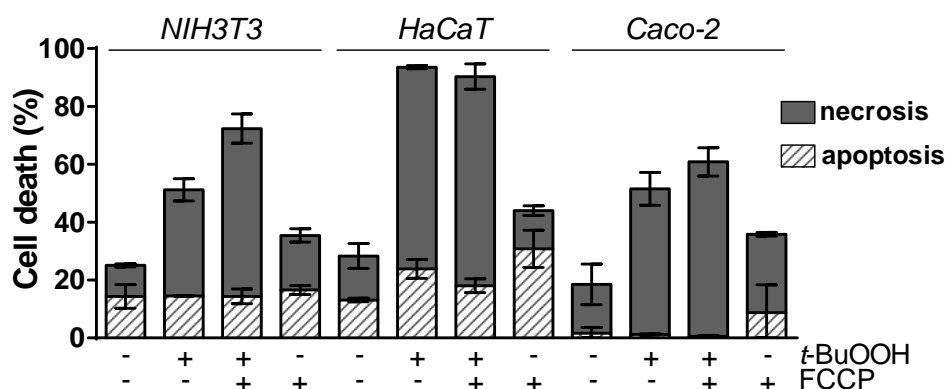
Fig. 48 Uncoupling of ATP synthesis by FCCP does not rescue cells from t-BuOOH-induced necrosis. Cells were either untreated or treated with t-BuOOH (NIH3T3: 30 µM; HaCaT: 200 µM; Caco-2: 100 µM) in the absence or the presence of the protonophore FCCP (10 µM) for 6 h. Subsequently, cells were stained with AnnexinV-FITC (apoptosis) / PI (necrosis) and cell death was analyzed via flow cytometry (mean ± SD of n = 2). Similar results were obtained in the presence of 0.1 µM and 1 µM FCCP, respectively (data not shown).

4.2.7 Necrostatin-1 inhibits t-BuOOH-induced necrosis independent of RIPK1 and RIPK3

Since a crucial role of DDR-related proteins and loss of the MMP in t-BuOOH-induced necrosis has been excluded according to the presented results, involvement of RIPK1 and RIPK3 was investigated. Besides a yet proven key function of RIPK1 in the execution of H_2O_2-induced necroptosis (Shen et al., 2004; Temkin et al., 2006), the existence of distinct RIPK1- and / or RIPK3-dependent RN subroutines has been widely reported upon oxidative stress (Galluzzi et al., 2012, 2014; Conrad et al., 2016; Galluzzi et al., 2018).

According to Figure 49A-C, flow cytometric analysis after AnnexinV-FITC / PI staining indicated significant inhibition of *t*-BuOOH-induced necrosis upon pretreatment of NIH3T3, HaCaT and Caco-2 cells with Nec-1 – a widely investigated RIPK1 inhibitor (Degterev et al., 2005). Similar results were obtained in serum-depleted NIH3T3 and HaCaT cells (Appendix I, Figure A6).
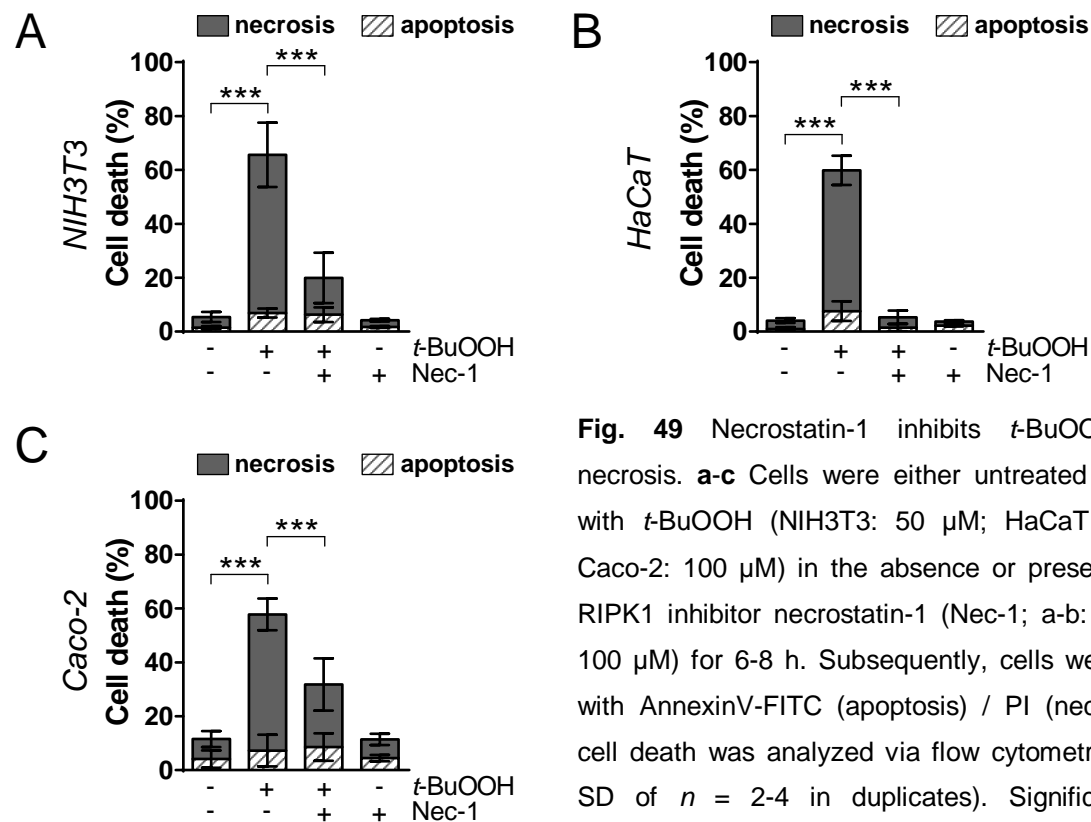
Fig. 49 Necrostatin-1 inhibits *t*-BuOOH-induced necrosis. **a-c** Cells were either untreated or treated with *t*-BuOOH (NIH3T3: 50 µM; HaCaT: 200 µM; Caco-2: 100 µM) in the absence or presence of the RIPK1 inhibitor necrostatin-1 (Nec-1; a-b: 50 µM; c: 100 µM) for 6-8 h. Subsequently, cells were stained with AnnexinV-FITC (apoptosis) / PI (necrosis) and cell death was analyzed via flow cytometry (mean ± SD of *n* = 2-4 in duplicates). Significance was calculated with *** $p \leq 0.001$.

To confirm these data, as well as to explore a possible involvement of RIPK3 in *t*-BuOOH-induced necrosis, more selective RIPK1 (GSK '728, GSK '963) and RIPK3 (GSK '843, GSK '872) inhibitors were investigated in accordance to their IC$_{50}$ values. In this context, NIH3T3 were analyzed in first line since these cells should be capable to undergo necroptosis (Shen et al., 2004; Zhang et al., 2011). Although the efficacy of these RIP kinase inhibitors has been widely reported (Dondelinger et al. 2014; Mandal et al. 2014; Berger et al., 2015), AnnexinV-FITC / PI staining followed by flow cytometry did not demonstrate any significant inhibition of *t*-BuOOH-induced necrosis (Figure 50A-B). Similar results were obtained upon *t*-BuOOH exposure of NIH3T3 and HaCaT cells in the presence of higher RIPK1 and RIPK3 inhibitor concentrations (analysis conducted by D. Faust; Wenz et al., 2018).
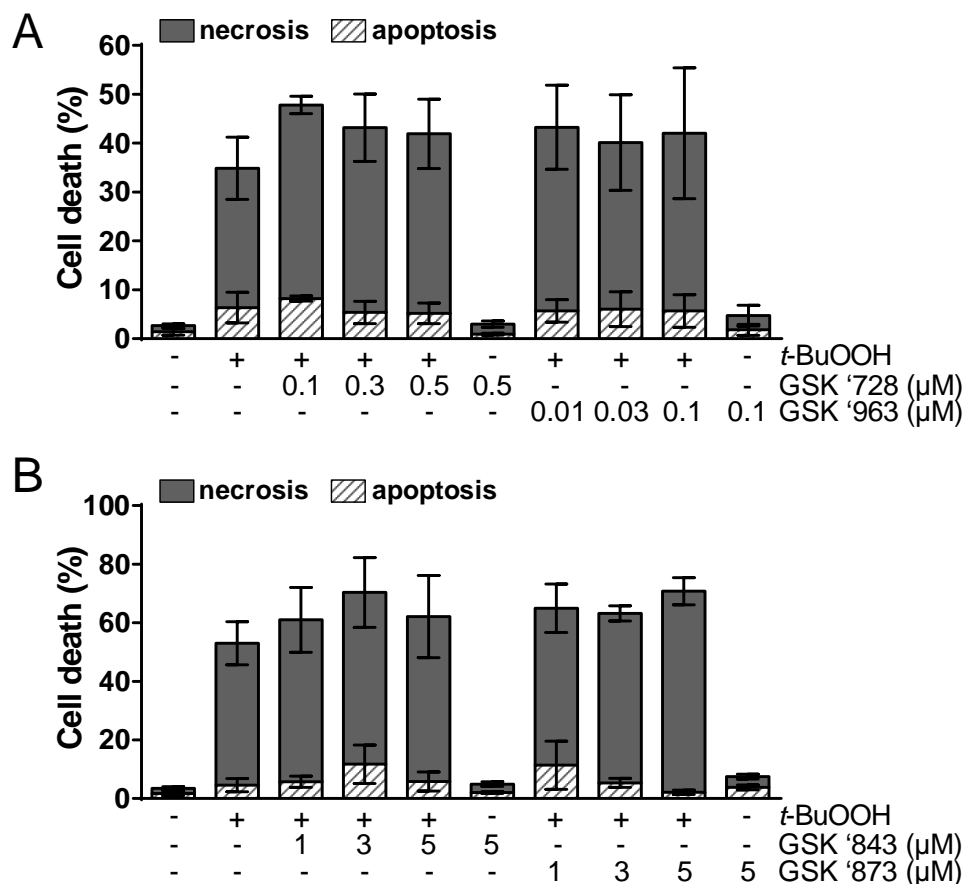
Fig. 50 *t*-BuOOH-induced necrosis is not blocked by more specific RIPK1 and RIPK3 inhibitors. **a-b** NIH3T3 cells were either untreated or treated with *t*-BuOOH (50 µM) in the absence or presence of (**a**) RIPK1 inhibitors (GSK '728: IC_{50} = 100 nM; GSK '963: IC_{50} = 10 nM) and (**b**) RIPK3 inhibitors (GSK '843, GSK '873: IC_{50} = 1 µM), respectively for 6 h. Subsequently, cells were stained with AnnexinV-FITC (apoptosis) / PI (necrosis) and cell death was analyzed via flow cytometry (mean ± SD of *n* = 2 in duplicates).

Due to different effects of Nec-1 compared to the other RIP kinase inhibitors on *t*-BuOOH-induced necrosis, a positive control for these chemical inhibitors was established via induction of necroptosis by TNFα. As the presence of RIPK1 and RIPK3 is crucial for the execution of this RN pathway (Galluzzi et al., 2012), the expression of these kinases was just investigated with help of Western Blot analysis in a set of murine and human cells (NIH3T3, MEF, HaCaT, Caco-2). According to Figure 51A, MEF, HaCaT and Caco-2 cells demonstrated a remarkable expression of both RIP kinase isoforms. Finally, MEF cells were selected for establishment of the inhibitor positive control since (i) NIH3T3 exhibited RIPK3 deficiency, and on the other hand, (ii) most of the experiments were so far conducted in murine fibroblasts. In this context, flow cytometric analysis after AnnexinV-FITC / PI staining clearly demonstrated a necrotic cell death induced by the presence of TNFα, the pancaspase inhibitor z-VAD-fmk and the protein synthesis inhibitor cycloheximide

(Figure 51B) – a combination so far described to induce necroptosis in MEF cells (Sosna et al., 2014). Although Nec-1, as well as the other more selective RIP kinase inhibitors efficiently blocked TNFα-induced necroptosis, *t*-BuOOH-induced necrosis was solely blocked by the presence of Nec-1 (Figure 51C). Hence, Nec-1 provided an unspecific off-target effect in our cell system.
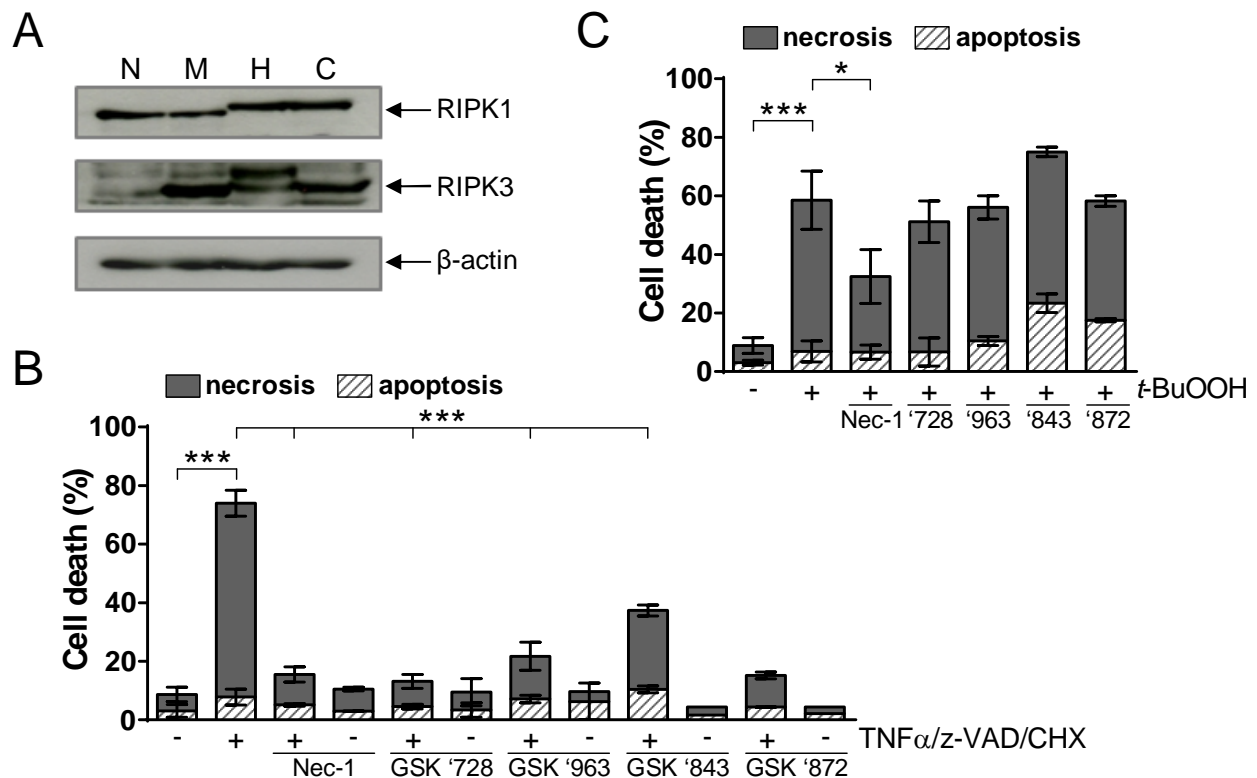
Fig. 51 Upon expression of RIPK1 and RIPK3, TNFα-induced necroptosis is inhibited by the presence of specific RIPK1 and RIPK3 inhibitors in contrast to *t*-BuOOH-induced necrosis in MEF cells. **a** Untreated murine NIH3T3 (N) and MEF (M) cells, as well as human HaCaT (H) and Caco-2 (C) cells were harvested for Western Blot analysis of RIPK1 (murine: 74 kDa; human: 76 kDa) and RIPK3 (murine, human: 57 kDa) expression with β-actin as loading control. **b-c** MEF cells were either (**b**) treated with TNFα (100 ng / mL), z-VAD-fmk (z-VAD: 20 µM) and cycloheximide (CHX: 1 µg / mL) for 24 h or (**c**) treated with *t*-BuOOH (100 µM) for 6 h, both in the absence or presence of necrostatin-1 (Nec-1: 100 µM), RIPK1 inhibitors (GSK '728, GSK '963: 10 µM) and RIPK3 inhibitors (GSK '843, GSK '873: 10 µM), respectively. Subsequently, cells were stained with AnnexinV-FITC (apoptosis) / PI (necrosis) and cell death was analyzed via flow cytometry (mean ± SD of $n = 2$ in duplicates).

A possible role of RIPK1 and RIPK3 in *t*-BuOOH-induced necrosis was finally excluded by analysis of NIH3T3 RIPK1 and RIPK3 CRISPR/Cas9 cell clones since siRNA-mediated knockdown of RIPK1 was not efficient enough to block TNFα-necroptosis (Appendix I, A7). Western Blot analysis provided evidence for RIPK1 and RIPK3 deficiency in these cell clones in accordance to the given knockout status

(Figure 52A). Moreover, cell death analysis after AnnexinV-FITC / PI staining clearly demonstrated inhibition of TNFα-induced necroptosis in RIPK1$^{-/-}$ and RIPK3$^{-/-}$ NIH3T3 cells, whereby *t*-BuOOH-induced necrosis was not affected but rather accelerated after 6 h of exposure compared to parental cells (Figure 52B; Wenz et al., 2018). Hence, Nec-1 inhibits *t*-BuOOH-induced necrosis independent of the presence of RIPK1 and RIPK3. Interestingly, despite Nec-1 was able to prevent *t*-BuOOH-induced necrosis, loss of the MMP ($\Delta\psi_m$) and the formation of DNA DSBs was not inhibited by this agent (Appendix I, Figure A8).
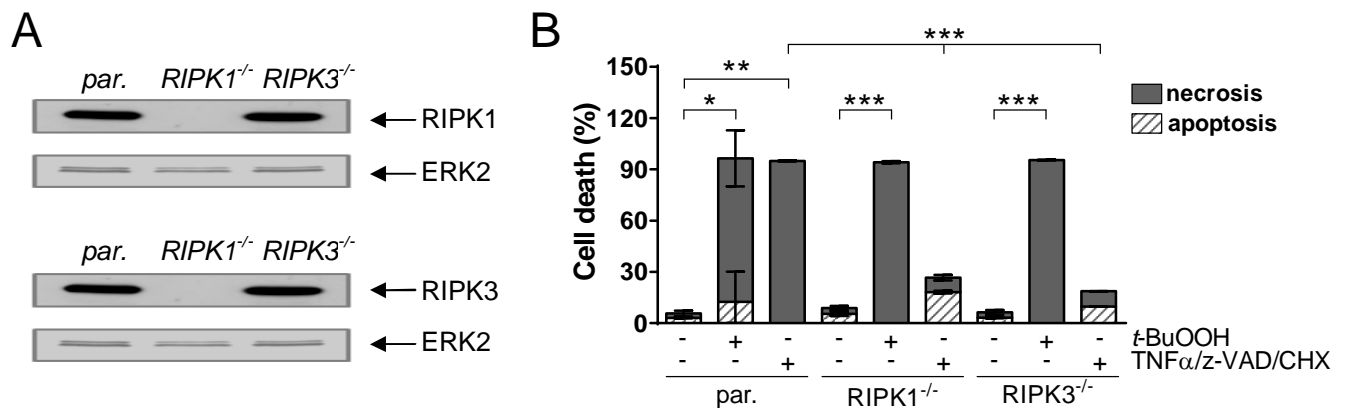
Fig. 52 Knockout of RIPK1 and RIPK3 rescues cells from TNFα-induced necroptosis but not from t-BuOOH-induced necrosis. Parental (par.) NIH3T3* cells, as well as RIPK1$^{-/-}$ and RIPK3$^{-/-}$ CRISPR/Cas cell clones (see 2.6) were either (**a**) harvested for Western Blot analysis of RIPK1 or RIPK3 expression with ERK2 as loading control (conducted by D. Faust), or (**b**) cells were treated with *t*-BuOOH (50 µM) or treated with TNFα (100 ng / mL), z-VAD-fmk (z-VAD: 20 µM) and cycloheximide (CHX: 1 µg / mL) for 24 h Subsequently, cells were stained with AnnexinV-FITC (apoptosis) / PI (necrosis) and cell death was analyzed via flow cytometry (mean ± SD of n = 3 in duplicates). Significance was calculated with * $p \leq 0.05$, ** $p \leq 0.01$, *** $p \leq 0.001$.

4.2.8 *t*-BuOOH is a novel inducer of ferroptosis

Although recent studies have been controversially discussed (Dixon et al., 2012), Nec-1 has been already described to inhibit the RN subroutine of ferroptosis via different off-target effects (Friedmann Angeli et al. 2014; Eling et al. 2015). So far, crucial drivers of ferroptosis comprise iron overload, lipid peroxidation, or blockage of ROS detoxification via the GSH / GPX4 system (Dixon et al., 2012; Friedmann Angeli et al., 2014; Linkermann et al., 2014; Yang et al., 2014; Cao & Dixon, 2016; Xie et al. 2016; Yang & Stockwell 2016; Dixon, 2017).

Since *t*-BuOOH-mediated necrosis was sensitive to inhibition by Nec-1, the induction of ferroptosis by *t*-BuOOH was evaluated with help of the specific ferroptosis inhibitor ferrostatin-1 (FS), which is known to inhibit lipid peroxidation (Dixon et al., 2012; Friedmann Angeli et al., 2014; Skouta et al., 2014; Yang et al., 2014; Dong et al., 2015). According to Figure 53A-C, FS was able to significantly inhibit *t*-BuOOH-induced necrosis in NIH3T3, HaCaT and Caco-2 cells. Interestingly, and similar to Nec-1, FS could not inhibit loss of the MMP ($\Delta\psi_m$) nor the formation of DNA DSBs in the presence of *t*-BuOOH (conducted by D. Faust; Wenz et al., 2018).

Fig. 53 *t*-BuOOH induces ferroptosis. **a-c** Cells were either untreated or treated with *t*-BuOOH (NIH3T3: 50 µM; HaCaT: 200 µM; Caco-2: 100 µM) in the absence or presence of the specific ferroptosis inhibitor ferrostatin-1 (FS; a-c: 1 µM) for 6 h. Subsequently, cells were stained with AnnexinV-FITC (apoptosis) / PI (necrosis) and cell death was analyzed via flow cytometry (mean ± SD of *n* = 3 in duplicates). Significance was calculated with *** $p \leq 0.001$.

In addition to the selective ferroptosis inhibitor FS, also the presence of the biosynthetic GSH precursor NAC has been described to block ferroptosis via prevention of GSH depletion (Aruoma et al., 1998; Gao et al., 2015; Lörincz et al., 2015; Li et al., 2018; Wu et al., 2018). Indeed, combined treatment of NIH3T3, HaCaT and Caco-2 cells with *t*-BuOOH and NAC was able to prevent necrosis as demonstrated by flow cytometry after AnnexinV-FITC / PI staining (Figure 54A-C). Since NAC and the selective inhibitor FS efficiently blocked *t*-BuOOH-induced necrosis in all of the tested cell lines, ferroptosis appears as the main cell death mechanism induced by the presence of *t*-BuOOH.

A

B

C
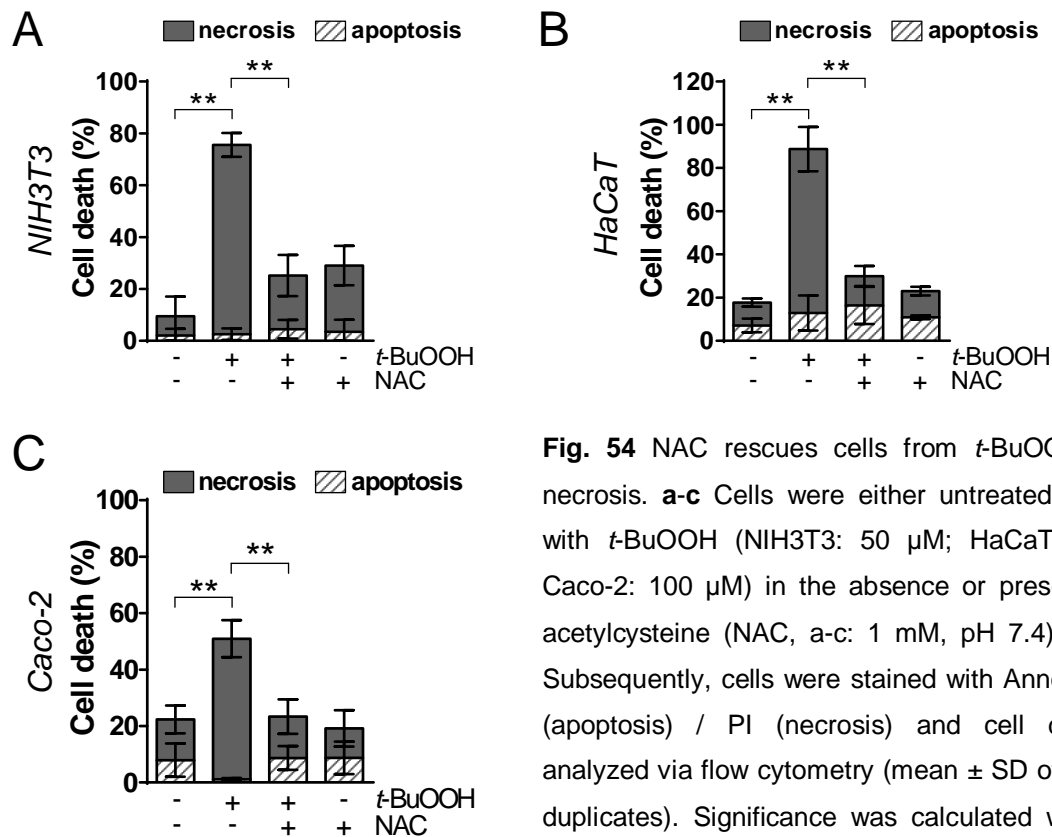
Fig. 54 NAC rescues cells from *t*-BuOOH-induced necrosis. **a-c** Cells were either untreated or treated with *t*-BuOOH (NIH3T3: 50 µM; HaCaT: 200 µM; Caco-2: 100 µM) in the absence or presence of *N*-acetylcysteine (NAC, a-c: 1 mM, pH 7.4) for 6-8 h. Subsequently, cells were stained with AnnexinV-FITC (apoptosis) / PI (necrosis) and cell death was analyzed via flow cytometry (mean ± SD of *n* = 2-3 in duplicates). Significance was calculated with ** *p* ≤ 0.01.

4.2.9 Ca^{2+} chelation rescues cells from *t*-BuOOH-induced ferroptosis and inhibits cellular damage

To date, a crucial role of Ca^{2+} as secondary messenger for the execution of different RN subroutines has been widely demonstrated (Vanden Berghe et al., 2014). Besides a tight regulation of the intracellular Ca^{2+} level during cell-cell contact-driven proliferation and differentiation (Nagar et al., 1996; Müller et al., 2006; Bhagavathula et al., 2007), the impact of Ca^{2+} signaling on ferroptosis remains to be elucidated. Therefore, a possible role of intracellular Ca^{2+} in *t*-BuOOH-induced ferroptosis was investigated in NIH3T3 and Caco-2 cells.

Indeed, cell death analysis after AnnexinV-FITC / PI staining demonstrated significant inhibition of *t*-BuOOH-induced ferroptosis by the Ca^{2+} chelator BAPTA AM (Figure 55A). Similar results were obtained in MEF and HaCaT cells (Appendix I, Figure A9). Besides inhibition of *t*-BuOOH-induced ferroptosis, Ca^{2+} chelation by BAPTA AM rescued cells from (i) a decrease in NAD$^+$, and (ii) loss of the MMP ($\Delta\psi_m$) as demonstrated by the NAD$^+$ cycling assay, as well as by DiOC6 / PI staining and flow cytometry (Figure 55B-C).
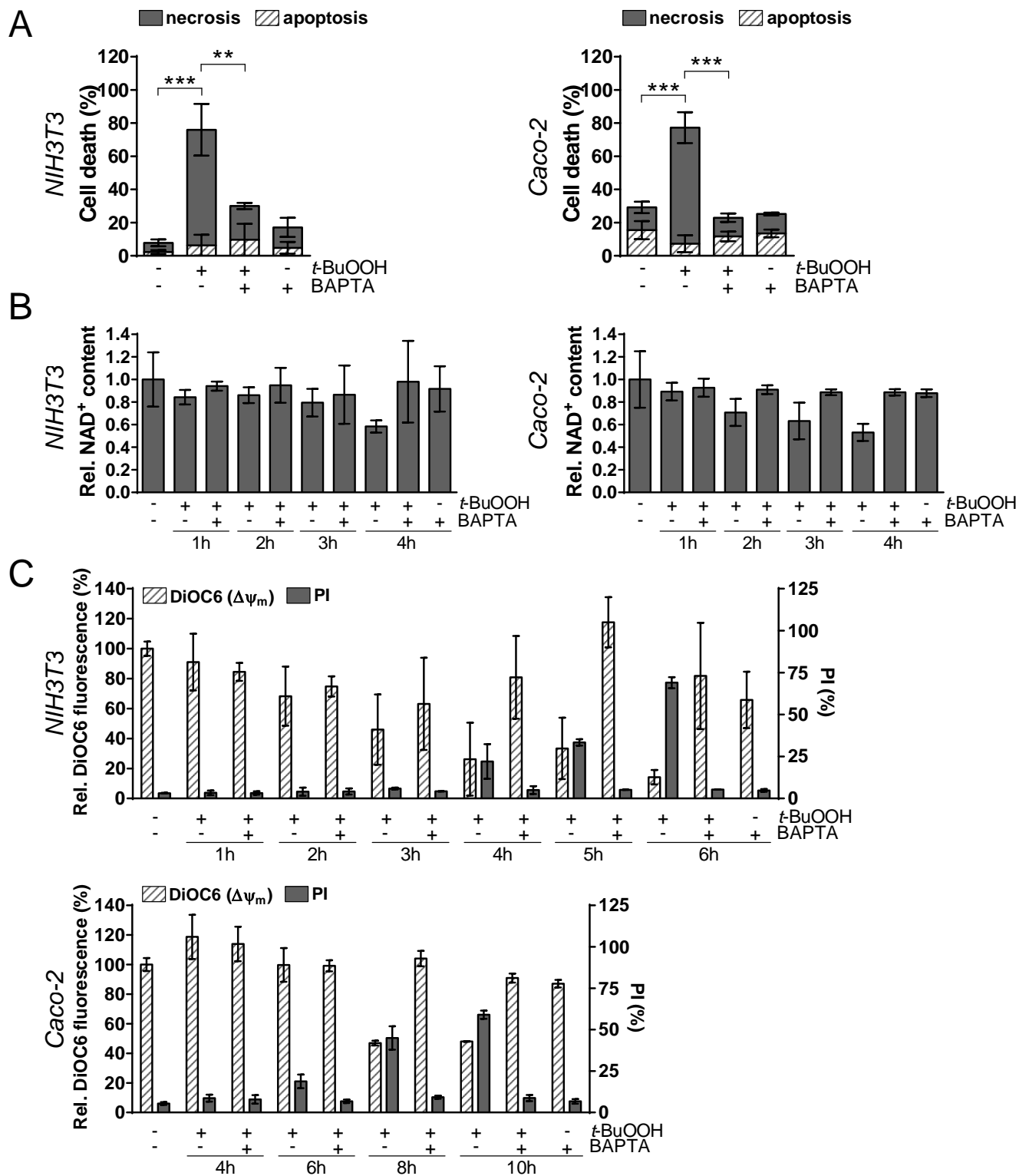
Fig. 55 *t*-BuOOH-induced ferroptosis, the decrease in intracellular NAD$^+$ and loss of the MMP ($\Delta\psi_m$) are prevented by the presence of the Ca^{2+} chelator BAPTA AM. **a-c** Cells were untreated or treated with *t*-BuOOH (NIH3T3: 50 µM; Caco-2: 100 µM; a: 6-8 h) in the absence or presence of BAPTA AM (NIH3T3: 5 µM; Caco-2: 10 µM). Subsequently, cells were either stained with (**a**) AnnexinV-FITC (apoptosis) / PI (necrosis) and cell death was analyzed (mean ± SD of *n* = 2-3 in duplicates), or with (**c**) DiOC6 to assess $\Delta\psi_m$ (relative to untreated cells = 100 %) and with PI to detect necrosis (mean ± SD of *n* = 2 in duplicates), both via flow cytometry. (**b**) The intracellular NAD$^+$ level (relative to untreated

control) was determined via the NAD$^+$ cycling assay (mean ± SD of n = 2 in triplicates). Significance was calculated with ** p ≤ 0.01, *** p ≤ 0.001.

Performance of the neutral Comet assay and laser scanning microscopy further revealed that also the formation of t-BuOOH-induced DNA DSBs could be efficiently blocked by the presence of BAPTA AM (Figure 56A-B).
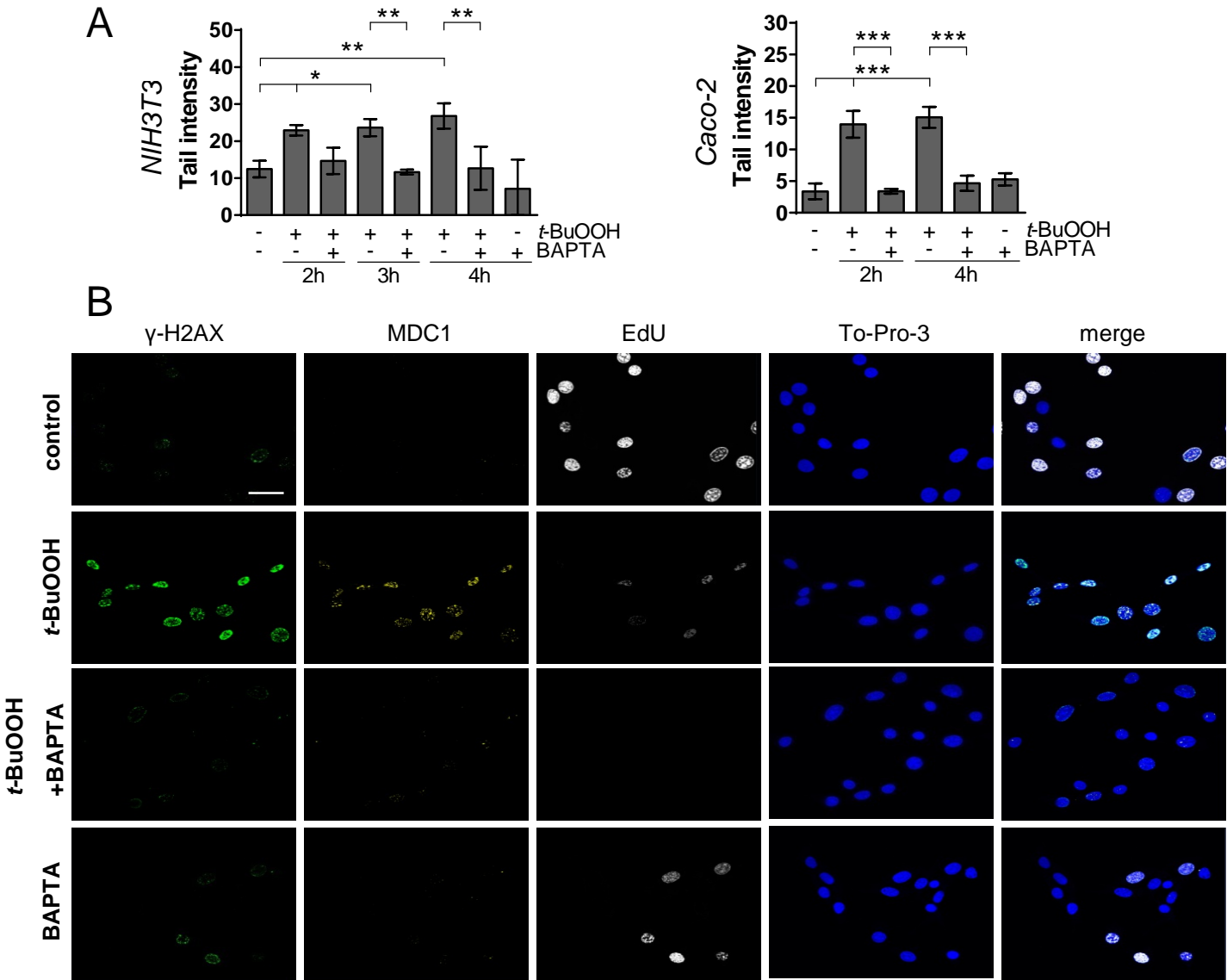
Fig. 56 Ca^{2+} chelation rescues cells from DNA DSB formation upon t-BuOOH exposure. **a-b** Cells were untreated (= control) or treated with t-BuOOH (a-b: NIH3T3, 50 µM; a: Caco-2, 100 µM; b: 4 h) in the absence or presence of BAPTA AM (NIH3T3: 5 µM; Caco-2: 10 µM). (**a**) After treatment, DSB formation was assessed by neutral Comet assay. Results are expressed as tail intensity and presented as mean ± SD of n = 2-4 with 50 cells analyzed per sample; * p ≤ 0.05, *** p ≤ 0.001). (**b**) Cells were incubated with the S phase marker EdU prior to treatment. Afterwards, cells were stained with primary and secondary antibody for detection of γ-H2AX and MDC1 foci. Nucleic DNA was stained by To-Pro-3 prior to analysis via laser scanning microscopy (bar = 50 µm).

Results of the neutral Comet assay were confirmed by immunochemical analysis of the co-localization of γ-H2AX and MDC1 – both coordinating the formation of DSB foci in order to stimulate their repair (Dickey et al., 2011). In addition, EdU staining was combined to evaluate the extent of DNA replication. In this context, laser scanning microscopy qualitatively supported an increase in co-localized γ-H2AX / MDC1 foci, as well as a DNA replication block in *t*-BuOOH-treated NIH3T3 cells. Besides reduction in EdU incorporation by the presence of BAPTA AM alone, Ca^{2+} chelation rescued NIH3T3 cells from *t*-BuOOH-induced DSB formation.

Since Ca^{2+} seemed to play a crucial role in *t*-BuOOH-induced ferroptosis, the intracellular Ca^{2+} level of confluent and semiconfluent (prol.) cells (NIH3T3, Caco-2) was finally investigated. Interestingly, flow cytometric analysis after staining with the cytosolic Ca^{2+} indicator Fluo-4 AM showed not only a significantly lower cytosolic Ca^{2+} level in untreated confluent compared to semiconfluent cells but also in the presence of *t*-BuOOH, confluent cells were almost resistant against a significant increase in cytosolic Ca^{2+} (Figure 57A-B). Besides a possible role of lipid ROS regulation in the resistance of confluent cells against *t*-BuOOH (conducted by D. Faust), Ca^{2+} seems to play a crucial role in the resistance of confluent cultures since BAPTA AM was the only agent which inhibited *t*-BuOOH-induced ferroptosis and cellular damage (e.g., MMP loss and DNA damage).
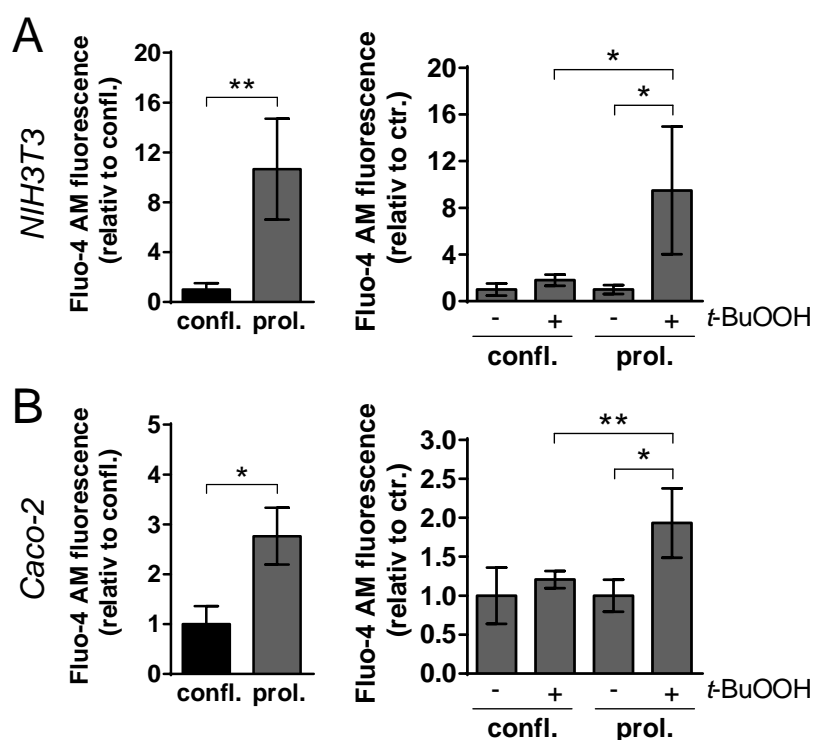
Fig. 57 Confluent cells exhibit a lower basal and *t*-BuOOH-induced Ca^{2+} level compared to semiconfluent cells. **a-b** Confluent (confl.) and semi-confluent (proliferating, prol.) cells were seeded and cultivated upon setup I. Cells were either (*left*) untreated or (*right*) treated with *t*-BuOOH (NIH3T3: 50 µM; Caco-2: 100 µM; a-b: 4 h). Subsequently, cells were stained with Fluo-4 AM for cytosolic Ca^{2+} detection (relative to confluent cells (*left*) or untreated control (*right*)) via flow cytometry (mean ± SD of *n* = 2-4 in duplicates). Significance was calculated with * $p ≤ 0.05$, ** $p ≤ 0.01$. ctr. = control.

In summary, the present work strongly indicates that the presence of cell-cell contacts protects murine fibroblasts (NIH3T3) and human epithelial cells (HaCaT, Caco-2) against t-BuOOH-induced toxicity independent of a G1 arrest. Besides protection of confluent versus semiconfluent cultures against cellular, not primary toxic lesions induced by t-BuOOH – (i) a decrease in cellular ATP and NAD^+, (ii) loss of the MMP ($\Delta\psi_m$), and (iii) the increase in DNA DSBs and cytosolic Ca^{2+} – characterization of t-BuOOH-induced necrosis revealed ferroptosis as the primary killing mechanism but also identified the presence of intracellular Ca^{2+} as crucial prerequisite for t-BuOOH-induced ferroptosis and cellular damage.

5 Discussion

5.1 Cell-cell contacts provide resistance against *t*-BuOOH-induced cytotoxicity and genotoxicity in mammalian cells

Oxidative stress as result of excessive intracellular ROS formation is highly involved in the etiology of diverse human pathologies, such as cardiovascular or neurodegenerative diseases and cancer. In this context, previous findings of our group demonstrated that contact-inhibited compared to proliferating murine fibroblasts (NIH3T3) were protected against the toxicity of the ROS-inducing chemical *t*-BuOOH (B. Linz, MD thesis, 2013). Remarkably, this short-chain hydroperoxide mimics lipid ROS patterning of oxidative stress-related pathological conditions *in vivo*, for instance, ischemia / reperfusion injury, neurological disorders and cancer (Lemasters & Nieminen, 1997; Garcia-Cohen et al., 2000; Lemasters et al., 2009; Ayala et al., 2014). On the other hand, there has been so far a scientific consensus, regarding the G1 arrest upon contact inhibition as the molecular key to resistance against ROS- and genotoxin-induced cell death due to a lower formation of replication-dependent DNA lesions (Berman et al, 1978; Rancourt et al., 2002; Naderi et al., 2003; Boonstra & Post, 2004; Roos & Kaina, 2006). However, Bar and coworkers (2004) support the idea that cell-cell contacts protect against ROS-induced toxicity as independent parameter, i.e. independent of cell cycle-driven effects. In the light of this leading hypothesis, the resistance of confluent compared to semiconfluent mammalian cells against *t*-BuOOH-induced toxicity was evaluated and characterized as first working part of this PhD thesis.

Confluent versus semiconfluent murine fibroblasts (NIH3T3), as well as cultures of human epithelial cell lines (HaCaT: keratinocytes; Caco-2: colon carcinoma cells) were compared in their sensitivity to *t*-BuOOH upon experimental setup I+II. In this context, analysis of the cell vitality via Trypan blue exclusion assays and flow cytometry proved resistance of confluent compared to semiconfluent cells against the toxicity of *t*-BuOOH. The leading hypothesis, suggesting cell-cell contacts rather than a G1 arrest as key mediator for the resistance against *t*-BuOOH, was strengthened by the following findings: (i) semiconfluent cultures (serum-depleted; U0126-treated) that exhibited a similar amount of cells in G1 as confluent cells at the time point of *t*-BuOOH exposure, were comparably sensitive to *t*-BuOOH as

semiconfluent, proliferating cells. Furthermore, data obtained by analysis of the cell cycle distribution, proliferation rate, p27 expression and EdU incorporation confirmed the assumption that (ii) confluent cells were not G1-arrested and proliferated at the time point of *t*-BuOOH exposure due to early cell confluence upon setup I+II. This early confluence only initiated the mechanism of contact inhibition but had not yet accomplished it. In accordance with these results, a complete proliferation stop due to the presence of cell-cell contacts occurred in MEF cells not before 4-5 days of cultivation after cells had been plated to confluence (Curto et al., 2007). Further support of a rather similar than distinct proliferation behavior of early confluent and proliferating cells comes from an *in vitro* study in epithelial cells, indicating a mostly similar regulation of intracellular signaling in early confluent and proliferating cultures (Rothen-Rutishauser et al., 1998). These findings stimulate the hypothesis that resistance against *t*-BuOOH-induced toxicity might be a unique defense system provided by the presence of cell-cell contacts against oxidative stress independent of cell cycle-driven effects.

The study of Rothen-Rutishauser et al. (1998) further suggests that early versus late confluent epithelial cells show remarkable differences in intracellular signaling. Therefore, the early confluent status of the cultures analyzed in the context of this work should be kept in mind upon comparison with other reports since lacking discrimination between early and late confluent cells might have already resulted in overlooking publications that possibly support the findings of this work. For instance, confluent compared to proliferating HaCaT cells have been reported to be more resistant against the toxicity of H_2O_2, $O_2^{\bullet-}$ and peroxynitrite (Bakondi et al., 2003). In this study, the authors declare HaCaT cultures that have been seeded to confluence and cultivated overnight as "differentiated", whereby lacking experimental data to prove the differentiated status, as well as own working experience with these cells makes differentiation overnight unlikely. Thus, this report might rather describe resistance of early confluent compared to proliferating HaCaT cells against oxidative stress-induced toxicity, and might therefore provide additional evidence for the findings of this work.

A positive correlation between the extent of intercellular adhesion and the resistance against *t*-BuOOH-induced toxicity arises by the comparison of Trypan blue assay results of NIH3T3, HaCaT and Caco-2 cells. With regard to the time necessary to singularize cells after trypsin incubation (HaCaT > Caco-2 > NIH3T3), and even the sufficiency for pre-incubation of HaCaT cells with a higher EDTA concentration to loosen cell-cell contacts (unpublished observation + methods section), the strength of intercellular contact seems to determine the sensitivity to *t*-BuOOH (HaCaT: 200 µM > Caco-2: 100 µM > NIH3T3: 30 or 50 µM). The assumption that cell-to-cell contacts rather than cell-to-matrix contacts might be crucial drivers of the resistance against *t*-BuOOH-induced toxicity is further supported by the study of Ko et al. (2000), which indicates that cell-cell contacts display a 30-fold higher stability as compared to cell-matrix contacts in human fibroblasts. The outcome of the mentioned study is strengthened by the observation that, although cells had already detached from the culture plate, intercellular contacts still remained, to the highest extent in HaCaT but also in Caco-2 cells (unpublished observation).

In general, an inverse correlation of cadherin-mediated cell-cell contact and β-integrin / receptor tyrosine kinase (RTK)-induced cell-matrix contact is assumed upon contact inhibition (Levenberg et al., 1998; von Schlippe et al., 2000). Therefore, the activation of β-integrin / RTK-induced mitogenic pathways, tightly correlated with EGFR, Ras or *c*-Src signaling, are inhibited in the presence of cell-cell contacts (Suarez Pestana et al., 1999; Nelson & Daniel 2002; Küppers et al., 2011). Interestingly, although these signaling cascades are not completely but most likely suppressed to the same extent in confluent, serum-depleted and U0126-treated NIH3T3 cells, solely confluent cultures were resistant against *t*-BuOOH-induced cell death. Moreover, semiconfluent cells were equally sensitive to *t*-BuOOH-induced toxicity in the absence and presence of FBS, further excluding a crucial role of growth factor-associated signaling in the regulation of *t*-BuOOH-induced toxicity in our cell systems. In addition, also secretion of soluble factors (e.g., growth hormones or immune modulatory stimuli) that might be released into the culture medium to render confluent cells resistant, were ruled out in confluent HaCaT cells upon H_2O_2 and peroxynitrite exposure (Bakondi et al. 2003). Hence, there appears no major role for cell-matrix contacts, growth factor stimuli and associated mitogenic signaling in the resistance of confluent cells against *t*-BuOOH-induced toxicity, but rather the presence of intercellular contacts seems to make the cell fate decision.

Steric hindrance of *t*-BuOOH uptake by the presence of cell-cell contacts, possibly being responsible for survival of confluent cultures, could be also excluded for the following reasons: the initial intracellular level of (i) cytosolic ROS as detected by CM-H2DCFDA staining and flow cytometry, (ii) oxidative DNA lesions, such as 8-oxo-dG (Wenz et al., 2019), as well as (iii) formation and repair of DNA SSBs assessed by alkaline Comet assays, were almost comparable in confluent and semiconfluent NIH3T3 cells upon setup I. Moreover, data obtained by EdU incorporation and laser scanning microscopy clearly showed a similar block of DNA replication in *t*-BuOOH-treated confluent and semiconfluent cultures upon setup II, and therefore, further support the assumption that a comparable amount of *t*-BuOOH molecules entered the cells. In this context, also To-Pro-3 staining of untreated confluent and semiconfluent cells was absolutely similar although this dye has a higher molecular weight compared to *t*-BuOOH and bears therefore a higher risk for impaired uptake in case of steric hindrance (unpublished observation).

On the other hand, a reduced formation of ROS, or *vice versa*, an increased level or regeneration capacity of intracellular antioxidants, such as GSH, was examined as potential molecular key for the survival of confluent in contrast to semiconfluent cells upon *t*-BuOOH exposure. So far, it is known that receptor tyrosine phosphatases (RTP), being upregulated in contact-inhibited but not in serum-depleted fibroblasts, are able to antagonize RTK-induced NADH oxidase activation, which results in a lowered basal ROS level (Dietrich et al., 1997; Pani et al., 2000; Boonstra & Post, 2004). RTK-induced ROS generation is, *vice versa*, stimulated in proliferating cells via cell-matrix contacts and growth factors like EGF (Boonstra & Post, 2004). Since (i) cell-matrix contacts and growth factor stimuli were excluded as crucial mediators of the resistance against *t*-BuOOH (described before), and (ii) early confluent cells rather resemble a proliferating phenotype, the above described mechanism might be not involved in the resistance of confluent cells.

These assumptions further fit flow cytometric data of this work, demonstrating no remarkable difference of the cytosolic ROS level in confluent versus semiconfluent (proliferating; serum-depleted) NIH3T3 and Caco-2 cells at the time point of *t*-BuOOH exposure. This data also provide evidence that serum depletion has no major effect on the intracellular ROS level and thereby rule out that the lack of antioxidative serum components (iron chelators like albumin or detoxifying enzymes like catalase) might increase basal ROS and render serum-depleted cells more sensitive to *t*-BuOOH.

Moreover, analysis of CM-H2DCFDA fluorescence provided strong evidence for a similar, time-dependent increase in t-BuOOH-derived cytosolic free radical species (OH·, t-BuO·, t-BuOO·) in confluent and semiconfluent cells prior to cell death induction (< 4 h). In this context, a huge number of reports have already described an increase in cytosolic ROS when mammalian cells, e.g., hepatocytes, macrophages or thymocytes were exposed to t-BuOOH (Palozza et al., 2002; Kanupriya et al., 2007; Lemasters et al., 2009). On the one hand, this work clearly indicates that survival of confluent cells is not mediated by a reduced formation of cytosolic ROS, neither on the basal level, nor upon t-BuOOH exposure.

Vice versa, it was tempting to speculate that also the antioxidative capacity might be similar in confluent and semiconfluent cells. As a first step, confluent and semiconfluent (proliferating) cells were treated with t-BuOOH in the context of experimental setup II. This second setup was able to rule out an increased detoxification of t-BuOOH in confluent compared to semiconfluent cells as a possible consequence of the higher plated cell number in case of setup I. Moreover, many reports have yet demonstrated that detoxification of t-BuOOH to t-butanol is mediated by GSH (Brigelius et al., 1983; Lombardi et al., 2002; Park et al., 2002; Tormos et al., 2004). This reaction is assumed to be catalyzed by the orchestrated action of GPXs, NAD(P)H-dependent GSH reductase and thioredoxin (Sies et al., 1978; Fratelli et al., 2003; Bindoli et al., 2008; Lemasters et al., 2009). On the other hand, catalase seems to play no crucial role in the detoxification of t-BuOOH since (i) this peroxide is poorly hydrolyzed by catalase (Winston et al., 1983; Watters et al., 1999; Awe et al., 2002), (ii) t-BuOOH acts as a suicide substrate for catalase (Pichorner et al., 1993), and (iii) the presence of catalase was able to block H_2O_2-, but not t-BuOOH-induced toxicity in vitro and ex vivo (Abe & Saito, 1998; Andrade et al., 2001). Thus, the intracellular GSH level appeared to primarily decide about the cell fate decision in case of t-BuOOH, and was therefore assessed by DTNB staining and photometric analysis.

In this context, other in vitro studies have surprisingly shown rather an oxidized than reduced GSH status during transition from a proliferating to a G1-arrested and / or differentiated cell phenotype, e.g., in epithelial intestine cells (Attene-Ramos et al., 2005; Circu & Aw, 2012). However, in concordance with results on the basal ROS level and the above described assumption of a similar intracellular signaling in (early) confluent and proliferating cells, the GSH level was almost similar

in confluent and semiconfluent (proliferating; serum-depleted) cultures of three different cell lines at the time point of *t*-BuOOH exposure (NIH3T3; HaCaT, MEF: unpublished data). Despite data could not be securely reproduced in the presence of *t*-BuOOH due to the low assay sensitivity, *t*-BuOOH seemed to provoke a comparable, time-dependent reduction of GSH in confluent and semiconfluent (proliferating; serum-depleted) NIH3T3 cells (unpublished data). Nevertheless, an increased GSH regenerative capacity upon confluence, e.g., via GSH reductase or thioredoxin, remains to be finally ruled out. In this context and to ascertain already obtained data, the DTNB assay can be combined with HPLC for more accurate, quantitative detection of intracellular GSH (Brigelius et al., 1983).

In contrast to the other cell lines, the basal GSH level of confluent Caco-2 cells was clearly diminished compared to semiconfluent (proliferating; serum-depleted) cultures at the time point of *t*-BuOOH exposure, whereby a significant difference of the measured GSH amount solely occurred between confluent and proliferating Caco-2 cells. This finding is supported by other groups, indicating a tight cell-cell contact-dependent regulation of GSH in Caco-2 cells (Noda et al., 2001; Nkabyo et al. 2002). Furthermore, confluent and to a much higher extent, semiconfluent Caco-2 cells surprisingly displayed rather an upregulated than a decreased level of GSH upon *t*-BuOOH exposure (unpublished data). The phenomenon that cells upregulate GSH upon challenge with *t*-BuOOH has been similarly observed in neuronal cells (Ekshyyan & Aw, 2005). The observed cell-cell contact-dependent GSH regulation, as well as GSH upregulation upon *t*-BuOOH exposure might be a tumorigenic characteristic of Caco-2 cells (Buhrke et al., 2011). In this context, a variety of reports describe upregulation of the antioxidative capacity (e.g., GSH and Nrf2) in tumor cells, rendering these cells more resistant to ROS, and therefore to chemo- and irradiation therapy (overview in Barrera, 2012).

Furthermore, the amount of intracellular ROS and GSH is assumed to crucially decide about replication and repair of mammalian DNA. For instance, the study by Russo et al. (1995) showed block of DNA replication through induction of a p53- and p21-dependent G1 arrest in response to intracellular ROS formation and GSH depletion in human fibroblasts. Moreover, as already described for H_2O_2-treated NIH3T3 cells by other groups, also *t*-BuOOH induced block of DNA replication – notably, to a similar extent in confluent and semiconfluent NIH3T3, HaCaT and Caco-2 cells as assessed by EdU incorporation and laser scanning microscopy (data of this

work; Chen et al., 1998; Chen et al., 2000; Barnouin et al., 2002). Hence, these data imply again a comparable intracellular ROS formation and detoxification of t-BuOOH by GSH in confluent and semiconfluent cells. Moreover, several findings of other groups have yet indicated a general link between ROS-induced DNA lesions and simultaneously arresting the cell cycle in order to stimulate DNA repair and thereby, to reduce the risk for the genetic transfer of mutagenic lesions during DNA replication (Rancourt et al., 2002; Boonstra & Post, 2004).

Besides block of DNA replication, also the level of t-BuOOH-induced oxidative DNA lesions (e.g., 8-oxo-dG) was similar in confluent and semiconfluent (proliferating; serum-depleted) NIH3T3 cells as assessed by modified FPG Comet assays (Wenz et al., 2019). These results were contradictory to previous findings of our and other groups at first sight since (i) the repair of H_2O_2-induced oxidative DNA lesions via the BER pathway was impaired in differentiated versus proliferating muscle cells (Narciso et al., 2007), and (ii) contact-inhibited NIH3T3 cells demonstrated downregulated mRNA levels of crucial BER components (e.g., OGG1, FEN1 or LIG1), what also hinted towards impairment of oxidative DNA damage repair in the presence of cell-cell contacts (Küppers et al., 2010). Due to the afore described assumption of Rothen-Rutishauser et al. (1998), these contradictory results might be explained by a distinct intracellular signaling in late confluent or differentiated cells versus early confluent cultures that were analyzed in the context of this work.

In addition to the oxidation of purine and pyrimidine bases, t-BuOOH has been yet reported to induce DNA SSBs, resulting from damage to the sugar-phosphate backbone or AP sites, as well as to provoke replication-dependent, highly toxic DNA DSBs in different cellular systems (Ochi et al., 1989; Altman et al., 1994; Latour et al., 1995; Park et al. 2003; Tormos et al., 2004). According to the data obtained by alkaline Comet assays, a similar, concentration-dependent SSB formation and repair velocity was observed in confluent and semiconfluent NIH3T3 cells upon t-BuOOH exposure, further supporting a similar uptake of t-BuOOH, as well as a comparable intracellular ROS formation in confluent and semiconfluent cells. However, although the same is assumed for t-BuOOH uptake and ROS formation in Caco-2 cells, confluent compared to proliferating cultures were more resistant to t-BuOOH-induced SSB formation. In this context, cell cycle-dependent effects were primarily excluded since serum-depleted Caco-2 cells were even more sensitive to t-BuOOH-induced SSB formation as compared to confluent and proliferating cells (unpublished data).

On the other hand, a similar repair of *t*-BuOOH-induced SSBs in confluent and proliferating Caco-2 cells brought no explanation for the observed resistance of confluent cells against these DNA lesions. However, although the amount of SSBs formed upon *t*-BuOOH exposure in confluent and proliferating Caco-2 cells was significantly different from the statistical view, comparison of the tail intensity values in consideration of the calculated standard deviations triggers the assumption that the resistance of confluent Caco-2 cells might be not pronounced enough to have a remarkable effect *in vivo*. Nevertheless, an improved SSB repair in confluent compared to semiconfluent Caco-2 cells cannot be completely ruled out since SSB repair was analyzed by a small number of experiments. In this context, a possible role of Gadd45a might be worth to be investigated due to (i) its role as cellular stress sensor in DNA repair and cell survival, as well as due to (ii) upregulation of Gadd45a in partially differentiated tumors (e.g., melanoma), increasing the resistance against chemotherapy upon the presence of cell-cell contacts (Vairapandi et al., 2000; Azam et al., 2001; Maeda et al., 2002; Ji et al., 2007; Liebermann & Hoffman, 2008; Shan et al., 2012; Morano et al., 2014; Liu et al., 2018).

In contrast to distinct results on the formation of *t*-BuOOH-induced SSBs in NIH3T3 and Caco-2 cells, neutral Comet assays and detection of γ-H2AX via Western Blot analysis (unpublished data) and laser scanning microscopy provided evidence that confluent in contrast to semiconfluent cultures of both cell lines were protected against the time-dependent increase in DNA DSBs, which was observed from the time point of cell death induction (3 - 4 h) onwards. Interestingly, the level of *t*-BuOOH-induced DSBs during the early treatment phase (1-2 h) was comparable in confluent and semiconfluent NIH3T3 and Caco-2 cells. These results, yet again, strengthen a similar uptake of *t*-BuOOH, as well as an equal ROS formation in confluent and semiconfluent cultures. Since mammalian DNA replication is averagely accomplished during 24 h, it is tempting to speculate that *t*-BuOOH induced here rather direct instead of replication-dependent DSBs via formation of "clustered lesions" by topoisomerases or along with the process of transcription (Cooper, 2000; Sedelnikova et al., 2010).

In the light of the above described findings, one explanation for the observed resistance of confluent cells against the time-dependent increase in DNA DSBs and cell death might be an improved DSB repair capacity. However, after a similar, initial DSB increase in confluent and semiconfluent NIH3T3 cells prior to *t*-BuOOH-induced

cell death, the DSB level in confluent cultures did not fully recover to the level of untreated control cells later on but rather a " DSB steady state level" was observable. In contrast, confluent Caco-2 cells were able to completely recover DSBs to the level of untreated controls till the time point cell death was induced in semiconfluent cells. However, in the light of other findings that will follow here and in the next discussion section, confluence-mediated protection against the increase in t-BuOOH-induced DSBs might be not a direct consequence of an improved DSB repair capacity but rather based on the prevention of t-BuOOH-induced mitochondrial damage.

In this context, analysis of the MMP ($\Delta\psi_m$) via DiOC6 staining and simultaneous detection of t-BuOOH-induced cell death by PI revealed resistance of confluent cells against the time-dependent loss of $\Delta\psi_m$, which occurred in semiconfluent (prol.; sd) NIH3T3 and HaCaT cells clearly prior to cell death induction (1-3 h). These findings are supported by (i) MTT assays, (ii) Mitotracker staining upon setup II, and (iii) several reports, describing loss of $\Delta\psi_m$ by the presence of t-BuOOH in other cellular systems (Nieminen et al., 1997; Kroemer et al., 1998; Kanupriya et al., 2007; Wu et al., 2018). Besides confluent Caco-2 cells were similarly resistant against the loss of the MMP, $\Delta\psi_m$ was comparatively late and lesser impaired in proliferating Caco-2 cultures as in NIH3T3 cells. Interestingly, where proliferating NIH3T3 cells exhibited a complete breakdown of $\Delta\psi_m$ at the time point of cell death induction (3-4 h), proliferating Caco-2 cells still maintained 50 % of $\Delta\psi_m$ till the onset of t-BuOOH-induced cell death (4-5 h). This comparatively long retention of $\Delta\psi_m$ in semiconfluent Caco-2 cells might be a consequence of the already described upregulation of GSH upon t-BuOOH exposure, and therefore, possibly an additional tumorigenic characteristic of these colon carcinoma cells.

Since $\Delta\psi_m$ is the major driving force for the activity of the F_0/F_1 ATPase within the mitochondrial electron transport chain (ETC) (Kroemer et al., 1998; Brookes et al., 2004), a negative correlation between the loss of $\Delta\psi_m$ and mitochondrial ATP synthesis was expected in t-BuOOH-treated semiconfluent cultures. Indeed, in NIH3T3 and HaCaT cells, a clear decrease in luciferase-detected intracellular ATP was observable but not before $\Delta\psi_m$ almost completely collapsed and cell death was initiated (3-4 h). The unexpected, almost stable ATP level in these cells upon a yet remarkable depolarization of $\Delta\psi_m$ during the early phase of t-BuOOH treatment (1-3 h) might be explained by another correlation of ATP and $\Delta\psi_m$ since mitochondrial ATP acts as a buffering system to maintain $\Delta\psi_m$. In this context, mitochondria have

been yet described to store huge amounts of ATP in order to supply this vital molecule for energy-dependent reactions in the cytosol or the nucleus in response to cellular stress conditions (Zorova et al., 2018). Thus, the early decrease in $\Delta\psi_m$ observed in t-BuOOH-exposed semiconfluent cultures might be a sign for the release of ATP from mitochondria, but might also hint towards ETC impairment and / or induction of reversible PTPC opening as discussed below and in the following section. However, since the intracellular ATP level was not fully depleted at the time point of cell death induction in semiconfluent NIH3T3 and HaCaT cells, not only the availability of ATP appears to decide about cell survival but also the extent of cellular damage seems to crucially dedicate the onset of t-BuOOH-induced cell death.

In contrast, confluent NIH3T3 and HaCaT cells exhibited a stable ATP level throughout the whole treatment duration of t-BuOOH exposure, whereas in the absence of t-BuOOH, the basal level of ATP was not significantly different in confluent and semiconfluent cultures. However, previous reports have yet described rather a decrease in $\Delta\psi_m$ and ATP in contact-inhibited versus proliferating mammalian cells, what might be again explained by different signaling in early and late confluent cells as discussed already before (Wilden et al., 1998; Agathocleous & Harris, 2013; Xiaoyun et al., 2017). Additionally, these results favor the hypothesis that the time-dependent DSB increase, observed in semiconfluent NIH3T3 cells, might be a downstream event of t-BuOOH-induced mitochondrial dysfunction since the DSB increase did not occur before $\Delta\psi_m$ collapsed and ATP was significantly reduced. This hypothesis is further strengthened by the fact that mitochondrial vitality, tightly coupled to ATP synthesis, crucially decides about the efficacy of DNA repair (Kroemer et al., 1998; Lans et al., 2012). On the other hand, some further results were somehow striking in the context of this hypothesis at first glance since, e.g., FCCP, known to uncouple ATP synthesis from oxidative phosphorylation, and therefore from $\Delta\psi_m$, rather increased than prevented t-BuOOH-induced cell death (data of this work; Hanstein, 1976; Jarvis et al., 2007).

However, impairment of the mitochondrial ETC, possibly coming along with the loss of $\Delta\psi_m$ in t-BuOOH-treated semiconfluent NIH3T3 and HaCaT cells, is likely and supported by results of the NAD$^+$ cycling assay that clearly demonstrate an early, time-dependent reduction of NAD$^+$ prior to cell death induction (1-3 h). This is in accordance with the fact that $\Delta\psi_m$ is established by an ETC-driven electron transfer and the release of protons from oxidized NADH (Alberts et al., 2002; Brayden et al.,

2014). Thus, the application of NAD$^+$ reducing agents like, for instance, β-hydroxybutyrate might be able to restore $\Delta\psi_m$. In addition, results of the NAD$^+$ cycling assay and previous findings of another group stimulate the assumption that t-BuOOH induces an irreversible oxidation of (mitochondrial) NADH (Nieminen et al., 1997). Interestingly, in the light of this assumption, the increase in t-BuOOH-induced cell death by FCCP becomes plausible at second glance since FCCP- driven proton trapping might reduce the available amount of NADH followed by a limited regeneration of oxidized GSH (GSSG), and finally, might promote mitochondrial dysfunction and impairment of ATP synthesis due to a lesser efficient GSH-mediated detoxification of t-BuOOH (Gunter & Pfeiffer, 1990; Circu & Awe, 2012).

Remarkably, confluent cells were not only completely resistant against the time-dependent decrease in NAD$^+$ upon t-BuOOH exposure, but also in the absence of the peroxide, confluent cells exhibited significantly elevated amounts of NAD$^+$ compared to proliferating cultures. However, in contrast to the other cell lines (NIH3T3, HaCaT), a similar initial decline in NAD$^+$ became visible in t-BuOOH-treated confluent and semiconfluent Caco-2 cells. Interestingly, confluent in contrast to semiconfluent Caco-2 cells were able to completely restore NAD$^+$ levels prior to cell death induction. With regard to the already described upregulation of GSH in confluent and semiconfluent Caco-2 cells upon t-BuOOH challenge, and the fact that NADH is an essential cofactor to regenerate oxidized GSH (GSSG) (Gunter & Pfeiffer, 1990; Circu & Awe, 2012), the initially observed reduction of NAD$^+$ in confluent and semiconfluent Caco-2 cells might be a synergistic effect of (i) an irreversible NADH oxidation by t-BuOOH-derived radicals and (ii) in contrast to the other cell lines, an increased need for NADH to regenerate GSSG.

Nevertheless, a significant upregulation of NAD$^+$ prior to t-BuOOH exposure was also detected in confluent Caco-2 cells. In this context, an increased reduction of the redox couple NAD$^+$/NADH has been so far observed when intestine cells initiated proliferation stop upon contact inhibition (Attene-Ramos et al., 2005). On the other hand, NADPH-dependent t-BuOOH detoxification was upregulated upon differentiation of neuronal cells, rendering these cultures more resistant to t-BuOOH-induced cell death (Ekshyyan & Aw, 2005). In contrast to these described reports, favoring an increased NAD$^+$ regeneration capacity in confluent cells, results presented in this work imply rather upregulation of the NAD$^+$ *de novo* synthesis by the presence of cell-cell contacts since the NAD$^+$ cycling assay is a direct measure

for the intracellular availability of NAD$^+$ independent of the cellular capacity to reduce the oxidized form of this cofactor (Bernofsky & Swan, 1973). Hence, there seems to be a crucial link between the intracellular NAD$^+$ level and survival of confluent cells upon *t*-BuOOH exposure.

In summary, this work proves that (early) confluent compared to semiconfluent murine fibroblasts (NIH3T3) and human epithelial cells (HaCaT, Caco-2) are protected against *t*-BuOOH-induced cell death independent of a G1 arrest. Upon a similar cytosolic ROS formation and block of DNA replication, cell-cell contacts are able to provide resistance against (i) irreversible NADH oxidation, (ii) reduction of ATP, (iii) loss of $\Delta\psi_m$, and (iv) the time-dependent increase in DNA DSBs induced by *t*-BuOOH exposure (see Figure 58). Moreover, in contrast to a similar basal GSH level and a comparable amount of *t*-BuOOH-induced DNA SSBs detected in confluent and semiconfluent, non-tumorigenic cultures (NIH3T3, HaCaT), a tight cell-cell contact-dependent regulation of these two parameters occurred in tumorigenic Caco-2 cells, rendering these cells probably more resistant to cancer therapy upon confluence. An overview of all, potentially crucial mediators that might be responsible for the resistance of confluent cells against *t*-BuOOH-induced toxicity can be found in the last discussion section (Figure 60).
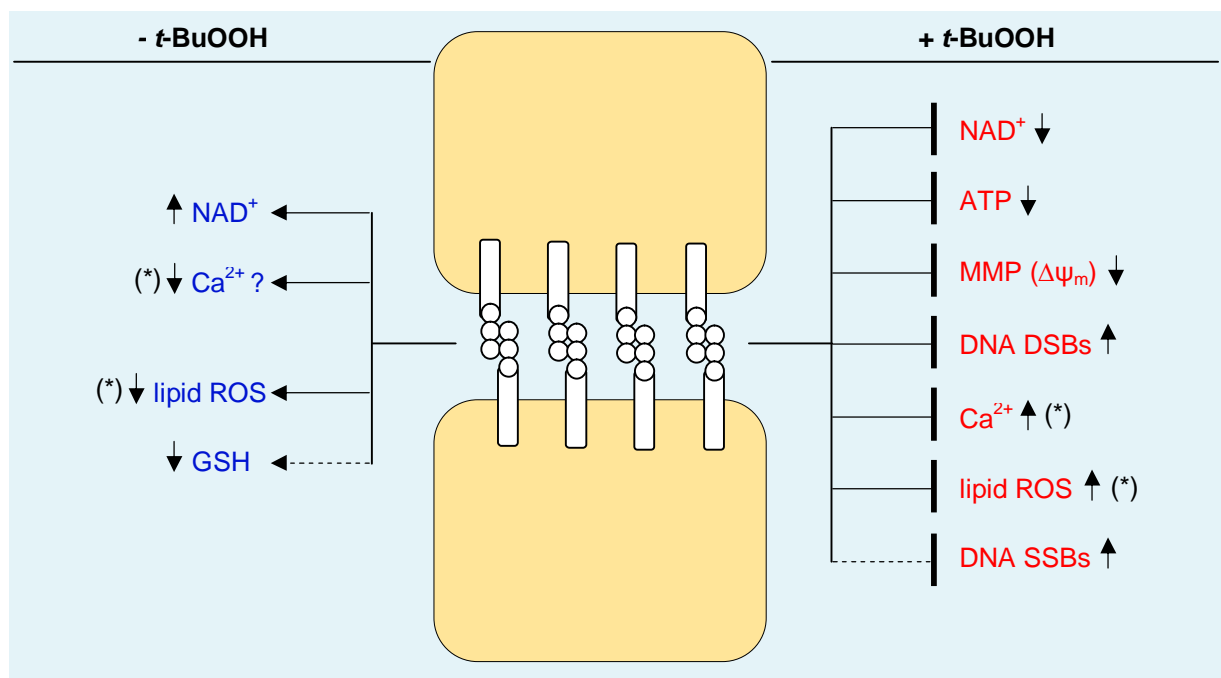
Fig. 58 Molecular effects of cell-cell contacts on the physiological status (- *t*-BuOOH, *left*) of mammalian cells and protection against *t*-BuOOH-induced toxicity and related cellular damage (+ *t*-BuOOH, *right*). (*dashed lines*) Effect only observed in tumorigenic Caco-2 cells in contrast to non-tumorigenic cells (NIH3T3, HaCaT). (*) for further explanation, see the last discussion section (6.3).

5.2 *t*-BuOOH induces Ca^{2+}-dependent ferroptosis *in vitro*

To identify the lethal trigger of *t*-BuOOH-induced necrosis in semiconfluent murine fibroblasts (NIH3T3) and human epithelial cultures (HaCaT, Caco-2), possibly providing hints towards the crucial mediator that renders confluent cultures resistant, *t*-BuOOH-induced cell death was characterized as second working part of this PhD thesis. In this context, the cell morphology induced by *t*-BuOOH in semiconfluent NIH3T3, HaCaT and Caco-2 cultures strongly hinted towards a necrotic cell death. Further evidence for rapid induction (~ 3-5 h) of a necrotic-like cell death mechanism by *t*-BuOOH (NIH3T3: 30 or 50 µM; HaCaT: 200 µM; Caco-2: 100 µM) was provided by AnnexinV-FITC / PI staining followed by flow cytometry and laser scanning microscopy. Thus, different key regulators of necrotic cell death subroutines that can occur in a tightly orchestrated manner upon as referred to "regulated necrosis" (RN) were evaluated in terms of *t*-BuOOH-induced necrosis (Galluzzi et al., 2012, 2014).

Involvement of caspases in *t*-BuOOH-induced necrosis, for instance, as described for the RN subroutine of pyrroptosis, was excluded due to (i) the absence of caspase 3 or caspase 3-induced PARP-1 cleavage detected by Western Blot analysis, (ii) the absence of caspase-mediated DNA fragmentation as assessed by flow cytometric subG1 analysis, as well as due to (ii) the lacking effect of the *pan*caspase inhibitor z-VAD-fmk on *t*-BuOOH-induced necrosis despite significant inhibition of cisplatin-induced apoptosis. Contrarily to this work, *t*-BuOOH has been already described to be a potent inducer of apoptosis, e.g., in macrophages, liver carcinoma cells, or PC12 cells as model cell line for neuronal cell differentiation (Amoroso et al., 2002; Kanupriya et al., 2007; Wu et al., 2018). On the other hand, there is also evidence that higher amounts of *t*-BuOOH (75 µM instead of 2.5 µM) can trigger regulated necrosis in the latter cell line (Wu et al., 2018).

Besides a more general explanation by cell type-specific effects that might be responsible for the induction of distinct cell death mechanisms by *t*-BuOOH, the existence of an intracellular ROS level threshold, as well as the intracellular site of ROS generation seem to crucially decide about the switch between apoptotic and necrotic cell death. In the end, these two parameters appear to determine whether (i) intracellular caspases are inactivated by SH-group oxidation, and (ii) if the ATP level is sufficient to mediate highly energy-consuming apoptotic cell death mechanisms (Kroemer et al., 1998; Kim et al., 2003; Vairetti et al., 2005). Further support for this

hypothesis comes from the report of Panieri et al. (2013), regarding H_2O_2-induced ROS formation *in vitro*. Moreover, components of the antioxidative defense (e.g., GSH) or the DNA damage response (e.g., PARP-1) might influence the intracellular ROS level threshold but they appear to act rather downstream of caspases and ATP in making the cell death mechanism switch (Bakondi et al., 2003).

Flow cytometric cell death analysis in *t*-BuOOH-treated NIH3T3, HaCaT and Caco-2 cells additionally provided first evidence for *t*-BuOOH to be a so far unknown inducer of ferroptosis – a yet recognized RN subroutine, which is selectively inhibited by FS (Dixon et al. 2012; Friedmann Angeli et al. 2014; Skouta et al. 2014; Yang et al. 2014; Dong et al. 2015). These findings were strengthened by further experiments in our lab, demonstrating inhibition of *t*-BuOOH-induced necrosis in NIH3T3 cells by other agents that have been already described to block ferroptotic cell death through (i) an antioxidative defense mechanism as mediated by FS against cytosolic and lipid ROS formation (e.g., liproxstatin-1, LX; α-tocopherol), or by (ii) iron chelation (e.g., deferoxamine) (Dixon et al. 2012; Skouta et al. 2014; Dong et al. 2015; Kabiraj et al., 2015; Zilka et al., 2017; Wenz et al., 2018). Besides lipid ROS formation and iron overload, GSH depletion or inhibition of GPX4 activity, have been also described to be crucial mediators of ferroptosis *in vitro* and *in vivo* (Yang & Stockwell, 2008; Dixon et al. 2012; Linkermann et al., 2013; Dixon et al., 2014; Friedmann Angeli et al., 2014; Linkermann et al., 2014; Xie et al., 2016; Yang & Stockwell 2016; Yang et al., 2016; Yang & Stockwell, 2016; Yu et al., 2017; Galluzzi et al., 2018). In the course of this, *t*-BuOOH-induced ferroptosis was also inhibited by the presence of NAC – a widely known ROS scavenger, which enhances the GSH *de novo* synthesis by supply of cysteine, and thus being yet described to block ferroptosis upon prevention of lipid ROS-mediated cellular damage and GSH depletion (Aruoma et al., 1998; Yang et al., 2014; Gao et al., 2015; Lörincz et al., 2015; Xie et al., 2016; Yu et al., 2017; Li et al., 2018; Wu et al., 2018).

Notably, the hypothesis of a ferroptotic cell death, being induced by the presence of *t*-BuOOH, has arisen at secondary glance, since a remarkably similar formation of cytosolic ROS and block of DNA replication was observed in *t*-BuOOH-treated confluent and semiconfluent cultures, and therefore, also an equally similar lipid ROS level has been initially assumed. Furthermore, semiconfluent cells of all analyzed cell lines were rescued from *t*-BuOOH-induced necrosis by the RIPK1 inhibitor Nec-1. Evaluation of *t*-BuOOH as ferroptosis inducer was finally stimulated

by the following findings: (i) flow cytometric analysis in the presence of other more specific RIPK1 (and RIPK3) inhibitors, as well as in RIPK1$^{-/-}$ (and RIPK3$^{-/-}$) NIH3T3 knockout cell clones proved an unspecific off-target effect of Nec-1 in accordance with results of other groups (Vandenabeele et al., 2013; Friedmann Angeli et al., 2014; Eling et al. 2015). Moreover, (ii) several reports have, still controversially, but yet described inhibition of ferroptosis by Nec-1 in an unspecific manner (Dixon et al., 2012; Friedmann Angeli et al., 2014; Eling et al., 2015).

Besides inhibition of t-BuOOH-induced necrosis by distinct ferroptosis inhibitors and strong hints towards detoxification of t-BuOOH by GSH, further analyses of our lab revealed lipid peroxidation as another marker of ferroptosis: (i) an increase in lipid ROS with its maximum prior to cell death induction as assessed by C11-BODIPY staining and flow cytometry, and (ii) elevated amounts of the secondary, toxic lipid ROS breakdown product MDA as detected by the photometric TBARS assay in t-BuOOH-exposed NIH3T3 cells (Wenz et al., 2018). Both findings clearly fit reports of other groups, demonstrating that t-BuOOH is a prominent lipid ROS inducer, which is able to deplete GSH in $vitro$ and remarkably resembles lipid ROS pattering of various human pathologies, such as ischemia / reperfusion injury, neurodegenerative disorders and cancer (Masaki et al., 1989; Coleman et al., 1989; Barr & Mason, 1995; Lemasters & Nieminen, 1997; Garcia-Cohen et al., 2000; Lombardi et al., 2002; Park et al., 2002; Mateos et al., 2004; Tormos et al., 2004; Lemasters et al., 2009; Ayala et al., 2014). Further data obtained by flow cytometric analyses showed also inhibition of t-BuOOH-induced necrosis by the ferroptosis inhibitor XJB-5-131 (mitochondria-selective) or JP4-039, and identified thereby, the peroxidation of mitochondrial cardiolipin (CL) as the primary toxic lesion for the underlying cell death mechanism (Wipf et al., 2005; Ji et al., 2012; Krainz et al., 2016; Wenz et al., 2018). Surprisingly, neither FS and LX, nor XJB-5-131 and JP4-039 were able to prevent loss of the MMP ($\Delta\psi_m$), and solely LX partially blocked the increase in t-BuOOH-induced DNA DSBs (Wenz et al., 2018).

In contrast to t-BuOOH, an equitoxic concentration of H_2O_2 was able to induce an increase in cytosolic, but not in lipid ROS formation in NIH3T3 cells as assessed by further analyses of our lab (Wenz et al., 2018). In addition to the assumption that H_2O_2 might trigger, in principal, another oxidative stress patterning than t-BuOOH, there is also evidence that the equitoxic concentration of H_2O_2 was possibly not high enough to induce lipid ROS formation in NIH3T3 cells since H_2O_2 and t-BuOOH have

been yet reported to similarly induce lipid ROS formation, for instance, in isolated thymocytes (Palozza et al., 2002). This hypothesis is strengthened also by the fact that H_2O_2 has a higher susceptibility to react with macromolecules than t-BuOOH, so that t-BuOOH is more capable than H_2O_2 to reach deeply located cellular sites, such as lipid ROS-sensitive mitochondria (Baker & He, 1991; Alia et al., 2005).

Further analyses of this work revealed that the DDR components p53 and PARP-1 are not crucially involved in t-BuOOH-induced ferroptosis. In this context, the activation of p53 and PARP-1 by t-BuOOH as detected by Western Blot analysis and / or laser scanning microscopy might be a general consequence of ROS-induced DNA damage in order to stimulate DNA repair, and / or cell cycle arrest (Levine, 1997; Pan et al., 2009; Swindall et al., 2013). The assumption that p53 and PARP-1 are no key regulators of t-BuOOH-induced ferroptosis is supported by the following findings via flow cytometry or Western Blot analysis: (i) t-BuOOH induced ferroptosis also in p53-mutated HaCaT cells and p53-deficient Caco-2 cells, (ii) p53$^{-/-}$ fibroblasts were not rescued but rather slightly sensitized to t-BuOOH-induced ferroptosis (Wenz et al., 2018), and (iii) although the PARP-1 inhibitor olaparib partially restored NAD$^+$ at later time points of t-BuOOH exposure, the inhibitor failed to protect cells against ferroptosis.

Moreover, Western Blot analysis provided evidence that t-BuOOH induced activation (phosphorylation) of the DDR-related stress kinases p38 and JNK in accordance to previous findings of other groups (Chen et al., 2010; Wu et al., 2018). Interestingly, cell death analysis in the presence of a chemical p38 (SB203580) or JNK (SP600125) inhibitor clearly demonstrated a prosurvival function of both stress kinases, so far being solely described in the context of apoptosis (Sabapathy et al., 1999; Pereira et al., 2013; Deng et al., 2001). However, there are contradictory findings that inhibition of p38 and JNK rescues cells from ferroptosis, what might be a cell-type or agent-specific effect (Xie et al., 2016). Nevertheless, it is likely that prosurvival activation of these DDR-related kinases by t-BuOOH might end up in an NF-κB-driven survival response since activation of NF-κB via p38 and JNK has been yet reported upon oxidative stress, for instance, upon H_2O_2 exposure (Craig et al., 2000; Siomek, 2012). Interestingly, NF-κB is able to upregulate antioxidative capacities that are needed for the detoxification of t-BuOOH-derived lipid ROS (e.g., GPX and thioredoxin), and *vice versa*, intracellular lipid ROS-generating systems are downregulated (e.g., LOX-5 and LOX-12) (overview in Morgan & Liu, 2011).

On the other hand, also the ATR- or ATM- related target kinases Chk1 and Chk2 were activated (phosphorylated) by the presence of t-BuOOH as shown by Western Blot analysis. Surprisingly, cell death analysis in the presence of a chemical ATR (VE-821) and ATM (Ku60019) inhibitor clearly demonstrated a general, prosurvival role for ATR, whereby ATM acted only in NIH3T3 and HaCaT cells (C. Turmann, MD thesis, in preparation), but not in Caco-2 cultures in a prosurvival manner upon t-BuOOH-induced ferroptosis. In this context, chemical inhibition of ATR or ATM might generally potentiate t-BuOOH-induced cell death due to an impaired repair of DNA SSB and DSBs that are formed in the presence of this peroxide. However, there is also increasing evidence that ATR activation might also end up in a prosurvival, NF-κB-mediated response mechanism. For instance, an ATR-Chk1-related anti-apoptotic pathway, which involves downstream activation of NF-κB, has been yet reported (Rocha et al., 2005). Anyway, a molecular mechanism, which might result in NF-κB activation via ATM, remains to be elucidated.

Since lipid ROS-blocking agents like FS, LX, XJB-5-131 and JP4-039 were able to inhibit t-BuOOH-induced ferroptosis, but failed to restore $\Delta\psi_m$, and did not (FS) or only partially (LX) block the increase in DSBs, both cellular lesions were not crucial for t-BuOOH-induced ferroptosis (data of this work; Wenz et al., 2018). On the other hand, these results imply the existence of another trigger, being responsible for these cellular lesions upon t-BuOOH exposure independent of lipid ROS formation. Remarkably, a huge number of *in vitro* and *in vivo* studies have yet described Ca^{2+} as crucial regulator of the apoptotic, as well as necrotic killing machinery and their related cellular damage (Decrock et al., 2013). Fitting reports of other groups that have already described inhibition of, e.g. H_2O_2-induced cell death by Ca^{2+} chelation, the cell-permeable Ca^{2+} chelator BAPTA AM significantly inhibited t-BuOOH-induced ferroptosis in NIH3T3, HaCaT and Caco-2 cells (data of this work; Bakondi et al., 2003; Bentle et al., 2006). Further cell death analyses conducted by our group in t-BuOOH-treated NIH3T3 cells with the Ca^{2+} indicator Fura-2, which is known to act as Ca^{2+}-chelating agent, clearly showed similar results as obtained by flow cytometry in the presence of BAPTA AM (unpublished data; (Neher, 1995). Thus, it can be excluded that BAPTA AM protects against t-BuOOH-induced ferroptosis via its ability to bind other divalent metal ions, such as lipid ROS- promoting iron.

In accordance with these findings, data obtained by Fluo-4 AM staining and flow cytometry revealed a remarkable increase in cytosolic Ca^{2+} at the time point of cell death induction (3-4 h), coming along with the detected maximum of lipid peroxidation, the collapse of $\Delta\psi_m$ and increasing amounts of DSBs upon t-BuOOH exposure in NIH3T3 cells. In macrophages and isolated hepatocytes, a similar increase in cytosolic Ca^{2+} has been observed in the presence of t-BuOOH (Kmonickova et al., 2000; Kanupriya et al., 2007). In general, it is assumed that oxidants are able to disturb intracellular Ca^{2+} homeostasis due to the modification of cellular metabolism and structural elements that are crucial for Ca^{2+} regulation (Ermak & Davies, 2002). Upon physiological conditions the cytosolic Ca^{2+} level is mostly maintained and kept low by plasma membrane Ca^{2+} ATPases, catalyzing the efflux of incoming, high amounts of Ca^{2+} from the extracellular medium in addition to action of voltage- or ligand-dependent Ca^{2+} channels (e.g., IP3-activated Ca^{2+} channels) or Ca^{2+} / $2Na^+$ exchanger (Gunter et al., 1994; Ermak & Davies, 2002; Strehler & Zacharias, 2001). On the other hand, Ca^{2+} ATPases catalyze ER-mediated sequestration of cytosolic Ca^{2+} (Ermak & Davies, 2002; Giorgi et al., 2009). Since Ca^{2+} ATPases are highly sensitive to the oxidation by ROS, provoking inhibition of these ATP-driven pumps, it is likely that radical oxygen species derived from t-BuOOH (OH·, t-BuO·, t-BuOO·) via the Fe^{2+}-catalyzed Fenton reaction mediate Ca^{2+} ATPase oxidation, and therefore provoke an increase in cytosolic Ca^{2+} (Ermak & Davies, 2002; Decrock et al., 2013; Zhang et al., 2016).

A more detailed hypothesis of this work hints towards an increase in cytosolic Ca^{2+} upon t-BuOOH exposure not as a result of ER depletion but rather via Ca^{2+} ATPase inactivation, as well as via ROS-induced disintegration of the plasma membrane for the following reasons: (i) Ca^{2+} release from ER is mediated via IP3-activated Ca^{2+} channels, whereby IP3 synthesis is dependent on the presence of growth factors in contrast to t-BuOOH-induced ferroptosis (data of this work; Li et al., 2004). (ii) An *in situ* study in mouse skeletal muscles provides evidence that ATPase-mediated uptake of cytoslic Ca^{2+} to the SR is inhibited in the presence of t-BuOOH (Andrade et al., 2001). (iii) t-BuOOH treatment did not affect IP3-releasable Ca^{2+} pools in endothelial cells (Elliott & Doan, 1993). Furthermore, (iv) low or moderate oxidative stress (e.g., provided by H_2O_2), rather initiating apoptosis, is related to a cytosolic Ca^{2+} increase by IP3-mediated ER depletion. In contrast, (v) high concentrations of H_2O_2 are known to provoke an increase in cytosolic Ca^{2+} by

inhibition of Ca^{2+} ATPases and / or plasma membrane disintegration upon induction of necrotic cell death (Roveri et al., 1992; Hampton & Orrenius, 1997; Leist et al., 1997; Ermak & Davies, 2002; Nicotera & Melino, 2004; Saito et al., 2006).

However, first experiments in NIH3T3 and Caco-2 cells indicated only a partial reduction of the cytosolic Ca^{2+} increase when cells were exposed to t-BuOOH in Ca^{2+}-free medium as assessed by Fluo-4 AM staining (unpublished data). Therefore, the increase in cytosolic Ca^{2+} by t-BuOOH might be not only a consequence of (i) an impaired Ca^{2+} efflux across the plasma membrane in case of Ca^{2+} ATPase inactivation or (ii) an increased Ca^{2+} influx from the extracellular medium due to plasma membrane disintegration, but seems to be simultaneously provoked by (iii) Ca^{2+} release from intracellular stores apart from the ER, like for instance, the mitochondria. This hypothesis is further strengthened by the study of Bakondi et al. (2003), clearly demonstrating resistance of confluent HaCaT cells against H_2O_2- and peroxynitrite-induced toxicity, as well as inhibition of cell death in semiconfluent cultures by the presence of BAPTA AM. These results are in remarkable accordance to the presented data of this work with regard to t-BuOOH. Interestingly, Bakondi's group (2003) further showed that ROS-inducing peroxynitrite provoked an increase in cytosolic Ca^{2+} by release of Ca^{2+} from intracellular stores, as well as by Ca^{2+} influx from the culture medium. Hence, t-BuOOH might act in a similar manner.

Mitochondrial Ca^{2+} accumulation, and therefore, the release of Ca^{2+} from these organelles into the cytosol when being overloaded, is explicitly favored as additional source for increased amounts of cytosolic Ca^{2+} upon t-BuOOH exposure by further flow cytometric analyses of our lab and the lab of Dr. Wolfgang Greffrath (Medical Faculty Mannheim, Germany) with help of the Ca^{2+}-sensitive fluorescent probe Fura-2 AM. These measurements provide evidence for an increase in free Ca^{2+} after exposure of NIH3T3 cells to t-BuOOH (unpublished data). Comparing these results with the data that were generated by Fluo-4 AM staining and flow cytometry, a significant increase in cytosolic Ca^{2+} accordingly occurred at the time point of cell death induction (3-4 h) (data of this work). Remarkably, it has been so far assumed that Fura-2 and its cell-permeable AM form are indicators of cellular, free Ca^{2+}, but there is huge evidence that Fura-2, and especially Fura-2 AM, rather detect mitochondrial Ca^{2+} changes since both indicators can be trapped by mitochondria of mammalian cells (overview in Gunter et al., 1994; Ricken et al., 1998). Moreover, these *in vitro* studies showed that Fura-2, but especially its AM form, accumulates in

"hotspot areas" located to the mitochondria of mammalian cells as assessed by (i) costaining with mitochondrial markers, or (ii) simultaneous detection of mitochondria-located NAD(P)H autofluorescence at 364 nm via laser scanning microscopy.

To further control the above described hypothesis, t-BuOOH treatment in combination with either CCP, FCCP or antimycin A should quench increased Fura-2 AM fluorescence in case of accumulated mitochondrial Ca^{2+} because these agents are known to induce the release of Ca^{2+} from the organelles (Gunter et al., 1994; Ricken et al., 1998). *Vice versa*, Fura-2 AM fluorescence is expected to increase upon Ca^{2+} release of the SR / ER (Gunter et al., 1994). Since the study by Ricken and coworkers (1998) clearly showed no accumulation of Fura-2 in HT29 cells, when the non-AM form of the Ca^{2+} indicator was loaded, and in consideration of the other existing reports, it is very likely that (i) the detected increase in Fura-2 AM fluorescence reflects an increase in mitochondrial, free Ca^{2+}, and that (ii) Fura-2 AM blocked ferroptosis via mitochondrial Ca^{2+} chelation in t-BuOOH-exposed NIH3T3 cells (unpublished data).

Upon physiological conditions, mitochondrial Ca^{2+} has been yet demonstrated to stimulate the activity of TCA cycle-related dehydrogenases, isoforms of adenine nucleotide translocators (ANTs) or the synthesis of ATP via the F_0/F_1 ATPase (Gunter et al., 1994; Rimessi et al., 2008; Zhang et al., 2016). Besides maintenance of cellular metabolism and energy homeostasis, also the mitochondrial membrane potential $\Delta\psi_m$ is preserved, e.g., by Ca^{2+}-dependent "flickering" of the MPT pore (PTPC) in response to the intracellular level of, e.g., NADH, GSH and ATP. Upon binding of NAD^+, GSSG or ADP / PI to redox-sensitive sites of the MPT pore itself or to modulatory PTPC components like ANT, transient PTPC opening is induced upon an increase in mitochondrial Ca^{2+} (Gunter et al., 1994; Brookes et al., 2004; Rimessi et al., 2008; Wei & Dirksen, 2012). In this case, the SR / ER is assumed as the main source for mitochondrial Ca^{2+}, which is transferred via locally linked mitochondria / ER membrane hotspot areas without affecting the cytosolic Ca^{2+} level (Brookes et al., 2004; Giorgi et al., 2009; Akl & Bultynck, 2013).

On the other hand, further reports showed induction of MPT-driven necrosis by mitochondrial Ca^{2+} overload upon oxidative stress since Ca^{2+} is able to induce permanent PTPC opening, e.g., by (i) activation of the redox-sensitive PTPC component CypD via ETC-derived ROS (Nguyen et al., 2011; Hwang et al., 2014; Gutiérrez-Aguilara & Baines, 2015; Zhang et al., 2016), (ii) inhibition of ANT upon

peroxidation of mitochondrial CL (Pestana et al., 2009; Paradies et al., 2014a), or (iii) Ca^{2+}-induced loss of the c-subunit of the F_0/F_1 ATPase – another yet proposed component of the MPT pore – followed by, for instance, CypD- and ANT-dependent PTPC opening (Bonora et al., 2013; Gutiérrez-Aguilara & Baines, 2015; Galluzzi et al., 2018). Although most of the above described modes of Ca^{2+}-driven MPT upon oxidative stress can be blocked by the presence of the CypD inhibitor CsA, there is also evidence for CsA-insensitive mechanisms of MPT-induced cell death (Kanno et al., 2002; Wei & Dirksen, 2012).

Surprisingly, a role of Ca^{2+}-driven MPT has been so far excluded for the mechanism of ferroptosis, although the data of this work and other reports provide enormous evidence for t-BuOOH to induce MPT-driven cell death upon mitochondrial Ca^{2+} overload in diverse cellular systems (Gunter & Pfeiffer, 1990; Imberti et al., 1993; Nieminen et al., 1995; Lemasters et al., 2009; Dixon et al., 2012). In this context, the study by Nieminen and coworkers (1995) proposed a mechanism for MPT-driven necrosis in response to t-BuOOH treatment of hepatocytes, which is initiated by (i) mitochondrial Ca^{2+} accumulation due to the oxidation of NADH and GSH by t-BuOOH, followed by a (ii) secondary ROS burst via the mitochondrial respiratory chain, (iii) loss of the MMP ($\Delta\psi_m$) and finally (iv) induction of MPT-driven necrosis. In the light of t-BuOOH-induced ferroptosis, the herein presented data provide a lot of evidence for a similar mechanism of mitochondrial dysfunction.

In this context, it is tempting to speculate that t-BuOOH might induce an early depolarization of $\Delta\psi_m$ due to the oxidation of NADH as described in the previous discussion section. Moreover, further loss of $\Delta\psi_m$ might be provoked by t-BuOOH through reversible PTPC opening, which is potentially stimulated by binding of NAD^+ and / or GSSG to PTPC redox-sensitive sites or ANT, followed by an increase in mitochondrial Ca^{2+}. These events might further promote ETC-mediated ROS formation and finally initiation of a positive feedback loop in the context of reversible, not lethal PTPC opening. Notably, the cellular availability of NADH instead of GSH might be more crucial to prevent mitochondrial depolarization and might act upstream of GSH in reversible PTPC opening since NADH is an essential cofactor to regenerate oxidized GSH (GSSG) (Gunter & Pfeiffer, 1990; Circu & Awe, 2012).

The above proposed mechanism for reversible PTPC opening and mitochondrial Ca^{2+} accumulation upon t-BuOOH-induced ferroptosis is supported by the following results of this work, as well as other reports already mentioned before:

(i) ferroptosis-blocking agents (e.g., FS) rescued cells from t-BuOOH-induced necrosis but were not able to restore $\Delta\psi_m$, what implies that loss of the MMP was not directly lethal for the cells. Furthermore, (ii) t-BuOOH, which should be not directly affected by inhibitors like FS as these agents only scavenge t-BuOOH-derived radical species (OH·, t-BuO·, t-BuOO·), can directly oxidize GSH and NADH. (iii) t-BuOOH detoxification is dependent on GSH as shown via inhibition of t-BuOOH-induced ferroptosis by the presence of NAC and other reports. (iv) t-BuOOH induced a time-dependent irreversible oxidation of NADH, which came along with loss of the MMP ($\Delta\psi_m$). (v) Ca^{2+} chelation via BAPTA AM significantly inhibited late (3-4 h) but not early (1-2 h) NADH oxidation upon t-BuOOH exposure. (vi) t-BuOOH induced, most likely, an increase in mitochondrial, free Ca^{2+} as assessed by Fura-2 AM staining and flow cytometry, and (vii) BAPTA AM was able to completely restore the MMP as assessed by DiOC6 staining and flow cytometry. Furthermore, (viii) post-treatment of t-BuOOH-exposed NIH3T3 cells with BAPTA AM inhibited ferroptosis till the maximum of lipid peroxidation and collapse of the MMP (≤ 2 h).

Since ferroptosis inhibitors like FS and LX were able to block t-BuOOH-induced cell death and lipid ROS formation but only slightly (~ 30 %) attenuated the increase in Fura-2 AM-detected Ca^{2+} (unpublished data; Wenz et al., 2018), there might be another toxic trigger than accumulated Ca^{2+} within the mitochondria, potentially inducing permanent PTPC opening and finally onset of MPT-driven ferroptosis. In this context, several studies have already described a "two-hit" hypothesis for MPT-driven cell death, proposing the need for a toxic mitochondrial lesion in the presence of accumulated Ca^{2+} for permanent and, therefore, lethal PTPC opening (Gunter et al., 1994; Brookes et al., 2004; Peng & Jou, 2010).

Remarkably, this model is also assumed for renal, cardiac, hepatic and neuronal ischemia / reperfusion injury *in vitro* and *in vivo*, whereby several findings have yet indicated the occurrence of both cell death mechanisms, MPT-driven necrosis and ferroptosis, upon these pathological conditions (Gunter et al., 1994; Ermak & Davies, 2002; Brookes et al., 2004; Degterev et al., 2005; Lemasters et al., 2009; Paradies et al., 2009; Xie et al., 2016; Tonnus & Linkermann, 2017; Galluzzi et al., 2018). Furthermore, so far defined morphological characteristics of ferroptosis, such as mitochondrial swelling, are closely related to the mechanism of MPT (Gunter et al., 1994; Kanno et al., 2002; Lemasters et al., 2009; Friedmann Angeli et al., 2014; Doll et al., 2017; Maiorino et al., 2018; Abdalkader et al., 2018; Ingold et al.,

2018). Since CL is almost exclusively located at the inner mitochondrial membrane and lipid ROS assays, as well as inhibitor experiments clearly demonstrated peroxidation of CL as the primarily toxic lesion, which is induced by t-BuOOH (Paradies et al., 2009; Wenz et al., 2018), the peroxidation of CL is very likely the crucial mitochondrial lesion for permanent PTPC opening in the presence of accumulated mitochondrial Ca^{2+}.

However, further analyses by our lab have indicated that solely blocking CL peroxidation by the mitochondria-selective inhibitor XJB-5-13 was sufficient to inhibit t-BuOOH-induced ferroptosis in NIH3T3 cells (Wenz et al., 2018). In this context, it is likely that the increase in free (mitochondrial) Ca^{2+} as detected in t-BuOOH-treated NIH3T3 cells by Fura-2 AM might be comparably not influenced by XJB-5-13 since this chemical has been described to act in the same manner as FS. This result leads to the idea that CL peroxidation *per se* might induce permanent, CsA-insensitive PTPC opening for induction of MPT-driven ferroptosis. In this context, oxidized CL has been already described to induce MPT, either via (i) activation of CypD (CsA-sensitive) due to mitochondrial $O_2^{\bullet-}$ generation (Hwang et al., 2014), or via (ii) inhibition of ANT (CsA-insensitive) (Pestana et al., 2009; Paradies et al., 2014a). With regard to the finding that CsA only partially restored the MMP ($\Delta\psi_m$) but was not able to block t-BuOOH-induced ferroptosis, the hypothesis arises that t-BuOOH might induce early, reversible PTPC opening upon NADH oxidation, what might be responsible for the loss of $\Delta\psi_m$ followed by an increase in mitochondrial Ca^{2+} as discussed before.

In the presence of oxidized CL, PTPC opening seems to be switched to a lethal trigger for MPT-induced ferroptosis upon permanent pore opening. This mechanism appears to be most likely provoked by a cooperative modulation of ANT and CypD in the case of t-BuOOH-induced ferroptosis due to the before mentioned results and findings of other groups. Moreover in this context, rather inhibition of ANT appears as the major driving force for initiating permanent PTPC opening and therefore MPT since CypD inhibition failed to block t-BuOOH-induced ferroptosis. On the other hand, if only CL peroxidation might be necessary for permanent PTPC opening and therefore MPT, the question arises, how BAPTA AM, as well as Fura-2 AM were able to rescue cells from t-BuOOH-induced ferroptosis?

In general, a tight Ca^{2+}-dependent regulation of lipid metabolism is assumed in mammalian cells. Besides the fact that certain enzymes of lipogenesis and lipolysis are sensitive to the presence of intracellular Ca^{2+}, the report of Brinckmann et al. (1998) clearly demonstrate that Ca^{2+} induces translocation and activation of 15-LOX, which is crucially associated to lipid ROS formation during ferroptosis, (Ritz et al., 1980; Friedmann Angeli et al., 2014; Yang et al., 2016). On the other hand, being in accordance with the "two-hit" model for induction of MPT-induced cell death, the presence of Ca^{2+} has been reported by distinct groups to be essential for mitochondrial CL peroxidation (Pestana et al., 2009; Hwang et al., 2014; Paradies et al., 2014b). In this context, the existence of a general, positive correlation between the presence of Ca^{2+} and lipid peroxidation has been accordingly described by some authors in the literature (Babizhayev, 1988; Selvam, 2002).

Further, diverse *in vitro* and *in vivo* studies indicated in this context a crucial link of intracellular Ca^{2+} and CL peroxidation during mitochondrial dysfunction-induced diseases (Paradies et al., 2009). The hypothesis that the presence of Ca^{2+} is generally needed for CL peroxidation is strengthened by further flow cytometric experiments of our lab, clearly demonstrating that BAPTA AM is able to inhibit the increase in *t*-BuOOH-induced lipid ROS in NIH3T3 cells (unpublished data). Since other experiments, as described above, have yet proven that CL might be the intracellular lipid, which is mostly and crucially oxidized by the presence of *t*-BuOOH (Wenz et al., 2018), *t*-BuOOH-induced ferroptosis appears dependent on the presence of Ca^{2+} for CL peroxidation. This hypothesis is strongly supported by findings of this work and Petrosillo et al. (2006 a,b; 2009), proposing a lowered threshold for mitochondrial Ca^{2+} to induce MPT-induced necrosis via peroxidation of CL by *t*-BuOOH-derived radical oxygen species.

Moreover, with regard to the fact that 99.9 % of mitochondrial Ca^{2+} is bound to CL, other anionic phospholipids and proteins (Gunter et al., 1994; Spät et al., 2008), the increase in free (mitochondrial) Ca^{2+} as detected by Fura-2 AM might be a consequence of an altered balance between bound and free Ca^{2+} within the mitochondrial matrix. This hypothesis is strengthened by reports, arguing against a direct uptake of Ca^{2+} by mitochondria from the cytosol or ER but rather favoring the assumption that mitochondrial protein and lipid oxidation increases the amount of free Ca^{2+} within the mitochondrial matrix (Gunter et al., 1994). Furthermore, an early (< 3 h) increase in mitochondrial Ca^{2+} was probably not detectable, since the

fluorescence of the Ca^{2+} sensor Fura-2 AM might reflect only an average value over a very huge number of mitochondria within one cell. These measurements might underestimate the beginning of Ca^{2+}-driven MPT upon oxidation of CL in the presence of t-BuOOH since the induction of MPT has been yet described rather as a transition or chain reaction than a direct, ultimate change of the mitochondrial status within one cell (Gunter et al., 1994). This means that release of Ca^{2+} from already overloaded, dysfunctioning mitochondria affect the remaining vital ones followed by sequential MPT induction within the mitochondria of one cell. In this case, studies on isolated mitochondria might help to get a more detailed picture of cellular Ca^{2+} changes during t-BuOOH exposure.

On the other hand, the increase in Fluo-4 AM-detected, cytosolic Ca^{2+} at the maximum of lipid ROS formation, and most likely also at the maximum of mitochondrial Ca^{2+} accumulation as potentially assessed by Fura-2 AM staining (3-4 h), might be a consequence of Ca^{2+} release from overloaded mitochondria, and a late occurring Ca^{2+} efflux from the extracellular environment due to plasma membrane disintegration. This explanation for a relatively late occurring, cytosolic Ca^{2+} increase in the presence of t-BuOOH is strengthened by an *in vitro* study of Bellomo and coworkers (1982) since t-BuOOH provoked an increase in cytosolic Ca^{2+} from two distinct compartments: (i) release of Ca^{2+} from mitochondria triggered by NAD(P)H oxidation, which was blocked by inhibition of GSH reductase, and (ii) Ca^{2+} increase in the cytosol from an extramitochondrial compartment, most likely from the disintegrated plasma membrane, being sensitive to the oxidation of GSH.

Besides DNA DSBs that were partially provoked by lipid ROS formation upon t-BuOOH exposure (Wenz et al., 2018), the release of Ca^{2+} from overloaded, dysfunctioning mitochondria upon MPT induction might be the reason for the time-dependent increase in t-BuOOH-induced DSBs as described and already in part discussed in the previous section. This assumption is further supported by inhibition of t-BuOOH-induced DSBs in the presence of BAPTA AM as shown by this work via neutral Comet assays, as well as detection of colocalized γ-H2AX / MDC1 foci via laser scanning microscopy. In mammalian cells, several findings of other groups have yet indicated that release of Ca^{2+} from overloaded mitochondria or an increase in cytosolic Ca^{2+} via plasma membrane disintegration crucially impairs the DNA repair capability or even, induce DNA damage upon stimulation of Ca^{2+}-driven endonucleases (Gafter et al., 1997; Salas & Corcoran, 1997; Ramirez et al., 2013).

Vice versa, treatment of NIH3T3 cells with BAPTA AM in the absence of *t*-BuOOH induced block of DNA replication as assessed by EdU incorporation and laser scanning microscopy, hinting towards an opposite situation, namely that Ca^{2+} chelation might stimulate DNA repair upon induction of a cell cycle arrest (data of this work; Rancourt et al., 2002; Boonstra & Post, 2004). Since there is evidence for an ATP-driven physiological Ca^{2+} gradient between the cytosol and the nucleus, stimulating (i) DNA synthesis, (ii) recruitment of DDR-related components (e.g., PARP-1), and (iii) the repair of DNA SSBs and DSBs, the precise role of Ca^{2+} in the regulation of the DNA damage response machinery upon pathological conditions might be worth to be further investigated (Nicotera et al., 1992; Bakondi et al., 2003; Bugreev & Mazin, 2004; Ramirez et al., 2013; Ralec et al., 2017).

However, also a secondary ROS burst, possibly provoked by *t*-BuOOH in the course of Ca^{2+}-driven MPT appears as an explanation for the observed time-dependent increase in DNA DSBs, whereby some authors support the assumption that an increase in mitochondrial ROS might be rather a consequence of depleting antioxidative capacities than directly of Ca^{2+}-driven MPT (Hansson et al., 2008). Finally, it remains to be elucidated to what extent a possible secondary ROS burst upon mitochondrial dysfunction, depletion of antioxidative capacities or an increase in cytosolic Ca^{2+} might be crucial for the time-dependent increase in *t*-BuOOH-induced DNA DSBs, whereby rather an interplay than solely one of these cellular lesions might determine the extent of DNA damage, as well as the cellular capability to repair these DNA lesions in the presence of *t*-BuOOH.

Surprisingly, a role for Ca^{2+} in the regulation of ferroptosis has been not yet described since (i) there is so far no evidence that Ca^{2+} chelation rescues cells from ferroptosis, as well as (ii) no increase of the cellular Ca^{2+} amount was detectable in the presence of prominent ferroptosis inducers, such as erastin or RSL-3 (Wolpaw et al., 2011; Dixon et al., 2012; Yu et al., 2017). This might be due to two reasons: evidence suggests that NADH oxidation alone can drive unspecific permeabilization of the inner mitochondrial membrane independent of Ca^{2+}-driven PTPC opening, what might be the case for the above described ferroptosis inducers (Hannson et al., 2008). On the other hand, intracellular Ca^{2+} signaling is often completely remodeled in solid tumor cells, such as in pancreatic, hepatic, colon, lung, prostate and breast tumor cells, representing the model systems that were widely applied to study ferroptosis (Dixon et al., 2012; Schwarz et al., 2013; Schaal et al., 2015; Monteith et

al., 2017; Yu et al., 2017; Lu et al., 2018). Therefore, ferroptosis inducers, such as erastin and probably also *t*-BuOOH, might be not able to modulate the intracellular Ca^{2+} level in certain tumor cells. Additionally, APAP has been yet described as inducer of ferroptosis, whereby other, from ferroptosis isolated studies indicated that APAP provokes a cellular Ca^{2+} increase (Salas & Corcoran, 1997; Holownia et al., 1998; Lörincz et al., 2015). Finally, the existence of a Ca^{2+}-dependent regulatory mechanism in *t*-BuOOH-induced ferroptosis, possibly linked to MPT upon CL peroxidation, is favored by the present work. However, the dependency of *t*-BuOOH-induced ferroptosis on intracellular Ca^{2+} might be restricted to healthy, non-tumorigenic cells (e.g., NIH3T3, HaCaT cells) and tumor cells (e.g., Caco-2), still or (re)expressing cell-cell contacts. An overview of the discussed results and theoretic assumptions of this section are summarized as proposal for a model mechanism of *t*-BuOOH-induced ferroptosis in NIH3T3 cells (Figure 59).
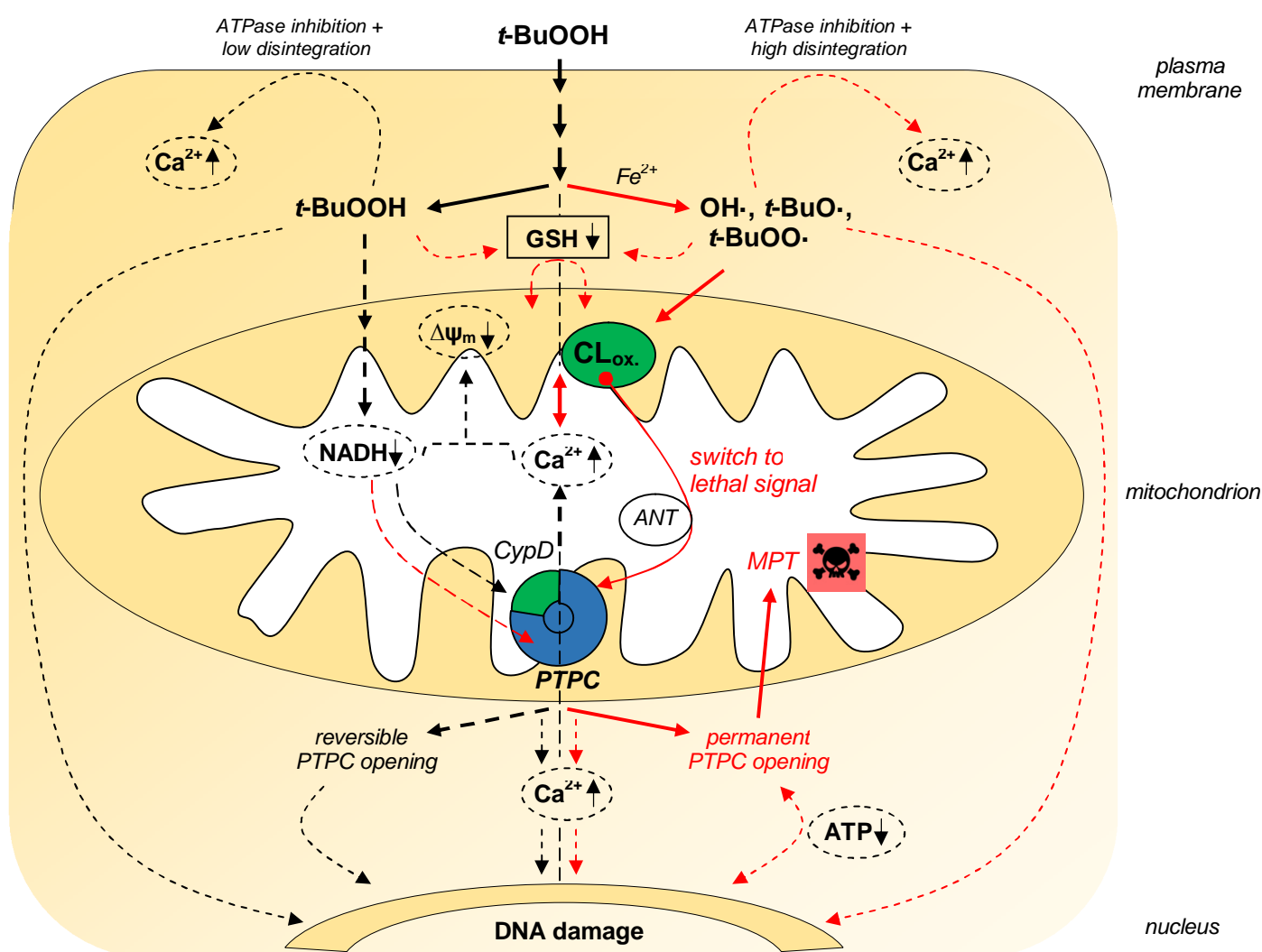
Fig. 59 Model mechanism for *t*-BuOOH-induced ferroptosis in NIH3T3 cells according to the presented results and discussed assumptions. Non-lethal cellular effects / lesions (*dark, dashed lines*) seem to

be directly induced by the presence of t-BuOOH via NADH oxidation-induced reversible PTPC opening within the mitochondrion and increased amounts of cellular (cytosolic + mitochondrial) Ca^{2+} independent of iron (Fe^{2+})-catalyzed metabolism. In contrast, radical species derived from t-BuOOH appear to mediate the lethal mechanism (*red lines*) of MPT-driven ferroptosis via CL peroxidation and increased amounts of free Ca^{2+} that provoke permanent PTPC opening within the mitochondrion. In addition, other t-BuOOH-induced cellular lesions might critically promote lethality (*red, dashed lines*).

5.3 Cell-cell contacts protect mammalian cells against t-BuOOH-induced ferroptosis: *in vitro* and *in vivo* implications

Besides resistance of (early) confluent compared to semiconfluent murine fibroblasts (NIH3T3) and human epithelial cells (HaCaT, Caco-2) against cellular, not primary toxic lesions induced by t-BuOOH – (i) irreversible NADH oxidation, (ii) a decrease in ATP, (iii) loss of the MMP ($\Delta\psi_m$), and (iv) the increase in DNA DSBs – characterization of t-BuOOH-induced necrosis revealed not only ferroptosis as the primary killing mechanism but also identified key mediators of t-BuOOH-induced cell death: (v) the presence of intracellular Ca^{2+}, most likely as prerequisite for (vi) mitochondrial CL peroxidation via t-BuOOH-derived lipid ROS (data of this work; unpublished data; Wenz et al., 2018, 2019).

In this context, Fluo-4 AM staining and flow cytometry demonstrated resistance of confluent compared to semiconfluent (proliferating) NIH3T3 and Caco-2 cells against an increase in cytosolic Ca^{2+} upon t-BuOOH exposure. Furthermore, also in the absence of t-BuOOH, a significantly lower cytosolic Ca^{2+} level was detectable in the presence of cell-cell contacts at first sight. At a second glance, further experiments by the lab of Dr. Wolfgang Greffrath (Medical Faculty Mannheim, Germany) with help of Fura-2 AM support resistance of confluent in contrast to proliferating NIH3T3 cells against an increase in free, cellular Ca^{2+} in the presence of t-BuOOH (unpublished data). However, further control experiments of our lab indicated probe leakage of Fluo-4 AM in untreated confluent NIH3T3 cells over time, and a similar Ca^{2+} level was detected by Fura-2 AM in untreated confluent and proliferating NIH3T3 cells (unpublished data). Hence, a physiological regulation of the intracellular Ca^{2+} level via the presence of cell-cell contacts is so far not supported by these findings.

Nevertheless, since Fura-2 AM possibly detects rather mitochondrial than cytosolic Ca^{2+} as discussed before, and probe leakage of Fluo-4 AM might be a consequence of upregulated Ca^{2+} efflux mechanisms across the plasma membrane, the cytosolic and mitochondrial Ca^{2+} level remain to be elucidated in detail, at the basal level and upon challenge with t-BuOOH. For instance, (i) combined analysis of cytosolic and mitochondrial Ca^{2+} by more specific, fluorescent Ca^{2+} indicators with a very narrow and distinct emission spectrum, as well as (ii) usage of Ca^{2+}-free medium or (iii) substances that, e.g., provoke mitochondrial Ca^{2+} release, such as FCCP (see section before), might help to decipher intracellular Ca^{2+} patterning in confluent and semiconfluent cultures upon t-BuOOH exposure.

In addition, the resistance of confluent compared to semiconfluent cells against an increase in cytosolic (Fluo-4 AM) and, most likely, mitochondrial (Fura-2 AM) Ca^{2+} in the presence of t-BuOOH might be a downstream event of the already discussed oxidation of NADH, limiting the capacity to regenerate GSSG and potentially provoking reversible PTPC opening (data of this work; unpublished data). In the light of this hypothesis, elevated amounts of NAD^+ as detected in confluent NIH3T3, HaCaT and Caco-2 cultures might be involved in mediating the resistance against not primarily toxic, Ca^{2+}-dependent cellular lesions (e.g., loss of the MPP) that are induced by t-BuOOH (data of this work). Besides a crucial role of mitochondrial $NAD(P)^+$ transhydrogenase is assumed in t-BuOOH catabolism (Lemasters et al., 2009), an *in vitro* study by Ekshyyan and Aw (2005) demonstrated an increased capacity of differentiated neuronal cells to detoxify t-BuOOH in a NADPH-dependent manner, thereby protecting these cells from cell death. Moreover, since NADH oxidation might be also the driving force for Ca^{2+}-independent PTPC opening in the presence of other ferroptosis inducers (e.g., erastin) as discussed before, the regulation of cellular $NAD(P)^+$ via cell-cell contacts might be worth to be further investigated as defense mechanism against ROS-induced cell death.

Importantly, the TBARS assay, as well as C11-BODIPY staining and flow cytometry provided evidence for a decreased lipid ROS formation in confluent compared to proliferating NIH3T3 cells, not only upon t-BuOOH exposure but also at the basal level (Wenz et al., 2019). In the light of these further investigations by our lab, this finding appears as a possible explanation for the resistance of confluent in contrast to semiconfluent cells against t-BuOOH-induced ferroptosis. The same protective effect, which was mediated by the presence of cell-cell contacts against

the formation of lipid ROS, was observed in erastin-treated NIH3T3 cells (Wenz et al., 2019). Interestingly, the report by Pani et al., (2000) has already indicated a diminished LOX activity within the arachidonic acid (AA) cascade in contact- inhibited mammalian cells. Contrarily, a transcriptome analysis of our lab proved significantly upregulated mRNA levels of the arachidonate 5-lipoxygenase activating protein (ALOX5AP or FLAP) in contact-inhibited compared to proliferating NIH3T3 cultures (Küppers et al., 2010). Notably, FLAP assists 5-LOX in the oxidation of AA during leukotriene synthesis by promoting translocation of the enzyme to the plasma membrane during, e.g., inflammation-associated diseases, such as atherosclerosis, stroke or colorectal cancer (Evans et al., 2008; Postula et al., 2016). With regard to these controversial findings, a direct regulation of lipid ROS formation by the presence of cell-cell contacts via, e.g., inhibition of LOX activity remains to be elucidated regarding the resistance of confluent cultures against t-BuOOH-induced ferroptosis and cellular damage.

However, a reduced lipid ROS formation in t-BuOOH-treated confluent versus semiconfluent NIH3T3 cells appears somehow contradictory with regard to the comparable formation of (i) cytosolic radical oxygen species, (ii) oxidative DNA lesions and SSBs, as well as a comparable (iii) block of DNA replication as already discussed in the first section. Furthermore, CM-H2DCFDA / DCFDA and C11-BODIPY should principally detect the same type of t-BuOOH-derived free radical oxygen species (OH·, t-BuO·, t-BuOO·). In principle, the localization of these dyes – either cytosolic or incorporated into cellular membranes – should be the only different parameter with regard to the quantitative analysis of ROS via flow cytometry (Drummen et al., 2002; Armstrong, 2010; Cheloni & Slaveykova, 2013). Thus, as additionally theory, C11-BODIPY fluorescence might be rather a measure for the susceptibility of cellular membranes to be attacked by radical oxygen species than a direct measure for the formation of lipid ROS. This assumption leads to the hypothesis that C11-BODIPY is potentially incorporated into cellular membranes dependent on the amount of PUFAs. Although the cellular distribution of C11-BODIPY has been already investigated and declared to be not organelle-specific, there is evidence that C11-BODIPY might primarily accumulate within the mitochondria, in the absence of any stimulus but also upon cellular stress conditions (Drummen et al., 2002; Kriska et al., 2006).

Due to the high content of CL (~ 20 % compared to total lipid) within the inner mitochondrial membrane, and with regard to results of our lab that indicate CL peroxidation as the primarily toxic lesion upon t-BuOOH-induced ferroptosis, it is tempting to speculate that C11-BODIPY might accumulate within the mitochondria proportional to the amount of PUFAs that are incorporated into CL (Dudek, 2017; Wenz et al., 2018). Further analysis of lipid peroxidation in the presence of the mitochondria-selective ferroptosis inhibitor XJB-5-131, which is known to block CL peroxidation, or staining of confluent and semiconfluent NIH3T3 cells with C11-BODIPY, MitoTracker Red as mitochondrial marker and fluorescent labeling of CL might support this hypothesis via laser scanning microscopy. Additionally, manipulation of the CL unsaturation index via application of, e.g., ω-6 PUFAs, as explained later, might give insights in the way, how the PUFA index of CL possibly affects the resistance of confluent cells against t-BuOOH-induced ferroptosis.

In general, the presented findings of this PhD thesis might have important implications for the outcome of prospective *in vitro* studies since most previous analyses have been exclusively performed in proliferating cells. Thus, recapitulation of these studies in confluent cultures might rather display the situation of solid, non-transformed tissues *in vivo* as these cells comparably underlie the regulation via the presence of cell-cell contacts, and might, therefore, reveal new results on the cytotoxic and genotoxic effects of ROS-inducing agents. Remarkably, the regulation of cell death via the presence of cell-cell contacts is likely a global, conserved effect in mammalian cells since (i) 6 distinct cell lines of murine or human fibroblasts (NIH3T3, FH109, MEF, Swiss3T3) and human epithelial cells (HaCaT; Caco-2) exhibited resistance against t-BuOOH-induced toxicity upon cell confluence, and (ii) resistance of confluent cultures was not restricted to t-BuOOH but also observable against toxic effects of H_2O_2, UV-C irradiation and the genotoxin MMS that are known to induce apoptotic cell death (data of this work; unpublished data; Lackinger et al., 2001; Yamauchi et al., 2011; Jiang et al., 2012). Thus, the presence of cell-cell contacts might protect also against caspase-dependent (e.g., apoptosis) and other caspase-independent (e.g., MPT-driven necrosis, PARP-1-mediated parthanatos or RIPK1 / RIPK3-induced necroptosis) cell death mechanisms.

Besides several findings also implicate a crucial role for tight and gap junctions in making the cell fate decision, intercellular contact and therefore maintenance of physiological tissue homeostasis, is largely mediated by cadherin-based adherence junctions, with E-cadherin being the most abundant cell contact molecule in mammalian cells (Cavallaro & Christofori, 2001; Juliano, 2002; Hutnik et al., 2008; Kim et al., 2012; Decrock et al., 2013; Gangwar et al., 2017). In this context, previous studies and findings of other groups indicated expression of different cadherin molecules in the cell model systems that were analyzed in the context of this work: NIH3T3 = N-cadherin; HaCaT = E-cadherin; Caco-2 = E-cadherin and N-cadherin (Goméz et al., 1999; Dietrich et al. 2002; Wever et al., 2004; Peignon et al., 2006; Wei et al., 2005; Kobayashi et al., 2006; Saito et al., 2012; Yan et al., 2015). Notably, a role of E-cadherin and N-cadherin has been so far solely described to regulate apoptotic cell death (Peluso et al., 1996; Li et al., 2001; Peluso et al., 2001; Erez et al., 2004; Galaz et al., 2005; Chae et al., 2009; Han et al., 2014; Lü et al., 2015). Hence, the presented work is the first *in vitro* study which demonstrates regulation of ferroptosis by the presence of cell-cell contacts.

On the other hand, results of this work might help to understand why solid tumors (e.g., pancreatic, hepatic, colon, lung, prostate and breast tumor cells, glioblastoma and melanoma) that have been so far resistant against conventional, apoptosis-inducing chemotherapy, are sensitized to conventional chemotherapeutic drugs (e.g., cisplatin or temozolomide) or even directly killed by the presence of ferroptosis-inducing agents (e.g., erastin or RSL3). With regard to the protective effect provided by cell-cell contacts against ferroptosis, the here presented findings might be further useful to find out how cells of the healthy surrounding tissue compared to solid tumor cells appear more resistant to cytotoxic effects of this novel, ferroptosis-inducing cancer therapy approach (Dixon et al., 2012; Yu et al., 2017; Lu et al., 2018). In this context, results of this work can be, in theory, transferred to this pathophysiological situation since cell-cell contact-expressing (early and late) confluent cultures resemble the situation in healthy tissues *in vivo*, whereas proliferating cultures rather reflect a tumor-related cell phenotype with regard to the classical three-stage model of carcinogenesis (Pitot, 1993; Hanahan & Weinberg, 2000; Valluru et al., 2014).

Remarkably, most of the above described solid tumors arise from epithelial tissues by loss of, e.g., E-cadherin, which has been widely reported to promote survival, proliferation and resistance of solid tumor cells against ROS-inducing chemo- and irradiation therapy upon permanent activation of the Wnt / β-catenin signal pathway (Cavallaro & Christofori, 2001; Moh & Shen, 2009; Ciu et al., 2012; Kim et al., 2012; Saito et al., 2012; Victorino et al., 2014; Morry et al., 2017; Nussinov et al., 2017). Moreover, also inhibition of the Hippo pathway downstream of β-catenin signaling, as well as permanent activation of the Notch-1-dependent signal pathway are tightly associated to the loss of cell-cell contact molecules and can act synergistically to promote chemoresistance in solid tumors, for instance, via upregulation of the Nrf2-mediated antioxidative defense (Glick & Yuspa, 2005; Pan, 2010; Mo et al., 2013; Plouffe et al., 2015; Wood, 2015; Plouffe et al., 2016; Sparaneo et al., 2016; Gujral & Kirschner, 2017; Park et al., 2018).

As hypothesized by this work, a lower amount of PUFAs (e.g., ω-6 PUFAs) that might be incorporated into CL in the presence of cell-cell contacts can be found as an inverted image upon the tumor situation. In this context, increasing evidence suggests that loss of cell-cell contact molecules like E-cadherin promotes reprogramming of (i) lipid metabolism, and (ii) lipid membrane composition to fulfill the high energy demand of aberrant cancer cell proliferation (Beloribi-Djefaflia et al., 2016; Vergara et al., 2017; Long et al., 2018; Maan et al., 2018; Yi et al., 2018; Yin et al., 2019). For instance, permanent activation of β-catenin has been reported to increase the unsaturation index of cellular lipids via activation of the enzyme stearoyl-CoA desaturase in a model cancer stem cell line (Yi et al., 2018). The study by Yi et al. (2018) further proved that oncogenic activation of this enzyme ends up in a positive feedback loop, which further promotes aberrant β-catenin signaling but also drives oncogenic signaling of certain Hippo pathway components and upregulation of NF-κB activity. *Vice versa* to the tumor situation, Notch-1 deficiency has resulted in a decreased content of mitochondrial lipids in hepatocytes (Song et al., 2016).

Furthermore, a study in Caco-2 cells shows that the incorporation of ω-3 PUFAs, yet being suggested as tumor-suppressing agent for colon cancer therapy, is negatively correlated with the presence of CL and ω-6 PUFAs, with huge evidence for the latter to act as tumor promoter (Benais-Pont et al., 2006; Berquin et al., 2008; Monteiro-Cardoso et al., 2014). This implies that a low level of both, ω-6 PUFAs and CL, might be associated to inhibition of carcinogenesis and therefore to the presence

of cell-cell contacts upon the classical image of carcinogenesis. *Vice versa*, a high level of ω-6 PUFAs and CL might act in a tumor-promoting way and might be, therefore, rather related to the loss of cell-cell contacts. In this context, the assumption of a high ω-6 PUFA level in tumors fits reports that ferroptosis is mainly induced by peroxidation of ω-6 PUFAs, such as AA, what might be the reason for the high sensitivity of certain tumors to ferroptosis-inducing agents (Yang et al., 2016; Doll et al., 2017; Kagan et al., 2017).

On the other hand, a high expression of human CL synthase and therefore huge amounts of mitochondrial CL are related to organs with a high energy demand like the heart, liver or kidney (Chen et al., 2006; Kiebish, 2008). Thus, is tempting to speculate that, as already proved for ω-6 PUFAs, tumor cells might exhibit also a higher amount of CL to cover their high energy demand (Berquin et al., 2008; Long et al., 2018). Beyond that, first studies indicate a correlation between cell-cell contact-driven signaling and remodeling of the fatty acid composition of CL via the transacylase activity of TAZ – a downstream effector of the Hippo signal pathway, which is frequently upregulated in human cancer to promote malignant cell proliferation, cell survival and metastasis upon loss of cell-cell contact (Pan, 2010; Fajardo et al., 2017; Gopinath et al., 2018; Lou et al., 2018; Park et al., 2018). Interestingly, the study by Lou et al. (2018) demonstrated not only a decreased myoblast differentiation in TAZ-knockout cells but also mitochondrial defects, related to an increase in mitochondrial ROS, as well as accumulation of remodeled monolyso-CL (Lou et al., 2018).

In this context, the hypothesis arises that the amount of CL and / or the amount of ω-6 PUFAs that are incorporated into CL and are especially sensitive to ferroptosis-related peroxidation (e.g., AA), might be regulated by the presence of cell-cell contacts (Yang et al., 2016; Doll et al., 2017; Kagan et al., 2017). Thus, it is tempting to speculate that a lower amount of CL and / or a decreased incorporation index of ω-6 PUFAs (e.g., AA) within CL might be the reason for the resistance of confluent cells against *t*-BuOOH-induced ferroptosis. One possibility to examine this hypothesis might be the increase of CL unsaturation by application of ω-6 PUFAs (e.g., AA) what might render confluent cells more sensitive to *t*-BuOOH-induced ferroptosis (Chang et al., 2018). *Vice versa*, chemical or genetic inhibition of TAZ in semiconfluent cultures possibly results in resistance against *t*-BuOOH-induced ferroptosis. In the end, combining (i) siRNA-mediated knockdown or CRISPR/ Cas9-

induced knockout of, e.g., E-cadherin or N-cadherin with either (ii) Western Blot analysis of mitochondrial CL expression, or (iii) the analysis of the PUFA composition of CL via LC-MS in confluent cultures might help to elucidate the underlying molecular mechanism. However, some findings even suggest a role of ω-3 PUFAs or 4-HNE as upstream regulators of cell-cell contact-associated signaling (Usatyuk et al., 2006; Pizzimenti et al., 2008; Yin et al., 2016).

Although a physiological regulation of intracellular Ca^{2+} via cell-cell contacts was not elucidated by this work, the obtained data provide evidence that the presence of Ca^{2+} is a crucial prerequisite for t-BuOOH-induced ferroptosis upon mitochondrial CL peroxidation (data of this work; Wenz et al., 2018). Thus, the additional hypothesis arises that Ca^{2+} might be an upstream regulator of lipid peroxidation, which is strengthened by a tight Ca^{2+}-dependent regulation of lipid metabolism as already discussed in the previous section. On the other hand, in many types of human cancer that are related to the loss of, e.g., E-cadherin, a high intracellular Ca^{2+} level can be found due to disruption of the physiological Ca^{2+} homeostasis, comprising not only deregulation of (i) Ca^{2+} uptake and release mechanisms via channels, ion exchangers or ATP-driven pumps from intracellular stores but also (ii) Ca^{2+} flux mechanisms across the plasma membrane (Sano et al., 2009; Monteith et al., 2012; Akl & Bultynck, 2013; Schwarz et al., 2013; Prevarskaya et al., 2014; Telford et al., 2015; Godwin et al., 2019). Besides the idea that an increased amount of mitochondrial CL and / or an increased level of ω-6 PUFAs, incorporated into CL, might render solid tumor cells more susceptible to t-BuOOH-induced ferroptosis, these findings suggests that the absence of cell-cell contacts in tumor cells is highly correlated with an increase in cellular Ca^{2+}, possibly sensitizing these cells as a secondary mechanism to ferroptosis when compared to healthy tissues. In this context, some authors even suggests to target Ca^{2+} signaling in tumor cells as potential key to overcome multicellular drug resistance of certain human cancers (Büsselberg & Florea, 2017).

However, the presented findings of this work suggest that colon carcinoma cells might be in part resistant to the novel approach of ferroptosis-inducing cancer therapy since confluent Caco-2 cells were protected against t-BuOOH-induced ferroptosis (data of this work). On the other hand, there was a discrepancy regarding certain cellular parameters (basal GSH amount or t-BuOOH-induced SSB formation) in confluent Caco-2 cells compared to the other non-tumorigenic cell lines (e.g.,

NIH3T3 or HaCaT) that might be explained by the expression of N-cadherin (data of this work). Interestingly, N-cadherin is mainly expressed during embryogenesis or in a few types of adult mammalian cells, such as in fibroblasts (Derycke & Bracke, 2004). On the other hand, the re-expression or *de novo* synthesis of N-cadherin is highly associated to the loss of E-cadherin, tumor formation and EMT-promoted metastasis (Tomita et al., 2000; Cavallaro & Christofori, 2001; Derycke & Bracke, 2004; Saito et al., 2012). In this context, there is huge evidence for a negative correlation between the expression of N-cadherin, mediating a fibroblastic and metastasic phenotype of solid tumors, and E-cadherin, acting, *vice versa*, as tumor suppressor by promotion of a more differentiated phenotype (Tomita et al., 2000; Li et al., 2001; Cavallaro & Christofori, 2001; Morry et al., 2017). Thus, it is tempting to speculate that simultaneous expression of E- and N-cadherin in Caco-2 cells in contrast to the non-tumorigenic cell lines (as described before) might be responsible for a differential regulation of the above mentioned cellular parameters. On the other hand, N-cadherin might mediate different functions in confluent, tumorigenic Caco-2 cells compared to confluent, non-tumorigenic cells (e.g., NIH3T3). Thus, further investigations might be worth to uncover the precise role of N-cadherin in *t*-BuOOH-induced ferroptosis in non-tumorigenic versus tumorigenic cell lines.

In general, the presented data strongly indicate that the presence of cell-cell contacts may render also other tumor cells more resistant to *t*-BuOOH-induced ferroptosis and other ROS-induced cell death mechanisms that are induced by chemo- or irradiation therapy since, in contrast to the classical image of EMT upon a complete loss of cell-cell contact molecules, many types of solid tumors (e.g., glioblastoma, breast or colon carcinoma) and related metastases (i) still express E-cadherin, (ii) re-express E-cadherin or (iii) establish cell-cell contacts via the *de novo* synthesis of N-cadherin (Friedl & Gilmour, 2009; Lewis-Tuffin et al., 2010; Rodriguez et al., 2012; Shih & Yamada, 2012; Aceto et al., 2014; Chung et al., 2016; Borcherding et al., 2018; Elisha et al., 2018; Yamashita et al., 2018). Especially differentiated tumors, such as melanomas, are able to escape even the novel chemotherapeutic approach of ferroptosis due to the re-expression of E-cadherin (Brabletz et al., 2001; Tsoi et al., 2018).

Interestingly, there are reports suggesting a positive correlation between the expression of N-cadherin and overactivation of PKCδ, with both being involved in the regulation of cell proliferation, differentiation and cell death (Derycke & Bracke, 2004; Glick & Yuspa, 2005; Breitkreutz et al., 2007; Pan et al., 2009; Basu & Pal, 2010; Garg et al., 2014). To overcome ferroptosis resistance in melanoma, Tsoi et al. (2018) have suggested MAPK inhibition to induce cell dedifferentiation and therefore loss of cell-cell contact molecules to rendering melanoma cells – in concordance to the here presented findings – more susceptible to ferroptosis. However, also inhibition of PKCδ combined with a ferroptosis-inducing agent, such as erastin, might overcome multicellular drug resistance of melanoma cells since previous studies of our lab could demonstrate cell dedifferentiation in HaCaT cells upon PKCδ inhibition during wound healing (Dietrich et al., 2001; Heit et al., 2001). In the light of these ideas, further investigations might elucidate a crucial role of PKCδ in the regulation of physiological and oncogenic cell-cell contact-driven signaling, possibly deciding about the resistance of solid cancer cells against chemo-and irradiation therapy.

Also other cellular mechanisms, such as iron metabolism, autophagy or the antioxidative defense against lipid peroxidation (e.g., GPX4 or selenoprotein P) that are tightly regulated by the presence of cell-cell contacts, might be crucial for the resistance of confluent cultures against *t*-BuOOH-induced ferroptosis but remain to be elucidated (Lötscher et al., 1979; Swat et al., 2009; Küppers et al., 2010; Chen et al., 2012; Dixon et al., 2012; Gao et al., 2016; Wenz et al., 2018; Yi et al., 2018; Wenz et al., 2019). Apart from implications that might be helpful to understand and potentially to overcome chemoresistance of human cancer, there is huge evidence for ferroptosis to be involved in inflammation-related human pathologies, as well as chronic neurodegenerative disorders, such as Parkinson or Alzheimer's disease (Kers et al., 2016; Yang & Stockwell, 2016; Müller et al., 2017; Tonnus & Linkermann, 2017). Thus, the presented data and findings might additionally help to develop novel preventive or regenerative approaches against these severe diseases by providing a more detailed view on (i) the protective effect of cell-cell contacts against ferroptosis, as well as on (ii) the mechanism of ferroptotic cell death, which strongly implicates involvement of Ca^{2+}-dependent MPT in the presence of *t*-BuOOH. In the context of the latter, the present work might further provide knowledge to complement cell death characterization of ferroptosis, which is of great importance, e.g., to better assess the risk of ferroptosis-inducing chemotherapy, which might even

promote the outgrowth of certain tumors, or might induce neurological disorders and lipid ROS-related chronic diseases. Furthermore with regard to the mode of action induced by *t*-BuOOH, comparison of the here presented results with other studies from the literature triggers the assumption for the existence of many other agents, e.g., redox cycler or lipid ROS-inducing agents, such as TGHQ, AAPH or capsaicin that might be potential inducers of ferroptosis (Park et al., 2002; Boreddy & Srivastava, 2012; Ramirez et al., 2013). Finally, exploring the mode of action of other ferroptosis inducers more detailed might be useful to understand the so far unknown physiological function of ferroptosis (Stockwell et al., 2017). In this context, the findings and described hypothesis of the presented work suggests a physiological role of ferroptosis in organs with a high, frequent exposure to lipid ROS, such as the skin or colon, or tissues with a high CL expression upon an increased energy demand as in the heart, kidney or liver (Chen et al., 2006; Kiebish, 2008; Erdelyi et al., 2009; Narendhirakannan & Hannah, 2013).
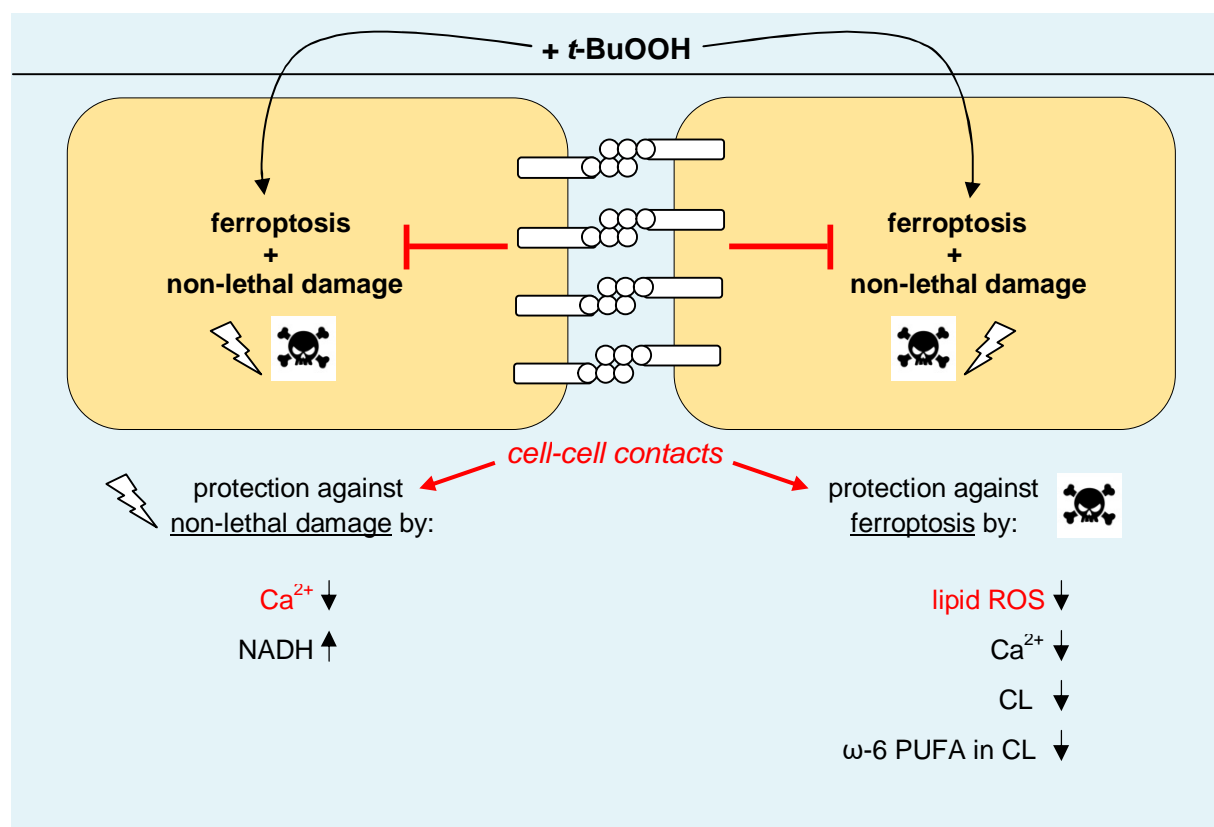
Fig. 60 Protection against *t*-BuOOH-induced ferroptosis and non-lethal cellular damage by cell-cell contact molecules (e.g., E-cadherin or N-cadherin) in mammalian cells via regulation of cellular parameters according to the presented and / or published results (*red colored*), as well as with regard to additional hypotheses (*black colored*) of this work.

In summary, the present work elucidates protection of (early) confluent versus semiconfluent mammalian cells against t-BuOOH-induced ferroptosis and cellular damage. Findings of this work and further investigations of our lab trigger the assumption that resistance of confluent cultures against t-BuOOH-induced ferroptosis is most likely mediated by (i) a reduced lipid peroxidation of CL, and / or (ii) a lowered intracellular Ca^{2+} level. Additional hypotheses are (iii) a decreased CL expression and / or (iv) a lowered incorporation index of ω-6 PUFAs within CL upon the presence of cell-cell contacts molecules, such as E-cadherin or N-cadherin. With regard to t-BuOOH-induced cellular damage, not being lethal for the cells (e.g., loss of the MMP or DNA DSBs), (i) an increased NAD^+ availability, or (ii) lowered amounts of (mitochondrial) Ca^{2+} might be responsible for the resistance of confluent cultures (for overview, see Figure 60). In the end, this study might provide knowledge to improve and / or to establish novel human therapies: on the one hand against ferroptosis-induced diseases, such as neurodegenerative disorders, but also might help to overcome drug resistance of solid cancers. Hence, more intensive *in vitro* and *in vivo* studies are needed to understand the complex, tightly orchestrated interaction of cell-cell contacts, lipid metabolism and Ca^{2+} in making the cell fate decision.

6 Summary

Oxidative stress due to excessive intracellular ROS formation can result in macromolecule damage and cell death. *In vitro*, ROS-induced apoptosis has been almost exclusively investigated in proliferating cells, although *in vivo*, cells establish cell-cell contacts and reside in the G1 cell cycle phase. Previous studies indicated that contact-inhibited compared to proliferating murine fibroblasts (NIH3T3) are resistant against *t*-BuOOH – a lipid ROS inducer, resembling oxidative stress in, e.g. neurodegenerative diseases and cancer. A role of cell-cell contacts in the resistance against ROS-induced cell death independent of a G1 arrest is so far not known.

Resistance of early confluent versus semiconfluent NIH3T3 cells and human epithelial cells (HaCaT, Caco-2) against *t*-BuOOH-induced necrosis was proved via setup I+II independent of a G1 arrest. Vitality assays, flow cytometry, Western Blot analysis and laser scanning microscopy demonstrated that (i) confluent cells proliferated at the time point of *t*-BuOOH exposure, and (ii) semiconfluent cultures (serum-depleted; U0126-treated) that exhibited a similar amount of cells in G1 as confluent cultures, were comparably sensitive to *t*-BuOOH as semiconfluent, proliferating cultures. Increased detoxification of *t*-BuOOH due to a higher cell number in confluent cultures was excluded via setup II. Further analyses and comet assays revealed a similar (i) cytosolic ROS increase, (ii) basal GSH level, (iii) replication block, as well as (iv) DNA SSB formation / repair in confluent and semiconfluent NIH3T3 cells. Confluent cultures were in contrast protected against (i) NADH oxidation, (ii) a decrease in ATP, (iii) collapse of the MMP ($\Delta\psi_m$), and (iv) an increase in DNA DSBs in the presence of *t*-BuOOH. Further experiments identified (i) *t*-BuOOH as a novel inducer of lipid ROS-induced ferroptosis, (ii) a prosurvival role of p38, JNK and ATR, as well as (iii) Ca^{2+} as crucial mediator of ferroptosis and cellular damage.

In summary, these findings present cell-cell contacts and Ca^{2+} as crucial regulators of *t*-BuOOH-induced ferroptosis *in vitro* and might help to develop therapies against ROS-induced diseases or multicellular resistance of solid tumors.

7 Zusammenfassung

Oxidativer Stress durch eine übermäßige Bildung von intrazellulären reaktiven Sauerstoffspezies (ROS) kann zur Schädigung von Makromolekülen und zum Zelltod führen. *In vitro* wurde die ROS-induzierte Apoptose fast ausschließlich in proliferierenden Zellen untersucht, obwohl Zellen *in vivo* Zell-Zell-Kontakte ausbilden und in der G1-Zellzyklusphase verbleiben. Bisherige Studien zeigten, dass kontaktinhibierte verglichen mit proliferierenden Mausfibroblasten (NIH3T3) resistent sind gegenüber *t*-BuOOH – einem Agens, das Lipid ROS ähnlich oxidativem Stress z.B. bei neurodegenerativen Erkrankungen und Krebs auslöst. Eine Rolle von Zell-Zell-Kontakten bei der Resistenz gegenüber dem ROS-induzierten Zelltod unabhängig von einem G1-Arrest ist bislang nicht bekannt.

Die Resistenz früh konfluenter versus semikonfluenter NIH3T3- und humaner Epithel-Zellen (HaCaT, Caco-2) gegenüber der *t*-BuOOH-induzierten Nekrose wurde unabhängig von einem G1-Arrest mithilfe Setup I+II nachgewiesen. Vitalitäts-analysen, Durchflusszytometrie, Western Bot Analysen und Laserscanmikroskopie zeigten, dass (i) konfluente Zellen zum Zeitpunkt der *t*-BuOOH-Exposition proliferierten und (ii) semikonfluente Kulturen (serum-depletiert oder U0126-behandelt), welche eine zu konfluenten Kulturen ähnliche Menge an Zellen in G1 aufwiesen, genauso sensitiv gegenüber *t*-BuOOH waren wie semikonfluente, proliferierende Kulturen. Eine verstärkte Entgiftung von *t*-BuOOH durch eine höhere Zellzahl in konfluenten Kulturen wurde ausgeschlossen mittels Setup II. Weitere Analysen und Comet assays zeigten einen ähnlichen (i) zytosolischen ROS-Anstieg, (ii) basalen GSH-Level, (iii) Replikationsblock und (iv) Bildung / Reparatur von DNA-Einzelstrangbrüchen in konfluenten und semikonfluenten NIH3T3-Zellen. Konfluente Zellen waren dahingegen geschützt vor (i) NADH-Oxidation, (ii) ATP-Abnahme, (iii) MMP ($\Delta\psi_m$)-Kollaps, und (iv) dem Anstieg von DNA-Doppelstrangbrüchen durch *t*-BuOOH. Weitere Experimente identifizierten (i) *t*-BuOOH als Induktor der Lipid ROS-induzierten Ferroptose, (ii) eine „prosurvival" Rolle von p38, JNK und ATR, als auch (iii) Ca^{2+} als zentralen Vermittler der Ferroptose und der zellulären Schäden.

Zusammenfassend präsentieren diese Ergebnisse Zell-Zell-Kontakte und Ca^{2+} als zentrale Regulatoren der *t*-BuOOH-induzierten Ferroptose *in vitro* und mögen hilfreich sein, um Therapien gegen ROS-induzierte Erkrankungen und die multizelluläre Resistenz von soliden Tumoren zu entwickeln.

8 Literature

Abdalkader, M., R. Lampinen, K. M. Kanninen, T. M. Malm, and J. R. Liddell. 2018. "Targeting Nrf2 to Suppress Ferroptosis and Mitochondrial Dysfunction in Neurodegeneration." *Front Neurosci* 12:466. doi: 10.3389/fnins.2018.00466.

Abe, K., and H. Saito. 1998. "Characterization of t-butyl hydroperoxide toxicity in cultured rat cortical neurones and astrocytes." *Pharmacol Toxicol* 83 (1):40-6.

Abercrombie, M. 1979. "Contact inhibition and malignancy." *Nature* 281 (5729):259-62.

Abraham, C., B. Scaglione-Sewell, S. F. Skarosi, W. Qin, M. Bissonnette, and T. A. Brasitus. 1998. "Protein kinase C alpha modulates growth and differentiation in Caco-2 cells." *Gastroenterology* 114 (3):503-9.

Aceto, N., A. Bardia, D. T. Miyamoto, M. C. Donaldson, B. S. Wittner, J. A. Spencer, M. Yu, A. Pely, A. Engstrom, H. Zhu, B. W. Brannigan, R. Kapur, S. L. Stott, T. Shioda, S. Ramaswamy, D. T. Ting, C. P. Lin, M. Toner, D. A. Haber, and S. Maheswaran. 2014. "Circulating tumor cell clusters are oligoclonal precursors of breast cancer metastasis." *Cell* 158 (5):1110-1122. doi: 10.1016/j.cell.2014.07.013.

Adan, A., Y. Kiraz, and Y. Baran. 2016. "Cell Proliferation and Cytotoxicity Assays." *Curr Pharm Biotechnol* 17 (14):1213-1221.

Agathocleous, M., and W. A. Harris. 2013. "Metabolism in physiological cell proliferation and differentiation." *Trends Cell Biol* 23 (10):484-92. doi: 10.1016/j.tcb.2013.05.004.

Aguilar, F., H. Navarro, and M. Peréz. 2016. Endogenous Antioxidants: A Review of their Role in Oxidative Stress [E-book]. Intech.

Akl, H., and G. Bultynck. 2013. "Altered Ca(2+) signaling in cancer cells: proto-oncogenes and tumor suppressors targeting IP3 receptors." *Biochim Biophys Acta* 1835 (2):180-93. doi: 10.1016/j.bbcan.2012.12.001.

Alberts, B., A. Johnson, J. Lewis, and et al. 2002. "Molecular Biology of the Cell. 4th Edition [E-book]." In. New York: Garland Science.

Alfadda, A. A., and R. M. Sallam. 2012. "Reactive oxygen species in health and disease." *J Biomed Biotechnol* 2012:936486. doi: 10.1155/2012/936486.

Altman, S. A., T. H. Zastawny, L. Randers, Z. Lin, J. A. Lumpkin, J. Remacle, M. Dizdaroglu, and G. Rao. 1994. "tert.-butyl hydroperoxide-mediated DNA base damage in cultured mammalian cells." *Mutat Res* 306 (1):35-44.

Alía, M., S. Ramos, R. Mateos, L. Bravo, and L. Goya. 2005. "Response of the antioxidant defense system to tert-butyl hydroperoxide and hydrogen peroxide in a human hepatoma cell line (HepG2)." *J Biochem Mol Toxicol* 19 (2):119-28. doi: 10.1002/jbt.20061.

Amoroso, S., A. D'Alessio, R. Sirabella, G. Di Renzo, and L. Annunziato. 2002. "Ca(2+)-independent caspase-3 but not Ca(2+)-dependent caspase-2 activation induced by oxidative stress leads to SH-SY5Y human

neuroblastoma cell apoptosis." *J Neurosci Res* 68 (4):454-62. doi: 10.1002/jnr.10199.

Amé, J. C., C. Spenlehauer, and G. de Murcia. 2004. "The PARP superfamily." *Bioessays* 26 (8):882-93. doi: 10.1002/bies.20085.

Andrabi, S. A., T. M. Dawson, and V. L. Dawson. 2008. "Mitochondrial and nuclear cross talk in cell death: parthanatos." *Ann N Y Acad Sci* 1147:233-41. doi: 10.1196/annals.1427.014.

Andrade, F. H., M. B. Reid, and H. Westerblad. 2001. "Contractile response of skeletal muscle to low peroxide concentrations: myofibrillar calcium sensitivity as a likely target for redox-modulation." *FASEB J* 15 (2):309-11. doi: 10.1096/fj.00-0507fje.

Armstrong, D., and et al. 2010. "Advanced Protocols in Oxidative Stress II [E-book]." In. Springer New York Dordrecht Heidelberg: Humana Press.

Aruoma, O. I., B. Halliwell, B. M. Hoey, and J. Butler. 1989. "The antioxidant action of N-acetylcysteine: its reaction with hydrogen peroxide, hydroxyl radical, superoxide, and hypochlorous acid." *Free Radic Biol Med* 6 (6):593-7.

Attene-Ramos, M. S., K. Kitiphongspattana, K. Ishii-Schrade, and H. R. Gaskins. 2005. "Temporal changes of multiple redox couples from proliferation to growth arrest in IEC-6 intestinal epithelial cells." *Am J Physiol Cell Physiol* 289 (5):C1220-8. doi: 10.1152/ajpcell.00164.2005.

Avery, S. V. 2011. "Molecular targets of oxidative stress." *Biochem J* 434 (2):201-10. doi: 10.1042/BJ20101695.

Awe, S. O., and A. S. Adeagbo. 2002. "Analysis of tert-butyl hydroperoxide induced constrictions of perfused vascular beds in vitro." *Life Sci* 71 (11):1255-66.

Ayala, A., M. F. Muñoz, and S. Argüelles. 2014. "Lipid peroxidation: production, metabolism, and signaling mechanisms of malondialdehyde and 4-hydroxy-2-nonenal." *Oxid Med Cell Longev* 2014:360438. doi: 10.1155/2014/360438.

Azam, N., M. Vairapandi, W. Zhang, B. Hoffman, and D. A. Liebermann. 2001. "Interaction of CR6 (GADD45gamma) with proliferating cell nuclear antigen impedes negative growth control." *J Biol Chem* 276 (4):2766-74. doi: 10.1074/jbc.M005626200.

Babizhayev, M. A. 1988. "The biphasic effect of calcium on lipid peroxidation." *Arch Biochem Biophys* 266 (2):446-51.

Baines, C. P., R. A. Kaiser, N. H. Purcell, N. S. Blair, H. Osinska, M. A. Hambleton, E. W. Brunskill, M. R. Sayen, R. A. Gottlieb, G. W. Dorn, J. Robbins, and J. D. Molkentin. 2005. "Loss of cyclophilin D reveals a critical role for mitochondrial permeability transition in cell death." *Nature* 434 (7033):658-62. doi: 10.1038/nature03434.

Baker, M. A., and S. Q. He. 1991. "Elaboration of cellular DNA breaks by hydroperoxides." *Free Radic Biol Med* 11 (6):563-72.

Bakondi, E., M. Gönczi, E. Szabó, P. Bai, P. Pacher, P. Gergely, L. Kovács, J. Hunyadi, C. Szabó, L. Csernoch, and L. Virág. 2003. "Role of intracellular calcium mobilization and cell-density-dependent signaling in oxidative-stress-induced cytotoxicity in HaCaT keratinocytes." *J Invest Dermatol* 121 (1):88-95. doi: 10.1046/j.1523-1747.2003.12329.x.

Bar, J., E. Cohen-Noyman, B. Geiger, and M. Oren. 2004. "Attenuation of the p53 response to DNA damage by high cell density." *Oncogene* 23 (12):2128-37. doi: 10.1038/sj.onc.1207325.

Baritaud, M., L. Cabon, L. Delavallée, P. Galán-Malo, M. E. Gilles, M. N. Brunelle-Navas, and S. A. Susin. 2012. "AIF-mediated caspase-independent necroptosis requires ATM and DNA-PK-induced histone H2AX Ser139 phosphorylation." *Cell Death Dis* 3:e390. doi: 10.1038/cddis.2012.120.

Barnouin, K., M. L. Dubuisson, E. S. Child, S. Fernandez de Mattos, J. Glassford, R. H. Medema, D. J. Mann, and E. W. Lam. 2002. "H2O2 induces a transient multi-phase cell cycle arrest in mouse fibroblasts through modulating cyclin D and p21Cip1 expression." *J Biol Chem* 277 (16):13761-70. doi: 10.1074/jbc.M111123200.

Barr, D. P., and R. P. Mason. 1995. "Mechanism of radical production from the reaction of cytochrome c with organic hydroperoxides. An ESR spin trapping investigation." *J Biol Chem* 270 (21):12709-16. doi: 10.1074/jbc.270.21.12709.

Barrera, G. 2012. "Oxidative stress and lipid peroxidation products in cancer progression and therapy." *ISRN Oncol* 2012:137289. doi: 10.5402/2012/137289.

Barzilai, A., and K. Yamamoto. 2004. "DNA damage responses to oxidative stress." *DNA Repair (Amst)* 3 (8-9):1109-15. doi: 10.1016/j.dnarep.2004.03.002.

Basu, A., and D. Pal. 2010. "Two faces of protein kinase Cδ: the contrasting roles of PKCδ in cell survival and cell death." *ScientificWorldJournal* 10:2272-84. doi: 10.1100/tsw.2010.214.

Belizário, J., L. Vieira-Cordeiro, and S. Enns. 2015. "Necroptotic Cell Death Signaling and Execution Pathway: Lessons from Knockout Mice." *Mediators Inflamm* 2015:128076. doi: 10.1155/2015/128076.

Bellomo, G., S. A. Jewell, H. Thor, and S. Orrenius. 1982. "Regulation of intracellular calcium compartmentation: studies with isolated hepatocytes and t-butyl hydroperoxide." *Proc Natl Acad Sci U S A* 79 (22):6842-6. doi: 10.1073/pnas.79.22.6842.

Beloribi-Djefaflia, S., S. Vasseur, and F. Guillaumond. 2016. "Lipid metabolic reprogramming in cancer cells." *Oncogenesis* 5:e189. doi: 10.1038/oncsis.2015.49.

Benais-Pont, G., Y. M. Dupertuis, M. P. Kossovsky, P. Nouet, A. S. Allal, F. Buchegger, and C. Pichard. 2006. "Omega-3 polyunsaturated fatty acids and ionizing radiation: combined cytotoxicity on human colorectal adenocarcinoma cells." *Nutrition* 22 (9):931-9. doi: 10.1016/j.nut.2006.05.012.

Bennett, B. L., D. T. Sasaki, B. W. Murray, E. C. O'Leary, S. T. Sakata, W. Xu, J. C. Leisten, A. Motiwala, S. Pierce, Y. Satoh, S. S. Bhagwat, A. M. Manning, and D. W. Anderson. 2001. "SP600125, an anthrapyrazolone inhibitor of Jun N-terminal kinase." *Proc Natl Acad Sci U S A* 98 (24):13681-6. doi: 10.1073/pnas.251194298.

Bentle, M. S., K. E. Reinicke, E. A. Bey, D. R. Spitz, and D. A. Boothman. 2006. "Calcium-dependent modulation of poly(ADP-ribose) polymerase-1 alters

cellular metabolism and DNA repair." *J Biol Chem* 281 (44):33684-96. doi: 10.1074/jbc.M603678200.

Bergamini, C. M., S. Gambetti, A. Dondi, and C. Cervellati. 2004. "Oxygen, reactive oxygen species and tissue damage." *Curr Pharm Des* 10 (14):1611-26.

Berger, S. B., P. Harris, R. Nagilla, V. Kasparcova, S. Hoffman, B. Swift, L. Dare, M. Schaeffer, C. Capriotti, M. Ouellette, B. W. King, D. Wisnoski, J. Cox, M. Reilly, R. W. Marquis, J. Bertin, and P. J. Gough. 2015. "Characterization of GSK'963: a structurally distinct, potent and selective inhibitor of RIP1 kinase." *Cell Death Discov* 1:15009. doi: 10.1038/cddiscovery.2015.9.

Berman, J. J., C. Tong, and G. M. Williams. 1978. "Enhancement of mutagenesis during cell replication of cultured liver epithelial cells." *Cancer Lett* 4 (5):277-83.

Bernofsky, C., and M. Swan. 1973. "An improved cycling assay for nicotinamide adenine dinucleotide." *Anal Biochem* 53 (2):452-8.

Berquin, I. M., I. J. Edwards, and Y. Q. Chen. 2008. "Multi-targeted therapy of cancer by omega-3 fatty acids." *Cancer Lett* 269 (2):363-77. doi: 10.1016/j.canlet.2008.03.044.

Bhagavathula, N., A. W. Hanosh, K. C. Nerusu, H. Appelman, S. Chakrabarty, and J. Varani. 2007. "Regulation of E-cadherin and beta-catenin by Ca2+ in colon carcinoma is dependent on calcium-sensing receptor expression and function." *Int J Cancer* 121 (7):1455-62. doi: 10.1002/ijc.22858.

Bhattacharya, S. 2015. Reactive Oxygen Species and Cellular Defense System [E-book]. New Delhi: Springer.

Bhutia, S. K., S. K. Mallick, and T. K. Maiti. 2010. "Tumour escape mechanisms and their therapeutic implications in combination tumour therapy." *Cell Biol Int* 34 (5):553-63. doi: 10.1042/CBI20090206.

Bindoli, A., J. M. Fukuto, and H. J. Forman. 2008. "Thiol chemistry in peroxidase catalysis and redox signaling." *Antioxid Redox Signal* 10 (9):1549-64. doi: 10.1089/ars.2008.2063.

Bittner, M., P. Kupferer, and C. F. Morris. 1980. "Electrophoretic transfer of proteins and nucleic acids from slab gels to diazobenzyloxymethyl cellulose or nitrocellulose sheets." *Anal Biochem* 102 (2):459-71.

Bogoyevitch, M. A., and B. Kobe. 2006. "Uses for JNK: the many and varied substrates of the c-Jun N-terminal kinases." *Microbiol Mol Biol Rev* 70 (4):1061-95. doi: 10.1128/MMBR.00025-06.

Bonora, M., A. Bononi, E. De Marchi, C. Giorgi, M. Lebiedzinska, S. Marchi, S. Patergnani, A. Rimessi, J. M. Suski, A. Wojtala, M. R. Wieckowski, G. Kroemer, L. Galluzzi, and P. Pinton. 2013. "Role of the c subunit of the FO ATP synthase in mitochondrial permeability transition." *Cell Cycle* 12 (4):674-83. doi: 10.4161/cc.23599.

Boonstra, J., and J. A. Post. 2004. "Molecular events associated with reactive oxygen species and cell cycle progression in mammalian cells." *Gene* 337:1-13. doi: 10.1016/j.gene.2004.04.032.

Bootman, M. D., K. Rietdorf, T. Collins, S. Walker, and M. Sanderson. 2013. "Ca2+-sensitive fluorescent dyes and intracellular Ca2+ imaging." *Cold Spring Harb Protoc* 2013 (2):83-99. doi: 10.1101/pdb.top066050.

Borcherding, N., K. Cole, P. Kluz, M. Jorgensen, R. Kolb, A. Bellizzi, and W. Zhang. 2018. "Re-Evaluating E-Cadherin and β-Catenin: A Pan-Cancer Proteomic Approach with an Emphasis on Breast Cancer." *Am J Pathol* 188 (8):1910-1920. doi: 10.1016/j.ajpath.2018.05.003.

Boreddy, S. R., and S. K. Srivastava. 2013. "Pancreatic cancer chemoprevention by phytochemicals." *Cancer Lett* 334 (1):86-94. doi: 10.1016/j.canlet.2012.10.020.

Boukamp, P., R. T. Petrussevska, D. Breitkreutz, J. Hornung, A. Markham, and N. E. Fusenig. 1988. "Normal keratinization in a spontaneously immortalized aneuploid human keratinocyte cell line." *J Cell Biol* 106 (3):761-71. doi: 10.1083/jcb.106.3.761.

Brabletz, T., A. Jung, S. Reu, M. Porzner, F. Hlubek, L. A. Kunz-Schughart, R. Knuechel, and T. Kirchner. 2001. "Variable beta-catenin expression in colorectal cancers indicates tumor progression driven by the tumor environment." *Proc Natl Acad Sci U S A* 98 (18):10356-61. doi: 10.1073/pnas.171610498.

Bradford, M. M. 1976. "A rapid and sensitive method for the quantitation of microgram quantities of protein utilizing the principle of protein-dye binding." *Anal Biochem* 72:248-54.

Brayden, D. J., J. Gleeson, and E. G. Walsh. 2014. "A head-to-head multi-parametric high content analysis of a series of medium chain fatty acid intestinal permeation enhancers in Caco-2 cells." *Eur J Pharm Biopharm* 88 (3):830-39. doi: 10.1016/j.ejpb.2014.10.008.

Breinbauer, R., and M. Köhn. 2003. "Azide-alkyne coupling: a powerful reaction for bioconjugate chemistry." *Chembiochem* 4 (11):1147-9. doi: 10.1002/cbic.200300705.

Breitkreutz, D., L. Braiman-Wiksman, N. Daum, M. F. Denning, and T. Tennenbaum. 2007. "Protein kinase C family: on the crossroads of cell signaling in skin and tumor epithelium." *J Cancer Res Clin Oncol* 133 (11):793-808. doi: 10.1007/s00432-007-0280-3.

Brigelius, R., C. Muckel, T. P. Akerboom, and H. Sies. 1983. "Identification and quantitation of glutathione in hepatic protein mixed disulfides and its relationship to glutathione disulfide." *Biochem Pharmacol* 32 (17):2529-34.

Brinckmann, R., K. Schnurr, D. Heydeck, T. Rosenbach, G. Kolde, and H. Kühn. 1998. "Membrane translocation of 15-lipoxygenase in hematopoietic cells is calcium-dependent and activates the oxygenase activity of the enzyme." *Blood* 91 (1):64-74.

Brookes, P. S., Y. Yoon, J. L. Robotham, M. W. Anders, and S. S. Sheu. 2004. "Calcium, ATP, and ROS: a mitochondrial love-hate triangle." *Am J Physiol Cell Physiol* 287 (4):C817-33. doi: 10.1152/ajpcell.00139.2004.

Brozovic, A., G. Fritz, M. Christmann, J. Zisowsky, U. Jaehde, M. Osmak, and B. Kaina. 2004. "Long-term activation of SAPK/JNK, p38 kinase and fas-L

expression by cisplatin is attenuated in human carcinoma cells that acquired drug resistance." *Int J Cancer* 112 (6):974-85. doi: 10.1002/ijc.20522.

Bugreev, D. V., and A. V. Mazin. 2004. "Ca2+ activates human homologous recombination protein Rad51 by modulating its ATPase activity." *Proc Natl Acad Sci U S A* 101 (27):9988-93. doi: 10.1073/pnas.0402105101.

Buhrke, T., I. Lengler, and A. Lampen. 2011. "Analysis of proteomic changes induced upon cellular differentiation of the human intestinal cell line Caco-2." *Dev Growth Differ* 53 (3):411-26. doi: 10.1111/j.1440-169X.2011.01258.x.

Büsselberg, D., and A. M. Florea. 2017. "Targeting Intracellular Calcium Signaling ([Ca." *Cancers (Basel)* 9 (5). doi: 10.3390/cancers9050048.

Cadenas, E., and H. Sies. 1982. "Low level chemiluminescence of liver microsomal fractions initiated by tert-butyl hydroperoxide. Relation to microsomal hemoproteins, oxygen dependence, and lipid peroxidation." *Eur J Biochem* 124 (2):349-56.

Campbell, N.A., and J.B. Reece. 2005. The Cell Cycle [PowerPoint Lectures for Biology, 9th edition]. San Francisco: Pearson Eduction.

Cao, J. Y., and S. J. Dixon. 2016. "Mechanisms of ferroptosis." *Cell Mol Life Sci* 73 (11-12):2195-209. doi: 10.1007/s00018-016-2194-1.

Cavallaro, U., and G. Christofori. 2001. "Cell adhesion in tumor invasion and metastasis: loss of the glue is not enough." *Biochim Biophys Acta* 1552 (1):39-45.

Chae, B., K. M. Yang, T. I. Kim, and W. H. Kim. 2009. "Adherens junction-dependent PI3K/Akt activation induces resistance to genotoxin-induced cell death in differentiated intestinal epithelial cells." *Biochem Biophys Res Commun* 378 (4):738-43. doi: 10.1016/j.bbrc.2008.11.120.

Chaitanya, G. V., A. J. Steven, and P. P. Babu. 2010. "PARP-1 cleavage fragments: signatures of cell-death proteases in neurodegeneration." *Cell Commun Signal* 8:31. doi: 10.1186/1478-811X-8-31.

Chang, W. H., H. C. Ting, W. W. Chen, J. F. Chan, and Y. H. Hsu. 2018. "Omega-3 and omega-6 fatty acid differentially impact cardiolipin remodeling in activated macrophage." *Lipids Health Dis* 17 (1):201. doi: 10.1186/s12944-018-0845-y.

Chapman, J. R., M. R. Taylor, and S. J. Boulton. 2012. "Playing the end game: DNA double-strand break repair pathway choice." *Mol Cell* 47 (4):497-510. doi: 10.1016/j.molcel.2012.07.029.

Cheloni, G., and V. I. Slaveykova. 2013. "Optimization of the C11-BODIPY(581/591) dye for the determination of lipid oxidation in Chlamydomonas reinhardtii by flow cytometry." *Cytometry A* 83 (10):952-61. doi: 10.1002/cyto.a.22338.

Chen, D., X. Y. Zhang, and Y. Shi. 2006. "Identification and functional characterization of hCLS1, a human cardiolipin synthase localized in mitochondria." *Biochem J* 398 (2):169-76. doi: 10.1042/BJ20060303.

Chen, H., L. Zhou, C. Y. Lin, M. C. Beattie, J. Liu, and B. R. Zirkin. 2010. "Effect of glutathione redox state on Leydig cell susceptibility to acute oxidative stress." *Mol Cell Endocrinol* 323 (2):147-54. doi: 10.1016/j.mce.2010.02.034.

Chen, Q. M., J. C. Bartholomew, J. Campisi, M. Acosta, J. D. Reagan, and B. N. Ames. 1998. "Molecular analysis of H2O2-induced senescent-like growth

arrest in normal human fibroblasts: p53 and Rb control G1 arrest but not cell replication." *Biochem J* 332 (Pt 1):43-50. doi: 10.1042/bj3320043.

Chen, Q. M., V. C. Tu, Y. Wu, and J. J. Bahl. 2000. "Hydrogen peroxide dose dependent induction of cell death or hypertrophy in cardiomyocytes." *Arch Biochem Biophys* 373 (1):242-8. doi: 10.1006/abbi.1999.1558.

Chen, Z., D. Zhang, F. Yue, M. Zheng, Z. Kovacevic, and D. R. Richardson. 2012. "The iron chelators Dp44mT and DFO inhibit TGF-β-induced epithelial-mesenchymal transition via up-regulation of N-Myc downstream-regulated gene 1 (NDRG1)." *J Biol Chem* 287 (21):17016-28. doi: 10.1074/jbc.M112.350470.

Cheung, T. H., and T. A. Rando. 2013. "Molecular regulation of stem cell quiescence." *Nat Rev Mol Cell Biol* 14 (6):329-40. doi: 10.1038/nrm3591.

Cho, Y. S., S. Y. Park, H. S. Shin, and F. K. Chan. 2010. "Physiological consequences of programmed necrosis, an alternative form of cell demise." *Mol Cells* 29 (4):327-32. doi: 10.1007/s10059-010-0066-3.

Christmann, M., M. T. Tomicic, W. P. Roos, and B. Kaina. 2003. "Mechanisms of human DNA repair: an update." *Toxicology* 193 (1-2):3-34.

Chung, Y. C., W. C. Wei, C. N. Hung, J. F. Kuo, C. P. Hsu, K. J. Chang, and W. T. Chao. 2016. "Rab11 collaborates E-cadherin to promote collective cell migration and indicates a poor prognosis in colorectal carcinoma." *Eur J Clin Invest* 46 (12):1002-1011. doi: 10.1111/eci.12683.

Circu, M. L., and T. Y. Aw. 2012. "Glutathione and modulation of cell apoptosis." *Biochim Biophys Acta* 1823 (10):1767-77. doi: 10.1016/j.bbamcr.2012.06.019.

Coleman, J. B., D. Gilfor, and J. L. Farber. 1989. "Dissociation of the accumulation of single-strand breaks in DNA from the killing of cultured hepatocytes by an oxidative stress." *Mol Pharmacol* 36 (1):193-200.

Conrad, M., J. P. Angeli, P. Vandenabeele, and B. R. Stockwell. 2016. "Regulated necrosis: disease relevance and therapeutic opportunities." *Nat Rev Drug Discov* 15 (5):348-66. doi: 10.1038/nrd.2015.6.

Cooper, G.M. 2000. "The Cell: A Molecular Approach. 2nd Edition [E-book]." In. Sunderland (MA): Sinauer Associates.

Cottet-Rousselle, C., X. Ronot, X. Leverve, and J. F. Mayol. 2011. "Cytometric assessment of mitochondria using fluorescent probes." *Cytometry A* 79 (6):405-25. doi: 10.1002/cyto.a.21061.

Craig, R., A. Larkin, A. M. Mingo, D. J. Thuerauf, C. Andrews, P. M. McDonough, and C. C. Glembotski. 2000. "p38 MAPK and NF-kappa B collaborate to induce interleukin-6 gene expression and release. Evidence for a cytoprotective autocrine signaling pathway in a cardiac myocyte model system." *J Biol Chem* 275 (31):23814-24. doi: 10.1074/jbc.M909695199.

Cuenda, A., J. Rouse, Y. N. Doza, R. Meier, P. Cohen, T. F. Gallagher, P. R. Young, and J. C. Lee. 1995. "SB 203580 is a specific inhibitor of a MAP kinase homologue which is stimulated by cellular stresses and interleukin-1." *FEBS Lett* 364 (2):229-33.

Cui, J., W. Jiang, S. Wang, L. Wang, and K. Xie. 2012. "Role of Wnt/β-catenin signaling in drug resistance of pancreatic cancer." *Curr Pharm Des* 18 (17):2464-71.

Curto, M., B. K. Cole, D. Lallemand, C. H. Liu, and A. I. McClatchey. 2007. "Contact-dependent inhibition of EGFR signaling by Nf2/Merlin." *J Cell Biol* 177 (5):893-903. doi: 10.1083/jcb.200703010.

Dahl, M., V. Maturi, P. Lönn, P. Papoutsoglou, A. Zieba, M. Vanlandewijck, L. P. van der Heide, Y. Watanabe, O. Söderberg, M. O. Hottiger, C. H. Heldin, and A. Moustakas. 2014. "Fine-tuning of Smad protein function by poly(ADP-ribose) polymerases and poly(ADP-ribose) glycohydrolase during transforming growth factor β signaling." *PLoS One* 9 (8):e103651. doi: 10.1371/journal.pone.0103651.

Darzynkiewicz, Z., H. D. Halicka, and H. Zhao. 2010. "Analysis of cellular DNA content by flow and laser scanning cytometry." *Adv Exp Med Biol* 676:137-47.

David, K. K., S. A. Andrabi, T. M. Dawson, and V. L. Dawson. 2009. "Parthanatos, a messenger of death." *Front Biosci (Landmark Ed)* 14:1116-28.

Davis, B.J., and L. Ornstein. 1959. ""A new high resolution electrophoresis method"." *Delivered at the Society for the Study of Blood at the New York Academy of Medicine.*

Day, R. M., and Y. J. Suzuki. 2006. "Cell proliferation, reactive oxygen and cellular glutathione." *Dose Response* 3 (3):425-42. doi: 10.2203/dose-response.003.03.010.

De Wever, O., W. Westbroek, A. Verloes, N. Bloemen, M. Bracke, C. Gespach, E. Bruyneel, and M. Mareel. 2004. "Critical role of N-cadherin in myofibroblast invasion and migration in vitro stimulated by colon-cancer-cell-derived TGF-beta or wounding." *J Cell Sci* 117 (Pt 20):4691-703. doi: 10.1242/jcs.01322.

Decrock, E., M. De Bock, N. Wang, A. K. Gadicherla, M. Bol, T. Delvaeye, P. Vandenabeele, M. Vinken, G. Bultynck, D. V. Krysko, and L. Leybaert. 2013. "IP3, a small molecule with a powerful message." *Biochim Biophys Acta* 1833 (7):1772-86. doi: 10.1016/j.bbamcr.2012.12.016.

Degasperi, G. R., R. F. Castilho, and A. E. Vercesi. 2008. "High susceptibility of activated lymphocytes to oxidative stress-induced cell death." *An Acad Bras Cienc* 80 (1):137-48.

Degterev, A., Z. Huang, M. Boyce, Y. Li, P. Jagtap, N. Mizushima, G. D. Cuny, T. J. Mitchison, M. A. Moskowitz, and J. Yuan. 2005. "Chemical inhibitor of nonapoptotic cell death with therapeutic potential for ischemic brain injury." *Nat Chem Biol* 1 (2):112-9. doi: 10.1038/nchembio711.

Deng, X., L. Xiao, W. Lang, F. Gao, P. Ruvolo, and W. S. May. 2001. "Novel role for JNK as a stress-activated Bcl2 kinase." *J Biol Chem* 276 (26):23681-8. doi: 10.1074/jbc.M100279200.

Derycke, L. D., and M. E. Bracke. 2004. "N-cadherin in the spotlight of cell-cell adhesion, differentiation, embryogenesis, invasion and signalling." *Int J Dev Biol* 48 (5-6):463-76. doi: 10.1387/ijdb.041793ld.

Devin, A., Y. Lin, and Z. G. Liu. 2003. "The role of the death-domain kinase RIP in tumour-necrosis-factor-induced activation of mitogen-activated protein kinases." *EMBO Rep* 4 (6):623-7. doi: 10.1038/sj.embor.embor854.

Dickey, J. S., C. E. Redon, A. J. Nakamura, B. J. Baird, O. A. Sedelnikova, and W. M. Bonner. 2009. "H2AX: functional roles and potential applications." *Chromosoma* 118 (6):683-92. doi: 10.1007/s00412-009-0234-4.

Dietrich, C., N. Gumpert, I. Heit, M. Borchert-Stuhlträger, F. Oesch, and R. Wieser. 2001. "Rottlerin induces a transformed phenotype in human keratinocytes." *Biochem Biophys Res Commun* 282 (2):575-9. doi: 10.1006/bbrc.2001.4530.

Dietrich, C., J. Scherwat, D. Faust, and F. Oesch. 2002. "Subcellular localization of beta-catenin is regulated by cell density." *Biochem Biophys Res Commun* 292 (1):195-9.

Dietrich, C., K. Wallenfang, F. Oesch, and R. Wieser. 1997. "Differences in the mechanisms of growth control in contact-inhibited and serum-deprived human fibroblasts." *Oncogene* 15 (22):2743-7. doi: 10.1038/sj.onc.1201439.

Dixon, S. J. 2017. "Ferroptosis: bug or feature?" *Immunol Rev* 277 (1):150-157. doi: 10.1111/imr.12533.

Dixon, S. J., K. M. Lemberg, M. R. Lamprecht, R. Skouta, E. M. Zaitsev, C. E. Gleason, D. N. Patel, A. J. Bauer, A. M. Cantley, W. S. Yang, B. Morrison, and B. R. Stockwell. 2012. "Ferroptosis: an iron-dependent form of nonapoptotic cell death." *Cell* 149 (5):1060-72. doi: 10.1016/j.cell.2012.03.042.

Djelloul, S., M. E. Forgue-Lafitte, B. Hermelin, M. Mareel, E. Bruyneel, A. Baldi, A. Giordano, E. Chastre, and C. Gespach. 1997. "Enterocyte differentiation is compatible with SV40 large T expression and loss of p53 function in human colonic Caco-2 cells. Status of the pRb1 and pRb2 tumor suppressor gene products." *FEBS Lett* 406 (3):234-42.

Doll, S., B. Proneth, Y. Y. Tyurina, E. Panzilius, S. Kobayashi, I. Ingold, M. Irmler, J. Beckers, M. Aichler, A. Walch, H. Prokisch, D. Trümbach, G. Mao, F. Qu, H. Bayir, J. Füllekrug, C. H. Scheel, W. Wurst, J. A. Schick, V. E. Kagan, J. P. Angeli, and M. Conrad. 2017. "ACSL4 dictates ferroptosis sensitivity by shaping cellular lipid composition." *Nat Chem Biol* 13 (1):91-98. doi: 10.1038/nchembio.2239.

Dondelinger, Y., W. Declercq, S. Montessuit, R. Roelandt, A. Goncalves, I. Bruggeman, P. Hulpiau, K. Weber, C. A. Sehon, R. W. Marquis, J. Bertin, P. J. Gough, S. Savvides, J. C. Martinou, M. J. Bertrand, and P. Vandenabeele. 2014. "MLKL compromises plasma membrane integrity by binding to phosphatidylinositol phosphates." *Cell Rep* 7 (4):971-81. doi: 10.1016/j.celrep.2014.04.026.

Dong, T., D. Liao, X. Liu, and X. Lei. 2015. "Using Small Molecules to Dissect Non-apoptotic Programmed Cell Death: Necroptosis, Ferroptosis, and Pyroptosis." *Chembiochem* 16 (18):2557-61. doi: 10.1002/cbic.201500422.

Dorsey, J. F., M. L. Dowling, M. Kim, R. Voong, L. J. Solin, and G. D. Kao. 2010. "Modulation of the anti-cancer efficacy of microtubule-targeting agents by cellular growth conditions." *Cancer Biol Ther* 9 (10):809-18. doi: 10.4161/cbt.9.10.11453.

Drummen, G. P., L. C. van Liebergen, J. A. Op den Kamp, and J. A. Post. 2002. "C11-BODIPY(581/591), an oxidation-sensitive fluorescent lipid peroxidation probe: (micro)spectroscopic characterization and validation of methodology." *Free Radic Biol Med* 33 (4):473-90.

Dunai, Z., P. I. Bauer, and R. Mihalik. 2011. "Necroptosis: biochemical, physiological and pathological aspects." *Pathol Oncol Res* 17 (4):791-800. doi: 10.1007/s12253-011-9433-4.

Eagle, H., and E. M. Levine. 1967. "Growth regulatory effects of cellular interaction." *Nature* 213 (5081):1102-6.

Ebnet, K. 2008. "Organization of multiprotein complexes at cell-cell junctions." *Histochem Cell Biol* 130 (1):1-20. doi: 10.1007/s00418-008-0418-7.

Edgell, C. J., C. C. McDonald, and J. B. Graham. 1983. "Permanent cell line expressing human factor VIII-related antigen established by hybridization." *Proc Natl Acad Sci U S A* 80 (12):3734-7. doi: 10.1073/pnas.80.12.3734.

Ekshyyan, O., and T. Y. Aw. 2005. "Decreased susceptibility of differentiated PC12 cells to oxidative challenge: relationship to cellular redox and expression of apoptotic protease activator factor-1." *Cell Death Differ* 12 (8):1066-77. doi: 10.1038/sj.cdd.4401650.

Eling, N., L. Reuter, J. Hazin, A. Hamacher-Brady, and N. R. Brady. 2015. "Identification of artesunate as a specific activator of ferroptosis in pancreatic cancer cells." *Oncoscience* 2 (5):517-32. doi: 10.18632/oncoscience.160.

Elisha, Y., V. Kalchenko, Y. Kuznetsov, and B. Geiger. 2018. "Dual role of E-cadherin in the regulation of invasive collective migration of mammary carcinoma cells." *Sci Rep* 8 (1):4986. doi: 10.1038/s41598-018-22940-3.

Elliott, S. J., and T. N. Doan. 1993. "Oxidant stress inhibits the store-dependent Ca(2+)-influx pathway of vascular endothelial cells." *Biochem J* 292 (Pt 2):385-93. doi: 10.1042/bj2920385.

Ellman, G. L. 1959. "Tissue sulfhydryl groups." *Arch Biochem Biophys* 82 (1):70-7.

English, J. D., and J. D. Sweatt. 1996. "Activation of p42 mitogen-activated protein kinase in hippocampal long term potentiation." *J Biol Chem* 271 (40):24329-32. doi: 10.1074/jbc.271.40.24329.

Erdelyi, I., N. Levenkova, E. Y. Lin, J. T. Pinto, M. Lipkin, F. W. Quimby, and P. R. Holt. 2009. "Western-style diets induce oxidative stress and dysregulate immune responses in the colon in a mouse model of sporadic colon cancer." *J Nutr* 139 (11):2072-8. doi: 10.3945/jn.108.104125.

Erez, N., E. Zamir, B. J. Gour, O. W. Blaschuk, and B. Geiger. 2004. "Induction of apoptosis in cultured endothelial cells by a cadherin antagonist peptide: involvement of fibroblast growth factor receptor-mediated signalling." *Exp Cell Res* 294 (2):366-78. doi: 10.1016/j.yexcr.2003.11.033.

Ermak, G., and K. J. Davies. 2002. "Calcium and oxidative stress: from cell signaling to cell death." *Mol Immunol* 38 (10):713-21.

Evans, J. F., A. D. Ferguson, R. T. Mosley, and J. H. Hutchinson. 2008. "What's all the FLAP about?: 5-lipoxygenase-activating protein inhibitors for inflammatory diseases." *Trends Pharmacol Sci* 29 (2):72-8. doi: 10.1016/j.tips.2007.11.006.

Fahrer, J., R. Kranaster, M. Altmeyer, A. Marx, and A. Bürkle. 2007. "Quantitative analysis of the binding affinity of poly(ADP-ribose) to specific binding proteins as a function of chain length." *Nucleic Acids Res* 35 (21):e143. doi: 10.1093/nar/gkm944.

Fairbairn, D. W., P. L. Olive, and K. L. O'Neill. 1995. "The comet assay: a comprehensive review." *Mutat Res* 339 (1):37-59.

Fajardo, V. A., J. S. Mikhaeil, C. F. Leveille, C. Saint, and P. J. LeBlanc. 2017. "Cardiolipin content, linoleic acid composition, and tafazzin expression in response to skeletal muscle overload and unload stimuli." *Sci Rep* 7 (1):2060. doi: 10.1038/s41598-017-02089-1.

Faust, D., I. Dolado, A. Cuadrado, F. Oesch, C. Weiss, A. R. Nebreda, and C. Dietrich. 2005. "p38alpha MAPK is required for contact inhibition." *Oncogene* 24 (53):7941-5. doi: 10.1038/sj.onc.1208948.

Faust, D., S. Kletting, E. Ueberham, and C. Dietrich. 2013. "Aryl hydrocarbon receptor-dependent cell cycle arrest in isolated mouse oval cells." *Toxicol Lett* 223 (1):73-80. doi: 10.1016/j.toxlet.2013.08.022.

Faust, D., C. Schmitt, F. Oesch, B. Oesch-Bartlomowicz, I. Schreck, C. Weiss, and C. Dietrich. 2012. "Differential p38-dependent signalling in response to cellular stress and mitogenic stimulation in fibroblasts." *Cell Commun Signal* 10:6. doi: 10.1186/1478-811X-10-6.

Forman, H. J., H. Zhang, and A. Rinna. 2009. "Glutathione: overview of its protective roles, measurement, and biosynthesis." *Mol Aspects Med* 30 (1-2):1-12. doi: 10.1016/j.mam.2008.08.006.

Francis, G. L. 2010. "Albumin and mammalian cell culture: implications for biotechnology applications." *Cytotechnology* 62 (1):1-16. doi: 10.1007/s10616-010-9263-3.

Franco, R., M. I. Panayiotidis, and J. A. Cidlowski. 2007. "Glutathione depletion is necessary for apoptosis in lymphoid cells independent of reactive oxygen species formation." *J Biol Chem* 282 (42):30452-65. doi: 10.1074/jbc.M703091200.

Fratelli, M., H. Demol, M. Puype, S. Casagrande, P. Villa, I. Eberini, J. Vandekerckhove, E. Gianazza, and P. Ghezzi. 2003. "Identification of proteins undergoing glutathionylation in oxidatively stressed hepatocytes and hepatoma cells." *Proteomics* 3 (7):1154-61. doi: 10.1002/pmic.200300436.

Friedl, P., and D. Gilmour. 2009. "Collective cell migration in morphogenesis, regeneration and cancer." *Nat Rev Mol Cell Biol* 10 (7):445-57. doi: 10.1038/nrm2720.

Friedmann Angeli, J. P., M. Schneider, B. Proneth, Y. Y. Tyurina, V. A. Tyurin, V. J. Hammond, N. Herbach, M. Aichler, A. Walch, E. Eggenhofer, D. Basavarajappa, O. Rådmark, S. Kobayashi, T. Seibt, H. Beck, F. Neff, I. Esposito, R. Wanke, H. Förster, O. Yefremova, M. Heinrichmeyer, G. W. Bornkamm, E. K. Geissler, S. B. Thomas, B. R. Stockwell, V. B. O'Donnell, V. E. Kagan, J. A. Schick, and M. Conrad. 2014. "Inactivation of the ferroptosis regulator Gpx4 triggers acute renal failure in mice." *Nat Cell Biol* 16 (12):1180-91. doi: 10.1038/ncb3064.

Fulda, S. 2014. "Therapeutic exploitation of necroptosis for cancer therapy." *Semin Cell Dev Biol* 35:51-6. doi: 10.1016/j.semcdb.2014.07.002.

Gaballah, M., M. Slisz, and D. Hutter-Lobo. 2012. "Role of JNK-1 regulation in the protection of contact-inhibited fibroblasts from oxidative stress." *Mol Cell Biochem* 359 (1-2):105-13. doi: 10.1007/s11010-011-1004-1.

Gafter, U., T. Malachi, Y. Ori, and H. Breitbart. 1997. "The role of calcium in human lymphocyte DNA repair ability." *J Lab Clin Med* 130 (1):33-41.

Galaz, S., J. Espada, J. C. Stockert, M. Pacheco, F. Sanz-Rodríguez, R. Arranz, S. Rello, M. Cañete, A. Villanueva, M. Esteller, and A. Juarranz. 2005. "Loss of E-cadherin mediated cell-cell adhesion as an early trigger of apoptosis induced by photodynamic treatment." *J Cell Physiol* 205 (1):86-96. doi: 10.1002/jcp.20374.

Galluzzi, L., O. Kepp, S. Krautwald, G. Kroemer, and A. Linkermann. 2014. "Molecular mechanisms of regulated necrosis." *Semin Cell Dev Biol* 35:24-32. doi: 10.1016/j.semcdb.2014.02.006.

Galluzzi, L., I. Vitale, S. A. Aaronson, J. M. Abrams, D. Adam, P. Agostinis, E. S. Alnemri, L. Altucci, I. Amelio, D. W. Andrews, M. Annicchiarico-Petruzzelli, A. V. Antonov, E. Arama, E. H. Baehrecke, N. A. Barlev, N. G. Bazan, F. Bernassola, M. J. M. Bertrand, K. Bianchi, M. V. Blagosklonny, K. Blomgren, C. Borner, P. Boya, C. Brenner, M. Campanella, E. Candi, D. Carmona-Gutierrez, F. Cecconi, F. K. Chan, N. S. Chandel, E. H. Cheng, J. E. Chipuk, J. A. Cidlowski, A. Ciechanover, G. M. Cohen, M. Conrad, J. R. Cubillos-Ruiz, P. E. Czabotar, V. D'Angiolella, T. M. Dawson, V. L. Dawson, V. De Laurenzi, R. De Maria, K. M. Debatin, R. J. DeBerardinis, M. Deshmukh, N. Di Daniele, F. Di Virgilio, V. M. Dixit, S. J. Dixon, C. S. Duckett, B. D. Dynlacht, W. S. El-Deiry, J. W. Elrod, G. M. Fimia, S. Fulda, A. J. García-Sáez, A. D. Garg, C. Garrido, E. Gavathiotis, P. Golstein, E. Gottlieb, D. R. Green, L. A. Greene, H. Gronemeyer, A. Gross, G. Hajnoczky, J. M. Hardwick, I. S. Harris, M. O. Hengartner, C. Hetz, H. Ichijo, M. Jäättelä, B. Joseph, P. J. Jost, P. P. Juin, W. J. Kaiser, M. Karin, T. Kaufmann, O. Kepp, A. Kimchi, R. N. Kitsis, D. J. Klionsky, R. A. Knight, S. Kumar, S. W. Lee, J. J. Lemasters, B. Levine, A. Linkermann, S. A. Lipton, R. A. Lockshin, C. López-Otín, S. W. Lowe, T. Luedde, E. Lugli, M. MacFarlane, F. Madeo, M. Malewicz, W. Malorni, G. Manic, J. C. Marine, S. J. Martin, J. C. Martinou, J. P. Medema, P. Mehlen, P. Meier, S. Melino, E. A. Miao, J. D. Molkentin, U. M. Moll, C. Muñoz-Pinedo, S. Nagata, G. Nuñez, A. Oberst, M. Oren, M. Overholtzer, M. Pagano, T. Panaretakis, M. Pasparakis, J. M. Penninger, D. M. Pereira, S. Pervaiz, M. E. Peter, M. Piacentini, P. Pinton, J. H. M. Prehn, H. Puthalakath, G. A. Rabinovich, M. Rehm, R. Rizzuto, C. M. P. Rodrigues, D. C. Rubinsztein, T. Rudel, K. M. Ryan, E. Sayan, L. Scorrano, F. Shao, Y. Shi, J. Silke, H. U. Simon, A. Sistigu, B. R. Stockwell, A. Strasser, G. Szabadkai, S. W. G. Tait, D. Tang, N. Tavernarakis, A. Thorburn, Y. Tsujimoto, B. Turk, T. Vanden Berghe, P. Vandenabeele, M. G. Vander Heiden, A. Villunger, H. W. Virgin, K. H. Vousden, D. Vucic, E. F. Wagner, H. Walczak, D. Wallach, Y. Wang, J. A. Wells, W. Wood, J. Yuan, Z. Zakeri, B. Zhivotovsky, L. Zitvogel, G. Melino,

and G. Kroemer. 2018. "Molecular mechanisms of cell death: recommendations of the Nomenclature Committee on Cell Death 2018." *Cell Death Differ* 25 (3):486-541. doi: 10.1038/s41418-017-0012-4.

Galluzzi, L., I. Vitale, J. M. Abrams, E. S. Alnemri, E. H. Baehrecke, M. V. Blagosklonny, T. M. Dawson, V. L. Dawson, W. S. El-Deiry, S. Fulda, E. Gottlieb, D. R. Green, M. O. Hengartner, O. Kepp, R. A. Knight, S. Kumar, S. A. Lipton, X. Lu, F. Madeo, W. Malorni, P. Mehlen, G. Nuñez, M. E. Peter, M. Piacentini, D. C. Rubinsztein, Y. Shi, H. U. Simon, P. Vandenabeele, E. White, J. Yuan, B. Zhivotovsky, G. Melino, and G. Kroemer. 2012. "Molecular definitions of cell death subroutines: recommendations of the Nomenclature Committee on Cell Death 2012." *Cell Death Differ* 19 (1):107-20. doi: 10.1038/cdd.2011.96.

Gangwar, R., A. S. Meena, P. K. Shukla, A. S. Nagaraja, P. L. Dorniak, S. Pallikuth, C. M. Waters, A. Sood, and R. Rao. 2017. "Calcium-mediated oxidative stress: a common mechanism in tight junction disruption by different types of cellular stress." *Biochem J* 474 (5):731-749. doi: 10.1042/BCJ20160679.

Gao, M., P. Monian, Q. Pan, W. Zhang, J. Xiang, and X. Jiang. 2016. "Ferroptosis is an autophagic cell death process." *Cell Res* 26 (9):1021-32. doi: 10.1038/cr.2016.95.

Gao, M., P. Monian, N. Quadri, R. Ramasamy, and X. Jiang. 2015. "Glutaminolysis and Transferrin Regulate Ferroptosis." *Mol Cell* 59 (2):298-308. doi: 10.1016/j.molcel.2015.06.011.

Garcia-Cohen, E. C., J. Marin, L. D. Diez-Picazo, A. B. Baena, M. Salaices, and M. A. Rodriguez-Martinez. 2000. "Oxidative stress induced by tert-butyl hydroperoxide causes vasoconstriction in the aorta from hypertensive and aged rats: role of cyclooxygenase-2 isoform." *J Pharmacol Exp Ther* 293 (1):75-81.

Garg, R., L. G. Benedetti, M. B. Abera, H. Wang, M. Abba, and M. G. Kazanietz. 2014. "Protein kinase C and cancer: what we know and what we do not." *Oncogene* 33 (45):5225-37. doi: 10.1038/onc.2013.524.

Gautheron, J., M. Vucur, F. Reisinger, D. V. Cardenas, C. Roderburg, C. Koppe, K. Kreggenwinkel, A. T. Schneider, M. Bartneck, U. P. Neumann, A. Canbay, H. L. Reeves, M. Luedde, F. Tacke, C. Trautwein, M. Heikenwalder, and T. Luedde. 2014. "A positive feedback loop between RIP3 and JNK controls non-alcoholic steatohepatitis." *EMBO Mol Med* 6 (8):1062-74. doi: 10.15252/emmm.201403856.

Gibson, B. A., and W. L. Kraus. 2012. "New insights into the molecular and cellular functions of poly(ADP-ribose) and PARPs." *Nat Rev Mol Cell Biol* 13 (7):411-24. doi: 10.1038/nrm3376.

Giorgi, C., D. De Stefani, A. Bononi, R. Rizzuto, and P. Pinton. 2009. "Structural and functional link between the mitochondrial network and the endoplasmic reticulum." *Int J Biochem Cell Biol* 41 (10):1817-27. doi: 10.1016/j.biocel.2009.04.010.

Glick, A. B., and S. H. Yuspa. 2005. "Tissue homeostasis and the control of the neoplastic phenotype in epithelial cancers." *Semin Cancer Biol* 15 (2):75-83. doi: 10.1016/j.semcancer.2004.08.008.

Godwin, T. D., S. T. Kelly, T. P. Brew, N. M. Bougen-Zhukov, A. B. Single, A. Chen, C. E. Stylianou, L. D. Harris, S. K. Currie, B. J. Telford, H. G. Beetham, G. B. Evans, M. A. Black, and P. J. Guilford. 2019. "E-cadherin-deficient cells have synthetic lethal vulnerabilities in plasma membrane organisation, dynamics and function." *Gastric Cancer* 22 (2):273-286. doi: 10.1007/s10120-018-0859-1.

Gopinath, M., R. Di Liddo, F. Marotta, R. Murugesan, A. Banerjee, S. Sriramulu, G. Jothimani, V. D. Subramaniam, S. Narasimhan, S. Priya K, X. F. Sun, and S. Pathak. 2018. "Role of Hippo Pathway Effector Tafazzin Protein in Maintaining Stemness of Umbilical Cord-Derived Mesenchymal Stem Cells (UC-MSC)." *Int J Hematol Oncol Stem Cell Res* 12 (2):153-165.

Gough, D. R., and T. G. Cotter. 2011. "Hydrogen peroxide: a Jekyll and Hyde signalling molecule." *Cell Death Dis* 2:e213. doi: 10.1038/cddis.2011.96.

Gujral, T. S., and M. W. Kirschner. 2017. "Hippo pathway mediates resistance to cytotoxic drugs." *Proc Natl Acad Sci U S A* 114 (18):E3729-E3738. doi: 10.1073/pnas.1703096114.

Gunter, T. E., K. K. Gunter, S. S. Sheu, and C. E. Gavin. 1994. "Mitochondrial calcium transport: physiological and pathological relevance." *Am J Physiol* 267 (2 Pt 1):C313-39. doi: 10.1152/ajpcell.1994.267.2.C313.

Gunter, T. E., and D. R. Pfeiffer. 1990. "Mechanisms by which mitochondria transport calcium." *Am J Physiol* 258 (5 Pt 1):C755-86. doi: 10.1152/ajpcell.1990.258.5.C755.

Gutiérrez-Aguilar, M., and C. P. Baines. 2015. "Structural mechanisms of cyclophilin D-dependent control of the mitochondrial permeability transition pore." *Biochim Biophys Acta* 1850 (10):2041-7. doi: 10.1016/j.bbagen.2014.11.009.

Gómez, S., M. del Mont Llosas, J. Verdú, S. Roura, J. Lloreta, M. Fabre, and A. García de Herreros. 1999. "Independent regulation of adherens and tight junctions by tyrosine phosphorylation in Caco-2 cells." *Biochim Biophys Acta* 1452 (2):121-32.

Görlach, A., K. Bertram, S. Hudecova, and O. Krizanova. 2015. "Calcium and ROS: A mutual interplay." *Redox Biol* 6:260-271. doi: 10.1016/j.redox.2015.08.010.

Halestrap, A. P. 2009. "What is the mitochondrial permeability transition pore?" *J Mol Cell Cardiol* 46 (6):821-31. doi: 10.1016/j.yjmcc.2009.02.021.

Halliwell, B., and J. M. Gutteridge. 1985. "The importance of free radicals and catalytic metal ions in human diseases." *Mol Aspects Med* 8 (2):89-193.

Hampton, M. B., and S. Orrenius. 1997. "Dual regulation of caspase activity by hydrogen peroxide: implications for apoptosis." *FEBS Lett* 414 (3):552-6.

Han, H. J., H. Y. Kwon, E. J. Sohn, H. Ko, B. Kim, K. Jung, J. H. Lew, and S. H. Kim. 2014. "Suppression of E-cadherin mediates gallotannin induced apoptosis in Hep G2 hepatocelluar carcinoma cells." *Int J Biol Sci* 10 (5):490-9. doi: 10.7150/ijbs.7495.

Hanahan, D., and R. A. Weinberg. 2000. "The hallmarks of cancer." *Cell* 100 (1):57-70.

Hansson, M. J., R. Månsson, S. Morota, H. Uchino, T. Kallur, T. Sumi, N. Ishii, M. Shimazu, M. F. Keep, A. Jegorov, and E. Elmér. 2008. "Calcium-induced generation of reactive oxygen species in brain mitochondria is mediated by permeability transition." *Free Radic Biol Med* 45 (3):284-94. doi: 10.1016/j.freeradbiomed.2008.04.021.

Hanstein, W. G. 1976. "Uncoupling of oxidative phosphorylation." *Biochim Biophys Acta* 456 (2):129-48.

Harr, M. W., and C. W. Distelhorst. 2010. "Apoptosis and autophagy: decoding calcium signals that mediate life or death." *Cold Spring Harb Perspect Biol* 2 (10):a005579. doi: 10.1101/cshperspect.a005579.

Hartsock, A., and W. J. Nelson. 2008. "Adherens and tight junctions: structure, function and connections to the actin cytoskeleton." *Biochim Biophys Acta* 1778 (3):660-9. doi: 10.1016/j.bbamem.2007.07.012.

Heit, I., R. J. Wieser, T. Herget, D. Faust, M. Borchert-Stuhlträger, F. Oesch, and C. Dietrich. 2001. "Involvement of protein kinase Cdelta in contact-dependent inhibition of growth in human and murine fibroblasts." *Oncogene* 20 (37):5143-54. doi: 10.1038/sj.onc.1204657.

Hempel, S. L., G. R. Buettner, Y. Q. O'Malley, D. A. Wessels, and D. M. Flaherty. 1999. "Dihydrofluorescein diacetate is superior for detecting intracellular oxidants: comparison with 2',7'-dichlorodihydrofluorescein diacetate, 5(and 6)-carboxy-2',7'-dichlorodihydrofluorescein diacetate, and dihydrorhodamine 123." *Free Radic Biol Med* 27 (1-2):146-59.

Hengst, L., and S. I. Reed. 1996. "Translational control of p27Kip1 accumulation during the cell cycle." *Science* 271 (5257):1861-4.

Higuchi, M., T. Honda, R. J. Proske, and E. T. Yeh. 1998. "Regulation of reactive oxygen species-induced apoptosis and necrosis by caspase 3-like proteases." *Oncogene* 17 (21):2753-60. doi: 10.1038/sj.onc.1202211.

Hix, S., M. B. Kadiiska, R. P. Mason, and O. Augusto. 2000. "In vivo metabolism of tert-butyl hydroperoxide to methyl radicals. EPR spin-trapping and DNA methylation studies." *Chem Res Toxicol* 13 (10):1056-64.

Holownia, A., J. F. Menez, and J. J. Braszko. 1998. "The role of calcium in paracetamol (acetaminophen) cytotoxicity in PC12 cells transfected with CYP4502E1." *Inflammopharmacology* 6 (2):133-42. doi: 10.1007/s10787-998-0030-4.

Hudson, B., W. B. Upholt, J. Devinny, and J. Vinograd. 1969. "The use of an ethidium analogue in the dye-buoyant density procedure for the isolation of closed circular DNA: the variation of the superhelix density of mitochondrial DNA." *Proc Natl Acad Sci U S A* 62 (3):813-20. doi: 10.1073/pnas.62.3.813.

Hutnik, C. M., C. E. Pocrnich, H. Liu, D. W. Laird, and Q. Shao. 2008. "The protective effect of functional connexin43 channels on a human epithelial cell line exposed to oxidative stress." *Invest Ophthalmol Vis Sci* 49 (2):800-6. doi: 10.1167/iovs.07-0717.

Hwang, M. S., C. T. Schwall, E. Pazarentzos, C. Datler, N. N. Alder, and S. Grimm. 2014. "Mitochondrial Ca(2+) influx targets cardiolipin to disintegrate respiratory chain complex II for cell death induction." *Cell Death Differ* 21 (11):1733-45. doi: 10.1038/cdd.2014.84.

Imberti, R., A. L. Nieminen, B. Herman, and J. J. Lemasters. 1993. "Mitochondrial and glycolytic dysfunction in lethal injury to hepatocytes by t-butylhydroperoxide: protection by fructose, cyclosporin A and trifluoperazine." *J Pharmacol Exp Ther* 265 (1):392-400.

Ingold, I., C. Berndt, S. Schmitt, S. Doll, G. Poschmann, K. Buday, A. Roveri, X. Peng, F. Porto Freitas, T. Seibt, L. Mehr, M. Aichler, A. Walch, D. Lamp, M. Jastroch, S. Miyamoto, W. Wurst, F. Ursini, E. S. J. Arnér, N. Fradejas-Villar, U. Schweizer, H. Zischka, J. P. Friedmann Angeli, and M. Conrad. 2018. "Selenium Utilization by GPX4 Is Required to Prevent Hydroperoxide-Induced Ferroptosis." *Cell* 172 (3):409-422.e21. doi: 10.1016/j.cell.2017.11.048.

Janeway, C.A., J.P. Travers , M. Walport , and M.J. Shlomchik. 2001. "Immunobiology, 5th Edition: The Immune System in Health and Disease [E-book]." In. New York: Garland Science.

Jarvis, R. M., J. Göttert, M. P. Murphy, and E. C. Ledgerwood. 2007. "Mitochondria-targeted antioxidants do not prevent tumour necrosis factor-induced necrosis of L929 cells." *Free Radic Res* 41 (9):1041-6. doi: 10.1080/10715760701557153.

Ji, J., A. E. Kline, A. Amoscato, A. K. Samhan-Arias, L. J. Sparvero, V. A. Tyurin, Y. Y. Tyurina, B. Fink, M. D. Manole, A. M. Puccio, D. O. Okonkwo, J. P. Cheng, H. Alexander, R. S. Clark, P. M. Kochanek, P. Wipf, V. E. Kagan, and H. Bayır. 2012. "Lipidomics identifies cardiolipin oxidation as a mitochondrial target for redox therapy of brain injury." *Nat Neurosci* 15 (10):1407-13. doi: 10.1038/nn.3195.

Ji, J., R. Liu, T. Tong, Y. Song, S. Jin, M. Wu, and Q. Zhan. 2007. "Gadd45a regulates beta-catenin distribution and maintains cell-cell adhesion/contact." *Oncogene* 26 (44):6396-405. doi: 10.1038/sj.onc.1210469.

Jia, N., Y. Nakazawa, C. Guo, M. Shimada, M. Sethi, Y. Takahashi, H. Ueda, Y. Nagayama, and T. Ogi. 2015. "A rapid, comprehensive system for assaying DNA repair activity and cytotoxic effects of DNA-damaging reagents." *Nat Protoc* 10 (1):12-24. doi: 10.1038/nprot.2014.194.

Jiang, Y., X. Y. Zhang, L. Sun, G. L. Zhang, P. Duerksen-Hughes, X. Q. Zhu, and J. Yang. 2012. "Methyl methanesulfonate induces apoptosis in p53-deficient H1299 and Hep3B cells through a caspase 2- and mitochondria-associated pathway." *Environ Toxicol Pharmacol* 34 (3):694-704. doi: 10.1016/j.etap.2012.09.019.

Jin, H., Y. He, P. Zhao, Y. Hu, J. Tao, J. Chen, and Y. Huang. 2019. "Targeting lipid metabolism to overcome EMT-associated drug resistance via integrin β3/FAK pathway and tumor-associated macrophage repolarization using legumain-activatable delivery." *Theranostics* 9 (1):265-278. doi: 10.7150/thno.27246.

Juliano, R. L. 2002. "Signal transduction by cell adhesion receptors and the cytoskeleton: functions of integrins, cadherins, selectins, and immunoglobulin-

superfamily members." *Annu Rev Pharmacol Toxicol* 42:283-323. doi: 10.1146/annurev.pharmtox.42.090401.151133.

Jyonouchi, H., S. Sun, T. Abiru, S. Chareancholvanich, and D. H. Ingbar. 1998. "The effects of hyperoxic injury and antioxidant vitamins on death and proliferation of human small airway epithelial cells." *Am J Respir Cell Mol Biol* 19 (3):426-36. doi: 10.1165/ajrcmb.19.3.2862m.

Kabiraj, P., C. A. Valenzuela, J. E. Marin, D. A. Ramirez, L. Mendez, M. S. Hwang, A. Varela-Ramirez, K. Fenelon, M. Narayan, and R. Skouta. 2015. "The neuroprotective role of ferrostatin-1 under rotenone-induced oxidative stress in dopaminergic neuroblastoma cells." *Protein J* 34 (5):349-58. doi: 10.1007/s10930-015-9629-7.

Kagan, V. E., G. Mao, F. Qu, J. P. Angeli, S. Doll, C. S. Croix, H. H. Dar, B. Liu, V. A. Tyurin, V. B. Ritov, A. A. Kapralov, A. A. Amoscato, J. Jiang, T. Anthonymuthu, D. Mohammadyani, Q. Yang, B. Proneth, J. Klein-Seetharaman, S. Watkins, I. Bahar, J. Greenberger, R. K. Mallampalli, B. R. Stockwell, Y. Y. Tyurina, M. Conrad, and H. Bayır. 2017. "Oxidized arachidonic and adrenic PEs navigate cells to ferroptosis." *Nat Chem Biol* 13 (1):81-90. doi: 10.1038/nchembio.2238.

Kajstura, M., H. D. Halicka, J. Pryjma, and Z. Darzynkiewicz. 2007. "Discontinuous fragmentation of nuclear DNA during apoptosis revealed by discrete "sub-G1" peaks on DNA content histograms." *Cytometry A* 71 (3):125-31. doi: 10.1002/cyto.a.20357.

Kamata, H., and H. Hirata. 1999. "Redox regulation of cellular signalling." *Cell Signal* 11 (1):1-14.

Kango-Singh, M., and A. Singh. 2009. "Regulation of organ size: insights from the Drosophila Hippo signaling pathway." *Dev Dyn* 238 (7):1627-37. doi: 10.1002/dvdy.21996.

Kanno, T., H. Fujita, S. Muranaka, H. Yano, T. Utsumi, T. Yoshioka, M. Inoue, and K. Utsumi. 2002. "Mitochondrial swelling and cytochrome c release: sensitivity to cyclosporin A and calcium." *Physiol Chem Phys Med NMR* 34 (2):91-102.

Kanupriya, D. Prasad, M. Sai Ram, R. C. Sawhney, G. Ilavazhagan, and P. K. Banerjee. 2007. "Mechanism of tert-butylhydroperoxide induced cytotoxicity in U-937 macrophages by alteration of mitochondrial function and generation of ROS." *Toxicol In Vitro* 21 (5):846-54. doi: 10.1016/j.tiv.2007.02.007.

Kawamitsu, H., H. Hoshino, H. Okada, M. Miwa, H. Momoi, and T. Sugimura. 1984. "Monoclonal antibodies to poly(adenosine diphosphate ribose) recognize different structures." *Biochemistry* 23 (16):3771-7.

Kelliher, M. A., S. Grimm, Y. Ishida, F. Kuo, B. Z. Stanger, and P. Leder. 1998. "The death domain kinase RIP mediates the TNF-induced NF-kappaB signal." *Immunity* 8 (3):297-303.

Kers, J., J. C. Leemans, and A. Linkermann. 2016. "An Overview of Pathways of Regulated Necrosis in Acute Kidney Injury." *Semin Nephrol* 36 (3):139-52. doi: 10.1016/j.semnephrol.2016.03.002.

Khan, N., K. E. Lawlor, J. M. Murphy, and J. E. Vince. 2014. "More to life than death: molecular determinants of necroptotic and non-necroptotic RIP3 kinase signaling." *Curr Opin Immunol* 26:76-89. doi: 10.1016/j.coi.2013.10.017.

Kiebish, M. A., X. Han, H. Cheng, J. H. Chuang, and T. N. Seyfried. 2008. "Cardiolipin and electron transport chain abnormalities in mouse brain tumor mitochondria: lipidomic evidence supporting the Warburg theory of cancer." *J Lipid Res* 49 (12):2545-56. doi: 10.1194/jlr.M800319-JLR200.

Kim, J. S., L. He, and J. J. Lemasters. 2003. "Mitochondrial permeability transition: a common pathway to necrosis and apoptosis." *Biochem Biophys Res Commun* 304 (3):463-70.

Kim, O. S., Y. S. Kim, D. S. Jang, N. H. Yoo, and J. S. Kim. 2009. "Cytoprotection against hydrogen peroxide-induced cell death in cultured mouse mesangial cells by erigeroflavanone, a novel compound from the flowers of Erigeron annuus." *Chem Biol Interact* 180 (3):414-20.

Kim, W. D., Y. W. Kim, I. J. Cho, C. H. Lee, and S. G. Kim. 2012. "E-cadherin inhibits nuclear accumulation of Nrf2: implications for chemoresistance of cancer cells." *J Cell Sci* 125 (Pt 5):1284-95. doi: 10.1242/jcs.095422.

Kmoníčková, E., L. Kameníková, S. Hynie, and H. Farghali. 2000. "Cyclosporin A modifies cytoplasmic calcium levels in isolated hepatocytes exposed to oxidative stress due to tert-butyl hydroperoxide." *Physiol Res* 49 (4):471-4.

Ko, K., P. Arora, W. Lee, and C. McCulloch. 2000. "Biochemical and functional characterization of intercellular adhesion and gap junctions in fibroblasts." *Am J Physiol Cell Physiol* 279 (1):C147-57. doi: 10.1152/ajpcell.2000.279.1.C147.

Kobayashi, N., A. Ikesue, S. Majumdar, and T. J. Siahaan. 2006. "Inhibition of e-cadherin-mediated homotypic adhesion of Caco-2 cells: a novel evaluation assay for peptide activities in modulating cell-cell adhesion." *J Pharmacol Exp Ther* 317 (1):309-16. doi: 10.1124/jpet.105.097535.

Koning, A. J., P. Y. Lum, J. M. Williams, and R. Wright. 1993. "DiOC6 staining reveals organelle structure and dynamics in living yeast cells." *Cell Motil Cytoskeleton* 25 (2):111-28. doi: 10.1002/cm.970250202.

Krainz, T., M. M. Gaschler, C. Lim, J. R. Sacher, B. R. Stockwell, and P. Wipf. 2016. "A Mitochondrial-Targeted Nitroxide Is a Potent Inhibitor of Ferroptosis." *ACS Cent Sci* 2 (9):653-659. doi: 10.1021/acscentsci.6b00199.

Kreuzaler, P., and C. J. Watson. 2012. "Killing a cancer: what are the alternatives?" *Nat Rev Cancer* 12 (6):411-24. doi: 10.1038/nrc3264.

Kriska, T., V. V. Levchenko, W. Korytowski, B. P. Atshaves, F. Schroeder, and A. W. Girotti. 2006. "Intracellular dissemination of peroxidative stress. Internalization, transport, and lethal targeting of a cholesterol hydroperoxide species by sterol carrier protein-2-overexpressing hepatoma cells." *J Biol Chem* 281 (33):23643-51. doi: 10.1074/jbc.M600744200.

Kroemer, G., B. Dallaporta, and M. Resche-Rigon. 1998. "The mitochondrial death/life regulator in apoptosis and necrosis." *Annu Rev Physiol* 60:619-42. doi: 10.1146/annurev.physiol.60.1.619.

Küppers, M., D. Faust, B. Linz, and C. Dietrich. 2011. "Regulation of ERK1/2 activity upon contact inhibition in fibroblasts." *Biochem Biophys Res Commun* 406 (3):483-7. doi: 10.1016/j.bbrc.2011.02.080.

Küppers, M., C. Ittrich, D. Faust, and C. Dietrich. 2010. "The transcriptional programme of contact-inhibition." *J Cell Biochem* 110 (5):1234-43. doi: 10.1002/jcb.22638.

Lackinger, D., U. Eichhorn, and B. Kaina. 2001. "Effect of ultraviolet light, methyl methanesulfonate and ionizing radiation on the genotoxic response and apoptosis of mouse fibroblasts lacking c-Fos, p53 or both." *Mutagenesis* 16 (3):233-41. doi: 10.1093/mutage/16.3.233.

Laemmli, U. K. 1970. "Cleavage of Structural Proteins during the Assembly of the Head of Bacteriophage T4." 227 (5259):680-685.

Lans, H., J. A. Marteijn, and W. Vermeulen. 2012. "ATP-dependent chromatin remodeling in the DNA-damage response." *Epigenetics Chromatin* 5:4. doi: 10.1186/1756-8935-5-4.

Latour, I., J. B. Demoulin, and P. Buc-Calderon. 1995. "Oxidative DNA damage by t-butyl hydroperoxide causes DNA single strand breaks which is not linked to cell lysis. A mechanistic study in freshly isolated rat hepatocytes." *FEBS Lett* 373 (3):299-302.

Lee, T. H., Q. Huang, S. Oikemus, J. Shank, J. J. Ventura, N. Cusson, R. R. Vaillancourt, B. Su, R. J. Davis, and M. A. Kelliher. 2003. "The death domain kinase RIP1 is essential for tumor necrosis factor alpha signaling to p38 mitogen-activated protein kinase." *Mol Cell Biol* 23 (22):8377-85. doi: 10.1128/mcb.23.22.8377-8385.2003.

Leist, M., B. Single, A. F. Castoldi, S. Kühnle, and P. Nicotera. 1997. "Intracellular adenosine triphosphate (ATP) concentration: a switch in the decision between apoptosis and necrosis." *J Exp Med* 185 (8):1481-6. doi: 10.1084/jem.185.8.1481.

Leist, M., C. Volbracht, S. Kühnle, E. Fava, E. Ferrando-May, and P. Nicotera. 1997. "Caspase-mediated apoptosis in neuronal excitotoxicity triggered by nitric oxide." *Mol Med* 3 (11):750-64.

Lemasters, J. J., and A. L. Nieminen. 1997. "Mitochondrial oxygen radical formation during reductive and oxidative stress to intact hepatocytes." *Biosci Rep* 17 (3):281-91.

Lemasters, J. J., T. P. Theruvath, Z. Zhong, and A. L. Nieminen. 2009. "Mitochondrial calcium and the permeability transition in cell death." *Biochim Biophys Acta* 1787 (11):1395-401. doi: 10.1016/j.bbabio.2009.06.009.

Levenberg, S., B. Z. Katz, K. M. Yamada, and B. Geiger. 1998. "Long-range and selective autoregulation of cell-cell or cell-matrix adhesions by cadherin or integrin ligands." *J Cell Sci* 111 (Pt 3):347-57.

Levine, A. J. 1997. "p53, the cellular gatekeeper for growth and division." *Cell* 88 (3):323-31.

Lewis-Tuffin, L. J., F. Rodriguez, C. Giannini, B. Scheithauer, B. M. Necela, J. N. Sarkaria, and P. Z. Anastasiadis. 2010. "Misregulated E-cadherin expression

associated with an aggressive brain tumor phenotype." *PLoS One* 5 (10):e13665. doi: 10.1371/journal.pone.0013665.

Li, G., K. Satyamoorthy, and M. Herlyn. 2001. "N-cadherin-mediated intercellular interactions promote survival and migration of melanoma cells." *Cancer Res* 61 (9):3819-25.

Li, L., Y. Hao, Y. Zhao, H. Wang, X. Zhao, Y. Jiang, and F. Gao. 2018. "Ferroptosis is associated with oxygen-glucose deprivation/reoxygenation-induced Sertoli cell death." *Int J Mol Med* 41 (5):3051-3062. doi: 10.3892/ijmm.2018.3469.

Li, W. P., L. Tsiokas, S. C. Sansom, and R. Ma. 2004. "Epidermal growth factor activates store-operated Ca2+ channels through an inositol 1,4,5-trisphosphate-independent pathway in human glomerular mesangial cells." *J Biol Chem* 279 (6):4570-7. doi: 10.1074/jbc.M304334200.

Liebermann, D. A., and B. Hoffman. 2008. "Gadd45 in stress signaling." *J Mol Signal* 3:15. doi: 10.1186/1750-2187-3-15.

Linden, A., M. Gülden, H. J. Martin, E. Maser, and H. Seibert. 2008. "Peroxide-induced cell death and lipid peroxidation in C6 glioma cells." *Toxicol In Vitro* 22 (5):1371-6. doi: 10.1016/j.tiv.2008.02.003.

Linkermann, A., J. H. Bräsen, M. Darding, M. K. Jin, A. B. Sanz, J. O. Heller, F. De Zen, R. Weinlich, A. Ortiz, H. Walczak, J. M. Weinberg, D. R. Green, U. Kunzendorf, and S. Krautwald. 2013. "Two independent pathways of regulated necrosis mediate ischemia-reperfusion injury." *Proc Natl Acad Sci U S A* 110 (29):12024-9. doi: 10.1073/pnas.1305538110.

Linkermann, A., and D. R. Green. 2014. "Necroptosis." *N Engl J Med* 370 (5):455-65. doi: 10.1056/NEJMra1310050.

Linkermann, A., R. Skouta, N. Himmerkus, S. R. Mulay, C. Dewitz, F. De Zen, A. Prokai, G. Zuchtriegel, F. Krombach, P. S. Welz, R. Weinlich, T. Vanden Berghe, P. Vandenabeele, M. Pasparakis, M. Bleich, J. M. Weinberg, C. A. Reichel, J. H. Bräsen, U. Kunzendorf, H. J. Anders, B. R. Stockwell, D. R. Green, and S. Krautwald. 2014. "Synchronized renal tubular cell death involves ferroptosis." *Proc Natl Acad Sci U S A* 111 (47):16836-41. doi: 10.1073/pnas.1415518111.

Linz, B. 2013. "Sensitivität gegenüber t-BOOH und DNA-Reparatur in proliferierenden und konfluenten NIH3T3 und FH109-Kulturen [MD thesis].", University Medical Center of the Johannes Gutenberg-University Mainz.

Liu, J., G. Jiang, P. Mao, J. Zhang, L. Zhang, L. Liu, J. Wang, L. Owusu, B. Ren, Y. Tang, and W. Li. 2018. "Down-regulation of GADD45A enhances chemosensitivity in melanoma." *Sci Rep* 8 (1):4111. doi: 10.1038/s41598-018-22484-6.

Liu, Y., and W. F. Bodmer. 2006. "Analysis of P53 mutations and their expression in 56 colorectal cancer cell lines." *Proc Natl Acad Sci U S A* 103 (4):976-81. doi: 10.1073/pnas.0510146103.

Liu, Y., B. Clem, E. K. Zuba-Surma, S. El-Naggar, S. Telang, A. B. Jenson, Y. Wang, H. Shao, M. Z. Ratajczak, J. Chesney, and D. C. Dean. 2009. "Mouse fibroblasts lacking RB1 function form spheres and undergo reprogramming to

a cancer stem cell phenotype." *Cell Stem Cell* 4 (4):336-47. doi: 10.1016/j.stem.2009.02.015.

Lloyd, R. V., L. A. Erickson, L. Jin, E. Kulig, X. Qian, J. C. Cheville, and B. W. Scheithauer. 1999. "p27kip1: a multifunctional cyclin-dependent kinase inhibitor with prognostic significance in human cancers." *Am J Pathol* 154 (2):313-23. doi: 10.1016/S0002-9440(10)65277-7.

Lombardi, G., F. Varsaldi, G. Miglio, M. G. Papini, A. Battaglia, and P. L. Canonico. 2002. "Cabergoline prevents necrotic neuronal death in an in vitro model of oxidative stress." *Eur J Pharmacol* 457 (2-3):95-8.

Long, J., C. J. Zhang, N. Zhu, K. Du, Y. F. Yin, X. Tan, D. F. Liao, and L. Qin. 2018. "Lipid metabolism and carcinogenesis, cancer development." *Am J Cancer Res* 8 (5):778-791.

Lou, W., C. A. Reynolds, Y. Li, J. Liu, M. Hüttemann, M. Schlame, D. Stevenson, D. Strathdee, and M. L. Greenberg. 2018. "Loss of tafazzin results in decreased myoblast differentiation in C2C12 cells: A myoblast model of Barth syndrome and cardiolipin deficiency." *Biochim Biophys Acta Mol Cell Biol Lipids* 1863 (8):857-865. doi: 10.1016/j.bbalip.2018.04.015.

Lu, B., X. B. Chen, M. D. Ying, Q. J. He, J. Cao, and B. Yang. 2017. "The Role of Ferroptosis in Cancer Development and Treatment Response." *Front Pharmacol* 8:992. doi: 10.3389/fphar.2017.00992.

Lötscher, H. R., K. H. Winterhalter, E. Carafoli, and C. Richter. 1979. "Hydroperoxides can modulate the redox state of pyridine nucleotides and the calcium balance in rat liver mitochondria." *Proc Natl Acad Sci U S A* 76 (9):4340-4. doi: 10.1073/pnas.76.9.4340.

Lü, L., X. Liu, C. Wang, F. Hu, J. Wang, and H. Huang. 2015. "Dissociation of E-cadherin/β-catenin complex by MG132 and bortezomib enhances CDDP induced cell death in oral cancer SCC-25 cells." *Toxicol In Vitro* 29 (8):1965-76. doi: 10.1016/j.tiv.2015.07.008.

Lőrincz, T., K. Jemnitz, T. Kardon, J. Mandl, and A. Szarka. 2015. "Ferroptosis is Involved in Acetaminophen Induced Cell Death." *Pathol Oncol Res* 21 (4):1115-21. doi: 10.1007/s12253-015-9946-3.

Maan, M., J. M. Peters, M. Dutta, and A. D. Patterson. 2018. "Lipid metabolism and lipophagy in cancer." *Biochem Biophys Res Commun* 504 (3):582-589. doi: 10.1016/j.bbrc.2018.02.097.

Maeda, T., A. N. Hanna, A. B. Sim, P. P. Chua, M. T. Chong, and V. A. Tron. 2002. "GADD45 regulates G2/M arrest, DNA repair, and cell death in keratinocytes following ultraviolet exposure." *J Invest Dermatol* 119 (1):22-6. doi: 10.1046/j.1523-1747.2002.01781.x.

Maiorino, M., M. Conrad, and F. Ursini. 2018. "GPx4, Lipid Peroxidation, and Cell Death: Discoveries, Rediscoveries, and Open Issues." *Antioxid Redox Signal* 29 (1):61-74. doi: 10.1089/ars.2017.7115.

Mandal, P., S. B. Berger, S. Pillay, K. Moriwaki, C. Huang, H. Guo, J. D. Lich, J. Finger, V. Kasparcova, B. Votta, M. Ouellette, B. W. King, D. Wisnoski, A. S. Lakdawala, M. P. DeMartino, L. N. Casillas, P. A. Haile, C. A. Sehon, R. W. Marquis, J. Upton, L. P. Daley-Bauer, L. Roback, N. Ramia, C. M. Dovey, J. E.

Carette, F. K. Chan, J. Bertin, P. J. Gough, E. S. Mocarski, and W. J. Kaiser. 2014. "RIP3 induces apoptosis independent of pronecrotic kinase activity." *Mol Cell* 56 (4):481-95. doi: 10.1016/j.molcel.2014.10.021.

Masaki, N., M. E. Kyle, and J. L. Farber. 1989. "tert-butyl hydroperoxide kills cultured hepatocytes by peroxidizing membrane lipids." *Arch Biochem Biophys* 269 (2):390-9.

Mateos, R., L. Goya, and L. Bravo. 2004. "Determination of malondialdehyde by liquid chromatography as the 2,4-dinitrophenylhydrazone derivative: a marker for oxidative stress in cell cultures of human hepatoma HepG2." *J Chromatogr B Analyt Technol Biomed Life Sci* 805 (1):33-9. doi: 10.1016/j.jchromb.2004.02.004.

Matsuoka, S., G. Rotman, A. Ogawa, Y. Shiloh, K. Tamai, and S. J. Elledge. 2000. "Ataxia telangiectasia-mutated phosphorylates Chk2 in vivo and in vitro." *Proc Natl Acad Sci U S A* 97 (19):10389-94. doi: 10.1073/pnas.190030497.

McClatchey, A. I., and A. S. Yap. 2012. "Contact inhibition (of proliferation) redux." *Curr Opin Cell Biol* 24 (5):685-94. doi: 10.1016/j.ceb.2012.06.009.

Meister, A., and S. S. Tate. 1976. "Glutathione and related gamma-glutamyl compounds: biosynthesis and utilization." *Annu Rev Biochem* 45:559-604. doi: 10.1146/annurev.bi.45.070176.003015.

Miller, D. M., G. R. Buettner, and S. D. Aust. 1990. "Transition metals as catalysts of "autoxidation" reactions." *Free Radic Biol Med* 8 (1):95-108.

Mimmler, M., S. Peter, A. Kraus, S. Stroh, T. Nikolova, N. Seiwert, S. Hasselwander, C. Neitzel, J. Haub, B. H. Monien, P. Nicken, P. Steinberg, J. W. Shay, B. Kaina, and J. Fahrer. 2016. "DNA damage response curtails detrimental replication stress and chromosomal instability induced by the dietary carcinogen PhIP." *Nucleic Acids Res* 44 (21):10259-10276. doi: 10.1093/nar/gkw791.

Mo, J. S., J. H. Yoon, E. J. Ann, J. S. Ahn, H. J. Baek, H. J. Lee, S. H. Kim, Y. D. Kim, M. Y. Kim, and H. S. Park. 2013. "Notch1 modulates oxidative stress induced cell death through suppression of apoptosis signal-regulating kinase 1." *Proc Natl Acad Sci U S A* 110 (17):6865-70. doi: 10.1073/pnas.1209078110.

Moh, M. C., and S. Shen. 2009. "The roles of cell adhesion molecules in tumor suppression and cell migration: a new paradox." *Cell Adh Migr* 3 (4):334-6. doi: 10.4161/cam.3.4.9246.

Mohammad, R. M., I. Muqbil, L. Lowe, C. Yedjou, H. Y. Hsu, L. T. Lin, M. D. Siegelin, C. Fimognari, N. B. Kumar, Q. P. Dou, H. Yang, A. K. Samadi, G. L. Russo, C. Spagnuolo, S. K. Ray, M. Chakrabarti, J. D. Morre, H. M. Coley, K. Honoki, H. Fujii, A. G. Georgakilas, A. Amedei, E. Niccolai, A. Amin, S. S. Ashraf, W. G. Helferich, X. Yang, C. S. Boosani, G. Guha, D. Bhakta, M. R. Ciriolo, K. Aquilano, S. Chen, S. I. Mohammed, W. N. Keith, A. Bilsland, D. Halicka, S. Nowsheen, and A. S. Azmi. 2015. "Broad targeting of resistance to apoptosis in cancer." *Semin Cancer Biol* 35 Suppl:S78-S103. doi: 10.1016/j.semcancer.2015.03.001.

Monteiro-Cardoso, V. F., A. M. Silva, M. M. Oliveira, F. Peixoto, and R. A. Videira. 2014. "Membrane lipid profile alterations are associated with the metabolic adaptation of the Caco-2 cells to aglycemic nutritional condition." *J Bioenerg Biomembr* 46 (1):45-57. doi: 10.1007/s10863-013-9531-y.

Monteith, G. R., F. M. Davis, and S. J. Roberts-Thomson. 2012. "Calcium channels and pumps in cancer: changes and consequences." *J Biol Chem* 287 (38):31666-73. doi: 10.1074/jbc.R112.343061.

Monteith, G. R., N. Prevarskaya, and S. J. Roberts-Thomson. 2017. "The calcium-cancer signalling nexus." *Nat Rev Cancer* 17 (6):367-380. doi: 10.1038/nrc.2017.18.

Montero, J., C. Dutta, D. van Bodegom, D. Weinstock, and A. Letai. 2013. "p53 regulates a non-apoptotic death induced by ROS." *Cell Death Differ* 20 (11):1465-74. doi: 10.1038/cdd.2013.52.

Morano, A., T. Angrisano, G. Russo, R. Landi, A. Pezone, S. Bartollino, C. Zuchegna, F. Babbio, I. M. Bonapace, B. Allen, M. T. Muller, L. Chiariotti, M. E. Gottesman, A. Porcellini, and E. V. Avvedimento. 2014. "Targeted DNA methylation by homology-directed repair in mammalian cells. Transcription reshapes methylation on the repaired gene." *Nucleic Acids Res* 42 (2):804-21. doi: 10.1093/nar/gkt920.

Morciano, G., A. C. Sarti, S. Marchi, S. Missiroli, S. Falzoni, L. Raffaghello, V. Pistoia, C. Giorgi, F. Di Virgilio, and P. Pinton. 2017. "Use of luciferase probes to measure ATP in living cells and animals." *Nat Protoc* 12 (8):1542-1562. doi: 10.1038/nprot.2017.052.

Morgan, M. J., and Z. G. Liu. 2011. "Crosstalk of reactive oxygen species and NF-κB signaling." *Cell Res* 21 (1):103-15. doi: 10.1038/cr.2010.178.

Morry, J., W. Ngamcherdtrakul, and W. Yantasee. 2017. "Oxidative stress in cancer and fibrosis: Opportunity for therapeutic intervention with antioxidant compounds, enzymes, and nanoparticles." *Redox Biol* 11:240-253. doi: 10.1016/j.redox.2016.12.011.

Müller, E. J., R. Caldelari, C. Kolly, L. Williamson, D. Baumann, G. Richard, P. Jensen, P. Girling, F. Delprincipe, M. Wyder, V. Balmer, and M. M. Suter. 2006. "Consequences of depleted SERCA2-gated calcium stores in the skin." *J Invest Dermatol* 126 (4):721-31. doi: 10.1038/sj.jid.5700091.

Müller, T., C. Dewitz, J. Schmitz, A. S. Schröder, J. H. Bräsen, B. R. Stockwell, J. M. Murphy, U. Kunzendorf, and S. Krautwald. 2017. "Necroptosis and ferroptosis are alternative cell death pathways that operate in acute kidney failure." *Cell Mol Life Sci* 74 (19):3631-3645. doi: 10.1007/s00018-017-2547-4.

Naderi, J., M. Hung, and S. Pandey. 2003. "Oxidative stress-induced apoptosis in dividing fibroblasts involves activation of p38 MAP kinase and over-expression of Bax: resistance of quiescent cells to oxidative stress." *Apoptosis* 8 (1):91-100.

Nagar, B., M. Overduin, M. Ikura, and J. M. Rini. 1996. "Structural basis of calcium-induced E-cadherin rigidification and dimerization." *Nature* 380 (6572):360-4. doi: 10.1038/380360a0.

Nakagawa, Takashi, Shigeomi Shimizu, Tetsuya Watanabe, Osamu Yamaguchi, Kinya Otsu, Hirotaka Yamagata, Hidenori Inohara, Takeshi Kubo, and Yoshihide Tsujimoto. 2005. "Cyclophilin D-dependent mitochondrial permeability transition regulates some necrotic but not apoptotic cell death." 434 (7033):652-658.

Narciso, L., P. Fortini, D. Pajalunga, A. Franchitto, P. Liu, P. Degan, M. Frechet, B. Demple, M. Crescenzi, and E. Dogliotti. 2007. "Terminally differentiated muscle cells are defective in base excision DNA repair and hypersensitive to oxygen injury." *Proc Natl Acad Sci U S A* 104 (43):17010-5. doi: 10.1073/pnas.0701743104.

Narendhirakannan, R. T., and M. A. Hannah. 2013. "Oxidative stress and skin cancer: an overview." *Indian J Clin Biochem* 28 (2):110-5. doi: 10.1007/s12291-012-0278-8.

Neher, E. 1995. "The use of fura-2 for estimating Ca buffers and Ca fluxes." *Neuropharmacology* 34 (11):1423-42.

Neilsen, P. M., J. E. Noll, R. J. Suetani, R. B. Schulz, F. Al-Ejeh, A. Evdokiou, D. P. Lane, and D. F. Callen. 2011. "Mutant p53 uses p63 as a molecular chaperone to alter gene expression and induce a pro-invasive secretome." *Oncotarget* 2 (12):1203-17. doi: 10.18632/oncotarget.382.

Nelson, P. J., and T. O. Daniel. 2002. "Emerging targets: molecular mechanisms of cell contact-mediated growth control." *Kidney Int* 61 (1 Suppl):S99-105. doi: 10.1046/j.1523-1755.2002.0610s1099.x.

Neustadt, J., and S. R. Pieczenik. 2008. "Medication-induced mitochondrial damage and disease." *Mol Nutr Food Res* 52 (7):780-8. doi: 10.1002/mnfr.200700075.

Nguyen, T. T., M. V. Stevens, M. Kohr, C. Steenbergen, M. N. Sack, and E. Murphy. 2011. "Cysteine 203 of cyclophilin D is critical for cyclophilin D activation of the mitochondrial permeability transition pore." *J Biol Chem* 286 (46):40184-92. doi: 10.1074/jbc.M111.243469.

Nicotera, P., G. Bellomo, and S. Orrenius. 1992. "Calcium-mediated mechanisms in chemically induced cell death." *Annu Rev Pharmacol Toxicol* 32:449-70. doi: 10.1146/annurev.pa.32.040192.002313.

Nicotera, P., and G. Melino. 2004. "Regulation of the apoptosis-necrosis switch." *Oncogene* 23 (16):2757-65. doi: 10.1038/sj.onc.1207559.

Nieminen, A. L., A. M. Byrne, B. Herman, and J. J. Lemasters. 1997. "Mitochondrial permeability transition in hepatocytes induced by t-BuOOH: NAD(P)H and reactive oxygen species." *Am J Physiol* 272 (4 Pt 1):C1286-94. doi: 10.1152/ajpcell.1997.272.4.C1286.

Nieminen, A. L., A. K. Saylor, S. A. Tesfai, B. Herman, and J. J. Lemasters. 1995. "Contribution of the mitochondrial permeability transition to lethal injury after exposure of hepatocytes to t-butylhydroperoxide." *Biochem J* 307 (Pt 1):99-106. doi: 10.1042/bj3070099.

Nkabyo, Y. S., T. R. Ziegler, L. H. Gu, W. H. Watson, and D. P. Jones. 2002. "Glutathione and thioredoxin redox during differentiation in human colon epithelial (Caco-2) cells." *Am J Physiol Gastrointest Liver Physiol* 283 (6):G1352-9. doi: 10.1152/ajpgi.00183.2002.

Noda, T., R. Iwakiri, K. Fujimoto, and T. Y. Aw. 2001. "Induction of mild intracellular redox imbalance inhibits proliferation of CaCo-2 cells." *FASEB J* 15 (12):2131-9. doi: 10.1096/fj.01-0131com.

Nussinov, R., C. J. Tsai, and H. Jang. 2017a. "A New View of Pathway-Driven Drug Resistance in Tumor Proliferation." *Trends Pharmacol Sci* 38 (5):427-437. doi: 10.1016/j.tips.2017.02.001.

Nussinov, R., C. J. Tsai, and H. Jang. 2017b. "A New View of Pathway-Driven Drug Resistance in Tumor Proliferation." *Trends Pharmacol Sci* 38 (5):427-437. doi: 10.1016/j.tips.2017.02.001.

Oberley, T. D., J. L. Schultz, N. Li, and L. W. Oberley. 1995. "Antioxidant enzyme levels as a function of growth state in cell culture." *Free Radic Biol Med* 19 (1):53-65.

Ochi, T., and P. A. Cerutti. 1989. "Differential effects of glutathione depletion and metallothionein induction on the induction of DNA single-strand breaks and cytotoxicity by tert-butyl hydroperoxide in cultured mammalian cells." *Chem Biol Interact* 72 (3):335-45.

Ormerod, M. G. 1998. "The study of apoptotic cells by flow cytometry." *Leukemia* 12 (7):1013-25.

Palozza, P., E. Piccioni, L. Avanzi, S. Vertuani, G. Calviello, and S. Manfredini. 2002. "Design, synthesis, and antioxidant activity of FeAOX-6, a novel agent deriving from a molecular combination of the chromanyl and polyisoprenyl moieties." *Free Radic Biol Med* 33 (12):1724-35.

Pan, D. 2010. "The hippo signaling pathway in development and cancer." *Dev Cell* 19 (4):491-505. doi: 10.1016/j.devcel.2010.09.011.

Pan, J. S., M. Z. Hong, and J. L. Ren. 2009. "Reactive oxygen species: a double-edged sword in oncogenesis." *World J Gastroenterol* 15 (14):1702-7. doi: 10.3748/wjg.15.1702.

Pani, G., R. Colavitti, B. Bedogni, R. Anzevino, S. Borrello, and T. Galeotti. 2000. "A redox signaling mechanism for density-dependent inhibition of cell growth." *J Biol Chem* 275 (49):38891-9. doi: 10.1074/jbc.M007319200.

Panieri, E., V. Gogvadze, E. Norberg, R. Venkatesh, S. Orrenius, and B. Zhivotovsky. 2013. "Reactive oxygen species generated in different compartments induce cell death, survival, or senescence." *Free Radic Biol Med* 57:176-87. doi: 10.1016/j.freeradbiomed.2012.12.024.

Paradies, G., V. Paradies, V. De Benedictis, F. M. Ruggiero, and G. Petrosillo. 2014a. "Functional role of cardiolipin in mitochondrial bioenergetics." *Biochim Biophys Acta* 1837 (4):408-17. doi: 10.1016/j.bbabio.2013.10.006.

Paradies, G., V. Paradies, F. M. Ruggiero, and G. Petrosillo. 2014b. "Oxidative stress, cardiolipin and mitochondrial dysfunction in nonalcoholic fatty liver disease." *World J Gastroenterol* 20 (39):14205-18. doi: 10.3748/wjg.v20.i39.14205.

Paradies, G., G. Petrosillo, V. Paradies, and F. M. Ruggiero. 2009. "Role of cardiolipin peroxidation and Ca2+ in mitochondrial dysfunction and disease." *Cell Calcium* 45 (6):643-50. doi: 10.1016/j.ceca.2009.03.012.

Paredes, R. M., J. C. Etzler, L. T. Watts, W. Zheng, and J. D. Lechleiter. 2008. "Chemical calcium indicators." *Methods* 46 (3):143-51. doi: 10.1016/j.ymeth.2008.09.025.

Park, J. E., J. H. Yang, S. J. Yoon, J. H. Lee, E. S. Yang, and J. W. Park. 2002. "Lipid peroxidation-mediated cytotoxicity and DNA damage in U937 cells." *Biochimie* 84 (12):1199-205.

Park, J. H., J. E. Shin, and H. W. Park. 2018. "The Role of Hippo Pathway in Cancer Stem Cell Biology." *Mol Cells* 41 (2):83-92. doi: 10.14348/molcells.2018.2242.

Pastor, N., H. Weinstein, E. Jamison, and M. Brenowitz. 2000. "A detailed interpretation of OH radical footprints in a TBP-DNA complex reveals the role of dynamics in the mechanism of sequence-specific binding." *J Mol Biol* 304 (1):55-68. doi: 10.1006/jmbi.2000.4173.

Pastorino, J. G., S. T. Chen, M. Tafani, J. W. Snyder, and J. L. Farber. 1998. "The overexpression of Bax produces cell death upon induction of the mitochondrial permeability transition." *J Biol Chem* 273 (13):7770-5. doi: 10.1074/jbc.273.13.7770.

Peignon, G., S. Thenet, C. Schreider, S. Fouquet, A. Ribeiro, E. Dussaulx, J. Chambaz, P. Cardot, M. Pinçon-Raymond, and J. Le Beyec. 2006. "E-cadherin-dependent transcriptional control of apolipoprotein A-IV gene expression in intestinal epithelial cells: a role for the hepatic nuclear factor 4." *J Biol Chem* 281 (6):3560-8. doi: 10.1074/jbc.M506360200.

Peluso, J. J., A. Pappalardo, and G. Fernandez. 2001. "E-cadherin-mediated cell contact prevents apoptosis of spontaneously immortalized granulosa cells by regulating Akt kinase activity." *Biol Reprod* 64 (4):1183-90. doi: 10.1095/biolreprod64.4.1183.

Peluso, J. J., A. Pappalardo, and M. P. Trolice. 1996. "N-cadherin-mediated cell contact inhibits granulosa cell apoptosis in a progesterone-independent manner." *Endocrinology* 137 (4):1196-203. doi: 10.1210/endo.137.4.8625889.

Peng, T. I., and M. J. Jou. 2010. "Oxidative stress caused by mitochondrial calcium overload." *Ann N Y Acad Sci* 1201:183-8. doi: 10.1111/j.1749-6632.2010.05634.x.

Pereira, L., A. Igea, B. Canovas, I. Dolado, and A. R. Nebreda. 2013. "Inhibition of p38 MAPK sensitizes tumour cells to cisplatin-induced apoptosis mediated by reactive oxygen species and JNK." *EMBO Mol Med* 5 (11):1759-74. doi: 10.1002/emmm.201302732.

Persinger, R. L., W. M. Blay, N. H. Heintz, D. R. Hemenway, and Y. M. Janssen-Heininger. 2001. "Nitrogen dioxide induces death in lung epithelial cells in a density-dependent manner." *Am J Respir Cell Mol Biol* 24 (5):583-90. doi: 10.1165/ajrcmb.24.5.4340.

Pestana, C. R., C. H. Silva, G. L. Pardo-Andreu, F. P. Rodrigues, A. C. Santos, S. A. Uyemura, and C. Curti. 2009. "Ca(2+) binding to c-state of adenine nucleotide translocase (ANT)-surrounding cardiolipins enhances (ANT)-Cys(56) relative mobility: a computational-based mitochondrial permeability transition study." *Biochim Biophys Acta* 1787 (3):176-82. doi: 10.1016/j.bbabio.2008.12.013.

Petrosillo, G., G. Casanova, M. Matera, F. M. Ruggiero, and G. Paradies. 2006b. "Interaction of peroxidized cardiolipin with rat-heart mitochondrial membranes: induction of permeability transition and cytochrome c release." *FEBS Lett* 580 (27):6311-6. doi: 10.1016/j.febslet.2006.10.036.

Petrosillo, G., G. Colantuono, N. Moro, F. M. Ruggiero, E. Tiravanti, N. Di Venosa, T. Fiore, and G. Paradies. 2009. "Melatonin protects against heart ischemia-reperfusion injury by inhibiting mitochondrial permeability transition pore opening." *Am J Physiol Heart Circ Physiol* 297 (4):H1487-93. doi: 10.1152/ajpheart.00163.2009.

Petrosillo, G., N. Di Venosa, M. Pistolese, G. Casanova, E. Tiravanti, G. Colantuono, A. Federici, G. Paradies, and F. M. Ruggiero. 2006a. "Protective effect of melatonin against mitochondrial dysfunction associated with cardiac ischemia-reperfusion: role of cardiolipin." *FASEB J* 20 (2):269-76. doi: 10.1096/fj.05-4692com.

Picco, V., and G. Pagès. 2013. "Linking JNK Activity to the DNA Damage Response." *Genes Cancer* 4 (9-10):360-8. doi: 10.1177/1947601913486347.

Pichorner, H., G. Jessner, and R. Ebermann. 1993. "tBOOH acts as a suicide substrate for catalase." *Arch Biochem Biophys* 300 (1):258-64. doi: 10.1006/abbi.1993.1036.

Pisoschi, A. M., and A. Pop. 2015. "The role of antioxidants in the chemistry of oxidative stress: A review." *Eur J Med Chem* 97:55-74. doi: 10.1016/j.ejmech.2015.04.040.

Pitot, H. C. 1993. "The molecular biology of carcinogenesis." *Cancer* 72 (3 Suppl):962-70.

Pizzimenti, S., G. Barrera, E. Calzavara, L. Mirandola, C. Toaldo, M. U. Dianzani, P. Comi, and R. Chiaramonte. 2008. "Down-regulation of Notch1 expression is involved in HL-60 cell growth inhibition induced by 4-hydroxynonenal, a product of lipid peroxidation." *Med Chem* 4 (6):551-7.

Plouffe, S. W., A. W. Hong, and K. L. Guan. 2015. "Disease implications of the Hippo/YAP pathway." *Trends Mol Med* 21 (4):212-22. doi: 10.1016/j.molmed.2015.01.003.

Plouffe, S. W., Z. Meng, K. C. Lin, B. Lin, A. W. Hong, J. V. Chun, and K. L. Guan. 2016. "Characterization of Hippo Pathway Components by Gene Inactivation." *Mol Cell* 64 (5):993-1008. doi: 10.1016/j.molcel.2016.10.034.

Polyak, K., J. Y. Kato, M. J. Solomon, C. J. Sherr, J. Massague, J. M. Roberts, and A. Koff. 1994. "p27Kip1, a cyclin-Cdk inhibitor, links transforming growth factor-beta and contact inhibition to cell cycle arrest." *Genes Dev* 8 (1):9-22. doi: 10.1101/gad.8.1.9.

Poot, M., Y. Z. Zhang, J. A. Krämer, K. S. Wells, L. J. Jones, D. K. Hanzel, A. G. Lugade, V. L. Singer, and R. P. Haugland. 1996. "Analysis of mitochondrial morphology and function with novel fixable fluorescent stains." *J Histochem Cytochem* 44 (12):1363-72.

Postula, M., P. K. Janicki, M. Rosiak, C. Eyileten, M. Zaremba, A. Kaplon-Cieslicka, S. Sugino, D. A. Kosior, G. Opolski, K. J. Filipiak, and D. Mirowska-Guzel.

2016. "Targeted deep resequencing of." *Exp Ther Med* 12 (1):415-421. doi: 10.3892/etm.2016.3334.

Prevarskaya, N., H. Ouadid-Ahidouch, R. Skryma, and Y. Shuba. 2014. "Remodelling of Ca2+ transport in cancer: how it contributes to cancer hallmarks?" *Philos Trans R Soc Lond B Biol Sci* 369 (1638):20130097. doi: 10.1098/rstb.2013.0097.

Ralec, C., E. Henry, M. Lemor, T. Killelea, and G. Henneke. 2017. "Calcium-driven DNA synthesis by a high-fidelity DNA polymerase." *Nucleic Acids Res* 45 (21):12425-12440. doi: 10.1093/nar/gkx927.

Ramirez, Frances M, Serrine S Lau, and Terrence J Monks. 2013. "Perturbations in Intracellular Ca2+ Concentrations and DNA Damage are Coupled to the Activation of PARP-1 During ROS-induced Necrotic Cell Death." *The FASEB Journal* 27 (1_supplement):890.5-890.5. doi: 10.1096/fasebj.27.1_supplement.890.5.

Rancourt, R. C., D. D. Hayes, P. R. Chess, P. C. Keng, and M. A. O'Reilly. 2002. "Growth arrest in G1 protects against oxygen-induced DNA damage and cell death." *J Cell Physiol* 193 (1):26-36. doi: 10.1002/jcp.10146.

Renart, J., J. Reiser, and G. R. Stark. 1979. "Transfer of proteins from gels to diazobenzyloxymethyl-paper and detection with antisera: a method for studying antibody specificity and antigen structure." *Proc Natl Acad Sci U S A* 76 (7):3116-20. doi: 10.1073/pnas.76.7.3116.

Rennefahrt, U. E., B. Illert, E. Kerkhoff, J. Troppmair, and U. R. Rapp. 2002. "Constitutive JNK activation in NIH 3T3 fibroblasts induces a partially transformed phenotype." *J Biol Chem* 277 (33):29510-8. doi: 10.1074/jbc.M203010200.

Ricken, S., J. Leipziger, R. Greger, and R. Nitschke. 1998. "Simultaneous measurements of cytosolic and mitochondrial Ca2+ transients in HT29 cells." *J Biol Chem* 273 (52):34961-9. doi: 10.1074/jbc.273.52.34961.

Riddles, P. W., R. L. Blakeley, and B. Zerner. 1979. "Ellman's reagent: 5,5'-dithiobis(2-nitrobenzoic acid)--a reexamination." *Anal Biochem* 94 (1):75-81.

Rimessi, A., C. Giorgi, P. Pinton, and R. Rizzuto. 2008. "The versatility of mitochondrial calcium signals: from stimulation of cell metabolism to induction of cell death." *Biochim Biophys Acta* 1777 (7-8):808-16. doi: 10.1016/j.bbabio.2008.05.449.

Riss, T.L., R.A. Moravec, A.L. Niles, and et al. 2013; updated: 2016. Cell Viability Assays [Internet]. In *Assay Guidance Manual*: Eli Lilly & Company and the National Center for Advancing Translational Sciences.

Ritz, E., C. C. Heuck, and R. Boland. 1980. "Phosphate, calcium and lipid metabolism." *Adv Exp Med Biol* 128:197-208.

Rocha, S., M. D. Garrett, K. J. Campbell, K. Schumm, and N. D. Perkins. 2005. "Regulation of NF-kappaB and p53 through activation of ATR and Chk1 by the ARF tumour suppressor." *EMBO J* 24 (6):1157-69. doi: 10.1038/sj.emboj.7600608.

Rodriguez, F. J., L. J. Lewis-Tuffin, and P. Z. Anastasiadis. 2012. "E-cadherin's dark side: possible role in tumor progression." *Biochim Biophys Acta* 1826 (1):23-31. doi: 10.1016/j.bbcan.2012.03.002.

Roos, W. P., and B. Kaina. 2006. "DNA damage-induced cell death by apoptosis." *Trends Mol Med* 12 (9):440-50. doi: 10.1016/j.molmed.2006.07.007.

Roos, W. P., and B. Kaina. 2013. "DNA damage-induced cell death: from specific DNA lesions to the DNA damage response and apoptosis." *Cancer Lett* 332 (2):237-48. doi: 10.1016/j.canlet.2012.01.007.

Rothen-Rutishauser, B., S. D. Krämer, A. Braun, M. Günthert, and H. Wunderli-Allenspach. 1998. "MDCK cell cultures as an epithelial in vitro model: cytoskeleton and tight junctions as indicators for the definition of age-related stages by confocal microscopy." *Pharm Res* 15 (7):964-71.

Rottenberg, H., and S. Wu. 1998. "Quantitative assay by flow cytometry of the mitochondrial membrane potential in intact cells." *Biochim Biophys Acta* 1404 (3):393-404.

Rouleau, M., A. Patel, M. J. Hendzel, S. H. Kaufmann, and G. G. Poirier. 2010. "PARP inhibition: PARP1 and beyond." *Nat Rev Cancer* 10 (4):293-301. doi: 10.1038/nrc2812.

Roveri, A., M. Coassin, M. Maiorino, A. Zamburlini, F. T. van Amsterdam, E. Ratti, and F. Ursini. 1992. "Effect of hydrogen peroxide on calcium homeostasis in smooth muscle cells." *Arch Biochem Biophys* 297 (2):265-70.

Russo, T., N. Zambrano, F. Esposito, R. Ammendola, F. Cimino, M. Fiscella, J. Jackman, P. M. O'Connor, C. W. Anderson, and E. Appella. 1995. "A p53-independent pathway for activation of WAF1/CIP1 expression following oxidative stress." *J Biol Chem* 270 (49):29386-91. doi: 10.1074/jbc.270.49.29386.

Sabapathy, K., W. Jochum, K. Hochedlinger, L. Chang, M. Karin, and E. F. Wagner. 1999. "Defective neural tube morphogenesis and altered apoptosis in the absence of both JNK1 and JNK2." *Mech Dev* 89 (1-2):115-24.

Saito, M., D. K. Tucker, D. Kohlhorst, C. M. Niessen, and A. P. Kowalczyk. 2012. "Classical and desmosomal cadherins at a glance." *J Cell Sci* 125 (Pt 11):2547-52. doi: 10.1242/jcs.066654.

Saito, Y., K. Nishio, Y. Ogawa, J. Kimata, T. Kinumi, Y. Yoshida, N. Noguchi, and E. Niki. 2006. "Turning point in apoptosis/necrosis induced by hydrogen peroxide." *Free Radic Res* 40 (6):619-30. doi: 10.1080/10715760600632552.

Salas, V. M., and G. B. Corcoran. 1997. "Calcium-dependent DNA damage and adenosine 3',5'-cyclic monophosphate-independent glycogen phosphorylase activation in an in vitro model of acetaminophen-induced liver injury." *Hepatology* 25 (6):1432-8. doi: 10.1002/hep.510250621.

Sano, M., M. Sierant, M. Miyagishi, M. Nakanishi, Y. Takagi, and S. Sutou. 2008. "Effect of asymmetric terminal structures of short RNA duplexes on the RNA interference activity and strand selection." *Nucleic Acids Res* 36 (18):5812-21. doi: 10.1093/nar/gkn584.

Schaal, C., J. Padmanabhan, and S. Chellappan. 2015. "The Role of nAChR and Calcium Signaling in Pancreatic Cancer Initiation and Progression." *Cancers (Basel)* 7 (3):1447-71. doi: 10.3390/cancers7030845.

Schwarz, E. C., B. Qu, and M. Hoth. 2013. "Calcium, cancer and killing: the role of calcium in killing cancer cells by cytotoxic T lymphocytes and natural killer cells." *Biochim Biophys Acta* 1833 (7):1603-11. doi: 10.1016/j.bbamcr.2012.11.016.

Sedelnikova, O. A., C. E. Redon, J. S. Dickey, A. J. Nakamura, A. G. Georgakilas, and W. M. Bonner. 2010. "Role of oxidatively induced DNA lesions in human pathogenesis." *Mutat Res* 704 (1-3):152-9. doi: 10.1016/j.mrrev.2009.12.005.

Seluanov, A., C. Hine, J. Azpurua, M. Feigenson, M. Bozzella, Z. Mao, K. C. Catania, and V. Gorbunova. 2009. "Hypersensitivity to contact inhibition provides a clue to cancer resistance of naked mole-rat." *Proc Natl Acad Sci U S A* 106 (46):19352-7. doi: 10.1073/pnas.0905252106.

Selvam, R. 2002. "Calcium oxalate stone disease: role of lipid peroxidation and antioxidants." *Urol Res* 30 (1):35-47.

Sfeir, A., and L. S. Symington. 2015. "Microhomology-Mediated End Joining: A Back-up Survival Mechanism or Dedicated Pathway?" *Trends Biochem Sci* 40 (11):701-714. doi: 10.1016/j.tibs.2015.08.006.

Shan, Z., G. Li, Q. Zhan, and D. Li. 2012. "Gadd45a inhibits cell migration and invasion by altering the global RNA expression." *Cancer Biol Ther* 13 (11):1112-22. doi: 10.4161/cbt.21186.

Shapiro, A. L., E. Viñuela, and J. V. Maizel. 1967. "Molecular weight estimation of polypeptide chains by electrophoresis in SDS-polyacrylamide gels." *Biochem Biophys Res Commun* 28 (5):815-20.

Shen, H. M., Y. Lin, S. Choksi, J. Tran, T. Jin, L. Chang, M. Karin, J. Zhang, and Z. G. Liu. 2004. "Essential roles of receptor-interacting protein and TRAF2 in oxidative stress-induced cell death." *Mol Cell Biol* 24 (13):5914-22. doi: 10.1128/MCB.24.13.5914-5922.2004.

Shi, Y., F. Nikulenkov, J. Zawacka-Pankau, H. Li, R. Gabdoulline, J. Xu, S. Eriksson, E. Hedström, N. Issaeva, A. Kel, E. S. Arnér, and G. Selivanova. 2014. "ROS-dependent activation of JNK converts p53 into an efficient inhibitor of oncogenes leading to robust apoptosis." *Cell Death Differ* 21 (4):612-23. doi: 10.1038/cdd.2013.186.

Shih, W., and S. Yamada. 2012. "N-cadherin-mediated cell-cell adhesion promotes cell migration in a three-dimensional matrix." *J Cell Sci* 125 (Pt 15):3661-70. doi: 10.1242/jcs.103861.

Siems, W. G., T. Grune, and H. Esterbauer. 1995. "4-Hydroxynonenal formation during ischemia and reperfusion of rat small intestine." *Life Sci* 57 (8):785-9.

Sies, H. 2015. "Oxidative stress: a concept in redox biology and medicine." *Redox Biol* 4:180-3. doi: 10.1016/j.redox.2015.01.002.

Sies, H., C. Berndt, and D. P. Jones. 2017. "Oxidative Stress." *Annu Rev Biochem* 86:715-748. doi: 10.1146/annurev-biochem-061516-045037.

Sies, H., and E. Cadenas. 1985. "Oxidative stress: damage to intact cells and organs." *Philos Trans R Soc Lond B Biol Sci* 311 (1152):617-31. doi: 10.1098/rstb.1985.0168.

Sies, H., and K. M. Moss. 1978. "A role of mitochondrial glutathione peroxidase in modulating mitochondrial oxidations in liver." *Eur J Biochem* 84 (2):377-83.

Siomek, A. 2012. "NF-κB signaling pathway and free radical impact." *Acta Biochim Pol* 59 (3):323-31.

Skouta, R., S. J. Dixon, J. Wang, D. E. Dunn, M. Orman, K. Shimada, P. A. Rosenberg, D. C. Lo, J. M. Weinberg, A. Linkermann, and B. R. Stockwell. 2014. "Ferrostatins inhibit oxidative lipid damage and cell death in diverse disease models." *J Am Chem Soc* 136 (12):4551-6. doi: 10.1021/ja411006a.

Slater, T. F., B. Sawyer, and U. Straeuli. 1963. "Studies on succinate-tetrazolium reductase systems. III. Points of coupling of four different tetrazolium salts." *Biochim Biophys Acta* 77:383-93.

Smith, P. K., R. I. Krohn, G. T. Hermanson, A. K. Mallia, F. H. Gartner, M. D. Provenzano, E. K. Fujimoto, N. M. Goeke, B. J. Olson, and D. C. Klenk. 1985. "Measurement of protein using bicinchoninic acid." *Anal Biochem* 150 (1):76-85.

Smithies, O. 1959. "An improved procedure for starch-gel electrophoresis: further variations in the serum proteins of normal individuals." *Biochem J* 71 (3):585-7. doi: 10.1042/bj0710585.

Son, Y., Y. K. Cheong, N. H. Kim, H. T. Chung, D. G. Kang, and H. O. Pae. 2011. "Mitogen-Activated Protein Kinases and Reactive Oxygen Species: How Can ROS Activate MAPK Pathways?" *J Signal Transduct* 2011:792639. doi: 10.1155/2011/792639.

Song, N. J., U. J. Yun, S. Yang, C. Wu, C. R. Seo, A. R. Gwon, S. H. Baik, Y. Choi, B. Y. Choi, G. Bahn, S. Kim, S. M. Kwon, J. S. Park, S. H. Baek, T. J. Park, K. Yoon, B. J. Kim, M. P. Mattson, S. J. Lee, D. G. Jo, and K. W. Park. 2016. "Notch1 deficiency decreases hepatic lipid accumulation by induction of fatty acid oxidation." *Sci Rep* 6:19377. doi: 10.1038/srep19377.

Sosa, V., T. Moliné, R. Somoza, R. Paciucci, H. Kondoh, and M. E. LLeonart. 2013. "Oxidative stress and cancer: an overview." *Ageing Res Rev* 12 (1):376-90. doi: 10.1016/j.arr.2012.10.004.

Sosna, J., S. Voigt, S. Mathieu, A. Lange, L. Thon, P. Davarnia, T. Herdegen, A. Linkermann, A. Rittger, F. K. Chan, D. Kabelitz, S. Schütze, and D. Adam. 2014. "TNF-induced necroptosis and PARP-1-mediated necrosis represent distinct routes to programmed necrotic cell death." *Cell Mol Life Sci* 71 (2):331-48. doi: 10.1007/s00018-013-1381-6.

Sparaneo, A., F. P. Fabrizio, and L. A. Muscarella. 2016. "Nrf2 and Notch Signaling in Lung Cancer: Near the Crossroad." *Oxid Med Cell Longev* 2016:7316492. doi: 10.1155/2016/7316492.

Spät, A., G. Szanda, G. Csordás, and G. Hajnóczky. 2008. "High- and low-calcium-dependent mechanisms of mitochondrial calcium signalling." *Cell Calcium* 44 (1):51-63. doi: 10.1016/j.ceca.2007.11.015.

Steinkamp-Fenske, K., L. Bollinger, H. Xu, Y. Yao, S. Horke, U. Förstermann, and H. Li. 2007. "Reciprocal regulation of endothelial nitric-oxide synthase and NADPH oxidase by betulinic acid in human endothelial cells." *J Pharmacol Exp Ther* 322 (2):836-42. doi: 10.1124/jpet.107.123356.

Stewart, G. S., B. Wang, C. R. Bignell, A. M. Taylor, and S. J. Elledge. 2003. "MDC1 is a mediator of the mammalian DNA damage checkpoint." *Nature* 421 (6926):961-6. doi: 10.1038/nature01446.

Stockwell, B. R., J. P. Friedmann Angeli, H. Bayir, A. I. Bush, M. Conrad, S. J. Dixon, S. Fulda, S. Gascón, S. K. Hatzios, V. E. Kagan, K. Noel, X. Jiang, A. Linkermann, M. E. Murphy, M. Overholtzer, A. Oyagi, G. C. Pagnussat, J. Park, Q. Ran, C. S. Rosenfeld, K. Salnikow, D. Tang, F. M. Torti, S. V. Torti, S. Toyokuni, K. A. Woerpel, and D. D. Zhang. 2017. "Ferroptosis: A Regulated Cell Death Nexus Linking Metabolism, Redox Biology, and Disease." *Cell* 171 (2):273-285. doi: 10.1016/j.cell.2017.09.021.

Strehler, E. E., and D. A. Zacharias. 2001. "Role of alternative splicing in generating isoform diversity among plasma membrane calcium pumps." *Physiol Rev* 81 (1):21-50. doi: 10.1152/physrev.2001.81.1.21.

Suárez Pestana, E., T. Tenev, S. Gross, B. Stoyanov, M. Ogata, and F. D. Böhmer. 1999. "The transmembrane protein tyrosine phosphatase RPTPsigma modulates signaling of the epidermal growth factor receptor in A431 cells." *Oncogene* 18 (28):4069-79. doi: 10.1038/sj.onc.1202794.

Swat, A., I. Dolado, J. M. Rojas, and A. R. Nebreda. 2009. "Cell density-dependent inhibition of epidermal growth factor receptor signaling by p38alpha mitogen-activated protein kinase via Sprouty2 downregulation." *Mol Cell Biol* 29 (12):3332-43. doi: 10.1128/MCB.01955-08.

Swindall, A. F., J. A. Stanley, and E. S. Yang. 2013. "PARP-1: Friend or Foe of DNA Damage and Repair in Tumorigenesis?" *Cancers (Basel)* 5 (3):943-58. doi: 10.3390/cancers5030943.

Tandon, V., B.M. Gupta, and R. Tandon. 2005. "Free Radicals / Reactive Oxygen Species." *JK-Practitioner* 12:143-148.

Telford, B. J., A. Chen, H. Beetham, J. Frick, T. P. Brew, C. M. Gould, A. Single, T. Godwin, K. J. Simpson, and P. Guilford. 2015. "Synthetic Lethal Screens Identify Vulnerabilities in GPCR Signaling and Cytoskeletal Organization in E-Cadherin-Deficient Cells." *Mol Cancer Ther* 14 (5):1213-23. doi: 10.1158/1535-7163.MCT-14-1092.

Telford, W. G., L. E. King, and P. J. Fraker. 1992. "Comparative evaluation of several DNA binding dyes in the detection of apoptosis-associated chromatin degradation by flow cytometry." *Cytometry* 13 (2):137-43. doi: 10.1002/cyto.990130205.

Temkin, V., Q. Huang, H. Liu, H. Osada, and R. M. Pope. 2006. "Inhibition of ADP/ATP exchange in receptor-interacting protein-mediated necrosis." *Mol Cell Biol* 26 (6):2215-25. doi: 10.1128/MCB.26.6.2215-2225.2006.

Tewari, M., L. T. Quan, K. O'Rourke, S. Desnoyers, Z. Zeng, D. R. Beidler, G. G. Poirier, G. S. Salvesen, and V. M. Dixit. 1995. "Yama/CPP32 beta, a

mammalian homolog of CED-3, is a CrmA-inhibitable protease that cleaves the death substrate poly(ADP-ribose) polymerase." *Cell* 81 (5):801-9.

Tice, R. R., E. Agurell, D. Anderson, B. Burlinson, A. Hartmann, H. Kobayashi, Y. Miyamae, E. Rojas, J. C. Ryu, and Y. F. Sasaki. 2000. "Single cell gel/comet assay: guidelines for in vitro and in vivo genetic toxicology testing." *Environ Mol Mutagen* 35 (3):206-21.

Todaro, G. J., and H. Green. 1963. "Quantitative studies of the growth of mouse embryo cells in culture and their development into established lines." *J Cell Biol* 17:299-313. doi: 10.1083/jcb.17.2.299.

Tomita, K., A. van Bokhoven, G. J. van Leenders, E. T. Ruijter, C. F. Jansen, M. J. Bussemakers, and J. A. Schalken. 2000. "Cadherin switching in human prostate cancer progression." *Cancer Res* 60 (13):3650-4.

Tonnus, W., and A. Linkermann. 2017. "The in vivo evidence for regulated necrosis." *Immunol Rev* 277 (1):128-149. doi: 10.1111/imr.12551.

Tormos, C., F. Javier Chaves, M. J. Garcia, F. Garrido, R. Jover, J. E. O'Connor, A. Iradi, A. Oltra, M. R. Oliva, and G. T. Sáez. 2004. "Role of glutathione in the induction of apoptosis and c-fos and c-jun mRNAs by oxidative stress in tumor cells." *Cancer Lett* 208 (1):103-13. doi: 10.1016/j.canlet.2003.11.007.

Towbin, H., T. Staehelin, and J. Gordon. 1979. "Electrophoretic transfer of proteins from polyacrylamide gels to nitrocellulose sheets: procedure and some applications." *Proc Natl Acad Sci U S A* 76 (9):4350-4. doi: 10.1073/pnas.76.9.4350.

Tsoi, J., L. Robert, K. Paraiso, C. Galvan, K. M. Sheu, J. Lay, D. J. L. Wong, M. Atefi, R. Shirazi, X. Wang, D. Braas, C. S. Grasso, N. Palaskas, A. Ribas, and T. G. Graeber. 2018. "Multi-stage Differentiation Defines Melanoma Subtypes with Differential Vulnerability to Drug-Induced Iron-Dependent Oxidative Stress." *Cancer Cell* 33 (5):890-904.e5. doi: 10.1016/j.ccell.2018.03.017.

Upreti, M., N. A. Koonce, L. Hennings, T. C. Chambers, and R. J. Griffin. 2010. "Pegylated IFN-α sensitizes melanoma cells to chemotherapy and causes premature senescence in endothelial cells by IRF-1 mediated signaling." *Cell Death Dis* 1:e67. doi: 10.1038/cddis.2010.43.

Usatyuk, P. V., N. L. Parinandi, and V. Natarajan. 2006. "Redox regulation of 4-hydroxy-2-nonenal-mediated endothelial barrier dysfunction by focal adhesion, adherens, and tight junction proteins." *J Biol Chem* 281 (46):35554-66. doi: 10.1074/jbc.M607305200.

Vairapandi, M., N. Azam, A. G. Balliet, B. Hoffman, and D. A. Liebermann. 2000. "Characterization of MyD118, Gadd45, and proliferating cell nuclear antigen (PCNA) interacting domains. PCNA impedes MyD118 AND Gadd45-mediated negative growth control." *J Biol Chem* 275 (22):16810-9. doi: 10.1074/jbc.275.22.16810.

Vairetti, M., A. Ferrigno, R. Bertone, P. Richelmi, F. Bertè, and I. Freitas. 2005. "Apoptosis vs. necrosis: glutathione-mediated cell death during rewarming of rat hepatocytes." *Biochim Biophys Acta* 1740 (3):367-74. doi: 10.1016/j.bbadis.2004.11.022.

Valko, M., D. Leibfritz, J. Moncol, M. T. Cronin, M. Mazur, and J. Telser. 2007. "Free radicals and antioxidants in normal physiological functions and human disease." *Int J Biochem Cell Biol* 39 (1):44-84. doi: 10.1016/j.biocel.2006.07.001.

Valko, M., C. J. Rhodes, J. Moncol, M. Izakovic, and M. Mazur. 2006. "Free radicals, metals and antioxidants in oxidative stress-induced cancer." *Chem Biol Interact* 160 (1):1-40. doi: 10.1016/j.cbi.2005.12.009.

Valluru, L., S. Dasari, and R. Wudayagiri. 2014. "Role of free radicals and antioxidants in gynecological cancers: current status and future prospects." *Oxid Antioxid Med Sci* 3:15-26. doi: 10.5455/oams.201113.rv.011.

Van Noorden, C. J. 2001. "The history of Z-VAD-FMK, a tool for understanding the significance of caspase inhibition." *Acta Histochem* 103 (3):241-51. doi: 10.1078/0065-1281-00601.

Vanden Berghe, T., A. Linkermann, S. Jouan-Lanhouet, H. Walczak, and P. Vandenabeele. 2014. "Regulated necrosis: the expanding network of non-apoptotic cell death pathways." *Nat Rev Mol Cell Biol* 15 (2):135-47. doi: 10.1038/nrm3737.

Vandenabeele, P., L. Galluzzi, T. Vanden Berghe, and G. Kroemer. 2010. "Molecular mechanisms of necroptosis: an ordered cellular explosion." *Nat Rev Mol Cell Biol* 11 (10):700-14. doi: 10.1038/nrm2970.

Vandenabeele, P., S. Grootjans, N. Callewaert, and N. Takahashi. 2013. "Necrostatin-1 blocks both RIPK1 and IDO: consequences for the study of cell death in experimental disease models." *Cell Death Differ* 20 (2):185-7. doi: 10.1038/cdd.2012.151.

Vanlangenakker, N., T. Vanden Berghe, and P. Vandenabeele. 2012. "Many stimuli pull the necrotic trigger, an overview." *Cell Death Differ* 19 (1):75-86. doi: 10.1038/cdd.2011.164.

Vaseva, A. V., N. D. Marchenko, K. Ji, S. E. Tsirka, S. Holzmann, and U. M. Moll. 2012. "p53 opens the mitochondrial permeability transition pore to trigger necrosis." *Cell* 149 (7):1536-48. doi: 10.1016/j.cell.2012.05.014.

Vergara, D., E. Stanca, F. Guerra, P. Priore, A. Gaballo, J. Franck, P. Simeone, M. Trerotola, S. De Domenico, I. Fournier, C. Bucci, M. Salzet, A. M. Giudetti, and M. Maffia. 2017. "β-Catenin Knockdown Affects Mitochondrial Biogenesis and Lipid Metabolism in Breast Cancer Cells." *Front Physiol* 8:544. doi: 10.3389/fphys.2017.00544.

Vermes, I., C. Haanen, H. Steffens-Nakken, and C. Reutelingsperger. 1995. "A novel assay for apoptosis. Flow cytometric detection of phosphatidylserine expression on early apoptotic cells using fluorescein labelled Annexin V." *J Immunol Methods* 184 (1):39-51.

Victorino, V. J., L. Pizzatti, P. Michelletti, and C. Panis. 2014. "Oxidative stress, redox signaling and cancer chemoresistance: putting together the pieces of the puzzle." *Curr Med Chem* 21 (28):3211-26.

Volwerk, J. J., G. B. Birrell, K. K. Hedberg, and O. H. Griffith. 1992. "A high level of cell surface phosphatidylinositol-specific phospholipase C activity is

characteristic of growth-arrested 3T3 fibroblasts but not of transformed variants." *J Cell Physiol* 151 (3):613-22. doi: 10.1002/jcp.1041510322.

von Schlippe, M., J. F. Marshall, P. Perry, M. Stone, A. J. Zhu, and I. R. Hart. 2000. "Functional interaction between E-cadherin and alphav-containing integrins in carcinoma cells." *J Cell Sci* 113 (Pt 3):425-37.

Vroegop, S. M., D. E. Decker, and S. E. Buxser. 1995. "Localization of damage induced by reactive oxygen species in cultured cells." *Free Radic Biol Med* 18 (2):141-51.

Wang, Y. 2008. "Bulky DNA lesions induced by reactive oxygen species." *Chem Res Toxicol* 21 (2):276-81. doi: 10.1021/tx700411g.

Wang-Heaton, H. 2016. """A novel role of human DNA damage checkpoint protein ATR in suppressing Ca^{2+} overload-induced PARP1-mediated necrosis" [Electronic Dissertation]." In. East Tennessee State University: Student Works at Digital Commons.

Watanabe, T., S. Sekine, I. Naguro, Y. Sekine, and H. Ichijo. 2015. "Apoptosis Signal-regulating Kinase 1 (ASK1)-p38 Pathway-dependent Cytoplasmic Translocation of the Orphan Nuclear Receptor NR4A2 Is Required for Oxidative Stress-induced Necrosis." *J Biol Chem* 290 (17):10791-803. doi: 10.1074/jbc.M114.623280.

Watters, D., P. Kedar, K. Spring, J. Bjorkman, P. Chen, M. Gatei, G. Birrell, B. Garrone, P. Srinivasa, D. I. Crane, and M. F. Lavin. 1999. "Localization of a portion of extranuclear ATM to peroxisomes." *J Biol Chem* 274 (48):34277-82. doi: 10.1074/jbc.274.48.34277.

Weber, A. M., and A. J. Ryan. 2015. "ATM and ATR as therapeutic targets in cancer." *Pharmacol Ther* 149:124-38. doi: 10.1016/j.pharmthera.2014.12.001.

Wei, C. J., R. Francis, X. Xu, and C. W. Lo. 2005. "Connexin43 associated with an N-cadherin-containing multiprotein complex is required for gap junction formation in NIH3T3 cells." *J Biol Chem* 280 (20):19925-36. doi: 10.1074/jbc.M412921200.

Wei, L., and R. T. Dirksen. 2012. "Perspectives on: SGP symposium on mitochondrial physiology and medicine: mitochondrial superoxide flashes: from discovery to new controversies." *J Gen Physiol* 139 (6):425-34. doi: 10.1085/jgp.201210790.

Weiss, C., D. Faust, H. Dürk, S. K. Kolluri, A. Pelzer, S. Schneider, C. Dietrich, F. Oesch, and M. Göttlicher. 2005. "TCDD induces c-jun expression via a novel Ah (dioxin) receptor-mediated p38-MAPK-dependent pathway." *Oncogene* 24 (31):4975-83. doi: 10.1038/sj.onc.1208679.

Weiss, C., D. Faust, I. Schreck, A. Ruff, T. Farwerck, A. Melenberg, S. Schneider, B. Oesch-Bartlomowicz, J. Zatloukalová, J. Vondrácek, F. Oesch, and C. Dietrich. 2008. "TCDD deregulates contact inhibition in rat liver oval cells via Ah receptor, JunD and cyclin A." *Oncogene* 27 (15):2198-207. doi: 10.1038/sj.onc.1210859.

Wenz, C., D. Faust, B. Linz, C. Turmann, T. Nikolova, J. Bertin, P. Gough, P. Wipf, A. S. Schröder, S. Krautwald, and C. Dietrich. 2018. "t-BuOOH induces

ferroptosis in human and murine cell lines." *Arch Toxicol* 92 (2):759-775. doi: 10.1007/s00204-017-2066-y.

Wenz, C., D. Faust, B. Linz, C. Turmann, T. Nikolova, and C. Dietrich. 2019. "Cell-cell contacts protect against t-BuOOH-induced cellular damage and ferroptosis in vitro." *Arch Toxicol.* doi: 10.1007/s00204-019-02413-w.

Wessel, D., and U. I. Flügge. 1984. "A method for the quantitative recovery of protein in dilute solution in the presence of detergents and lipids." *Anal Biochem* 138 (1):141-3.

Wieser, R. J., D. Faust, C. Dietrich, and F. Oesch. 1999. "p16INK4 mediates contact-inhibition of growth." *Oncogene* 18 (1):277-81. doi: 10.1038/sj.onc.1202270.

Wilden, P. A., Y. M. Agazie, R. Kaufman, and S. P. Halenda. 1998. "ATP-stimulated smooth muscle cell proliferation requires independent ERK and PI3K signaling pathways." *Am J Physiol* 275 (4):H1209-15. doi: 10.1152/ajpheart.1998.275.4.H1209.

Winston, G. W., W. Harvey, L. Berl, and A. I. Cederbaum. 1983. "The generation of hydroxyl and alkoxyl radicals from the interaction of ferrous bipyridyl with peroxides." *Biochem J* 216 (2):415-21. doi: 10.1042/bj2160415.

Winterbourn, C. C. 2008. "Reconciling the chemistry and biology of reactive oxygen species." *Nat Chem Biol* 4 (5):278-86. doi: 10.1038/nchembio.85.

Wipf, P., J. Xiao, J. Jiang, N. A. Belikova, V. A. Tyurin, M. P. Fink, and V. E. Kagan. 2005. "Mitochondrial targeting of selective electron scavengers: synthesis and biological analysis of hemigramicidin-TEMPO conjugates." *J Am Chem Soc* 127 (36):12460-1. doi: 10.1021/ja053679l.

Wolpaw, A. J., K. Shimada, R. Skouta, M. E. Welsch, U. D. Akavia, D. Pe'er, F. Shaik, J. C. Bulinski, and B. R. Stockwell. 2011. "Modulatory profiling identifies mechanisms of small molecule-induced cell death." *Proc Natl Acad Sci U S A* 108 (39):E771-80. doi: 10.1073/pnas.1106149108.

Wood, K. C. 2015. "Mapping the Pathways of Resistance to Targeted Therapies." *Cancer Res* 75 (20):4247-51. doi: 10.1158/0008-5472.CAN-15-1248.

Wu, C., W. Zhao, J. Yu, S. Li, L. Lin, and X. Chen. 2018. "Induction of ferroptosis and mitochondrial dysfunction by oxidative stress in PC12 cells." *Sci Rep* 8 (1):574. doi: 10.1038/s41598-017-18935-1.

Xia, M., R. Huang, K. L. Witt, N. Southall, J. Fostel, M. H. Cho, A. Jadhav, C. S. Smith, J. Inglese, C. J. Portier, R. R. Tice, and C. P. Austin. 2008. "Compound cytotoxicity profiling using quantitative high-throughput screening." *Environ Health Perspect* 116 (3):284-91. doi: 10.1289/ehp.10727.

Xiaoyun, X., H. Chaofei, Z. Weiqi, C. Chen, L. Lixia, L. Queping, P. Cong, Z. Shuang, S. Juan, and C. Xiang. 2017. "Possible Involvement of F1F0-ATP synthase and Intracellular ATP in Keratinocyte Differentiation in normal skin and skin lesions." *Sci Rep* 7:42672. doi: 10.1038/srep42672.

Xie, Y., W. Hou, X. Song, Y. Yu, J. Huang, X. Sun, R. Kang, and D. Tang. 2016. "Ferroptosis: process and function." *Cell Death Differ* 23 (3):369-79. doi: 10.1038/cdd.2015.158.

Xie, Y., S. Zhu, X. Song, X. Sun, Y. Fan, J. Liu, M. Zhong, H. Yuan, L. Zhang, T. R. Billiar, M. T. Lotze, H. J. Zeh, R. Kang, G. Kroemer, and D. Tang. 2017. "The

Tumor Suppressor p53 Limits Ferroptosis by Blocking DPP4 Activity." *Cell Rep* 20 (7):1692-1704. doi: 10.1016/j.celrep.2017.07.055.

Yagoda, N., M. von Rechenberg, E. Zaganjor, A. J. Bauer, W. S. Yang, D. J. Fridman, A. J. Wolpaw, I. Smukste, J. M. Peltier, J. J. Boniface, R. Smith, S. L. Lessnick, S. Sahasrabudhe, and B. R. Stockwell. 2007. "RAS-RAF-MEK-dependent oxidative cell death involving voltage-dependent anion channels." *Nature* 447 (7146):864-8. doi: 10.1038/nature05859.

Yamashita, N., E. Tokunaga, M. Iimori, Y. Inoue, K. Tanaka, H. Kitao, H. Saeki, E. Oki, and Y. Maehara. 2018. "Epithelial Paradox: Clinical Significance of Coexpression of E-cadherin and Vimentin With Regard to Invasion and Metastasis of Breast Cancer." *Clin Breast Cancer* 18 (5):e1003-e1009. doi: 10.1016/j.clbc.2018.02.002.

Yamauchi, T., S. Adachi, I. Yasuda, M. Nakashima, J. Kawaguchi, T. Yoshioka, Y. Hirose, O. Kozawa, and H. Moriwaki. 2011. "Ultra-violet irradiation induces apoptosis via mitochondrial pathway in pancreatic cancer cells." *Int J Oncol* 39 (6):1375-80. doi: 10.3892/ijo.2011.1188.

Yan, S., M. Sorrell, and Z. Berman. 2014. "Functional interplay between ATM/ATR-mediated DNA damage response and DNA repair pathways in oxidative stress." *Cell Mol Life Sci* 71 (20):3951-67. doi: 10.1007/s00018-014-1666-4.

Yan, X., L. Yan, S. Liu, Z. Shan, Y. Tian, and Z. Jin. 2015. "N-cadherin, a novel prognostic biomarker, drives malignant progression of colorectal cancer." *Mol Med Rep* 12 (2):2999-3006. doi: 10.3892/mmr.2015.3687.

Yang, J., Y. Yu, H. E. Hamrick, and P. J. Duerksen-Hughes. 2003. "ATM, ATR and DNA-PK: initiators of the cellular genotoxic stress responses." *Carcinogenesis* 24 (10):1571-80. doi: 10.1093/carcin/bgg137.

Yang, W. S., K. J. Kim, M. M. Gaschler, M. Patel, M. S. Shchepinov, and B. R. Stockwell. 2016. "Peroxidation of polyunsaturated fatty acids by lipoxygenases drives ferroptosis." *Proc Natl Acad Sci U S A* 113 (34):E4966-75. doi: 10.1073/pnas.1603244113.

Yang, W. S., R. SriRamaratnam, M. E. Welsch, K. Shimada, R. Skouta, V. S. Viswanathan, J. H. Cheah, P. A. Clemons, A. F. Shamji, C. B. Clish, L. M. Brown, A. W. Girotti, V. W. Cornish, S. L. Schreiber, and B. R. Stockwell. 2014. "Regulation of ferroptotic cancer cell death by GPX4." *Cell* 156 (1-2):317-331. doi: 10.1016/j.cell.2013.12.010.

Yang, W. S., and B. R. Stockwell. 2008. "Synthetic lethal screening identifies compounds activating iron-dependent, nonapoptotic cell death in oncogenic-RAS-harboring cancer cells." *Chem Biol* 15 (3):234-45. doi: 10.1016/j.chembiol.2008.02.010.

Yang, W. S., and B. R. Stockwell. 2016. "Ferroptosis: Death by Lipid Peroxidation." *Trends Cell Biol* 26 (3):165-176. doi: 10.1016/j.tcb.2015.10.014.

Yi, M., J. Li, S. Chen, J. Cai, Y. Ban, Q. Peng, Y. Zhou, Z. Zeng, S. Peng, X. Li, W. Xiong, G. Li, and B. Xiang. 2018. "Emerging role of lipid metabolism alterations in Cancer stem cells." *J Exp Clin Cancer Res* 37 (1):118. doi: 10.1186/s13046-018-0784-5.

Yin, X., X. W. Yu, P. Zhu, Y. M. Zhang, X. H. Zhang, F. Wang, J. J. Zhang, W. Yan, Y. Xi, J. B. Wan, J. X. Kang, Z. Q. Zou, and S. Z. Bu. 2016. "Endogenously synthesized n-3 fatty acids in fat-1 transgenic mice prevent melanoma progression by increasing E-cadherin expression and inhibiting β-catenin signaling." *Mol Med Rep* 14 (4):3476-84. doi: 10.3892/mmr.2016.5639.

Yu, H., P. Guo, X. Xie, Y. Wang, and G. Chen. 2017. "Ferroptosis, a new form of cell death, and its relationships with tumourous diseases." *J Cell Mol Med* 21 (4):648-657. doi: 10.1111/jcmm.13008.

Yuan, J., A. Najafov, and B. F. Py. 2016. "Roles of Caspases in Necrotic Cell Death." *Cell* 167 (7):1693-1704. doi: 10.1016/j.cell.2016.11.047.

Zhang, D. W., M. Zheng, J. Zhao, Y. Y. Li, Z. Huang, Z. Li, and J. Han. 2011. "Multiple death pathways in TNF-treated fibroblasts: RIP3- and RIP1-dependent and independent routes." *Cell Res* 21 (2):368-71. doi: 10.1038/cr.2011.3.

Zhang, J., X. Wang, V. Vikash, Q. Ye, D. Wu, Y. Liu, and W. Dong. 2016. "ROS and ROS-Mediated Cellular Signaling." *Oxid Med Cell Longev* 2016:4350965. doi: 10.1155/2016/4350965.

Zhang, S., Y. Lin, Y. S. Kim, M. P. Hande, Z. G. Liu, and H. M. Shen. 2007. "c-Jun N-terminal kinase mediates hydrogen peroxide-induced cell death via sustained poly(ADP-ribose) polymerase-1 activation." *Cell Death Differ* 14 (5):1001-10. doi: 10.1038/sj.cdd.4402088.

Zilka, O., R. Shah, B. Li, J. P. Friedmann Angeli, M. Griesser, M. Conrad, and D. A. Pratt. 2017. "On the Mechanism of Cytoprotection by Ferrostatin-1 and Liproxstatin-1 and the Role of Lipid Peroxidation in Ferroptotic Cell Death." *ACS Cent Sci* 3 (3):232-243. doi: 10.1021/acscentsci.7b00028.

Zong, W. X., and C. B. Thompson. 2006. "Necrotic death as a cell fate." *Genes Dev* 20 (1):1-15. doi: 10.1101/gad.1376506.

Zorova, L. D., V. A. Popkov, E. Y. Plotnikov, D. N. Silachev, I. B. Pevzner, S. S. Jankauskas, V. A. Babenko, S. D. Zorov, A. V. Balakireva, M. Juhaszova, S. J. Sollott, and D. B. Zorov. 2018. "Mitochondrial membrane potential." *Anal Biochem* 552:50-59. doi: 10.1016/j.ab.2017.07.009.

Appendix I: Supplemental data

Cell line	Cell population	% of cells in:			
		subG1	**G0/G1**	**S**	**G2/M**
MEF *(0.5 % FBS, 48 h)*	**confl.**	8	**74**	4	14
	prol.	16	45	8	31
	sd	12	**67**	6	15
Swiss3T3 *(0.1 % FBS, 48 h)*	**confl.**	5	**72**	4	19
	prol.	10	53	9	28
	sd	12	**72**	3	13
FH109 *(0.1 % FBS, 48 h)*	**confl.**	0	**75**	10	15
	prol.	1	50	29	20
	sd	16	**70**	7	7

Table 1: Confluent and serum-depleted cells show a similar cell cycle distribution and confluent cells are not arrested in G1 at the time point of *t*-BuOOH exposure. Confluent (confl.) and semiconfluent (proliferating, prol.; serum-depleted, sd) cells were seeded and cultivated according to setup I (*condition for serum depletion are separately indicated*). Afterwards, cell cycle analysis was conducted via PI staining and flow cytometry at the time point of *t*-BuOOH exposure (representative values out of *n* = 2-3 in duplicates). The analysis of FH109 cells was conducted by B. Linz.

| Cell line	Cell population	Cell treatment	% of cells in:			
			subG1	**G0/G1**	**S**	**G2/M**
NIH3T3	prol.	control	1	49	12	38
		6h 30µM *t*-BuOOH	1	42	18	39
		6h 50µM *t*-BuOOH	2	47	17	34
	sd	control	4	81	3	12
		6h 30µM *t*-BuOOH	8	75	4	13
		6h 50µM *t*-BuOOH	11	73	3	13
Caco-2	prol.	control	3	53	11	33
		6h 100µM *t*-BuOOH	2	48	10	39
		8h 100µM *t*-BuOOH	2	49	15	34
		10h 100µM *t*-BuOOH	2	45	14	39

Table 2: *t*-BuOOH-induced necrosis is executed in the absence of DNA fragmentation. Semiconfluent cells (proliferating, prol.; serum-depleted, sd) cells were seeded and cultivated according to experimental setup I. After *t*-BOOH exposure, subG1 analysis was conducted via PI staining and flow cytometry (mean of a single experiment performed in duplicates).
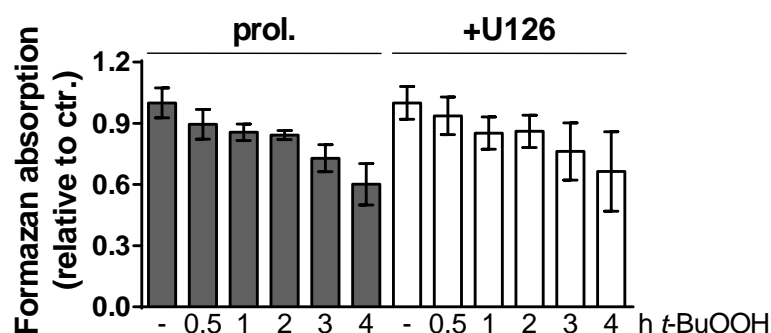
Fig. A1: *t*-BuOOH induces a similar time-dependent decrease of the intracellular dehydrogenase activity in proliferating and U0126-treated NIH3T3 cells. Semiconfluent cells were seeded according to setup I. Cells were cultivated in the presence of 10 % FBS and were either untreated (proliferating, prol.) or simultaneously treated with U0126 (50 µM; + U0126) for 24 h. After *t*-BuOOH treatment (30 µM) followed by incubation with MTT, formazan absorbance was assessed as a rough measure for intracellular dehyrogenase activity. Results are presented as mean ± SD of a representative experiment out of *n* = 2-3 in duplicates.
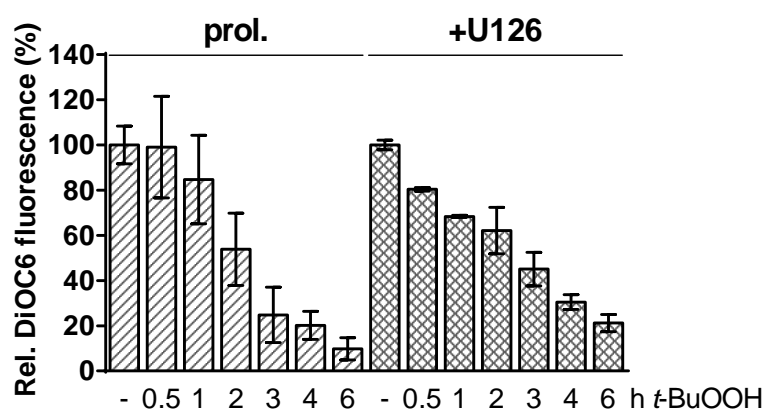
Fig. A2: *t*-BuOOH induces a similar time-dependent loss of the mitochondrial membrane potential ($\Delta\psi_m$) in proliferating and U0126-treated NIH3T3 cells. Semiconfluent cells were seeded according to setup I. Cells were cultivated in the presence of 10 % FBS and were either untreated (proliferating, prol.) or simultaneously treated with U0126 (50 µM; + U0126) for 24 h. After *t*-BuOOH treatment (50 µM), cells were stained with DiOC6 as marker for $\Delta\psi_m$ followed by flow cytometric analysis. Results are presented as mean ± SD of *n* = 2-3 in duplicates.
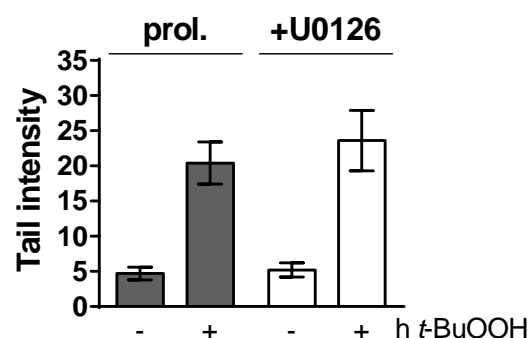
Fig. A3: Proliferating and U0126-treated NIH3T3 cells demonstrate a similar induction of *t*-BuOOH-induced DSBs. Semiconfluent cells were seeded according to setup I. Cells were cultivated in the presence of 10 % FBS and were either untreated (proliferating, prol.) or simultaneously treated with U0126 (50 µM; + U0126) for 24 h. After *t*-BuOOH treatment (50 µM), the neutral comet assay was performed. Results are expressed as tail intensity and presented as mean ± SD of *n* = 3 with 50 cells analyzed per sample.
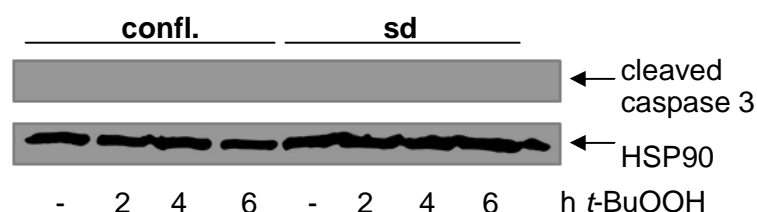

Fig. A4: *t*-BuOOH-induced necrosis is executed independent from caspases. Confluent (confl.) and serumdepleted (sd) NIH3T3 cells were seeded and cultivated upon setup I. After *t*-BuOOH treatment (50 µM) for the indicated time points, cells were harvested for Western Blot analysis of caspase 3 activation with HSP90 as loading control (conducted by D. Faust). Positive controls were simultaneously detected on blots for analysis of proliferating cells.
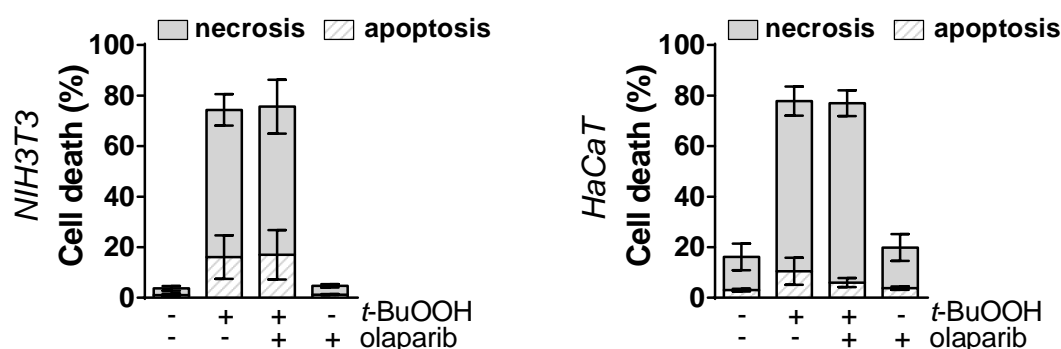
Fig. A5: PARP-1 inhibition fails to prevent *t*-BuOOH-induced necrosis. Serum-depleted NIH3T3 cells were seeded and cultivated according to setup I. Subsequently, cells were either untreated or treated with *t*-BuOOH (NIH3T3: 50 µM; HaCaT: 200 µM) in the absence or the presence of the PARP-1 inhibitor olaparib (0.5 µM) for 6 h. Subsequent, cells were stained with AnnexinV-FITC (apoptosis) / PI (necrosis) and cell death was analyzed via flow cytometry (mean ± SD of *n* = 2-3 in duplicates).
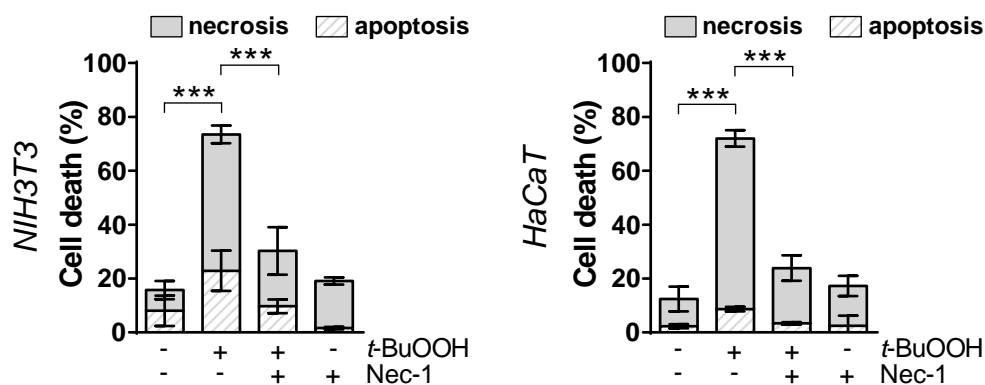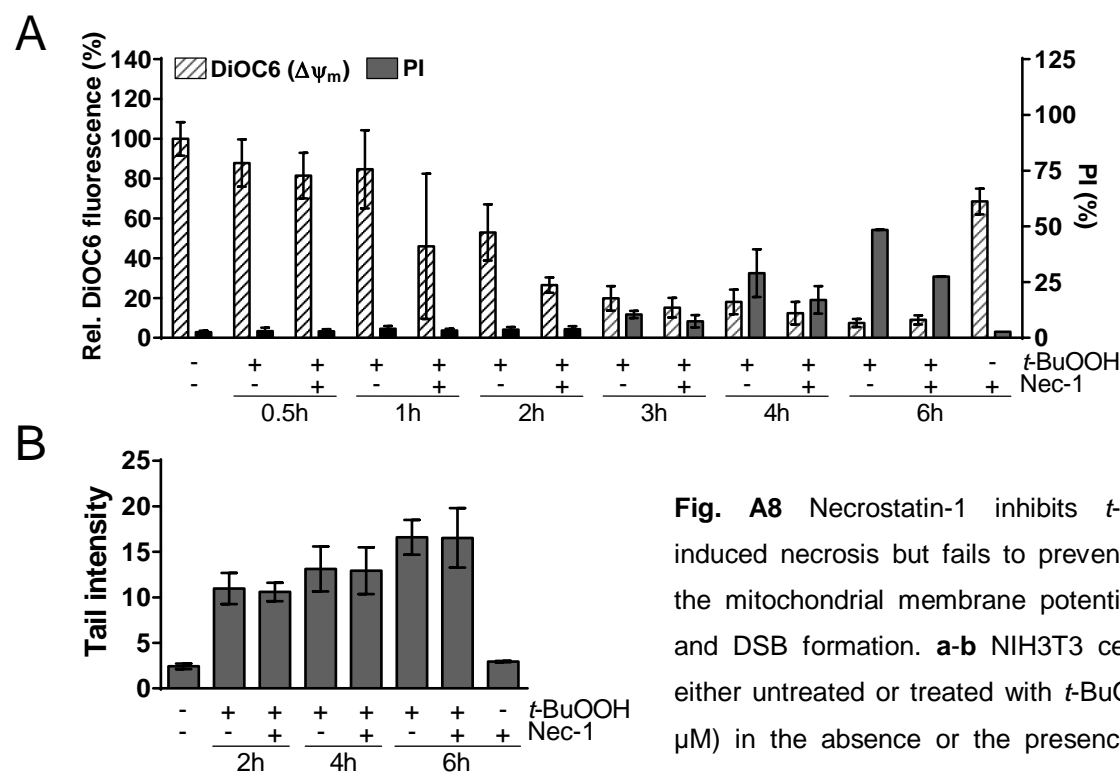
Fig. A6 Necrostatin-1 inhibits *t*-BuOOH-induced necrosis. Serum-depleted cells were seeded and cultivated according to setup I. Afterwards, cells were either untreated or treated with *t*-BuOOH (NIH3T3: 50 µM; HaCaT: 200 µM) in the absence or the presence of the RIPK1 inhibitor necrostatin-1 (Nec-1: 50 µM) for 6 h. Subsequently, cells were stained with AnnexinV-FITC (apoptosis) / PI (necrosis) and cell death was analyzed via flow cytometry (mean ± SD of *n* = 2-4 in duplicates). Significance was calculated with *** $p \leq 0.001$.
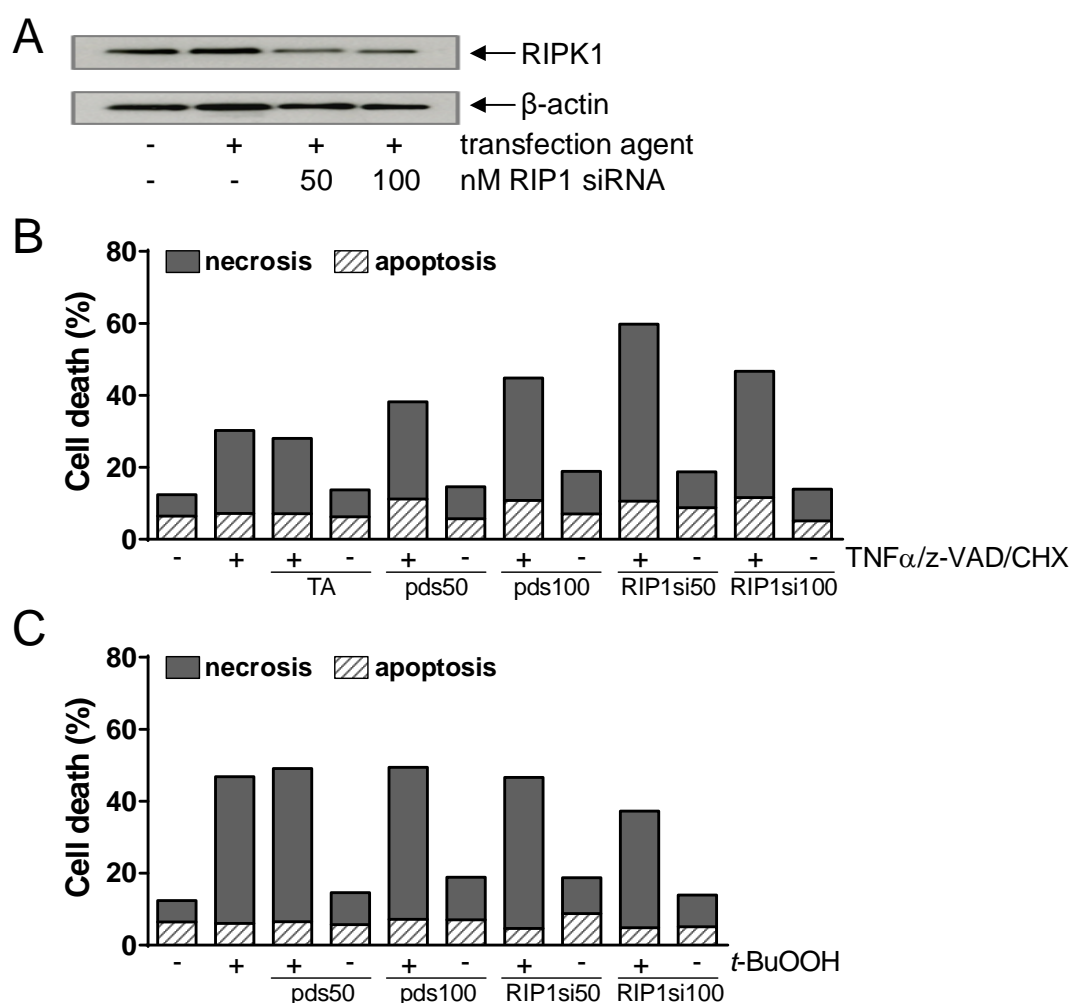

Fig. A7 siRNA-mediated RIPK1 knockdown was not sufficient to block TNFα-induced necroptosis or to inhibit *t*-BuOOH-induced necrosis. **a** Western Blot analysis of RIPK1 knockdown in MEF cells with β-actin as loading control after transfection with the indicated siRNA concentrations for 48 h. **b-c** After

RIPK1 knockdown, MEF cells were either (**b**) treated with TNFα (100 ng/mL), z-VAD-fmk (z-VAD: 20 µM) and cycloheximide (CHX: 1 µg/mL) for 24 h, or (**c**) treated with *t*-BuOOH (100 µM) for 6 h. Subsequently, cells were stained with AnnexinV-FITC (apoptosis) / PI (necrosis) and cell death was analyzed via flow cytometry (representative experiment out of n = 2-4). TA = transfection agent, pds50/100 = scrambled siRNA (50 nM, 100 nM), RIPsi50/100 = RIPK1 siRNA (50 nM, 100 nM).

Fig. A8 Necrostatin-1 inhibits *t*-BuOOH-induced necrosis but fails to prevent loss of the mitochondrial membrane potential ($\Delta\psi_m$) and DSB formation. **a-b** NIH3T3 cells were either untreated or treated with *t*-BuOOH (50 µM) in the absence or the presence of the RIPK1 inhibitor Necrostatin-1 (Nec-1; 50 µM). Afterwards, cells were either (**a**) stained with DiOC6 to assess $\Delta\psi_m$ and PI to detect necrosis, or (**b**) neutral comet assays were performed to detect DNA DSBs (mean ± SD of n = 2-3 in duplicates).
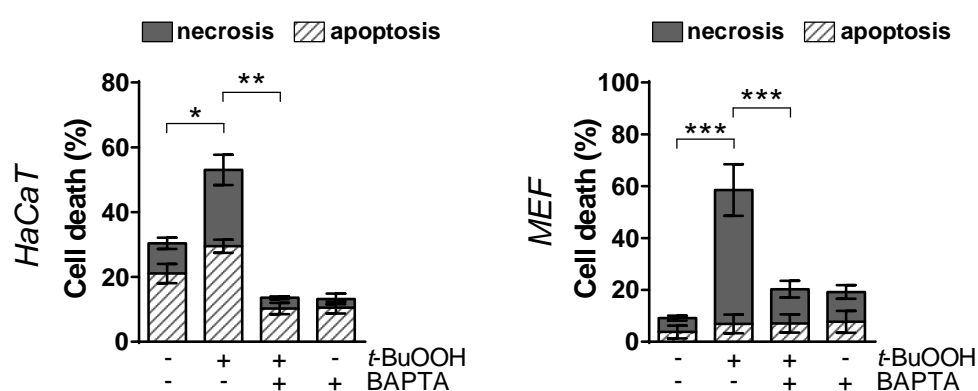
Fig. A9 *t*-BuOOH-induced necrosis is inhibited by the Ca^{2+} chelator BAPTA AM. Cells were untreated or treated with *t*-BuOOH (HaCaT: 200 µM; MEF: 100 µM) in the absence or in the presence of BAPTA AM (10 µM) for 6 h. Subsequently, cells were either stained with AnnexinV-FITC (apoptosis) / PI (necrosis) and cell death was analyzed. Mean ± SD of n = 2-3 in duplicates (HaCaT: representative experiment). Significance was calculated with * $p \le 0.05$, ** $p \le 0.01$, *** $p \le 0.001$.